FOREWORD

This work was conducted by the National Carbon Company, a Division of Union Carbide Corporation under USAF Contract AF 33(616)-6915. This Contract was initiated under Project No. 7350 "Refractory Inorganic Non-Metallic Materials," Task No. 735002 "Refractory Inorganic Nonmetallic Materials: Graphitic"; Project No. 7381 "Materials Application," Task No. 738102 "Materials Processes"; and Project No. 7-817 "Process Development for Graphite Materials." The work was administrated under the direction of the Directorate of Materials and Processes, Deputy for Technology, Aeronautical Systems Division, with Captain R. H. Wilson, L. J. Conlon, and W. P. Conrardy acting as Project Engineers.

This is a summary technical report covering the period from May 1, 1960 to April 30, 1963. The work reported was carried out in Laboratories of National Carbon Company located in Lawrenceburg, Tennessee, Fostoria, Ohio, Cleveland Ohio, and Niagara Falls, New York. The advanced Materials Project was under the direction of R. M. Bushong, R. C. Stroup was responsible for the Development work, W. P. Eatherly coordinated the Research activities and J. H. Brannan supervised the field application activities.

The reports issued under USAF Contract AF 33(616)-6915 including the present one are listed below:

WADD Technical Notes 61-18 and 61-18, Part II, progress reports covering work from the start of the Contract on May 1, 1960 to October 15, 1961, and the following volumes of WADD Technical Report 61-72 covering various subject phases of the work:

Volume I	Observations by Electron Microscopy of Dislocations in Graphite, by R. Sprague.
Volume II	Applications of Anisotropic Elastic Continuum Theory to Dislocations in Graphite, by G. B. Spence.
Volume III	Decoration of Dislocations and Low Angle Grain Boundaries in Graphite Single Crystals, by R. Bacon and R. Sprague.
Volume IV	Adaptation of Radiographic Principles to the Quality Control of Graphite, by R. W. Wallouch.
Volume V	Analysis of Creep and Recovery Curves for ATJ Graphite, by E. J. Seldin and R. N. Draper.
Volume VI	Creep of Carbons and Graphites in Flexure at High Temperatures, by E. J. Seldin.
Volume VII	High Density Recrystallized Graphite by Hot Forming, by E. A. Neel, A. A. Kellar, and K. J. Zeitsch.
Supplement to Volume VII	High Density Recrystallized Graphite by Hot Forming, by G. L. Rowe and M. B. Carter.

Volume VIII	Electron Spin Resonance in Polycrystalline Graphite, by L. S. Singer and G. Wagoner.
Volume IX	Fabrication and Properties of Carbonized Cloth Composites, by W. C. Beasley and E. L. Piper.
Volume X	Thermal Reactivity of Aromatic Hydrocarbons, by I. C. Lewis and T. Edstrom.
Supplement to Volume X	Thermal Reactivity of Aromatic Hydrocarbons, by I. C. Lewis and T. Edstrom.
Volume XI	Characterization of Binders Used in the Fabrication of Graphite Bodies, by E. de Ruiter, A. Halleux, V. Sandor and H. Tschamler.
Supplement to Volume XI	Characterization of Binders Used in the Fabrication of Graphite Bodies, by E. de Ruiter, J. F. M. Oth, V. Sandor and H. Tschamler.
Volume XII	Development of an Improved Large Diameter Fine Grain Graphite for Aerospace Applications, by C. W. Waters and E. L. Piper.
Volume XIII	Development of a Fine-Grain Isotropic Graphite for Structural and Substrate Applications, by R. A. Howard and E. L. Piper.
Supplement to Volume XIII	Development of a Fine-Grain Isotropic Graphite for Structural and Substrate Applications, by R.A. Howard and R. L. Racicot.
Volume XIV	Study of High-Temperature Tensile Properties of ZTA Grade Graphite, by R. M. Hale and W.M. Fassell, Jr.
Volume XV	Alumina-Condensed Furfuryl Alcohol Resins, by C. W. Boquist, E. R. Nielsen, H. J. O'Neil and R. E. Putcher.
Volume XVI	An Electron Spin Resonance Study of Thermal Decomposition Reactions of Organic Compounds, by L. S. Singer and I. C. Lewis.
Volume XVII	Radiography of Carbon and Graphite, by T. C. Furnas, Jr. and M. R. Rosumny.
Volume XVIII	High Temperature Tensile Creep of Graphite, by E. J. Seldin.
Volume XIX	Thermal Stresses in Anisotropic Hollow Cylinders, by Tu-Lung Weng.

Volume XX	The Electric and Magnetic Properties of Pyrolytic Graphite, by G. Wagoner and B. H. Eckstein.
Volume XXI	Arc Image Furnace Studies of Graphite, by M. R. Null and W. W. Lozier
Volume XXII	Photomicrographic Techniques for Carbon and Graphite, by G. L. Peters and H. D. Shade.
Volume XXIII	A Method for Determining Young's Modulus of Graphite at Elevated Temperatures, by S.O. Johnson and R. B. Dull.
Volume XXIV	The Thermal Expansion of Graphite in the c-Direction, by C. E. Lowell.
Volume XXV	Lamellar Compounds of Nongraphitized Petroleum Cokes, by H. F. Volk.
Volume XXVI	Physical Properties of Some Newly Developed Graphite Grades, by R. B. Dull.
Volume XXVII	Carbonization Studies of Aromatic Hydrocarbons, by I. C. Lewis and T. Edstrom.
Volume XXVIII	Polarographic Reduction of Polynuclear Aromatics, by I. C. Lewis, H. Leibecki, and S. L. Bushong.
Volume XXIX	Evaluation of Graphite Materials in a Subscale Solid Propellant Rocket Motor, by D. C. Hiler and R. B. Dull.
Supplement to Volume XXIX	Evaluation of Graphite Materials in a Subscale Solid Propellant Rocket Motor, by S. O. Johnson and R. B. Dull.
Volume XXX	Oxidation Resistant Graphite Base Composites, by K. J. Zeitsch and J. Criscione.
Volume XXXI	High Performance Graphite by Liquid Impregnation, by C. E. Waylett, M. A. Spring and M. B. Carter.
Volume XXXII	Studies of Binder Systems for Graphite, by T. Edstrom, I. C. Lewis, R. L. Racicot and C. F. Stout.
Volume XXXIII	Investigation of Hot Worked Recrystallized Graphites, by J. H. Turner and M. B. Carter.
Volume XXXIV	Oxidation Resistant Coatings for Graphite, by D.A. Schulz, P. H. Higgs and J. D. Cannon.
Volume XXXV	Methods of Measuring Mechanical Properties of Graphite in the 20° to 2700°C Temperature Range, by M. B. Manofsky and R. B. Dull.

Volume XXXVI	Studies of the Quality of Petroleum Coke from a Pilot Scale Delayed Coker, by C. F. Stout, M. Janes and J. A. Biehl.
Volume XXXVII	Studies of Graphite Deposited by Pyrolytic Processes, by P. H. Higgs, R. L. Finicle, R. J. Bobka, E. J. Seldin and K. J. Zeitsch.
Volume XXXVIII	Development of an Improved Large Diameter Ultra Fine-Grain Graphite, by R. A. Howard and R. L. Racicot.
Volume XXXIX	Diamagnetic Susceptibility of Graphite by the Faraday Method, by D. E. Soule and C. W. Nezbeda.
Volume XL	The Influence of Fillers on the Pyrolysis and Bonding Characteristics of Certain Synthetic Binders, by C. W. Boquist, H. J. O'Neil, R. E. Putcher and A. Dynako.
Volume XLI	Survey and Analytical Representation of the Measurements of the Specific Heat of Graphite, by G. B. Spence.
Volume XLII	Summary Technical Report.

ABSTRACT

This report gives a summary of a research and development program on graphite and graphite-base materials over the period May 1, 1960 to April 30, 1963. The efforts covered raw materials studies, basic investigations of the elemental graphite crystals, fabrication studies including scaleup to useful sizes, and characterization and evaluation for applicability to selected weapons systems.

A complete listing of other Technical Reports issued under this contract study is presented.

This report has been reviewed and is approved.

W. G. RAMKE
Chief, Ceramics and Graphite Branch
Metals and Ceramics Division
Air Force Materials Laboratory

TABLE OF CONTENTS

PAGE

1. INTRODUCTION 1

2. SUMMARY 2

2.1. Research Summary 2

2.1.1. Summary of Raw Materials Studies 2

2.1.2. Summary of Basic Research Studies 2

2.1.3. Summary of Applied Research 3

2.2. Development Summary 3

3. RESEARCH 5

3.1. Study of Raw Materials for Graphite 5

3.1.1. Pyrolysis Studies on Pure Compounds 5

3.1.1.1. Thermal Reactivity of Aromatic Hydrocarbons, Substituted Aromatics, and Heterocyclic Compounds 5

3.1.1.2. Quantitative DTA 5

3.1.1.3. Electron Spin Resonance Studies 7

3.1.1.4. Carbonization Studies 9

3.1.1.5. Application of Special Analytical Techniques 10

3.1.2. Pyrolysis Studies on Tars, Pitches, Resins, and Cokes . . 16

3.1.2.1. Characterization of Binders Used in the Fabrication of Graphite Bodies 16

3.1.2.2. Studies of Binder Reactions and Binder-Filler Interactions by Armour Research Foundation (ARF) 16

3.1.2.3. Thermogravimetric Analysis (TGA) 17

3.1.2.4. Atomic C/H Ratios and Carbonization 18

3.1.3. Study of Lamellar Compounds of Carbon and Graphite . . 20

3.2. Basic Studies of Graphite 21

3.2.1. Electronic Properties 21

TABLE OF CONTENTS (CONT'D.)

		PAGE
3.2.1.1.	Electron Spin Resonance of Graphite	21
3.2.1.2.	Diamagnetic Susceptibility of Graphite	22
3.2.1.3.	Electronic Properties of Pyrolytic Graphite	24
3.2.1.4.	Doping Studies	27
3.2.2.	Mechanical Properties of Graphite Crystal	31
3.2.2.1.	Studies of Dislocations	31
3.2.2.2.	Studies of Graphite Whiskers	38
3.2.2.3.	Crystallite Preferred Orientation Studies	41
3.2.2.4.	High Temperature X-Ray Diffraction Studies	47
3.2.2.5.	Specific Heat of Graphite	49
3.2.2.6.	Measurement of Thermal Conductivity at Elevated Temperatures	51
3.3.	Applied Research	57
3.3.1.	Studies of Creep of Graphite	57
3.3.2.	Tensile Stress-Strain Behavior of Grade ATJ Graphite	59
3.3.3.	Thermal Stresses in Anisotropic Hollow Cylinders	61
3.3.4.	Sonic Elastic Constants of Polycrystalline Graphite with Cylindrical Symmetry	62
3.3.5.	Study of High Temperature Tensile Properties of Grade ZTA Graphite	62
3.3.6.	Radiographic Examination of Carbon and Graphite	63
3.3.7.	Arc Image Furnace Studies	64
4.	DEVELOPMENT	66
4.1.	Raw Materials Studies	66
4.1.1.	Process Studies in Pilot Coker	66
4.1.2.	Binder Systems for Graphite	67

TABLE OF CONTENTS (CONT'D)

	PAGE
4.1.3. Calcination of Raw Petroleum Cokes	68
4.1.4. Preimpregnation of Raw Materials	69
4.2. Fabrication Studies	69
4.2.1. High Density Recrystallized Graphite (ZT Grades)	69
4.2.2. Pressure-cured Large Size Graphite	70
4.2.3. Substrate Graphite for Coatings	71
4.2.4. Oxidation Resistant Graphites	72
4.2.5. Liquid Impregnation of Graphite	75
4.2.6. Fibrous Carbon and Graphite Composites	75
4.2.7. Graphite from Pyrolytic Processes	75
4.2.8. Special Extrusion Techniques	76
4.2.9. Carbon and Graphite Whiskers	76
4.2.10. Carbon and Graphite Foams	76
4.2.11. Cements for Use with Carbon and Graphite	77
4.3. Material Characterization and Evaluation	77
4.3.1. Graphite Properties over a Range of Temperatures	77
4.3.2. Radiographic Techniques for Examination of Graphite	78
4.3.3. Photomicrographic Techniques for Examination of Graphite	78
4.3.4. Environmental Tests in Subscale Rocket Motors	79
4.3.5. Applications Technology	79
5. LIST OF REFERENCES	81
6. GLOSSARY	87
6.1. Abbreviations	87
6.2. National Carbon Company Grades	87
6.3 Terms	88

TABLE OF CONTENTS (CONT'D)

		PAGE
APPENDIX I.	MECHANICAL PROPERTIES OF GRAPHITE WHISKERS AT HIGH TEMPERATURE	89
APPENDIX II.	SONIC ELASTIC CONSTANTS OF POLY-CRYSTALLINE GRAPHITES	105
APPENDIX III.	CALCINATION OF RAW PETROLEUM COKES . .	119
APPENDIX IV.	IMPROVEMENT OF GRAPHITE PROPERTIES BY PREIMPREGNATION OF RAW MATERIALS . . .	138
APPENDIX V.	INDUCTION HEATING FOR PRESSURE CURING .	148
APPENDIX VI.	SPECIAL EXTRUSION TECHNIQUES	167
APPENDIX VII.	CARBON AND GRAPHITE WHISKERS	174
APPENDIX VIII.	CARBON AND GRAPHITE FOAMS - FEASIBILITY STUDIES	185
APPENDIX IX.	CEMENTS FOR USE WITH CARBON AND GRAPHITE	189

LIST OF FIGURES

FIGURE		PAGE
1.	Spectra of 9, 9'-Dibromofluorene in Solution and Heat-Treated	11
2.	Spectra of 10:1 m-Quinquephenyl:Acenaphthylene During Heating	13
3.	Absorption Spectra of Aromatic Hydrocarbon-Quinone Mixtures	14
4.	Thermogravimetric Analysis of Coal Tar Pitch	18
5.	Thermogravimetric Analysis of Coal Tar Pitch vs. Heating Rate, 110°C M.P. 30 Medium Pitch	19
6.	Diamagnetism and g-Value of Pyrolytic Graphite	25
7.	Spin Resonance g-Value of Pyrolytic Graphite vs. Deposition Temperature	26
8.	Schematic Diagram of Assembly for Hall Coefficient and Resistance Measurements. I - Leads for Main Current, H - Hall Effect Probes, R - Resistivity Probes	29
9.	Hall Coefficient of L113SP Potassium-Doped Graphite	30
10.	A. Relative Resistance of Potassium-Doped L113SP Graphite. B. Relative Magnetic Susceptibility of Potassium-Doped L113SP Graphite	30
11.	g-Value of Potassium-Doped Graphite vs. Potassium Concentration	31
12.	(a) Naphthalene Molecule $C_{10}H_8$. (b) Azulene Molecule $C_{10}H_8$	34
13.	Positions and Glide Zones of an Edge Dislocation Parallel to the c-Axis in Graphite	35
14.	Atomic Positions of a Type 1 Dislocation as Given by Linear Elasticity Theory: (a) Position 1, (b) Position 2, (c) Position 3	36
15.	Atomic Positions of a Type 4 Dislocation as Given by Linear Elasticity Theory: (a) Position 7, (b) Position 8, (c) Position 9	36

LIST OF FIGURES (CONT'D)

FIGURE		PAGE
16.	Atomic Positions of a Type 5 Dislocation as Given by Linear Elasticity Theory: (a) Position 10, (b) Position 11, (c) Position 12	37
17.	Atomic Positions of a Type 2 Dislocation as Given by Linear Elasticity Theory with Estimated Relaxation of Core Atoms: (a) Position 4, (b) Position 5, (c) Position 6	37
18.	Crystallite Orientation Distribution Function for Grade AGKSP Graphite. Solid Curve-Experimental. Dashed Curve - Analytical	42
19.	Orientation of a Crystallite With Respect to the Sample Symmetry Axis and to the Magnetic Field Direction	44
20.	Effect of Heat Treatment on Acenaphthylene Coke	49
21.	Specimen Environment in Thermal Conductivity Apparatus	52
22.	Correction Factor for Thermal Conductivity	53
23.	Diagram of Thermal Conductivity Apparatus	54
24.	Thermal Conductivity Apparatus Assembled in Vacuum Furnace	55
25.	Measurement of Effect of Transverse Heat Losses, i.e., Measurement of $dT(x)/dT_s$	56
26.	Measurement of κ_o, Uncorrected Thermal Conductivity.	56
27.	Flexural Creep of RVA Graphite at Room Temperature.	58
28.	Stress-Strain Data for Grade ATJ Graphite	60
I.1.	Graphite Whisker of 4-mm Length Mounted Between Two Graphite Rod Tensile Grips	92
I.2.	Diagram of Tensile Apparatus	93

LIST OF FIGURES (CONT'D)

FIGURE		PAGE
I.3.	Photograph of High Temperature Tensile Apparatus . . .	94
I.4.	Tensile Apparatus Shown with Pumping Station and Recording Equipment	95
I.5.	Typical Tension-Elongation Curve for a Graphite Whisker at Room Temperature	96
I.6.	Hysteresis Loop Resulting from Application and Subsequent Release of Force on a Whisker	96
I.7.	Relative Yield Stress at Room and High Temperatures on Whisker 7B	99
I.8.	Relative Yield Stress at Room and High Temperatures on Whisker 19	99
I.9.	Graphite Whisker Exploded Inside the Electron Microscope	101
I.10.	Tip of an Exploded Whisker Showing Hollow Inner Core. .	102
I.11.	Twisted Section of a Plastically Deformed Inner Core . .	103
II.1.	Sonic Young's Modulus for Grade ATJ Graphite Parallel to the Molding Direction Versus Density.	113
II.2.	Sonic Torsion Modulus for Grade ATJ Graphite Parallel to the Molding Direction Versus Density	113
II.3.	Orientation of Samples of Grade ATJ Graphite for Sonic Modulus Testing.	115
II.4.	Calculated Values of s_{13} as a Function of Orientation for Grade ATJ Sample 2A.	117
III.1.	Photomicrograph of Petroleum Coke 60-Flour, Pressure Calcined at 1350°C, 150X	120
III.2.	Photomicrograph of Petroleum Coke 60-Flour Control Calcined at 1350°C, 150X	120
III.3.	Puffing Diagram of Plugs Made from TA Coke Calcined to 1350°C as 60-Flour	126
III.4.	Puffing Diagram of Plugs Made from AX Coke Calcined to 1350°C as 60-Flour	126

LIST OF FIGURES (CONT'D.)

FIGURE		PAGE
III. 5.	Puffing Diagram of Plugs Made from AX Coke Calcined to 1350°C in Lump Form	127
III. 6.	Photomicrograph of TA Coke, Sulfur Calcined, 100X . .	128
III. 7.	Photomicrograph of TA Coke, Standard Calcined, 100X .	128
III. 8.	Photomicrograph of HT Coke, Sulfur Calcined, 100X . .	129
III. 9.	Photomicrograph of HT Coke, Standard Calcined, 100X .	129
III. 10.	Sulfur Calcination of Different TA Coke Samples, Calcined to 1350°C	131
III. 11.	Effect of Volatile Content and Calcining Rate on Sulfur Calcination of HK Coke, Calcined to 1350°C	132
III. 12.	Effect of Temperature on Sulfur Calcination of TA Coke .	133
III. 13.	Effect of Sulfur Concentration on Calcination of DK Coke, Calcined to 1350°C	134
III. 14.	Effect of Furnace Type on Sulfur Calcination of DK Coke, Calcined to 1350°C	135
III. 15.	Puffing Diagramsof Plugs Made from TA Coke, Calcined to 1200°C	136
III. 16.	Puffing Diagrams of Plugs Made from TA Coke, Calcined to 1350°C	136
III. 17.	Puffing Diagram of Plugs Made from TA Coke, Calcined to 1600°C	137
IV. 1.	AX Coke, Calcined to 1350°C, 100X	139
IV. 2.	AX Coke, Calcined to 1350°C, Pitch Impregnated, 100X .	139
IV. 3.	AX Coke, Calcined to 1350°C, Pitch Treated and Recalcined to 425°C, 100X	140
IV. 4.	AX Coke, Calcined to 1350°C, Pitch Treated and Recalcined to 450°C, 100X	140
IV. 5.	AX Coke, Calcined to 1350°C, Pitch Treated and Recalcined to 475°C, 100X	141

LIST OF FIGURES (CONT'D.)

FIGURE		PAGE
IV.6.	AX Coke, Calcined to 1350°C, Pitch Treated and Recalcined to 500°C, 100X	141
IV.7.	AX Coke, Calcined to 1350°C, Pitch Treated and Recalcined to 525°C, 100X	142
IV.8.	AX Coke, Calcined to 1350°C, Pitch Treated and Recalcined to 550°C, 100X	142
IV.9.	Density Comparison, Pressure Cured Blocks, Preimpregnated AX Coke Base and Standard AX Coke Base	145
IV.10.	Resistance Comparison, Pressure Cured Blocks Preimpregnated AX Coke Base and Standard AX Coke Base	146
IV.11.	Flexural Strength Comparison, Pressure Cured Blocks, Preimpregnated AX Coke Base and Standard AX Coke Base	147
V.1.	Run No. 1-X, Induction Heating Trial, Green RVA Plug	149
V.2.	Run No. 2-X, Induction Heating Trial, Cured RVA Plug	150
V.3.	Run No. 3-X, Induction Heating Trial, Green RVA Plug	151
V.4.	Fiber Glass Mold, Refractory Liner and Heat Exchanger Assembly for Induction Heating-Pressure Curing Process	152
V.5.	Cast Refractory Pressure Rams for Induction Heating-Pressure Curing Process	153
V.6.	Induction Heating-Pressure Curing Assembly	154
V.7.	Induction Heating-Pressure Curing Assembly, Front View	155
V.8.	Induction Heating-Pressure Curing Assembly, Rear View	156
V.9.	Trial No. 11-R, Induction Heating-Pressure Curing, RVA Grade, Conditions and Results	158
V.10.	Trial No. 11-R, Induction Heating-Pressure Curing, Temperatures of the Fiber Glass-Castable Liner Interface	159
V.11.	Top Pressure Ram for Induction Heating Pressure Curing Assembly	160
V.12.	Bottom Pressure Ram for Induction Heating Pressure Curing Assembly	161

LIST OF FIGURES (CONT'D.)

FIGURE		PAGE
V.13.	Trial No. 12-R, Induction Heating-Pressure Curing, RVA Grade, Conditions and Results	162
V.14.	Trial No. 13-R, Induction Heating-Pressure Curing, RVA Grade, Conditions and Results	163
V.15.	Induction Heating Pressure Curing Assembly Showing Position of "Heat Concentrators"	164
V.16.	Trial No. 11-R, Induction Heated Pressure Cured RVA Plug	165
V.17.	Trial No. 12-R, Induction Heated Pressure Cured RVA Plug	165
VI.1.	Extrusion with Applied Back Pressure, Back-Pressure Ram and Die Sleeve Assembly	169
VI.2.	Extrusion with Applied Back Pressure, Close-up View of Back-Pressure Ram and Die Sleeve	169
VI.3.	Auger Extruded with Expansion-Reduction-Back Pressure Assembly	170
VI.4.	Expansion-Reduction Die Used in Back-Pressure Experiments	170
VI.5.	Extrusion with 200 lbs. Back Pressure, Sawed Surface Showing Flow Line Patterns 45° to Direction of Mix Flow, 9X	172
VI.6.	Extrusion with no Back Pressure, Flow Lines Approximately Parallel to Direction of Mix Flow, 9X	172
VI.7.	Grain Orientation Resulting from Various Types of Extrusion	173
VII.1.	Graphite Whiskers from the Hot Working Process in Original Environment, 10X	175
VII.2.	Graphite Whisker from Hot Working Process, Internal Section of Single Whisker, 100X	176
VII.3.	Graphite Whiskers from Hot Working Process, Internal Section of the Same Whisker as Figure VII.2, 500X	176

LIST OF FIGURES (CONT'D.)

FIGURE		PAGE
VII. 4.	Graphite Whiskers from Hot Working Process, Showing Surface Contour and Variation in Size, 500X	177
VII. 5.	Graphite Whiskers from Hot Working Process, Showing Partial Fracture of Whisker, 500X	177
VII. 6.	1350°C Induction Heated, Coke Calcination Assembly. .	178
VII. 7.	Carbon Whiskers from Coke Calcination, 1000X . . .	179
VII. 8.	Single Carbon Whisker from Coke Calcination, 1000X .	179
VII. 9.	Carbon Whiskers from Coke Calcination, End View, 1000X	180
VII. 10.	Scaled Down 1350°C Induction Heated, Coke Calcination Assembly	181
VII. 11.	Carbon Whiskers from Coke Calcination, Grown on Coke Particle, 15X	182
VII. 12.	Carbon Whiskers from Coke Calcination, Grown on Exit End of Nitrogen Injection Tube, 2X	183
VII. 13.	Carbon Whiskers from Coke Calcination, Extracted From Area on Side Wall of Susceptor, 15X	184
VII. 14.	Carbon Whiskers from Coke Calcination, 25X	184
IX. 1.	Side View of a Segmented Nozzle after Testing Firing .	190
IX. 2.	Top View of a Segmented Nozzle After Test Firing. . .	191
IX. 3.	Tensile Fracture for TS-341 Cement on CFW Graphite, Specimen Tested at Room Temperature, Fracture Located in Joint	195
IX. 4.	Location of Tensile Fracture for TS-341 Cement on CFW Graphite, Specimen Tested at Room Temperature, Fracture Located in Stock	195
IX. 5.	Flexural Strength vs. Temperature on TS-341 and C-9 Cemented Joints, ZTA Graphite Specimens	197

LIST OF TABLES

Table		Page
1.	Heats of Reaction Estimated from DTA Peak Areas ΔH Values in Kcal/Mol	6
2.	New Absorption Bands Formed for Aromatic Hydrocarbons Dissolved in Concentrated Sulfuric Acid	15
3.	Comparison of Petroleum Coke and Graphite Properties	19
4.	Properties of Potassium-Doped L113SP Lampblack-Based Graphite	29
5.	Types of Edge Dislocations Parallel to the c-Axis in Graphite	36
6.	Schedule for Graphitization Series	48
7.	Organization of Development Program on Advanced Graphite Materials	66
I.1.	Tensile Test Results on Graphite Whiskers at Room Temperature	97
II.1.	Young's and Torsional Moduli for Grade ATJ Samples	115
II.2.	Elastic Compliance Constants for Grade ATJ Samples	117
III.1.	Effect of Pressure Calcination on VT Coke	121
III.2.	Effect of Pressure Calcination on TA Coke	122
III.3.	Effect of Pressure Calcination on DK Coke	123
III.4.	Effect of Pressure Calcination on NA Coke	124
III.5.	Effect of Pressure Calcination on AX Coke	125
III.6.	Effect of Sulfur Calcination on TA Coke.	131
III.7	Effect of Sulfur Calcination on HK Coke as Related to Initial Volatile Content and Calcining Rate	132
III.8.	Effect of Temperature on Sulfur Calcination of TA Coke	133
III.9.	Effect of Sulfur Concentration on Calcination of DK Coke	134
III.10.	Effect of Furnace Type Sulfur Calcination of DK Coke	135

LIST OF TABLES

Table		Page
IV.1.	Property Comparison of Pressure Cured Blocks, Preimpregnated AX Coke Base vs Standard AX Coke Base	145
V.1.	Induction Heating Pressure Curing, Before and After Cure Densities	166
VIII.1.	Formulation of Urethane Base Foams	185
VIII.2.	Curing Data - Urethane Foam System	186
VIII.3.	Flexural Strengths of Carbon Foam with Respect to Structure Type	187
IX.1.	Composition of TS-341 Cement	189
IX.2.	Flexural Strength vs. Temperature of TS-341 Cemented Joints, ZTA Graphite Specimens	190
IX.3.	Flexural Strengths of TS-341 Cemented Specimens, Varying Grain Size of TiB_2	192
IX.4.	Flexural Strengths of TS-341 Cement Joints on Dried and Undried CFW Graphite	192
IX.5.	Room Temperature Flexural Strengths of TS-341 Cemented Joints, With and Without Macerated Graphite Cloth Matrix, CFW Graphite Specimens	193
IX.6.	Tensile Strength vs. Temperature of Reacted TS-341 and Cured C-9 Cemented Joints, CFW Graphite Specimens	194
IX.7.	Flexural Strength vs. Temperature of TS-341 and C-9 Cemented Joints, ZTA Graphite Specimens	196
IX.8.	Composition of Modified C-9 Cement	197

1. INTRODUCTION

This Summary Technical Report is a synopsis of a three-year effort on a coordinated program of basic research and development for the advancement of graphite and graphite-base materials, including scaleup, characterization and evaluation. It is the last of a series of forty-two individual Volumes of WADD Technical Report 61-72 which constitutes the complete Technical Report on Contract No. AF 33(616)-6915. These forty-two reports along with their six Supplements listed in the Foreword cover work on individual study subjects.

The accomplishments on the overall program are outlined briefly in this Summary Technical Report which includes abstracts of the other Volumes of WADD Technical Report 61-72. The full report contains the following additional main sections:

2. SUMMARY
3. RESEARCH
4. DEVELOPMENT

APPENDICES I through IX

Section 2 is a capsule summary of the principal areas of investigation and progress.

Sections 3 and 4 contain short summaries of the individual Volumes. They also report on topics not covered by the individual Volumes of the Technical Reports. The more comprehensive topics are reported in Appendices I through IX.

The purpose of this report is to outline and emphasize the coordination of the graphite development program as it has been carried out over the past three years. This summary also provides abstracts and references so that the reader may be guided, for detailed information, to those reports within his field of interest.

Manuscript released by the authors August 1963 for publication as an ASD Technical Documentary Report.

2. SUMMARY

2.1. Research Summary

2.1.1. Summary of Raw Materials Studies

In recognition of its fundamental importance to graphite technology, research on raw materials has constituted the largest portion of the research effort. Studies of the pyrolysis of pure aromatic compounds have been exceedingly fruitful in advancing our understanding. Their use in combination with numerous techniques and skills including differential thermal analysis, absorption spectroscopy ranging between the microwave (electron spin resonance) and the ultraviolet regions of the spectrum, chromatography, and many others have outlined the principal steps through polymerization, condensation, and finally carbonization to graphite. Relations have been demonstrated between the original molecular structure and physical properties of the resultant graphite, including size, orientation, and perfection of the crystallites.

Concurrent investigations on complex mixtures of commercial interest such as tars and pitches derived from coal, residues from petroleum refining, and resins have approached the problem from the opposite viewpoint and have concentrated on the physical and chemical characterization by means of advanced techniques of both starting materials and the products of pyrolysis. Subcontract activity by Union Carbide European Research Associates has importantly supplemented our own activity.

A study of lamellar and residue compounds of carbon and graphite has shown important effects of impurities and additives, such as bromine, potassium, sulfur, iron and calcium, on the physical properties of the associated graphite.

2.1.2. Summary of Basic Research Studies

Basic studies of the elemental graphite crystal have contributed materially to our understanding of its electronic and magnetic properties and to the influence of stacking faults. Turbostraticity, present in pyrolytic graphites, produces marked effects in galvano-magnetic properties, the main characteristics of which are now understandable in terms of the quantum mechanical band theory of the graphite lattice.

Knowledge has been gained on the nature and the energetics of dislocations in graphite which is fundamental to an eventual understanding of the plastic flow properties of graphite. Studies of graphite whiskers have revealed unique stress-strain behavior and exceptionally large fracture strain.

Crystallite orientation has been measured by X-ray methods in polycrystalline graphite and considered in relation to the observed anisotropy of the diamagnetic susceptibility. High temperature X-ray studies have shown an influence of the degree of orientation and crystallinity of the polycrystalline body on the thermal expansion of the lattice cell along the c-direction.

2.1.3. Summary of Applied Research

Studies of the tensile creep at high temperatures made on a variety of grades and types of fabricated graphite have shown marked dependence of the creep rate on orientation, crystallinity, density, tensile stress, and temperature. The temperature dependence of the tensile creep rates indicates a thermally activated process with an activation energy of 124 kcal per mole, independent of the other variables. Flexural creep rates do not indicate any such invariant activation energy. Even low temperature stress-strain studies show a marked anelastic behavior.

Thermal stresses have been investigated analytically in anisotropic hollow cylinders by quasi-static thermal elasticity theory. The necessity for consideration of the anisotropic properties is clearly evident. The analysis, using typical graphite properties, has shown qualitative agreement with thermal shock behavior in rocket nozzle applications.

Measurements of the tensile strength of grade ZTA graphite at high temperatures have shown it to be dependent on grain orientation, load rate, prior degassing treatment, and on surrounding gas pressure.

Radiographic exposure techniques have been determined for attainment of high perceptibility of defects in high density graphite in the 4- to 16-inch thickness range.

The carbon arc image furnace has been used to measure the high temperature spectral emissivity and thermal conductivity of carbon and graphite materials and to study the oxidation behavior of graphite-refractory composites.

2.2. Development Summary

Studies of raw materials for graphite manufacture have included binder systems, processing of standard raw petroleum cokes and control of petroleum coke quality by the use of an experimental pilot scale delayed coker. The pilot coker studies are just beginning and represent an area for concentrated future work.

High density, recrystallized graphites, produced by a hot working process, possess properties intermediate to premium quality commercial graphites and pyrolytic graphite. These hot worked graphites have been scaled up as grades ZTA and ZTE to sizes as large as 14-inch diameter by 10-inch length and 30-inch diameter by 30-inch length, respectively.

Fabrication techniques, based on a pressure curing process and the use of a thermosetting binder system, have been developed and extended for the production of graphite bodies as large as 30-inch diameter by 40-inch length. Graphites produced by this pressure curing technique are fine-grain materials having structural integrity and strengths superior to and exhibiting less than one-third the variation in strength or bulk density of ATJ grade graphite.

The pressure curing process has also been extended to ultra fine-grain graphites in the 30-inch diameter size and to high thermal expansion graphite for use as a substrate material for oxidation resistant coatings. The latter graphite is an excellent substrate for silicon carbide coatings; because of the very similar thermal expansions of the two materials, the coated graphite can be cycled many times from room temperature to 1500°C without causing cracks in the coating. The substrate graphite has been produced in sizes up to 18-inch diameter by 18-inch length.

Fibrous forms of carbon and graphite, such as cloths and felts, have been fabricated by various methods into a unique class of bulk graphites. The unusual properties of these graphites include low density, high strength, low modulus of elasticity, low thermal conductivity, excellent thermal shock resistance and relative ease of fabrication and machining.

Composites of graphite with refractory metals and/or other additives produced by hot pressing have shown good resistance to oxidation at high temperatures.

Other miscellaneous forms of graphites and fabrication methods which have been investigated include carbon and graphite foams and whiskers, cements for use with carbon or graphite, special extrusion techniques and pyrolytic processes.

Materials testing and characterization have represented a relatively large effort under this contract. Included in this category are measurements of physical properties of graphites over a range of temperatures, photomicrographic and radiographic techniques for determination of structure and structural integrity, and environmental tests of materials in a subscale rocket motor. Supplying of property data and design information and samples for testing under conditions of actual use was handled as an applications technology function with close contact being maintained between the contracting parties and Governmental agencies and contractors.

3. RESEARCH

For the purposes of this report, the research program is discussed under the following headings: (1) raw materials studies, (2) basic studies, and (3) applied research. However, these divisions cannot always be completely unambiguous.

3.1. Study of Raw Materials for Graphite

Wide variations in the properties of fabricated graphite can be achieved through selection of the basic raw materials in combination with the methods and conditions of processing. In general, the raw materials are complex organic mixtures. A knowledge of their carbonization behavior requires an understanding of the thermal reactions of their chemical constituents.

Attention has been paid to complex mixtures of practical interest and the considerable progress outlined below has resulted from the use of advanced study techniques. However, greater advancement of our fundamental understanding has come from a study of the pyrolysis of pure organic compounds. Progress along both lines is described in the following sections.

3.1.1. Pyrolysis Studies on Pure Compounds

3.1.1.1. Thermal Reactivity of Aromatic Hydrocarbons, Substituted Aromatics, and Heterocyclic Compounds

A general survey has been made of the thermal reactivity of polynuclear aromatic hydrocarbons, substituted aromatics, and heterocyclic compounds to provide information basic to the understanding of the conversion of organic materials to carbon. Differential thermal analysis (DTA) was employed on 213 pure compounds and on 26 binary mixtures to delineate the thermal sequences during pyrolysis to 750°C. Absorption spectroscopy, electron spin resonance, chromatography, and molecular weight determinations have been used to determine the thermal mechanisms and structural changes which occur. Thermal reactivity of pure compounds has been related to molecular structure. These findings have been reported [1] in WADD Technical Report 61-72, Volume X and Supplement to Volume X.

3.1.1.2. Quantitative DTA

Most of the applications of DTA in this investigation, such as that mentioned in the preceding paragraph, have been qualitative. A limited study was made of the quantitative application of DTA for the determination of thermal quantities as outlined below.

In differential thermal analysis (DTA), the heat of a reaction is measured by the temperature difference it produces in a sample material when referred to the temperature of the reference environment.

A simplified theoretical treatment relating the DTA peak area to the heat of reaction[2], independent of most of the difficulties caused by apparatus and sample property parameters was tested in our apparatus by measuring the heats of fusion of standard pure compounds. The DTA peak area, A, was shown to be:

$$A = \int_{t_1}^{t_2} \theta \, dt = \frac{mq}{g}$$

where θ = differential temperature (T sample - T reference)
t = time
m = mass of sample
q = heat of reaction per unit mass
g = heat-transfer coefficient, an apparatus characteristic.

Using the known heats of fusion of standard compounds to calibrate our apparatus and determine the heat-transfer coefficient, the heats of reaction were calculated for a number of compounds and mixtures as listed in Table 1. The original thermograms for these systems are found in Reference 1.

Table 1. Heats of Reaction Estimated from DTA Peak Areas
ΔH Values in Kcal/Mol

Compound or Mixture	ΔH_{fusion}	$\Delta H_{reaction\ exotherm}$	$\Delta H_{reaction\ endotherm}$
Acenaphthene	5.4	---	---
Acenaphthylene	3.0	6.2	3.4
1:1 Acenaphthene-Acenaphthylene	7.8	---	1.2
Polyacenaphthylene	---	---	~ 24 (assume MW of 1000)
Decacyclene	2.8	1.5	---
Naphthoquinone	4.3	3.3	---
Bifluorylidene	3.4	3.6	---
Fluorene	4.1	---	---
Naphthacene	3.5	1.1	---
Pentacene	1.3	1.4	---
1:1 Acenaphthene-p-benzquinone	7.2	7.8	---
1:1 Anthracene-p-benzquinone	---	5.3	---
1:1 Acenaphthene-anthraquinone	---	2.8	---
1:3 Acenaphthene-acenaphthylene	---	5.1	2.4
di-p-Xylene	---	6.2	---
1:1-p-Benzquinone-fluorene	---	6.4	---
1:1-p-Benzquinone-naphthalene	4.7	---	---

These values are all based on the original weight of sample. No corrections were made for loss of sample during the DTA run. With thermogravimetric (TGA) results to supplement these data, this method of determining heats of reaction should be useful. Without the TGA data, only the heats of fusion have any validity and these are doubtful if sublimation occurs appreciably.

3.1.1.3. Electron Spin Resonance Studies

3.1.1.3.1. Electron Spin Resonance Studies of Thermal Decomposition and Carbonization Reactions

The first phase of an electron spin resonance (ESR) study of thermal decomposition and carbonization reactions of organic compounds has been completed. The goal of this investigation is to elucidate the mechanisms of the initial chemical reactions of carbonization. An understanding of these reactions will clarify the relations between the microscopic structure of carbons and the nature of the starting material.

The most important single result of this study has been the observation that thermal decomposition, including carbonization reactions, can be carried out in inert liquid solvents and the ESR observed simultaneously in situ. The use of such liquid systems offers the following advantages.

a. The free radicals which are formed in the liquid phase are free to tumble rapidly. This rapid molecular motion effectively averages out anisotropic nuclear hyperfine interactions and permits the observation of a well-resolved ESR spectrum. Such a spectrum is required for the identification of the radicals.

b. Since the solution of a carbonizable material in an inert solvent constitutes a homogeneous system, the different paths and rates of the various reactions can be altered and studied in a controlled manner by varying concentration, temperature and other experimental parameters.

c. The in situ ESR experiment, which is done in a specially designed heater cavity, has the advantage of enabling the course of a free radical reaction to be followed as it occurs.

The work has included the following topics which are summarized briefly in the discussion below and discussed in greater detail in WADD Technical Report 61-72, Volume XVI[3].

a. General ESR Survey of Pyrolysis.

A survey was made of the ESR of ~ 20 carbonizable organic compounds during the early stages of pyrolysis. Included were a number of aromatic hydrocarbons, substituted aromatics, several polymers, and one aromatic hydrocarbon-quinone mixture[3]. The observation of ESR during the initial stages of pyrolysis for every carbonizable compound which we have examined to date demonstrates the general importance of radical intermediates in the carbonization process.

b. Detailed ESR Investigations of the Model Aromatic Hydrocarbons Acenaphthylene, 9,9'-Bifluorenyl and 9,9'-Bifluorylidene.

Resolved hyperfine structures were obtained for all three compounds during pyrolysis in the inert solvent m-quinquephenyl. The results have been interpreted in terms of the initial thermal reactions and the subsequent graphitization behavior[3].

c. ESR Studies of the Thermal Decomposition of Several Aromatic Diazo Compounds.

Diazo decompositions are among the simplest examples of organic thermal decomposition reactions. Resolved ESR spectra have been obtained[3] during the decomposition of diphenyl diazomethane, diazobenzil, and diazofluorene. The radical intermediates observed in these systems are thought to be similar to those observed in the more complex carbonization reactions.

3.1.1.3.2. ESR at the Coke Stage

In addition to the ESR studies of the initial studies of pyrolysis, some investigations of the more advanced "coke" stage were carried out.

By the time carbonization has proceeded to the higher temperature coke stage, the carbonaceous solid is so complex that identification of the large number of paramagnetic species on a molecular scale is impossible. However, information concerning the general character of the unpaired electrons can in some cases be determined by ESR temperature dependence and line shape measurements. Measurements were made on both sucrose and acenaphthylene cokes.

Samples of sucrose chars were heated in a vacuum of better than 10^{-5} mm Hg to various temperatures between 600°C and 800°C. The ESR signals for charred sucrose were extremely sharp and intense, but, within experimental error, followed Curie's law between 100°K and 300°K. The sharpest line seen to date (~ 0.3 gauss) was observed in the 650°C heat-treated coke. The 800°C heat-treated coke exhibited a somewhat asymmetric line at 120°K, presumably due to g-factor anisotropy. The line widths for all these cokes either remained constant or decreased slightly with decreasing measuring temperature.

The most striking difference between the acenaphthylene cokes and sucrose cokes was that electrical conductivity, as evidenced by a skin-effect line shape, was observed for acenaphthylene heat-treated at only 600°C, whereas it was necessary to heat-treat sucrose to at least 800°C to obtain similar conductivity effects. This behavior is, of course, consistent with the idea that acenaphthylene cokes are much more "graphitic". This idea is also consistent with the observation of anisotropy broadening for acenaphthylene but not for sucrose. If one invokes "crystallite averaging" arguments, similar to those used by Singer and Wagoner[4] to explain the sharp lines in small crystallite-size polycrystalline graphites, the differences in ESR

properties of these two charred materials can be satisfactorily explained. This explanation also suggests that the observed spins may take part in the conduction process.

The asymmetries caused by anisotropy effects made quantitative determination of ESR susceptibilities difficult. However, the asymmetric line-shape was found to be very closely temperature independent so that relative integrated absorptions could still be determined from the width and height of the lines. The most detailed temperature dependence measurements were made on an acenaphthylene coke heat-treated at 750°C. The spin concentration increased by about a factor of 3 between 100°K and 500°K, implying a thermally populated paramagnetic state with an excitation energy of about 0.01 ev. A similar temperature dependence was observed for a 600°C heat-treated acenaphthylene coke.

These temperature dependence measurements prove that the ESR in these and presumably many other charred materials at the coke stage is not due to ordinary free radicals which follow Curie's law. This dependence is in contrast to the measurements for the lower temperature (400°C) acenaphthylene cokes and the sucrose cokes noted above, both of which did obey Curie's law. Thus, the identification of the paramagnetic species in cokes is still a very open question. In addition to temperature dependence measurements, a more careful study of the anisotropic ESR properties of oriented cokes might be helpful in elucidating the nature of the spins.

3.1.1.4. Carbonization Studies

3.1.1.4.1. Carbonization of Model Aromatic Hydrocarbons

The dependence of the graphitization on aromatic structure has been demonstrated by an X-ray comparison of synthetic graphites prepared from a wide variety of aromatic compounds.

Detailed investigations, employing a variety of chemical and physical techniques, have been conducted on the carbonization of two model hydrocarbons, acenaphthylene and 9, 9'-bifluorenyl. These compounds produce graphitic products of widely different types and this graphitization behavior has been discussed in terms of chemical mechanisms.

This work is presented in detail in WADD Technical Report 61-72, Volume XXVII[5].

3.1.1.4.2. Effects of Quinones on the Carbonization of Aromatics

Quinones are known to interact with aromatic hydrocarbons in at least three ways, through charge transfer complexing, dehydrogenation, and addition copolymerization. The effects of these interactions on carbonization behavior have been demonstrated for a variety of quinone-aromatic hydrocarbon mixtures. Studies have also been conducted on the effects of quinone additives on the carbonization of coal tar pitches. In nearly every instance

the quinone is seen to have a beneficial effect on increasing the coking value. The magnitude of the effects can be related to some extent to chemical reactivity parameters. These results have also been reported in more complete detail in WADD Technical Report 61-72, Volume XXVII[5].

3.1.1.5. Application of Special Analytical Techniques

In addition to the direct studies of pyrolysis of pure compounds already described, research was conducted for the purpose of developing special analytical techniques for studying carbonization. These techniques were directed specifically to the characterization of the aromatic products important in carbonization.

3.1.1.5.1. Polarographic Reduction of Polynuclear Aromatics

Half-wave reduction potentials ($E^1/_2$) for aromatic hydrocarbons have been recognized as generally useful structural parameters. The polarographic technique has therefore been investigated in an attempt to utilize $E^1/_2$ values to characterize the aromatic materials important in carbonization.

$E^1/_2$ values have been obtained for a number of polynuclear aromatic hydrocarbons and compared with other structural and reactivity parameters. Substituents on the aromatic ring have been shown to influence $E^1/_2$ values through electronic interaction. Half-wave potentials have also been obtained for pyrolytic aromatic residues derived from acenaphthylene. These results are discussed in detail in WADD Technical Report 61-72, Volume XXVIII[6].

3.1.1.5.2. High Temperature Ultraviolet Spectroscopy

In order to study thermal reactions chemically in situ, as well as to detect reversible thermal interactions, experiments were performed on measurements of ultraviolet spectra at high temperatures. A specially designed high temperature cell compartment was employed in conjunction with a Cary Model 14 spectrophotometer. Heating was accomplished by means of a platinum wound resistance wire and the temperature monitored with a thermocouple. Samples were deposited as thin films between two quartz plates which were inserted into the cell compartment. Spectra were obtained for several pure aromatic hydrocarbons and for some aromatic mixtures at their melting points, and in some cases at higher temperatures.

High temperature spectra were obtained for the aromatic compounds: (1) acenaphthene, (2) acenaphthylene, (3) anthracene, (4) p-benzoquinone, and (5) 9, 9'-dibromofluorene. The spectra for acenaphthene, acenaphthylene and anthracene were identical to those obtained in solution at room temperature except for slight wavelength shifts. p-Benzoquinone and 9, 9'-dibromofluorene showed the reversible formation of broad bands in the visible absorption region. The behavior of the latter material is illustrated in Figure 1. Volatility problems prevented spectral measurement for the compounds chloranil and benz(a)anthracene.

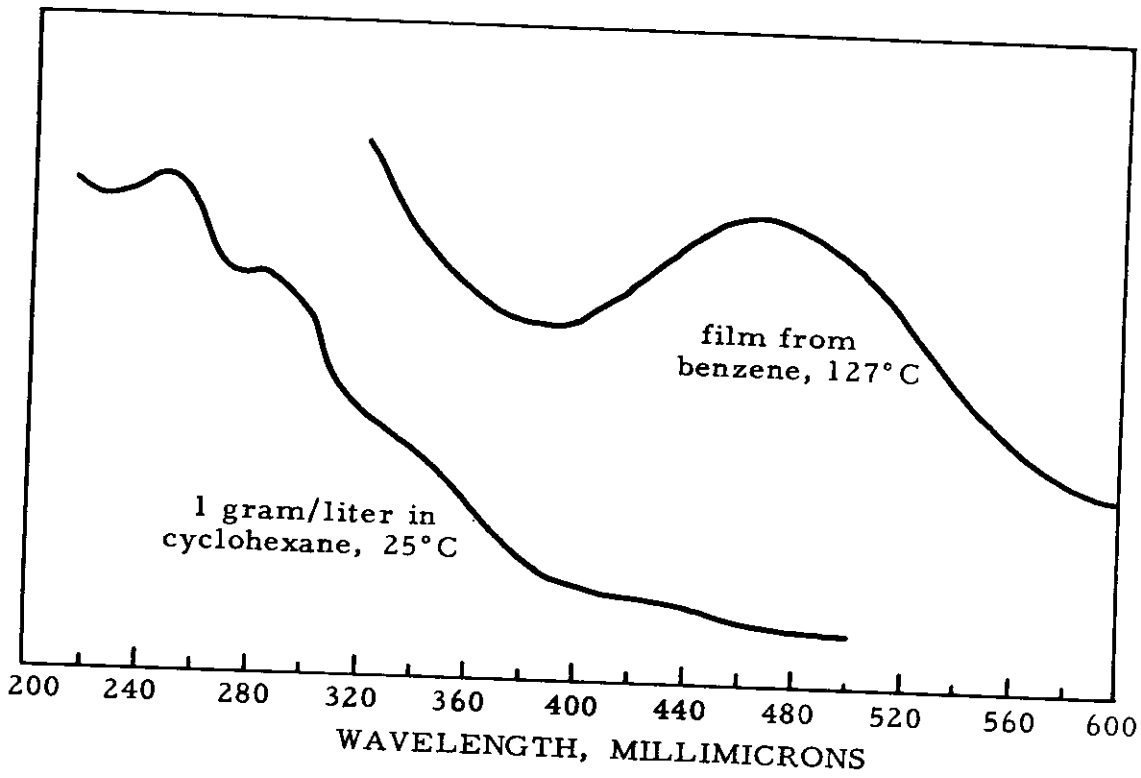

N-3529

Figure 1. Spectra of 9,9'-Dibromofluorene in Solution and Heat-Treated

This technique has also been employed to study the pyrolytic transformations of several pure compounds. Acenaphthylene, 9,9'-bifluorenyl and 9-diazofluorene have been examined in this manner. Shown in Figure 2 is a series of high temperature curves for the thermally reacting aromatic hydrocarbon acenaphthylene in the inert diluent m-quinquephenyl. The spectral transformations have already been interpreted chemically[3].

Reversible thermal interactions have also been demonstrated for some aromatic hydrocarbon-quinone mixtures. At melting temperatures, acenaphthene with both p-benzoquinone and chloranil gave rise to major absorption bands in the visible region.

Anthracene, when treated with these quinones, showed a pronounced change in its ultraviolet absorption spectrum. No new visible bands were detected however. The same behavior was observed for the aromatic hydrocarbons perylene and pyrene. Examples of these effects are shown in Figure 3.

No thermal interactions were observed for the following mixtures: benz(a)anthracene-chloranil, naphthacene-chloranil and benz(a)anthracene-p-benzoquinone.

3.1.1.5.3. Quantitative Determination of Aromatic and Aliphatic Hydrogen by Infrared Spectroscopy

Quantitative methods for determining aromatic to aliphatic hydrogen ratios by the use of infrared spectroscopy have been explored. Only a poor relationship was obtained employing the intensities of the fundamental aromatic and aliphatic C-H stretching vibrations in the 3.5 μ region as a criterion of aromatic and aliphatic content. Measurements on a wide variety of model compounds showed the intensity of these bands to have a strong dependence on molecular structure.

A precise relationship has been derived employing the near infrared (1.1 to 1.4 μ) second overtone aromatic and aliphatic C-H stretching frequencies. Application of this method to substituted aromatic hydrocarbons of varying structure led to the following quantitative expression:

$$n\text{-}H_{Ar}/n\text{-}H_{Al} = 1.097\ A\text{-}H_{Ar}/A\text{-}H_{Al}$$

$n\text{-}H_{Ar}/n\text{-}H_{Al}$ = Aromatic/Aliphatic Hydrogen Ratio

$A\text{-}H_{Ar}/A\text{-}H_{Al}$ = Ratio of Integrated Absorptions of the Respective IR Aromatic and Aliphatic C-H Bands.

3.1.1.5.4. Ultraviolet and Visible Spectroscopy of Aromatics in Sulfuric Acid

Polynuclear aromatic hydrocarbons are known to undergo reversible protonation and oxidation in concentrated sulfuric acid. This process leads

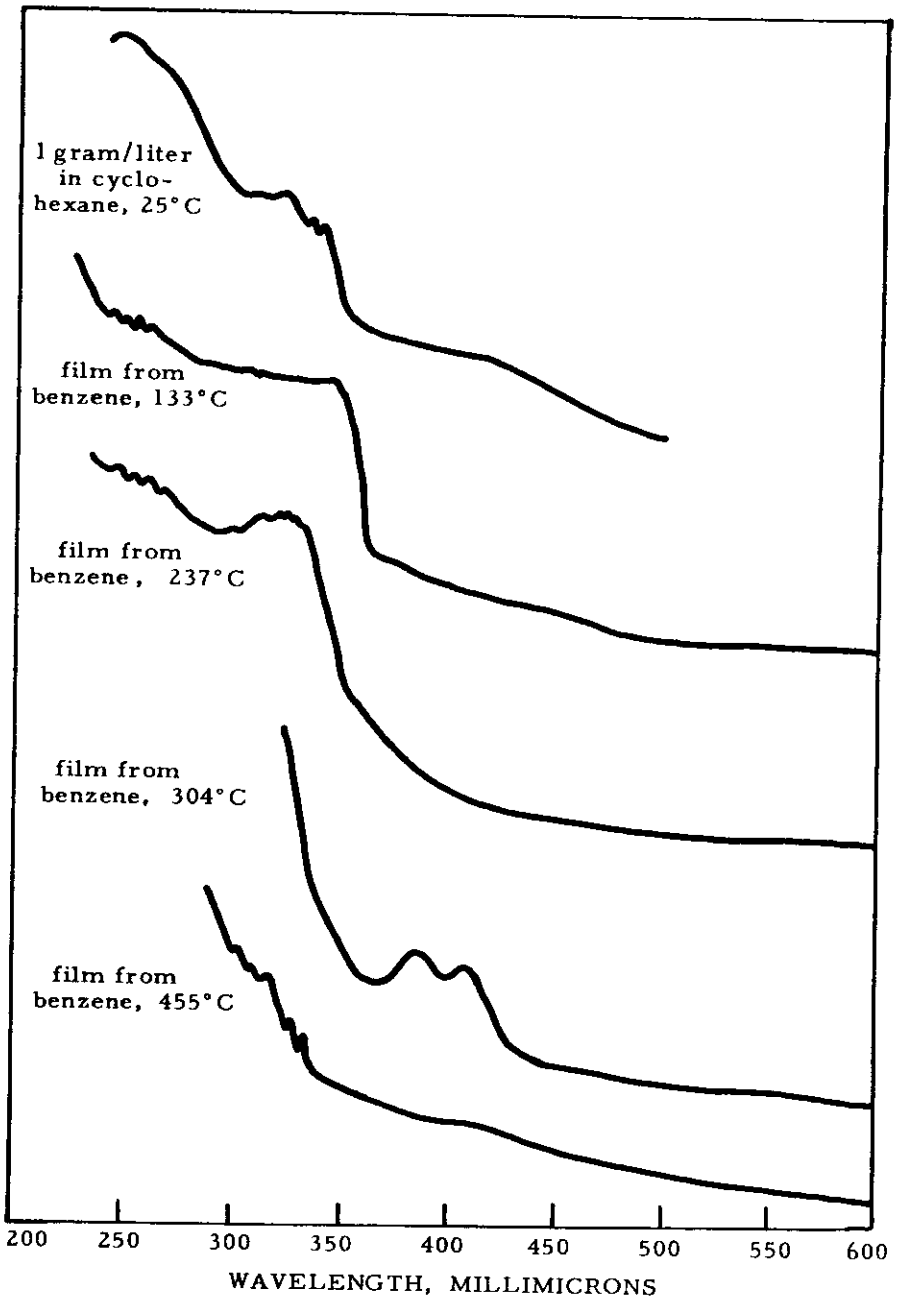

N-3587

Figure 2. Spectra of 10:1 m-Quinquephenyl:Acenaphthylene During Heating

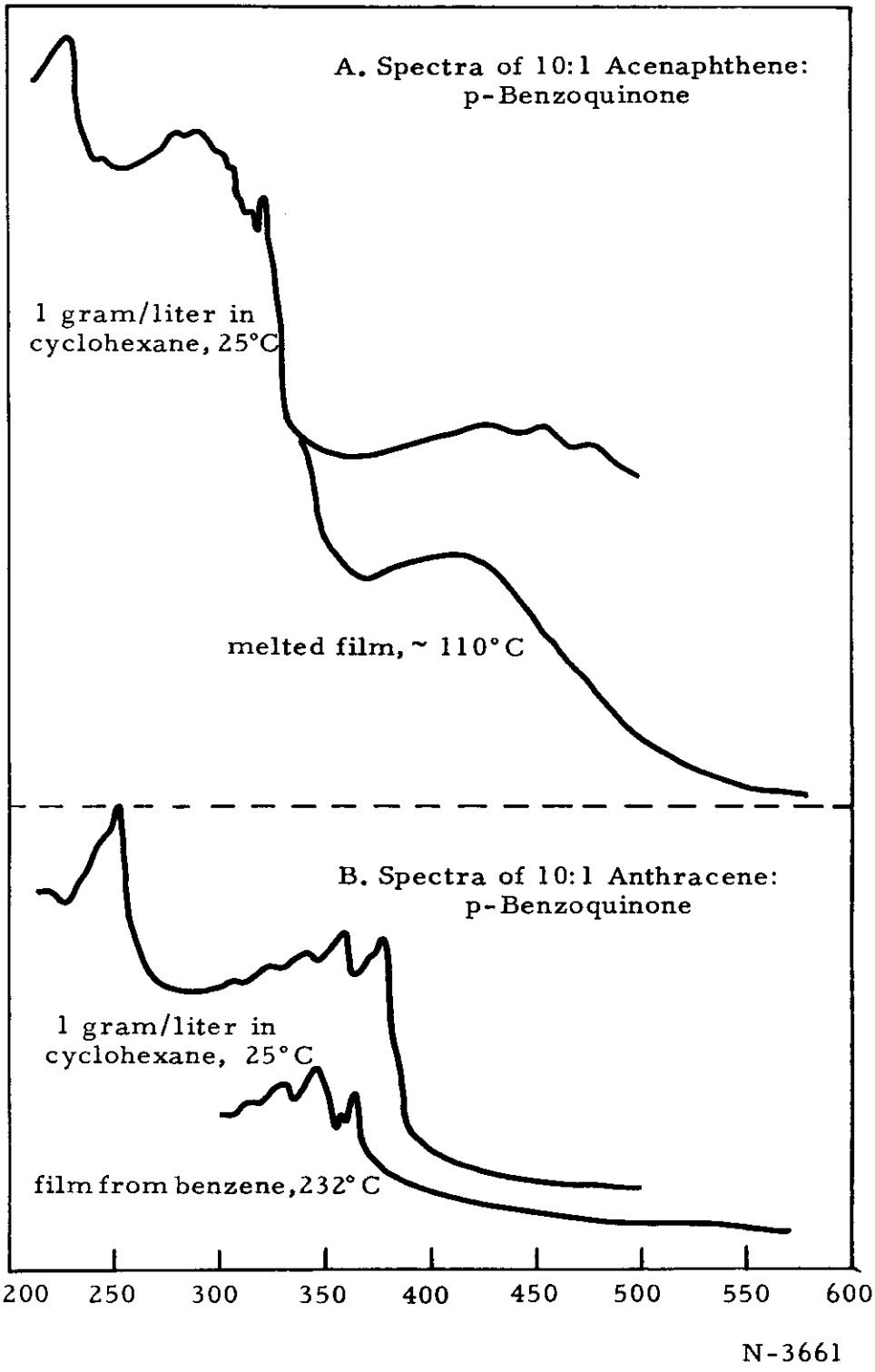

Figure 3. Absorption Spectra of Aromatic Hydrocarbon-Quinone Mixtures

$$ArH \overset{H^+}{\rightleftharpoons} ArH_2^{\oplus} \overset{-H\cdot}{\rightleftharpoons} ArH\cdot^{\oplus}$$

(I) (II)

to the formation of protonated ions (I) and radical ions (II), both of which exhibit significant absorptions in the visible spectral region. These absorptions are dependent on aromatic structure. In order to investigate the application of this technique for studying and characterizing aromatic pyrolysis products, investigations have been initiated on the behavior of some pure aromatic hydrocarbons in sulfuric acid.

Summarized in Table 2 are the initial results for 8 aromatic hydrocarbons. The wavelengths of the new visible absorption bands formed are listed in millimicrons. For a number of compounds the intensity and nature of specific bands vary with time due to the change in relative concentrations of (I) and (II). These data are also listed in Table 2.

Table 2. New Absorption Bands Formed for Aromatic Hydrocarbons Dissolved in Concentrated Sulfuric Acid

Compound	Time	Wavelength, mμ *
Acenaphthylene	3 hours	625s
Anthracene	0 hours	417s, 560w, 660w, 711s
9,10-Dibenzylanthracene	0 hours	442s, 535w, 627w
	3 hours	423w, 625w, 713s
9,10-Di(α -naphthyl)anthracene	3 hours	420w, 545w, 597w, 658w, 704w
9,10-Diphenylanthracene	0 hours	410s, 610w
	30 hours	430w, 530w, 588w, 637w, 743w
Naphthacene	0 hours	458s, 600s, 740s, 851s, 929w, 985w
2-Phenylanthracene	0 hours	505s, 631w, 685s, 752s, 870w
	3-1/2 hours	438w, 558s, 750w, 860w
9-Phenylanthracene	0 hours	417s, 540w, 583w, 652w, 707w
	3-1/2 hours	707w

* w = weak; s = strong

3.1.1.5.5. High Resolution Nuclear Magnetic Resonance

Initial experiments with high resolution proton magnetic resonance (NMR) have demonstrated the utility of this spectroscopic technique for studying the hydrogen distribution in pyrolytic residues. NMR is therefore believed to offer a powerful auxiliary spectroscopic technique for carbonization studies.

3.1.2. Pyrolysis Studies on Tars, Pitches, Resins, and Cokes

3.1.2.1. Characterization of Binders Used in the Fabrication of Graphite Bodies

Studies have been carried out under Subcontract by Union Carbide European Research Associates (ERA) in Brussels, Belgium, on coal tars, pitches, and other pyrolysis products. A series of chemical and physical methods, previously developed for use in the study of the constitution of coals, has been applied to the definition of structural parameters for thirteen tar and pitch samples which have a wide range of properties and which are of interest in the fabrication of graphite bodies.

Information obtained on the molecular size and composition indicates the presence of polycyclic compounds with a high degree of aromaticity. Evidence also points to the importance of large aromatic clusters.

Additional work has been concentrated on a selected sample of 30-medium pitch. The investigations have been extensively concerned with the separation of the pitch into fractions with respect to molecular weight. Furthermore, a structural analysis has been undertaken on several of the fractions obtained. Finally, the plastic behavior of some of the fractions has been determined. All of these results have been reported in detail in WADD Technical Report 61-72, Volume XI and Supplement to Volume XI[7].

3.1.2.2. Studies of Binder Reactions and Binder-Filler Interactions by Armour Research Foundation (ARF)

Studies were carried out under Subcontract by Armour Research Foundation to complement the other efforts of this Contract program. Objectives of the work at ARF were: (1) to study specific binder systems for carbon and graphite articles in relation to the filler properties, and (2) to understand the chemistry of the furfuryl alcohol polymer system. The results have been described in WADD Technical Report 61-72, Volumes XV[8] and XL[9].

The objective of the binder-filler systems investigations was to study the rheological properties and the pyrolysis mechanism for two binder systems as affected by filler materials with different chemical activities. The two binder systems were chosen because of their promising characteristics as binders suggested by earlier experience and because of their lending themselves to accurate characterization and future duplication. One binder was the alumina-condensed furfuryl alcohol polymer which has been developed at Armour Research Foundation and which thermosets to cured resin in yields of over 99 per cent and pyrolyzes to coke in yields of nearly 60 per cent. The other binder system was the acenaphthylene pitch developed by National Carbon Company and described in WADD Technical Report 61-72, Volume XXXII[10].

Filler materials chosen for study were: carbon and graphite particles, and flour derived from petroleum coke, silicon carbide, and aluminum oxide particles and flour.

Equipment and methods used in preparing resins of different viscosities have been briefly discussed; the equipment used in making the necessary analyses [8] was also described.

In the discussion of results [8,9], data obtained from fractional distillation, gas chromatography, differential thermal analysis, thermogravimetric analysis, X-ray studies, shrinkage measurements, and dynamic elastic modulus measurements have been presented, interpreted and correlated. Also included is information on the use of low viscosity resin as an impregnant, resin modifications, cured resin yield, and microstructures.

Pyrolysis of the two binder systems showed marked differences in the number and distribution in the gaseous decomposition products. The coke fillers appeared to have little effect on the pyrolysis of either the alumina-condensed resin or the acenaphthylene pitch. The alumina particles showed some catalytic effect on the pyrolysis reactions, especially for the resin binder.

3.1.2.3. Thermogravimetric Analysis (TGA)

Assessing thermal stability has long been a matter of interest in the preparation and utilization of materials. In the carbon industry, the determination of coking value, i.e., per cent carbon residue after heating a material to a specified temperature, has always been an important test of raw materials. The thermogravimetric analysis technique (TGA) which produces a continuous record of sample weight change during a heating cycle can be used to gain an insight into the thermal processes involved.

Because evidence of sample changes is available only as weight change data in TGA, the method is inherently limited to decompositions which are accompanied by volatilization. This limitation, however, is of little importance in the case of carbonaceous materials. TGA is not generally suited to measuring thermal stability in reactive atmospheres since weight increases can occur which complicate the weight loss data. All of our work to date has been conducted in a dry argon atmosphere flowing through the reaction tube. There are several potential sources of variation in TGA. Experimental details such as size and fineness of the sample material, the tightness of packing in the crucible, the size and shape of the sample crucible, the type of atmospheric gas and its flow rate, the rate of heating and condensation of sample volatiles on sensitive parts of the balance can cause large differences between repeat data records. Most of these variables can be controlled so that the corresponding errors are not significant; however, their effects must be recognized. Since we are interested in correlating our TGA data with our DTA results, comparable experimental conditions have been arbitrarily chosen for both in these initial trials.

3.1.2.3.1. TGA of Coal Tar Pitches

The TGA curves obtained on a sample of 15 vacuum pitch and a mixture of 95 wt. per cent 15 vacuum pitch and 5 wt. per cent 1, 4-naphthoquinone are shown in Figure 4. The heating rates were about 8°C per minute and dry

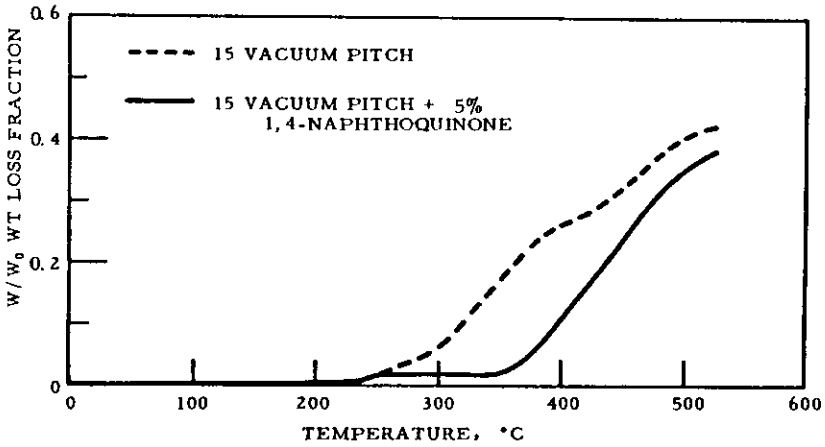

Figure 4. Thermogravimetric Analysis of Coal Tar Pitch

argon flowing at about 50 cc per minute was used to maintain an inert atmosphere. The samples in all cases described in this report were approximately 1 gram of finely ground powder packed into a stainless steel pan one inch in diameter by 3/16 inch deep. Under these conditions, it is seen that 15 vacuum pitch begins to volatilize around 220°C. The volatilization rate increases at 300°C, decreases between 390°C and 420°C, and then increases again to about 500°C. Above 500°C the rate of volatilization is low since this pitch gives about 50 per cent carbon yield at 1000°C using a fast heating rate. The addition of 1,4-naphthoquinone changes the volatilization curve considerably. After the initial small weight loss beginning at 225°C, the weight of the mixture remains constant to 345°C. This temperature region corresponds to the exothermic reaction region found in the DTA thermogram of 1,4-naphthoquinone. Above 350°C, the mixture begins to volatilize at a fairly constant rate to about 500°C at which point the rate decreases. On separate coking tests, the coking value of the mixture was approximately the same as that of the pitch alone. Considerably larger fractions of the naphthoquinone have been found necessary to produce an appreciable enhancement of coking value [10].

In Figure 5 will be found a series of TGA thermograms of 110°C melting 30 medium pitch. These curves illustrate the effects of different heating rates on the thermogram obtained. It is evident that the shape of the curve is retained but the relative volatilization rates are a function of the heating rate. Of particular interest is the reduced volatilization rate obtained in the temperature interval between 375° and 475°C. All of the curves approach a common coking value above 600°C.

3.1.2.4. Atomic C/H Ratios and Carbonization

Chemical studies on the carbonization of model compounds have suggested that materials which graphitize well also dehydrogenate at faster rates than

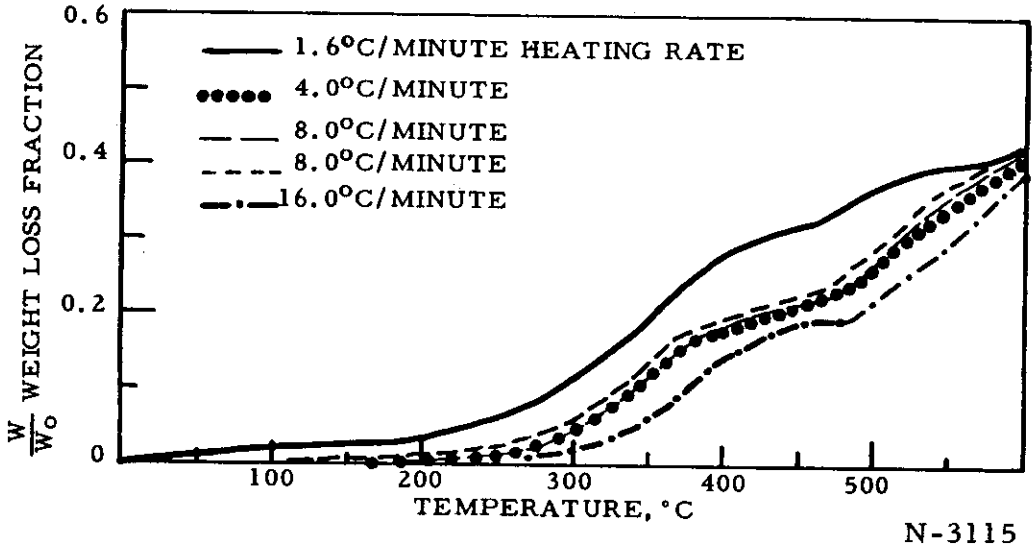

Figure 5. Thermogravimetric Analysis of Coal Tar Pitch vs. Heating Rate, 110°C M.P. 30 Medium Pitch

poorly graphitizing materials. Atomic C/H ratios of cokes heat-treated to comparable temperatures could therefore be related to coke structure.

As a simple test of this hypothesis, two commercial raw cokes of different quality have been heat-treated to 600°C to assure a comparable thermal history and their carbon-hydrogen analyses were then obtained. The results are summarized in Table 3 along with values of the thermal expansion coefficient for graphitized rods fabricated from each coke.

Table 3. Comparison of Petroleum Coke and Graphite Properties

Coke	Atomic C/H Ratio (600°C)	Coefficient of Thermal Expansion, * 10^{-7}/°C
(1) AX Coke	2.26	4.5
(2) DK Coke	1.91	15.0

* Average from room temperature to 100°C.

The coke which has the lower thermal expansion is seen to exhibit a substantially higher atomic C/H ratio at 600°C. These results, although far from conclusive, are in agreement with previous observations.

3.1.3. Study of Lamellar Compounds of Carbon and Graphite

A study has been made of lamellar compounds of graphite. Previous work in our laboratory as well as elsewhere has shown that some elements (e.g., K, Rb, Cs, Br) and numerous inorganic compounds (e.g., ICl, $FeCl_3$) can be intercalated between the graphite layer planes. The published studies on these compounds have been recently reviewed by Hennig [11] and Rudorff [12]. Although the bulk of the intercalated material can usually be removed with ease by reversing the procedure of formation and/or leaching with suitable solvents, a small quantity is often retained tenaciously (residue compounds) and profoundly affects the physical properties of the graphite. Some of these residue compounds are stable even at 2000°C.

From previous work in our laboratory it appeared possible that some of the impurities normally found in petroleum coke (e.g., S, Ca, Fe, V, Na) form similar residue compounds during graphitization. Such residue compounds might be related to some of the physical changes observed during the fabrication of graphite bodies formed from petroleum coke. A so-called "puffing" phenomenon, resulting in a volume expansion during baking in the temperature range 1500 - 2000°C, has been connected with the evolution of sulfurous complexes present in the coke [13]. The retention -- release behavior of sulfur from chars has been shown [14] to be affected by the presence of some ash materials, such as iron, but not by others, such as silica. Work was therefore undertaken to study preparation and properties of lamellar and residue compounds and the effects of their presence on the physical properties of the graphite.

3.1.3.1. Lamellar Compounds in Nongraphitized Petroleum Coke

Extensive analogies between sulfur-containing petroleum cokes and carbon-bromine lamellar residue compounds were found. For both materials, the irreversible volume expansion due to thermal expulsion of bromine or sulfur was found to be a function of coke crystallinity and could be prevented or modified by addition of iron or calcium. It was therefore concluded that sulfur in calcined petroleum coke is present as a lamellar residue compound. This fact was confirmed by the results of oxidation studies on sulfur-containing cokes, studies which also indicated that the carbon-sulfur lamellar residue compounds are formed by coking sulfur-containing carbonaceous material to temperatures in the range 1000° to 1200°C. Direct intercalation of sulfur into graphite or calcined petroleum coke has not been found possible. Iron or calcium react with sulfur-containing coke to form very stable carbon-sulfur-iron (or calcium) complexes, which were shown to be ternary lamellar residue compounds. In a similar reaction with bromine residue compounds, ternary carbon-bromine-iron (or calcium) compounds are formed. These ternary lamellar residue compounds are stable to temperatures near 2000°C and cannot be decomposed by boiling with concentrated hydrochloric acid. Hall coefficient and resistance measurements showed that the metal (iron or calcium) in these compounds is not ionized and functions only as spacer. WADD Technical Report 61-72, Volume XXV elaborates [15] these findings.

3.2. Basic Studies of Graphite

This category covers fundamental investigations of the graphite crystal, a complete knowledge of which is necessary for an ultimate understanding of the properties of polycrystalline graphite bodies. All of the properties of the graphite single crystal reflect strongly its anisotropic character, traceable to the structure. Properties which are considered involve both so-called electronic phenomena related to the charge carriers in the lattice and also mechanical properties involving interatomic interactions.

3.2.1. Electronic Properties

Studies of electron spin resonance, magnetic susceptibility and galvanomagnetic properties have been undertaken on both single crystal and polycrystalline graphite. Such studies are important both because of their intrinsic scientific interest and because a detailed knowledge of the electronic properties will ultimately be a most useful tool in scientifically characterizing the structure of polycrystalline graphite. The work reported here has played a major role in elucidating the electronic band structure of graphite and in determining the mechanism of the electronic processes. In addition, of all the physical properties of polycrystalline graphite, the electron spin resonance and the magnetic susceptibility have the simplest and most direct interpretation in terms of the single crystal values; hence these properties provide a logical starting point for obtaining a detailed understanding of artificial graphite.

3.2.1.1. Electron Spin Resonance of Graphite

3.2.1.1.1. Introduction

Prior to the start of this contract, experiments were carried out at this laboratory to determine the nature of the unpaired spins which give rise to the electron spin resonance in graphite. Investigation of the resonance in pure, relatively perfect single crystals of graphite [16] showed that the unpaired spins were those of the mobile charge carriers and that both electrons and holes in graphite contribute to a single resonance line. Dyson's theory of the line shape of a conduction electron spin resonance was found to describe the resonance line shape, and the band theoretical results of McClure accounted quite well for the resonant intensity. The g-shift of the single crystal resonance was found to be remarkably large for a material with the small spin-orbit coupling of carbon. Both the large magnitude and the dependence on temperature have been shown to be due to the presence of degenerate energy bands. The agreement between theory and experiment for the electron spin resonance of pure single crystals of graphite is reasonably satisfactory.

The work on pure single crystals has been extended to boron-doped single crystals [16] Boron goes into the graphite lattice substitutionally and, being trivalent, acts as an acceptor. Galvano-magnetic measurements, reported in Section 3.2.1.4.1., verify the acceptor action of boron and there is good qualitative agreement between theory and experiment. McClure and Yafet [17] have given the theory of the g-shift for both pure and doped graphite single

crystals. For the g-shift of doped crystals, since there is serious disagreement between theory and experiment, this work must be regarded as incomplete.

Electron spin resonance studies on single-crystal and polycrystalline, fabricated graphite, performed under this Contract, are reported in the following section. Additional spin resonance studies on pyrolytic graphite, together with susceptibility and galvano-magnetic work, are reported as a unit in Section 3.2.1.3. Similar studies on doped graphites are collected together in Section 3.2.1.4.

3.2.1.1.2. Results for Single-Crystal and Polycrystalline Graphite

The electron spin resonance work on single-crystal and polycrystalline graphite has been reported in detail in WADD Technical Report 61-72, Volume VIII[18] and will be reported only briefly here. As mentioned above, the spin resonance in perfect single crystals is due to charge carriers. It had been suggested[19] that in polycrystalline material the spin resonance is due to "dangling bonds" or "claw dislocations". The present work has shown that the resonance is due,rather, to charge carriers. This conclusion was established by comparison of the temperature dependence of the g-shift and spin susceptibility of polycrystalline graphite with that of single crystals. The intensity of the spin susceptibility is also in excellent agreement with McClure's theoretical predictions for charge carriers, and the temperature dependence of the g-shift is in satisfactory agreement with McClure's theoretical predictions. However, the temperature dependence of the line width is not yet understood.

Investigation of the effect of impurities on the electron spin resonance in graphite has indicated that two types of impurities can affect the resonance. Those impurities which become ionized and shift the Fermi level are discussed in Section 3.2.1.4. Large un-ionized atoms such as Si and Ge do not shift the Fermi level. They do, however, act as efficient scattering centers which shorten the spin-lattice relaxation time.

The proper interpretation of the spin resonance line shape in polycrystalline material depends on correctly accounting for the motional averaging of the charge carriers. Motional averaging effects have been studied in single crystals and in very fine-grained polycrystalline (lampblack) graphite, where the results are particularly simple.

Experimental complications incurred in measuring the spin resonance in polycrystalline conductive substances were discussed. These complications include the effects of skin depth and microwave heating and the dependence of line shape on crystallite size and sample purity.

3.2.1.2. Diamagnetic Susceptibility of Graphite

The following discussion summarizes an extensive series of studies which are fully reported in WADD Technical Report 61-72, Volume XXXIX[20].

The magnetic susceptibility is directly related to electronic properties of graphite common to both the single-crystal and polycrystalline forms, independent of a particular electronic scattering mechanism. The Faraday method of measuring susceptibility is the most suitable one because it measures the entire susceptibility throughout a sample, can be used to measure three orthogonal directions for the trace, and can account for ferromagnetic impurities. An apparatus employing this technique was constructed using specially shaped pole pieces to produce a constant H dH/dz region in which the sample is placed. A quartz microbalance having a "least count" under operating conditions of 0.5 μg was used to detect the small forces involved giving an overall accuracy for the susceptibility measurement of ± 1 per cent. It was operated in the magnetic field range from 10 to 22 kilogauss to allow corrections to be made for ferromagnetic impurities by the Honda-Owen method. A cryostat was incorporated in the apparatus enabling measurements to be made from 83°K to 660°K, although this feature has been perfected so recently that only room temperature results are reported here. Different representative types of graphite have been measured including single crystals, both natural and synthetic, several types of pyrolytic, and grades ZTA, AGKSP, CEP, ATJ and L113SP. The single crystals were in the form of small platelets 1 to 3 mm in diameter by 0.1 to 0.3 mm thick and the polycrystalline samples were cut into cubes 0.050 inch on a side to facilitate measurements in three perpendicular directions for trace values. Special suspensions were designed to restrict the sample from rotating in the magnetic field without contributing unduly to the measured value itself, in order to meet the requirements of the small size and high anisotropy of the samples. For more accurate measurements of $\chi_\perp$ on single crystals, a flexible suspension of fine Teflon monofilaments was devised to allow the crystal to orient itself with a minimal contribution from the suspension.

A careful study has been made of the anisotropy of the various forms of graphite by a direct observation of the orientation dependence. For the highly anisotropic single crystals, the component $\chi_\parallel$ parallel to the hexagonal axis averages $-21.8^3 \times 10^{-6}$ emu/g and is due almost entirely to the conduction electron contribution. The isotropic component $\chi_\perp$ in the basal plane, due to the ionic core electrons, was found to have an average value of -0.46×10^{-6} emu/g. For polycrystalline materials the anisotropy is much less. For example, the values of $\chi_\parallel / \chi_\perp$ range from 47 to 69 for single crystals and from 9 to 22 for pyrolytic graphites and are 2.1 for grade ZTA, 1.9 for grade AGKSP, 1.3 for grade ATJ, 1.02 for grade L113SP, and 1.01 for grade CEP graphite. It has been found for the first time by direct experimental observation that the orientation dependence of the susceptibility of both single crystals and polycrystalline graphites exactly obeys the theoretical cosine-squared relation. The magnitude of the angular variation of the susceptibility for polycrystalline materials measures the degree of preferred orientation of the crystallites in these materials. The crystallite orientation distribution has also been determined by X-ray measurements, as reported in Section 3.2.2.3.2. A comparison of the magnetic susceptibility and X-ray results is made in Section 3.2.2.3.3.

The susceptibility trace (sum of three perpendicular components) is invariant to a rotation of the measurement axes and, hence, is the same for a pure material in both the single crystal and polycrystalline forms. The susceptibility trace for single crystals was found to have the value -22.8 x 10^{-6} emu/g. The range of trace values measured on polycrystalline graphites runs from -21.9 x 10^{-6} emu/g for heat-treated pyrolytic to -19.1 x 10^{-6} emu/g for ZT. The decrease of the magnitude of the polycrystalline trace values of up to 16 per cent below the single crystal value is due to small fractions of the sample that may be composed of nongraphitic carbons, of microcrystals less than ~ 150 A in size, and of impurities. However, a section of the sample might have the rhombohedral (abcabc stacking scheme) modification or the two-dimensional turbostratic structure. In this case, since both of these structures have a theoretical susceptibility value of about -39 x 10^{-6} emu/g, this contribution would actually increase the measured trace.

Further magnetic susceptibility studies on pyrolytic graphite are reported in Section 3.2.1.3. Doping studies are reported in Section 3.2.1.4.

3.2.1.3. Electronic Properties of Pyrolytic Graphite

3.2.1.3.1. As-Deposited Materials

Studies of the electronic properties of pyrolytic graphite have yielded considerable information about the structure of this unique type of graphite. The materials on which these studies were made are comparatively simple forms of imperfect polycrystalline graphite, containing turbostratic stacking and trapping centers which affect the Fermi level. Since commercial polycrystalline graphites contain these imperfections in addition to others, an understanding of pyrolytic graphite is one of the first steps in understanding polycrystalline graphite.

A series of pyrolytic samples was prepared at deposition temperatures from 1600° to 2600°C. The details of the method of preparation and of the measurements of the electronic properties are given in WADD Technical Report 61-72, Volume XX[21]. In brief, the following results were obtained. X-ray work showed that the interlayer spacings of the as-deposited specimens ranged from 3.42 to 3.44 A. Hence, the samples all had from 87 to 100 per cent turbostratic stacking. In spite of their almost complete turbostratic character, these samples showed a marked and systematic variation in the magnetic susceptibility, g-shift, and Hall coefficient with deposition temperature. This variation is presumably due to changes in the Fermi level caused by different amounts of imperfections being formed at different temperatures.

The trace of the diamagnetic susceptibility of these specimens is shown in Figure 6 as a function of deposition temperature. The arrows correspond to single crystal values. The maximum value of -33.5 x 10^{-6} emu/g is the largest yet reported for any form of graphite and is to be compared with the value of -22.8 x 10^{-6} emu/g, given in the previous section, for the best single crystals. Theoretical considerations indicate that the large diamagnetism of

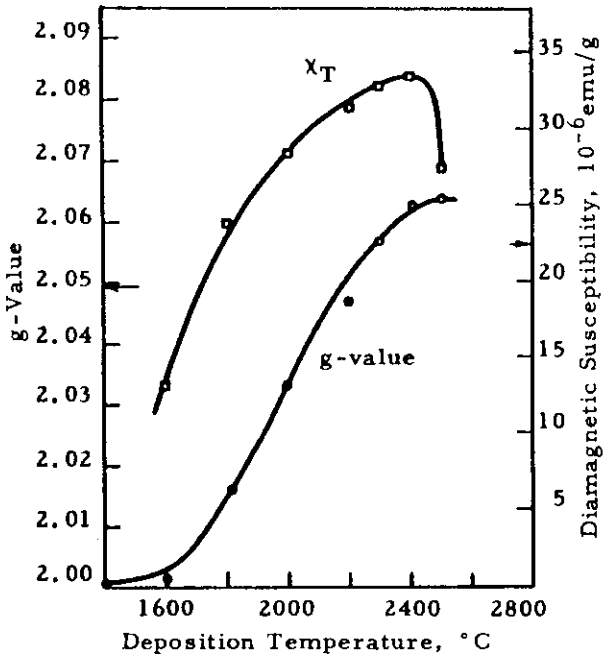

N-3857

Figure 6. Diamagnetism and g-Value of Pyrolytic Graphite

pyrolytic graphite is due to the effects of turbostratic stacking. According to calculations made by McClure [22], the susceptibility trace of two-dimensional graphite, which has no interlayer interactions, is -39×10^{-6} emu/g. McClure [23] has estimated that the diamagnetism of fully turbostratic graphite should be about 80 per cent of the value for two-dimensional graphite. The largest observed value is 86 per cent.

In addition to the diamagnetic susceptibility, the electron spin resonance g-value, Hall coefficient, resistivity, and magneto-resistance have been measured on the same samples. The resistivity and magneto-resistance are affected too much by structural irregularities to provide meaningful information about the electronic band structure of this material. The Hall coefficient is large and positive and has a maximum at a deposition temperature of about 2100°C. The large value of the Hall coefficient indicates the existence of electron traps but the nature of these traps is not known. The g-values are shown in Figure 6. At the higher deposition temperatures the g-values are the largest yet observed for any form of graphite. The g-shift of two-dimensional graphite, calculated from the formulas of McClure and Yafet [17] and from the Hall coefficient data, is not in agreement with the experimental results. It appears that the theory of the g-shift in turbostratic graphite must take into account the weak interplanar interactions as well as the shift in Fermi level.

3.2.1.3.2. Annealed Materials

The effect of annealing temperatures from 2000 to 3360°C upon the susceptibility trace and anisotropy have been investigated [20] on three specimens with deposition temperatures between 2000 and 2100°C. The first two specimens were studied by annealing different individual samples to different

temperatures. For the third specimen, two representative samples were remeasured after annealing at progressively higher temperatures. In addition, lattice spacings were measured concurrently on identical samples by X-rays. In general, an increase in $\chi_{||}$ and a decrease in $\chi_{\perp}$ were observed; this result was caused by the partial annealing which flattened the layer planes. This observation was substantiated by corresponding metallographic observations. The resulting changes in the anisotropy run from 9 to 13, 9 to 16, and 7 to 20 for these types, respectively. With increasing annealing temperature the behavior of the susceptibility trace reflects the competition between two processes: (a) the further graphitization of remaining nongraphitic carbon, as indicated by the observed growth in crystallite size which increases the magnitude of the trace, and (b) the transformation from a turbostratic two-dimensional structure to an ordered three-dimensional hexagonal structure, which decreases the magnitude of the trace. In one specimen the first process dominated and the trace changed from -19.0 to -19.8×10^{-6} emu/g. In the other two specimens the second process dominated and for one of these the trace changed from -24.5 to -21.9×10^{-6} emu/g at 2400°C with no further change at higher annealing temperatures. The interlayer spacing varied like the trace, starting from a turbostratic value of 3.41 A, dropping to almost the normal crystal value of 3.35 A at ~ 2400°C, and remaining constant at higher temperatures, indicating the effect of the turbostratic structure on the trace. The a-spacing remained essentially unchanged.

A somewhat different type of annealing experiment was made[21] on the series of samples described in the previous section. Each of these samples was annealed at ~ 3350°C. The change in the g-values is shown in Figure 7.

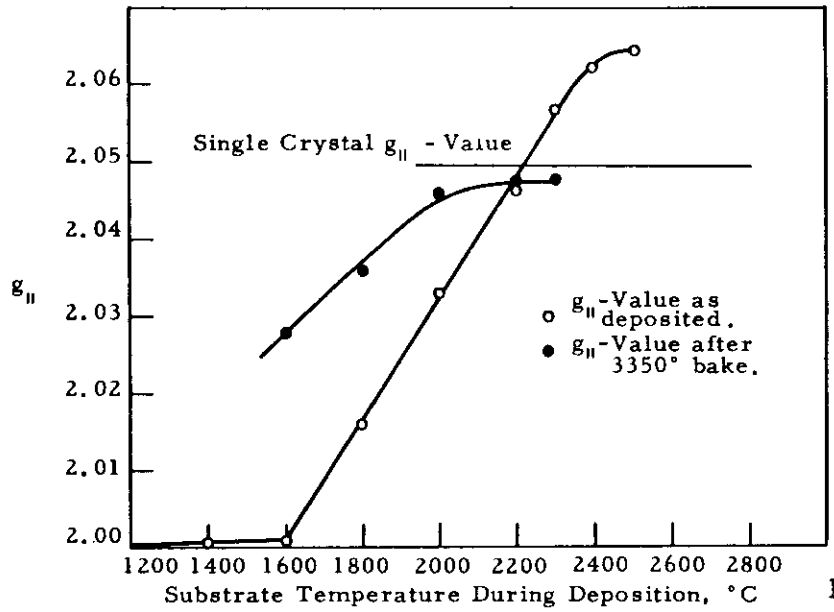

Figure 7. Spin Resonance g-Value of Pyrolytic Graphite vs. Deposition Temperature

For all samples the change was such as to bring the g-value closer to the single-crystal value, in agreement with the susceptibility results. The spin resonance work confirms the commonly observed result that pyrolytic graphite deposited at less than 2000°C under average conditions cannot be fully graphitized by annealing.

3.2.1.4. Doping Studies

Artificial graphites contain imperfections which both shift the Fermi level and change the band structure. As a preliminary step in studying naturally occurring imperfections, doping studies have been made on both natural and artificial graphites. Controlled doping has been used to change the Fermi level by known amounts without markedly changing the band structure. General agreement has been found between theory and experiment but certain details are in conflict.

3.2.1.4.1. Effect of Boron

The behavior of the diamagnetic susceptibility of three types of graphite (L113SP, AGKSP, and single crystals) was investigated [20] as a function of boron content in the range of 1 ppm up to 6000 ppm. Though this series of samples represents crystallite sizes from ~ 300 A to ~ 2 mm and anisotropy ratios from 1.02 to about 50, the relative behaviors are basically the same. The trace χ_T shows a strong shoulder on a semi-log plot in the range from ~ 10^{-4} to ~ 3×10^{-3} B/C atom ratio, changing from its pure graphite value to ~ -2×10^{-6} emu/g and becoming asymptotic to the isotropic boron insensitive component $^3\chi_{\text{ion core}}$. This shoulder is due to the rapid decrease of the large boron sensitive component $\chi_{\text{conduction}}$ as the Fermi level shifts through the band overlap region toward a p-type behavior governed by the acceptor boron. A reasonable agreement between the single crystal results and the theory of McClure is obtained by assuming an ionization efficiency of 75 ± 15 per cent. This figure was also arrived at independently [24] by applying the two-band model to the Hall effect results, where a maximum was observed in the same region corresponding to the transition from a mixed electron and hole conduction to that of hole conduction alone. Boron was chosen as a relatively ideal acceptor because of its small size (0.4 A diameter of the B^{+3} ion compared to the nearest-neighbor spacing in the graphite lattice of 1.42 A) and because it has one less valence electron than carbon. Though X-ray determinations show a slight distortion of the lattice and the electrical conductivity shows [24] an increase in the electron scattering, this study demonstrates that the susceptibility is a good indicator of the intrinsic shift of the Fermi level occurring within the crystallites, regardless of the macroscopic graphite type.

3.2.1.4.2. Effect of Potassium

Room temperature measurements of resistivity, Hall coefficient, electron spin resonance g-shift, and magnetic susceptibility have been made on lampblack-based, potassium-doped graphite. The potassium concentrations, ranging from 0.005 to 0.7 atom per cent, were limited on the low side by the

magnitude of the observed effects and on the high side by swelling and warping of the specimens due to lamellar compound formation.

The graphite samples were machined from National Carbon Company spectroscopic grade L113SP material and measured 5 cm x 1 cm x 0.1 cm thick. Each specimen was inspected under a microscope and those which showed cracks or other gross defects were rejected.

It was found that uniform doping could be achieved only at low potassium vapor pressures and high temperatures. Briefly, the experimental method involved the following procedure: The specimen was suspended from a quartz fiber in a long vertical quartz tube, which was surrounded by two independently controlled tube furnaces. The tube also contained a small amount of metallic potassium, which had been added under a blanket of argon. After evacuating to 10^{-5} mm Hg, the graphite sample was heated to the reaction temperature (400-600°C, depending on desired potassium concentration) and outgassed for one hour. Potassium in the lower section of the tube was then heated to a temperature between 160 and 210°C (vapor pressure 10^{-3} to 10^{-2} mm Hg). After 3 to 10 hours, the potassium reservoir was allowed to cool, while heating of the specimen was continued for at least one more hour in high vacuum. For the lowest potassium concentrations, this annealing process was carried out at 650°C, i.e., at 50 to 100°C higher than the reaction temperature.

The potassium concentration was determined from the weight gain. A microbalance with an accuracy of 2×10^{-5} g (sensitivity 3×10^{-6}g) was used. Since the specimens weighed approximately 0.8 g, this determination was sufficiently accurate only at concentrations higher than 0.03 atom per cent (~ 0.1 weight per cent). Lower concentrations were determined by X-ray fluorescence, which was also used to measure the uniformity of doping. Specimens with a concentration gradient of more than 5 per cent (~ 3 per cent at higher concentrations) were rejected.

The magnetic susceptibility was measured by the Gouy method in a field of 4440 gauss (permanent magnet, 1" pole pieces, 1/2" gap) with a quartz-spring balance and a traveling microscope (sensitivity 2×10^{-4}g, extension of spring 20 cm/g). The listed susceptibility values are believed to be accurate to $\pm 0.2 \times 10^{-6}$ emu/g.

For the Hall coefficient and resistivity measurements, the specimens were mounted between brass blocks acting as current carriers, and four knife-edged brass probes were gently pressed against the sample as shown in Figure 8. The entire assembly could be fitted between the pole-pieces of the magnet described above. The measurements were carried out at a current density of 0.3 ampere. Voltages were measured potentiometrically to $\pm$ 0.2 μV. For the Hall effect, the mean of four values, obtained by reversal of both current and field, was taken to eliminate errors due to misalignment of the probes and thermo-magnetic effects other than the Ettingshausen effect. By far the largest single error in these measurements was the determination of the sample thickness (0.1 cm, measured with a micrometer to $\pm$ 2 per cent). However, in the R/R_o and χ/χ_o values this

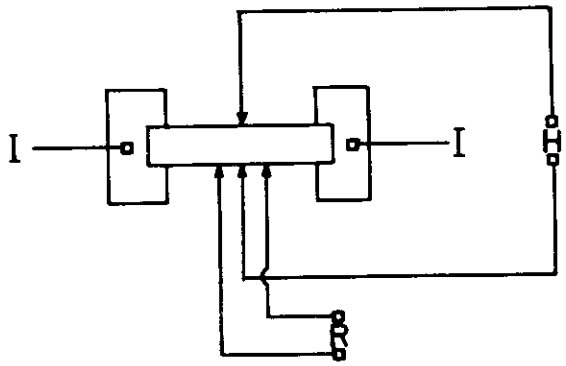

N-4091

Figure 8. Schematic Diagram of Assembly for Hall Coefficient and Resistance Measurements. I - Leads for Main Current, H - Hall Effect Probes, R - Resistivity Probes

error has been canceled out. The maximum error in the Hall coefficient is estimated to be ±0.005 cc/coulomb, and in the relative resistance to be ±0.3 per cent.

The results are listed in Table 4 and shown for the lower concentrations only in Figures 9 and 10. At low potassium concentrations the effect of doping on resistivity and susceptibility was of the same magnitude as the variations of these properties from one specimen to another. The values were therefore normalized by using the relative resistance R/R_o and relative susceptibility χ/χ_o (value after doping/before doping). The changes in Hall coefficient were sufficiently large even at the lowest concentrations so that normalizing was not necessary.

Table 4. Properties of Potassium-Doped L113SP Lampblack-Based Graphite

K Concentration		R_H cc/coulomb		R/R_o	$\chi 10^{-6}$ emu/g		χ/χ_o
Weight Per Cent	Atom Per Cent	Before	After		Before	After	
0.015	0.0045	-0.039	-0.070	1.004	-6.6	-6.5	0.985
0.034	0.0102	-0.029	-0.129	1.000	-6.5	-6.3	0.969
0.060	0.0180	-0.038	-0.215	0.969	-6.7	-6.0	0.896
0.060	0.0180	-0.039	-0.225	0.970	-6.0	-5.3	0.883
0.065	0.0195	-0.036	-0.210	0.953	-6.8	-5.8	0.853
0.076	0.0228	-0.030	-0.223	0.956	-6.4	-5.9	0.922
0.080	0.0230	-0.030	-0.223	0.956	-6.4	-5.9	0.922
0.081	0.0243	-0.038	-0.209	0.947	-6.4	-5.4	0.844
0.095	0.0285	-0.032	-0.217	0.934	-6.3	-5.3	0.841
0.115	0.0345	-0.038	-0.223	0.905	-6.5	-5.6	0.862
0.15	0.045	-0.030	-0.230	0.885	-6.4	-5.2	0.812
0.23	0.069	-0.037	-0.230	0.853	-6.3	-4.8	0.762
0.25	0.075	-0.037	-0.230	0.853	-6.3	-4.8	0.762
0.28	0.084	-0.030	-0.228	0.809	-6.4	-5.2	0.812
0.33	0.099	-0.030	-0.228	0.824	-6.6	-4.6	0.697
0.53	0.159	-0.038	-0.216	0.784	-6.2	-4.4	0.710
0.55	0.165	-0.033	-0.213	0.746	-6.3	-4.3	0.683
0.62	0.186	-0.033	-0.213	0.735	-6.3	-4.1	0.651
0.82	0.246	-0.033	-0.196	0.723	-6.6	-4.0	0.606
1.25	0.375	-0.028	-0.147	0.603	-6.2	-3.4	0.548
1.38	0.414	-0.036	-0.129	0.544	-6.6	-3.0	0.454
1.28	0.684	-0.027	-0.076	0.512	-6.5	-1.8	0.277

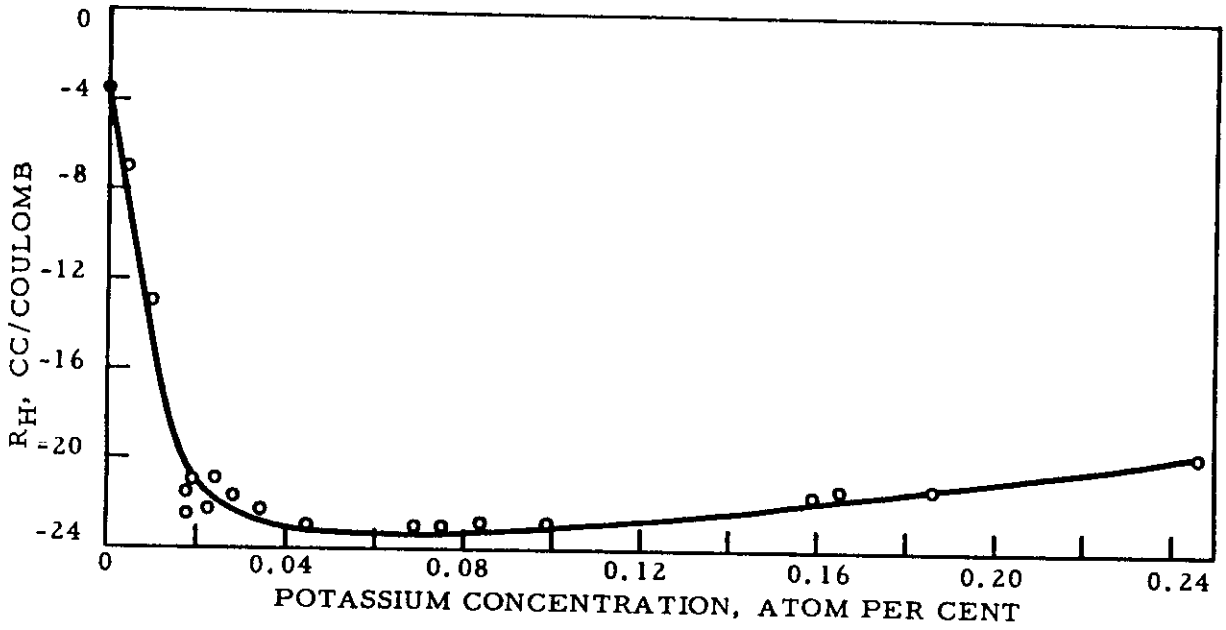

N-3603

Figure 9. Hall Coefficient of L113SP Potassium-Doped Graphite

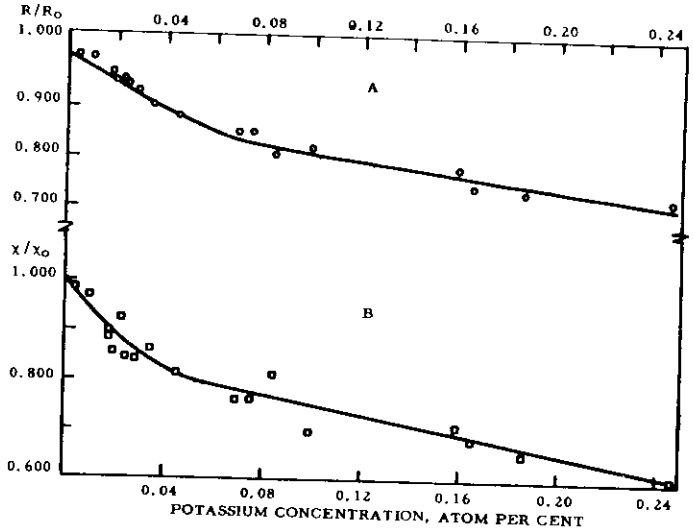

N-4093

Figure 10. A. Relative Resistance of Potassium-Doped L113SP Graphite.
B. Relative Magnetic Susceptibility of Potassium-Doped L113SP Graphite

The results were compared with those obtained by Dzurus and Hennig [25] on electrolytically prepared very dilute graphite $NH_4^+ \cdot n \cdot NH_3$ compounds. This comparison indicates that only about 10 per cent of the added potassium is ionized to K^+, except at potassium concentrations below 0.05 atom per cent, where the ionization efficiency is about 30 per cent. In the previous section the ionization efficiency of boron in L113SP graphite was found to be about 75 per cent in the same concentration range. Electron spin resonance g-shift measurements have been made on potassium-doped samples and the results are shown in Figure 11. Although the theory of the g-shift of doped graphite is not very satisfactory, the g-shift observations also seem to require a very low ionization efficiency for potassium.

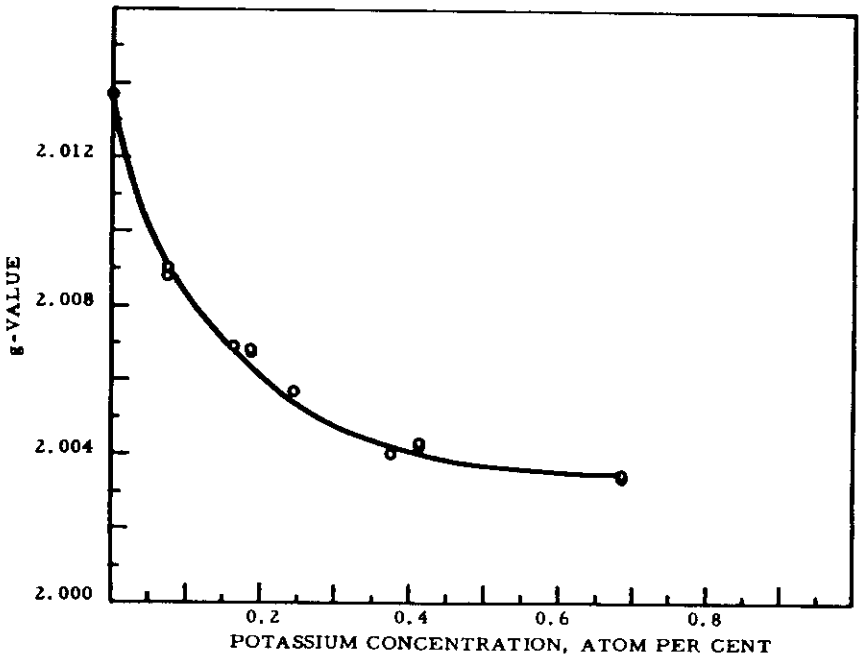

N-3413

Figure 11. g-Value of Potassium-Doped Graphite vs. Potassium Concentration

3.2.2. Mechanical Properties of Graphite Crystal

3.2.2.1. Studies of Dislocations

3.2.2.1.1. Observations of Dislocations by Electron Microscopy

An electron microscope study of dislocations and other imperfections in graphite single crystals was undertaken in order to gain an understanding of the basic mechanisms of plastic flow and fracture in graphite.

Techniques of sample preparation were developed which permitted cleaving of natural graphite single crystals to the thinness required for electron optical transmission, about 1000 A. These techniques are described in WADD Technical Report 61-72, Volume I[26]. This same report shows many examples of the variety of single dislocation networks, grain boundaries, moiré patterns, and other imperfections which are commonly observed in the microscope.

An attempt was made to study the effect of interlamellar impurities on the motion and configurations of dislocations. Three substances, bromine, cesium, and iron chloride, which form lamellar compounds with graphite, were introduced into the crystals by standard techniques. The most useful result of this study was that the impurities frequently precipitate or otherwise accumulate along dislocations or grain boundaries, thereby "decorating" them[27]. Brominated samples showed interesting contrast changes during observation, possibly as a result of changes in the interplanar spacing in regions where monolayers of bromine penetrated between graphite layers. Iron chloride was the most interesting from a visual standpoint, since it became fluid under the heating effect of the electron beam and moved about within internal pockets in the crystal. These observations clearly demonstrated the existence of these pockets, which were essentially interlayer cracks. Often they appeared to be bounded by tilt boundaries in the crystal.

Hohlstellen, which are lens-shaped blisters within the crystal, were observed in every type of sample we have studied, namely, natural and artificial single crystals and pyrolytic graphite flakes. Previously observed in graphite whiskers as well, the Hohlstellen are thought to be due to accumulation of entrapped gases or liquids between layers. Hohlstellen were observed to impede the motion of dislocations through them.

A 16 mm cine film was made by photographing the image directly from the electron microscope viewing screen. This film illustrates various dislocation processes, including the operation of a source of dislocations and of a grain boundary dislocation "sink". It also shows the motion of iron chloride within the internal cracks of a crystal and a rare example of the decoration of a dislocation network.

3.2.2.1.2. Theoretical Calculations on Dislocations

Calculations of dislocation interactions were undertaken to support the experimental work on dislocations by electron microscopy. The graphite single crystal is over fifty times more anisotropic in its elastic properties than is a typical metal crystal. This fact makes it mandatory that the formulas used in interpreting the experimental observations on graphite must correctly take into account elastic anisotropy. A general method for calculating the displacements of atoms and the components of the stress field surrounding a straight dislocation in an infinite anisotropic crystal has been derived by Eshelby, Read, and Shockley[28]. The work reported here is an application of the general theory to dislocations in certain directions of crystallographic symmetry for which much simpler and more explicit results can be obtained.

3.2.2.1.2.1. Atomic Displacements, Stress Fields, and Stacking Fault Energy of Dislocations in Symmetry Directions

Most of the theoretical work on dislocations has been reported in detail in WADD Technical Report 61-72, Volume II[29]. Formulas for the atomic displacements and the components of the stress field outside the core of a straight dislocation in an infinite anisotropic crystal have been derived. These formulas do not contain the complex numbers of the general theory and the dependence on the elastic moduli is given explicitly. These results are applicable to dislocations in and perpendicular to the basal plane of hexagonal crystals and to dislocations in certain directions of high symmetry in other crystal systems. The stress components for the anisotropic case were used to calculate the dependence of stacking fault energy on width of an extended dislocation, on width of a triple partial ribbon, and on the radius of curvature of an extended node. Experimental values obtained by electron microscopy of dislocation widths and radii of curvature in graphite have been used to obtain an approximate value of 0.6 ± 0.2 erg/cm^2 for the stacking fault energy of graphite.

The thickness of films used in electron microscopy is about 1000 A, which is about the same as the width of an extended dislocation in graphite and much less than the width of a triple partial ribbon. The stress-free surfaces of such films reduce the widths of dislocations and ribbons. The variation of width with distance of the dislocation from the surface has been calculated for an arbitrarily oriented dislocation in an isotropic solid with a single, plane surface and for a 30° extended dislocation and a symmetrical, screw triple partial ribbon in thin films cut parallel to the basal plane of a hexagonal crystal. A procedure for correcting the widths observed in electron microscopy of thin films has been given and the results were applied to graphite.

Some applications of the above results have been made to dislocations in hexagonal-close-packed and face-centered-cubic metals. In particular, it has been shown that approximate formulas relating stacking fault energy to width for dislocations in a general direction in a (111) plane in FCC crystals are not more than about 10 per cent in error, which should be a considerable improvement over formulas based on elastic isotropy.

3.2.2.1.2.2. Edge Dislocations Parallel to the c-Axis

The following work was done after the report[29] on the theory of dislocations was issued.

Edge dislocations parallel to the c-axis in graphite are of interest because a row of such dislocations would form a low-angle grain boundary between crystallites with a slight misalignment of their a-axes. Whether or not such dislocations actually occur depends on their energy of formation and the energy to move them into the crystal.

The energy of an edge dislocation parallel to the c-axis can be estimated as follows. The elastic field energy U_f outside the core of the dislocation can

be calculated from the results given in the Technical Report [30]. Assuming R/r_o in formula (3.1.2.) of that report is 4×10^3, one obtains

$$U_f = 22 \times 10^{-4} \text{ erg/cm} \quad .$$

This value is roughly twenty times larger than the total energy of dislocations lying in the basal plane. It has usually been assumed that the core energy of edge dislocations parallel to the c-axis is large due to the presence of "dangling" carbon bonds, as in the models proposed by Dawson and Follett [31]. Recently, Professor R. Smoluchowski pointed out [32] that the core structure might be very similar to that of the relatively stable azulene molecule (see Figure 12). Instead of a core energy of a few hundred kilocalories per mole due to breaking carbon-carbon bonds, the core energy should be approximately the same as the difference in energy between the azulene and naphthalene molecules. The difference in the heats of formation or combustion range [33] from 33.6 to 36.0 kilocal/mole, which gives the estimate for the core energy U_c of

$$\begin{aligned} U_c &= 35 \text{ kilocal/mole} \\ &= 0.7 \times 10^{-4} \text{ erg/cm} , \end{aligned}$$

assuming one azulene molecule per layer. The total line energy is approximately

$$U = U_f + U_c = (22 + 1)\ 10^{-4} \text{ erg/cm} \quad .$$

Due to the extreme stiffness of the graphite plane, the elastic field energy is roughly 10 times that of dislocations in other materials, but the core energy is roughly the same.

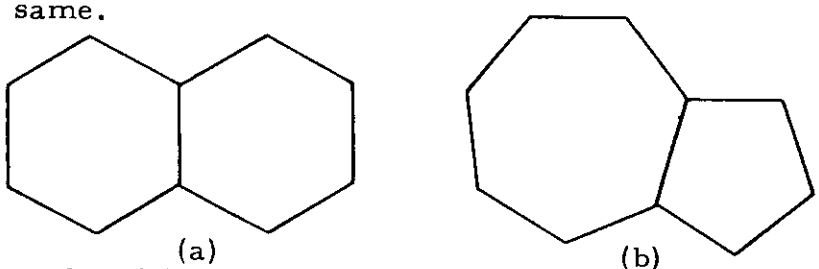

(a) (b) N-4094

Figure 12. (a) Naphthalene Molecule $C_{10}H_8$. (b) Azulene Molecule $C_{10}H_8$

In order to calculate the Peierls stress, it is necessary to know the change in core energy as the dislocation moves by glide through the crystal. Since the calculation of the core energy is long and difficult, it is important to know as much as possible about the different core structures before undertaking such calculations. The linear elastic continuum theory has been used to calculate the atomic positions around the dislocation for a number of positions of the dislocation within a unit cell of the crystal. Although the atomic positions within the core given by the linear theory are not exact, they appear to be sufficiently accurate to give a clear picture of the motion of the atoms as the dislocation glides through the crystal.

Because there are two layers and two atoms per layer within the unit cell of the graphite lattice, a dislocation cannot move without climb throughout the entire unit cell, but can only move within certain glide zones. "Nominal" glide zones for each layer are indicated in Figure 13. Even with no climb, a dislocation does not have to remain within its nominal glide zone; but if a dislocation moves without climb very much above its proper glide zone, then certain atoms in the core will be squeezed excessively close together. If a dislocation moves without climb very much below its proper glide zone, then a crack one Burgers vector wide will be opened up. There are five different types of dislocations which can be distinguished by the nominal glide zone of each layer. These are listed in Table 5. As a dislocation moves by glide under the influence of an applied stress, it will move from a position of minimum energy to a position where the energy surface has a saddle point and then to the next minimum energy position. The type of dislocation with lowest minimum energy, the type with lowest saddle point energy, and the type with lowest Peierls stress may not be the same. Evidently, a large number of dislocations of different types and different positions must be investigated for a complete understanding of the problem.

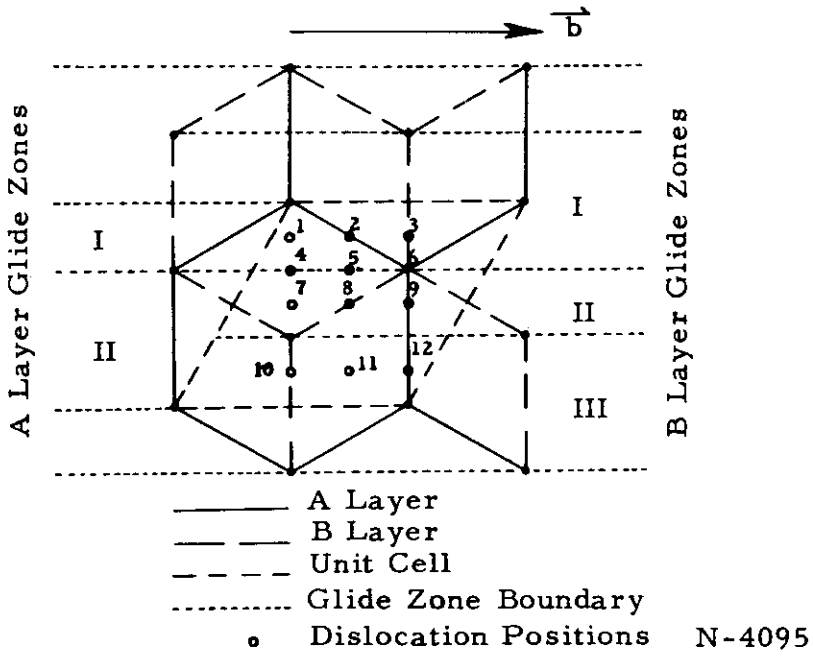

Figure 13. Positions and Glide Zones of an Edge Dislocation Parallel to the c-Axis in Graphite

Figures 14, 15 and 16 show the atomic positions given by linear elasticity theory for three positions each of dislocations of Types 1, 4 and 5. Dotted lines indicate bonds whose length, given by linear theory, either is less than 1.2 A or between 1.6 and 1.8 A. These bond lengths would doubtless change considerably in a core calculation with correct atomic forces. In the A layer in Figure 14(a) and in the B layer in Figure 15(c), the four

Table 5. Types of Edge Dislocations Parallel to the c-Axis in Graphite

Type	Layer and Glide Zone	
1	AI	BI
2	AI	BII
3	AII	BI
4	AII	BII
5	AII	BIII

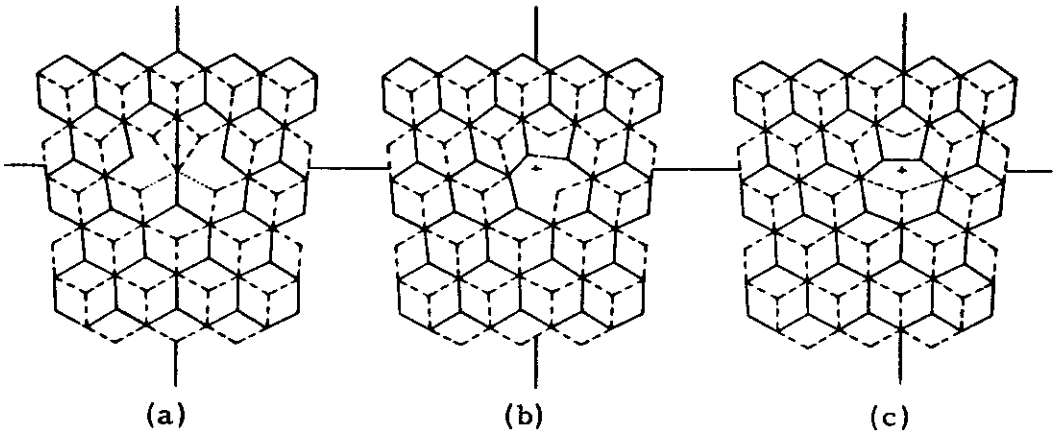

N-4096

Figure 14. Atomic Positions of a Type 1 Dislocation as Given by Linear Elasticity Theory: (a) Position 1, (b) Position 2, (c) Position 3

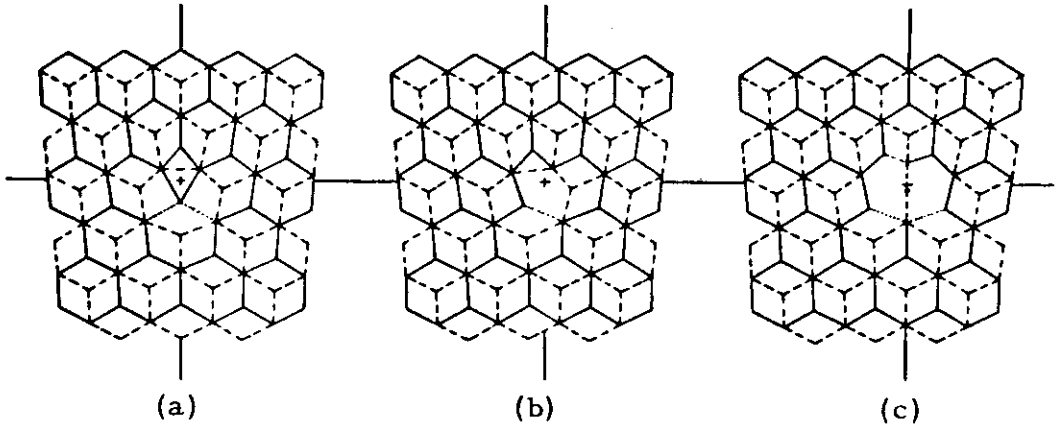

N-4097

Figure 15. Atomic Positions of a Type 4 Dislocation as Given by Linear Elasticity Theory: (a) Position 7, (b) Position 8, (c) Position 9

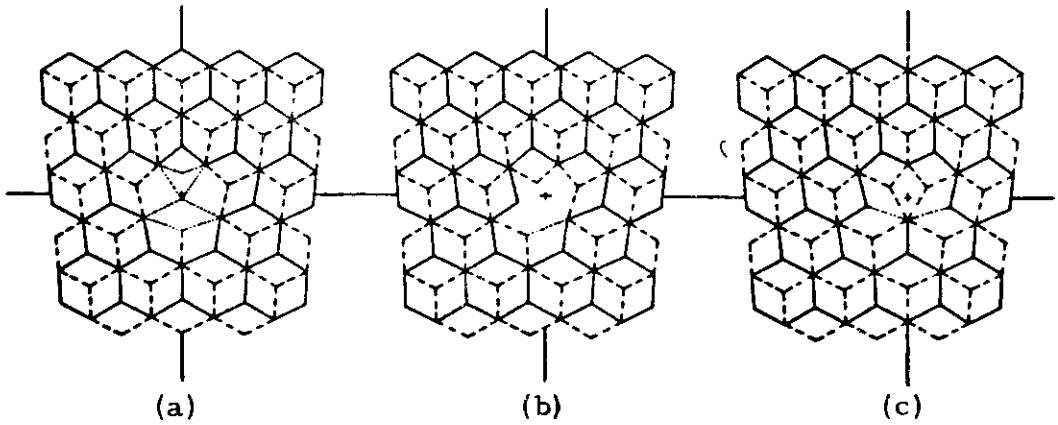

N-4098

Figure 16. Atomic Positions of a Type 5 Dislocation as Given by Linear Elasticity Theory: (a) Position 10, (b) Position 11, (c) Position 12

atoms closest to the origin along the vertical axis appear to be in unstable equilibrium if discrete atomic forces rather than an elastic continuum is considered. The two atoms closest to the origin would probably move slightly to the right and left of the vertical line and above and below the layer plane. This relaxation of linear theory positions would occur automatically in a core calculation; but if it does occur, then the symmetry position 1 or 9 of the dislocation is not the position of the saddle point in the energy. This further complicates the calculation of the saddle point energy and the Peierls stress.

Professor R. Smoluchowski's suggestion that the core atoms of the edge dislocation might have essentially the same positions as the carbon atoms in an azulene molecule is clearly confirmed by the linear theory calculations for an A layer of a Type 1 and a B layer of a Type 4 dislocation; only the Type 2 dislocation with its staggered glide zones on different layers has the azulene molecule core structure in both layers. This is illustrated in Figure 17 which has been drawn with an estimated relaxation of the positions of the central atoms on the vertical axis, as discussed above.

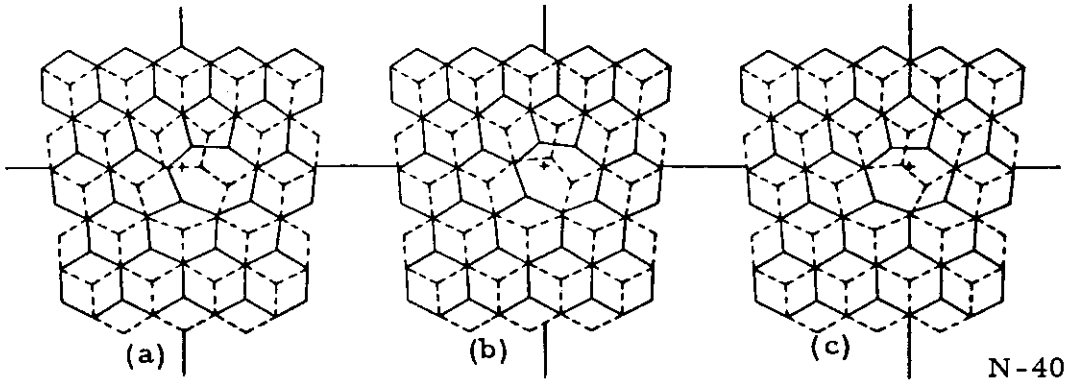

N-4099

Figure 17. Atomic Positions of a Type 2 Dislocation as Given by Linear Elasticity Theory with Estimated Relaxation of Core Atoms: (a) Position 4, (b) Position 5, (c) Position 6

The linear theory calculations suggest the following hypotheses with which to start a program of core calculations. The lowest dislocation energy probably occurs for a Type 2 dislocation near position 5. The Peierls stress for a Type 2 dislocation is likely to be relatively high and difficult to calculate. Because of its open core and lack of a stable chemical "molecular" core structure at any position, a Type 5 dislocation may have the lowest Peierls stress, although its energy should be higher than that of any other type except perhaps Type 3. It is also clear from Figures 14 through 17 that for certain atoms within the core the bond lengths, the bond angles, and even the number of bonds change significantly as the dislocation moves through the crystal. These changes will strongly affect the resonant electronic structure and hence will strongly affect the bond forces between core atoms. Accurate core calculations for an edge dislocation parallel to the c-axis must await a better understanding of these atomic forces within the irregular structure of the core.

3.2.2.2. Studies of Graphite Whiskers

3.2.2.2.1. Mechanical Properties of Whiskers at High Temperature

The stress-strain characteristics of graphite whiskers have been studied at room temperature and at temperatures up to 1550°C. The details of this work are given in Appendix I of this report.

A stress-strain device for testing whiskers at high temperatures was constructed for operation inside a bell-jar vacuum chamber. High temperature tests were performed in a vacuum, room temperature tests either in vacuum or in air.

The stress-strain diagram of graphite whiskers at room temperature showed an initial approximately linear region which was partly elastic and partly anelastic but also recoverable. This was followed by a long region of plastic slip to as much as 20 per cent elongation and a slowly falling applied force.

The room temperature anelastic or plastic behavior is interpreted as resulting from the unwinding or stretching of the scroll-type tubes of which the whisker is composed or from the slipping of one tube relative to the next concentric tube.

The high temperature behavior was essentially similar to that at room temperature, except that the yield point and the "modulus" or slope of the linear portion of the stress-strain curve were consistently lower. However, no clear-cut variation of these quantities with temperature has so far been determined.

This work has been hampered by the problem of slipping between graphite layers in the region near the grip, making it impossible to apply a reasonably pure tensile stress to the whisker in this region. However, the recent development of a suitable technique for stripping the outer layers from a whisker to prepare very small diameter "inner core" specimens will hopefully enable us more nearly to measure the intrinsic properties along the layer planes.

3.2.2.2.2. Theoretical Investigations of Whiskers

3.2.2.2.2.1. Statement of the Problem

For a flat single crystal of graphite strained parallel to its basal plane the experimentally measured Young's modulus is just the reciprocal of the elastic compliance constant s_{11} and the shear modulus is the reciprocal of $2(s_{11} - s_{12})$. Theoretical work was undertaken to see if, and how, these results were changed when the basal planes were in the form of the cylinders found in graphite whiskers.

As a simplified model of a whisker, it is assumed that the whisker is composed of cylindrical basal planes, instead of several planes rolled into a scroll. The neglect of the scroll-like structure will be discussed later. Every small volume element is assumed to have the elastic properties of a perfect hexagonal single crystal with the c-axis in the radial direction. This assumption surely breaks down near the central axis of the whisker; but if this core region is small compared with the total cross-sectional area of the whisker, the neglect of the true core structure will not cause an appreciable error. Since the c-axis varies in direction, the whisker is both anisotropic and nonhomogeneous.

In order to allow for hollow whiskers, consider a hollow cylinder of inner radius a_1 and outer radius a_2. The cylinder is fixed at one end and either pulled in tension or twisted by a pure torque at the other end. The inner and outer cylindrical surfaces are assumed to be stress-free. The stress-strain relations and the three equations of elastic equilibrium were derived in cylindrical coordinates and for the "cylindrical-hexagonal" symmetry discussed above. The equations of equilibrium were solved, subject to the appropriate boundary conditions, and from these solutions the effective Young's modulus and torsional rigidity were calculated.

3.2.2.2.2.2. Results for Young's Modulus

If F denotes the total force applied to one end of the whisker, then the average tensile stress is $F/\pi(a_2^2 - a_1^2)$ and the experimentally measured Young's modulus is obtained from

$$Y_w = \frac{F/\pi(a_2^2 - a_1^2)}{\text{strain}} \quad ,$$

where the subscript w denotes the Young's modulus of a whisker. The expression on the right is given in terms of the single crystal elastic compliance constants by the theoretical solutions of the equations of elastic equilibrium. The result is

$$Y_w = Y_{sc}\left\{1 + \frac{s_{13} - s_{12}}{s_{11}s_{33} - s_{13}^2 - s_{11}^2 + s_{12}^2}\left[s_{13} + s_{12}\right.\right.$$

$$\left.\left. - \frac{2}{(1-a^2)(1-a^{2m})}\left(\frac{s_{13} - s_{12}m}{m-1}(a - a^m)^2 + \frac{s_{13} + s_{12}m}{m+1}(1 - a^{1+m})^2\right)\right]\right\} ,$$

where

$$a = a_1/a_2 ,$$

$$m = \sqrt{\frac{c_{11}}{c_{33}}} = \sqrt{\frac{s_{11}s_{33} - s_{13}^2}{s_{11}^2 - s_{12}^2}} ,$$

and $$Y_{sc} = 1/s_{11}$$

is the Young's modulus for tension in the basal plane of a flat single crystal.

The general formula simplifies in two limiting cases. For a very thin-walled cylinder (a_1 approximately equal to a_2)

$$Y_w \simeq Y_{sc} .$$

For a solid cylinder ($a_1 = 0$)

$$Y_w = Y_{sc} \left[1 + \frac{(s_{13} - s_{12})^2}{\left[(s_{11}s_{33} - s_{13}^2)^{1/2} + (s_{11}^2 - s_{12}^2)^{1/2} \right]^2} \right] .$$

Using the presently estimated values of the s_{ij} of graphite crystals, one obtains for a solid cylinder

$$Y_w = 1.14\ Y_{sc} .$$

The stiffening of the whisker seems to be caused by a resistance, due to the cylindrical geometry, to the Poisson contraction which must accompany the extension of the whisker. In the limit $s_{12} = s_{13}$ of an isotropic material, the radial and tangential Poisson contractions are compatible with each other and there is no stiffening effect.

Since the effect of a scroll structure in which the layers of the scroll are not bonded together and the effect of a hollow core both make $Y_w \simeq Y_{sc}$, it appears that the experimentally measured values of Young's modulus should lie in the range

$$Y_{sc} \leq Y_w \leq 1.14\ Y_{sc}$$

and are probably closer to Y_{sc} .

3.2.2.2.2.3. Results for the Torsional Rigidity

If M denotes the total torque applied to one end of the whisker and τ denotes the twist per unit length produced by this torque, then the experimentally

measured torsional rigidity C of the whisker is obtained from

$$C = M/\tau \ .$$

From the solution of the equations of equilibrium one obtains

$$C = \tfrac{1}{2}(c_{11} - c_{12})\, I = 1/2\,(s_{11} - s_{12})\ ,$$

where

$$I = \tfrac{1}{2}\pi\,(a_2^4 - a_1^4)$$

is the moment of inertia of the hollow cylinder about its axis. For this mode of deformation there are no Poisson contractions and the expression for the torsional rigidity is the same as that for an isotropic cylinder with shear modulus $\frac{1}{2}(c_{11} - c_{12}) = 1/2\,(s_{11} - s_{12})$. Since the basal planes of hexagonal crystals are elastically isotropic, this result is to be expected.

3.2.2.3. Crystallite Preferred Orientation Studies

3.2.2.3.1. Introduction

The variation in the values of physical properties with direction in the sample is one of the important features of almost all grades of graphite. The origin of this anisotropy is mainly the preferred orientation in the distribution of crystallites within the polycrystalline body. Any fundamental investigation which attempts to interpret a physical property of a polycrystalline body in terms of the physical property of the single crystal must start from a knowledge of the crystallite distribution function.

X-ray techniques have recently been developed at this laboratory and elsewhere by which the crystallite orientation distribution function can be measured. In order to use the empirically determined function in other investigations it is desirable to fit the empirical curve by a reasonably simple analytical function. The theoretical work reported here was undertaken to find suitable functions and methods with which to fit the X-ray data.

The diamagnetic susceptibility of artificial graphite is determined almost completely by the crystallites and only slightly by the noncrystalline material between the grains. Consequently, the polycrystalline susceptibility should be one of the easiest physical properties to interpret. Preliminary work on this problem has been fairly successful.

Most polycrystalline graphite bodies have, to a high degree, an axis of cylindrical symmetry. This symmetry axis is approximately the molding or extrusion direction, although there may be local deviations of a few degrees between the symmetry axis and the molding or extrusion direction. Let ϕ be the angle between the c-axis of an individual crystallite and the symmetry axis. The crystallite distribution function $N(\phi)$ is defined by

$N(\phi) \sin \phi \, d\phi$ = probability of a crystallite having its c-axis between ϕ and $\phi + d\phi$.

The normalization condition is

$$\int_0^{\pi/2} N(\phi) \sin \phi \, d\phi = 1 \, .$$

For an isotropic distribution the function $N(\phi)$ has the constant value unity.

3.2.2.3.2. Curve-Fitting of X-Ray Data

An experimentally determined[34] distribution function for AGKSP extruded graphite is shown in Figure 18. This curve is normalized so that

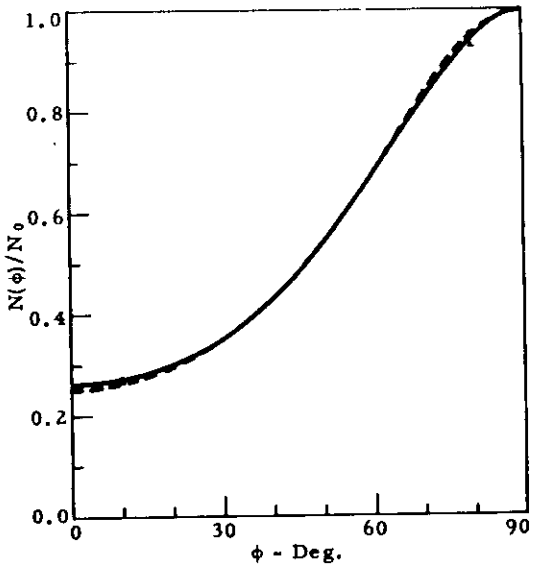

N-2776

Figure 18. Crystallite Orientation Distribution Function for Grade AGKSP Graphite. Solid Curve - Experimental. Dashed Curve - Analytical

the peak has the value unity. The narrowness of the maximum relative to the minimum is typical of both molded and extruded graphites and is extreme for pyrolytic graphite. Although this function could be fit with a Fourier series, this procedure is not too practical because a large number of terms are required to fit a strongly peaked function. Several different types of exponential functions were tried and functions of the following form were found to work well for pyrolytic, molded, and extruded graphites:

For Molded and Pyrolytic Graphite (peaked at $\phi = 0°$)

$$N(\phi) = N_0 \sum n_i \exp(-a_i^2 \sin^2 \phi) \, ,$$

For Extruded Graphite (peaked at $\phi = 90°$)

$$N(\phi) = N_0 \sum n_i \exp(-a_i^2 \cos^2 \phi).$$

If the auxiliary condition

$$\sum n_i = 1$$

is imposed, then $N(\phi)/N_0 = 1$ at the peak; and N_0 can be considered to be fixed by the normalization condition on $N(\phi)$. Substitution of these functions into the normalization condition yields the results:

For Molded and Pyrolytic Graphite

$$\frac{1}{N_0} = \sum \frac{n_i}{a_i} h(a_i),$$

where

$$h(x) = e^{-x^2} \int_0^x e^{t^2} dt$$

is a tabulated function[35], and

For Extruded Graphite

$$\frac{1}{N_0} = \sum \frac{\sqrt{\pi}\, n_i}{2a_i} \operatorname{erf}(a_i),$$

where

$$\operatorname{erf}(x) = \frac{2}{\sqrt{\pi}} \int_0^x e^{-t^2} dt$$

is the error function.

The analytical functions were fitted to the experimental curves for pyrolytic and grades ZTA, ATJ, and AGKSP graphite. Since only two terms were used, there were three adjustable parameters, a_1, a_2, and n_1. The analytical curve was forced to go through two preselected points (in addition to the maximum at $N(\phi)/N_0 = 1$) and come as close as possible elsewhere. The resulting fit is good but not optimum in the sense of least-squares. Both the analytical and experimental curves are shown in Figure 18 for grade AGKSP graphite. The experimental uncertainty, indicated by the vertical bars at 10° and 80°, is about the same as the difference between the analytical and experimental curves. For the analytical curve: $n_1 = 0.896$, $n_2 = 0.104$, $a_1 = 1.124$, $a_2 = 2.537$, and $N_0 = 1.51$.

3.2.2.3.3. Interpretation of Magnetic Susceptibility Data

The formulas expressing the polycrystalline susceptibilities in terms of the single crystal susceptibilities can be derived as follows. For every direction of the magnetic field each crystallite in the sample contributes to the measured magnetic susceptibility according to the formula

$$\chi_{sc}(\theta) = A_{sc} + B_{sc} \cos^2\theta \quad ,$$

where θ is the angle between the c-axis of the crystallite and the magnetic field and the subscript sc denotes single crystal values. The susceptibility χ_{pc} of the polycrystalline body is the sum of the susceptibility of each crystallite and is given by

$$\chi_{pc}(\textcircled{H}) = \frac{1}{2\pi} \sum c_i \int\int \chi_{sc,i}(\theta) N_i(\phi) \sin\phi \, d\phi \, d\psi ,$$

in which $\textcircled{H}$ is the angle between the magnetic field and the symmetry axis of the body and the summation is over all phases (coke, binder, etc.) which have different single crystal susceptibilities. The c_i are the mass fractions of the different phases, subject to the condition, $\sum c_i = 1$. The angle θ is related to $\textcircled{H}$, ϕ, and ψ as shown in Figure 19.

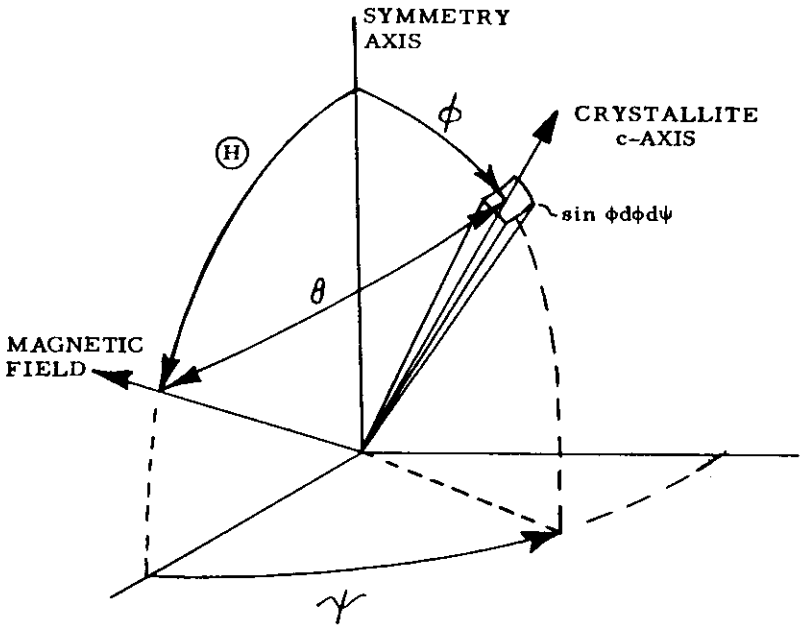

N-2771

Figure 19. Orientation of a Crystallite With Respect to the Sample Symmetry Axis and to the Magnetic Field Direction

On carrying out the integrations, one obtains

$$\chi_{pc}(\textcircled{H}) = A_{pc} + B_{pc} \cos^2 \textcircled{H} \quad ,$$

where

$$A_{pc} = \sum c_i A_{pc,i}$$

$$B_{pc} = \sum c_i B_{pc,i}$$

$$A_{pc,i} = A_{sc,i} + \tfrac{1}{2} I_i B_{sc,i}$$

$$B_{pc,i} = B_{sc,i} (1 - \tfrac{3}{2} I_i)$$

and

$$I_i = \int_0^{\pi/2} N_i(\phi) \sin^3 \phi \, d\phi$$

is the average value of $\sin^2 \phi$, averaged over the distribution of crystallites of the ith phase. By eliminating I_i one obtains the invariance of the trace relation for the ith phase:

$$\chi_{T,i} = 3A_{sc,i} + B_{sc,i} = 3A_{pc,i} + B_{pc,i} \quad .$$

It also follows that

$$\chi_T = \sum c_i \chi_{T,i} \quad ,$$

where

$$\chi_T = 3A_{pc} + B_{pc}$$

is the trace of the polycrystalline material. The experimental proof of the cosine squared variation of the susceptibility of both single crystals and polycrystalline material was reported in Section 3.2.1.2.

Note that, since the dependence on $\textcircled{H}$ factors out of the integral, the measurement of magnetic susceptibility as a function of $\textcircled{H}$ can yield information only about the quantities I_i, which are averages over the distributions. Even if there is only one phase, the distribution function itself cannot be determined by magnetic susceptibility measurements.

In the limit of perfect alignment of all c-axes along the symmetry axis ($\phi = 0$) one finds

$$I_i = 0$$

and

$$A_{pc,i} = A_{sc,i}$$

$$B_{pc,i} = B_{sc,i} \quad .$$

For an isotropic polycrystalline body

$$I_i = \tfrac{2}{3}$$

and

$$A_{pc,i} = A_{sc,i} + \tfrac{1}{3} B_{sc,i}$$

$$B_{pc,i} = 0 \ .$$

In the limit of perfect alignment of all c-axes perpendicular to the symmetry axis ($\phi = 90°$) one finds

$$I_i = 1$$

and

$$A_{pc,i} = A_{sc,i} + \tfrac{1}{2} B_{sc,i}$$

$$B_{pc,i} = -\tfrac{1}{2} B_{sc,i} \quad .$$

For all physically reasonable distribution functions, $0 \leq I_i \leq \frac{2}{3}$ for molded and pyrolytic graphite and $\frac{2}{3} \leq I_i \leq 1$ for extruded graphite.

For the analytical distribution functions discussed in the section on X-rays the integral expression for I (dropping the subscript) can be calculated by an integration by parts. The results are:

For Molded and Pyrolytic Graphite

$$I = 1 - \frac{N_0}{2} \sum \frac{n_i}{a_i^2} \left(1 - \frac{h(a_i)}{a_i} \right) \ ;$$

For Extruded Graphite

$$I = 1 - \frac{N_0}{2} \sum \frac{n_i}{a_i^2} \left(\frac{\sqrt{\pi}}{2a_i} \ \mathrm{erf}(a_i) - \exp(-a_i^2) \right) \ .$$

As yet, X-ray and magnetic susceptibility data taken on adjacent pieces of graphite are available for only one sample of grade AGKSP, which is an extruded graphite. For this sample $A_{pc} = -8.28$, $B_{pc} = 4.13$, and the

susceptibility trace is -20.71, all in units of 10^{-6} emu/g. The value of I for the crystallite distribution obtained by X-rays is 0.774. The fact that the magnitude of the trace for this sample of grade AGKSP is smaller than that of perfect single crystals means that the polycrystalline material cannot be considered as a single phase of perfect single crystals. Possible reasons for the low value of the trace have already been discussed in Section 3.2.1.2. Because of the way graphite is manufactured, it is likely that it will have to be considered as at least a two-phase system. However, it is of interest to see what the consequences would be of assuming that the material is a single phase of imperfect single crystals, that is, of crystals of unknown A_{sc} and B_{sc}. For a single phase the relevant equations which must be satisfied may be taken to be

$$3A_{pc} + B_{pc} = 3A_{sc} + B_{sc}$$

$$B_{pc} = B_{sc}\left(1-\tfrac{3}{2}I\right).$$

Substituting the values for the AGKSP graphite sample into these equations, one obtains $A_{sc} = 1.65$ and $B_{sc} = -25.65$. These values would require a paramagnetism for the magnetic field parallel to the basal plane and an even stronger diamagnetism than perfect single crystals for the magnetic field perpendicular to the basal plane. Whether this analysis is actually the case or whether a more complicated model of graphite must be employed can only be decided by further experimental work.

Some investigations of polycrystalline properties will require a detailed knowledge of $N(\phi)$. Other studies, for example, that of the coefficient of thermal expansion, require only a knowledge of the integral I. After the proper model of graphite has been determined, magnetic susceptibility measurements appear to be the easiest way of obtaining the value of I.

3.2.2.4. High Temperature X-Ray Diffraction Studies

3.2.2.4.1. Thermal Expansion of Graphites

Using a high temperature X-ray diffraction camera, the thermal expansion characteristics of grades CEP, ZTA, and ATJ of graphite and a nearly perfectly crystallized pyrolytic graphite were measured in the temperature range of 1000°K to 2600°K. By appropriate modification of the camera, the thermal expansion of these materials was determined in the temperature range of 6° to 298°K. The results of this work were reported in WADD Technical Report 61-72, Volume XXIV [36]. In brief, the expansivity in the c direction of the graphites increased with increasing orientation and crystallinity. For all of the graphites studied, the per cent change in a_o at elevated temperatures was less than the accuracy of the measurements, ~ 0.2 per cent.

3.2.2.4.2. Graphitization of Acenaphthylene Coke

Work was initiated to study the effect of time and temperature on the graphitization of acenaphthylene coke utilizing the high temperature X-ray camera. Samples in the form of 0.025 inch diameter rods were prepared by extrusion of a mixture of the coke, which was made in this laboratory, and a furfural-pitch binder. The samples were subsequently heated to 1000°C and then loaded into the camera for heat-treatment. Debye patterns were made according to the schedule in Table 6. Once hold temperature was reached, the sample was not cooled until either the heater evaporated or the 30 hour period was ended.

Table 6. Schedule for Graphitization Series

Film No.	T (°K)	Hold Time
1	298	pre hold
2	1273	pre hold
3	hold temp.	0 - 5 Min.
4	" "	5 - 10 Min.
5	" "	10 - 15 Min.
6	" "	15 - 20 Min.
7	" "	20 - 30 Min.
8	" "	30 - 40 Min.
9	" "	40 - 50 Min.
10	" "	50 - 60 Min.
11	" "	1.25 Hours
12	" "	1.5 Hours
13	" "	2.0 Hours
14	" "	2.5 Hours
15	" "	3.0 Hours
16	" "	4.0 Hours
17	" "	5.0 Hours
18	" "	6.0 Hours
19	" "	7.0 Hours
20	" "	24.0 Hours
21	" "	26.0 Hours
22	" "	30.0 Hours
23	298	post hold

Upon completion of a run the films were processed and the values of $\frac{1}{2}c$ were calculated. The results are summarized in Figure 20. The values of $\frac{1}{2}c$ at $t = \infty$ were determined from the thermal expansion behavior of fully graphitized acenaphthylene. An evaluation of the curves reveals the presence of three reactions corresponding to temperature ranges of up to 2200°K, 2400°K to 2600°K, and 2700°K and higher. Furthermore, at temperatures of 2600°K and above, $\frac{1}{2}c$ drops below the value determined for infinite hold time.

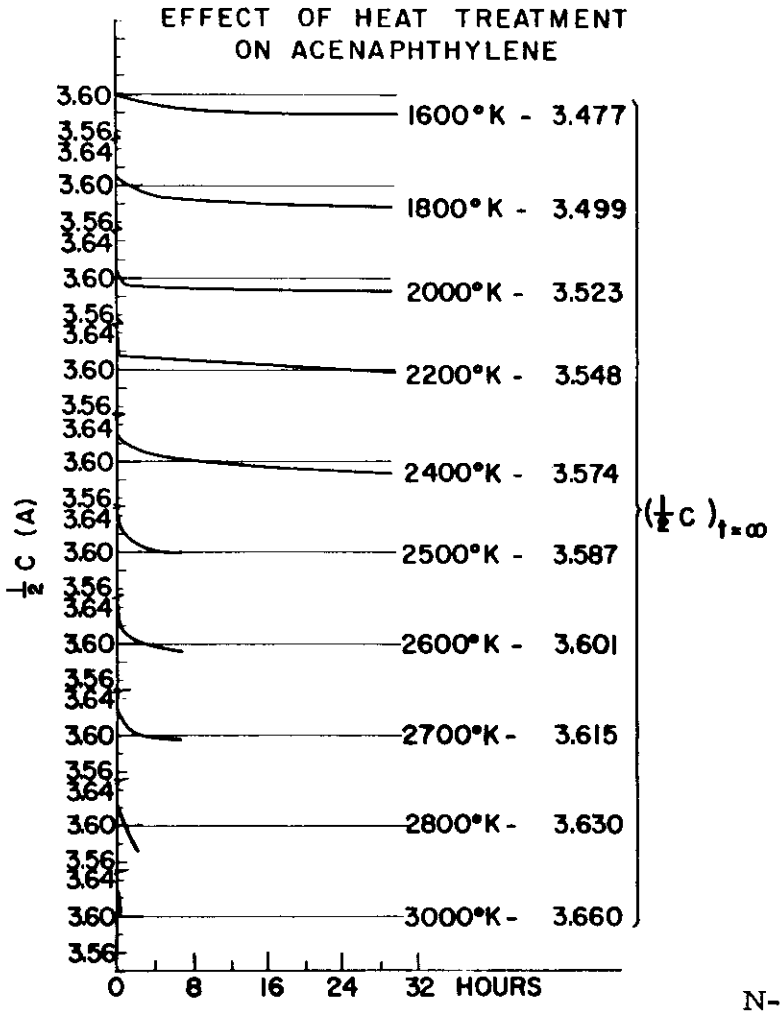

Figure 20. Effect of Heat Treatment on Acenaphthylene Coke

This would seem to confirm the results of the thermal expansion work which suggest that thermal expansivity is reduced in materials of poorer crystallinity as are the partially graphitized cokes. Thus, longer hold times at the highest temperatures should show a reversal in the curve.

Although the above results are but tentative at the present, they are of sufficient interest to warrant further investigation. Anticipating such work, attempts have been made to prolong the heater lifetime and extend the temperature range, efforts which have enabled the range to be extended to 3200°K with hold times up to twelve hours at 2800°K. For the coke presently under investigation, these extensions should be sufficient to allow graphitization to be carried to completion.

3.2.2.5. Specific Heat of Graphite

The uses of a knowledge of the specific heat of graphite extend from rocket nozzle studies at extremely high temperatures to basic science studies of

lattice vibrations at extremely low temperatures. Because of the increased importance of the specific heat, a large number of experimental measurements on different kinds of graphite have been made at various laboratories within the last decade. There does not appear to be any published evaluation and comparison of the recent specific heat measurements. Furthermore, the reviews which do exist of the older measurements give only average values with little or no indication of their accuracy.

The work reported here is an attempt to survey all the important specific heat measurements made since 1900 except those at extremely low temperatures of a few degrees absolute. The details are given in WADD Technical Report 61-72, Volume XLI[37]. Often the older literature did not give the specific heat at constant pressure c_p as a function of temperature T but instead gave the mean specific heat over a large temperature interval. In a few cases in the newer literature, the published c_p vs. T curves had an anomalous shape which appeared to be due in part to the analytical way in which the raw data had been evaluated. In order to obtain an independent evaluation of the original data, the experimental heat contents have been plotted against temperature, whenever possible. The specific heat has been obtained from the slope of these curves. The results of analyzing about twenty experiments are presented in graphical and tabular form together with an estimate of the probable errors. From these, a smooth curve has been selected to represent the specific heat over the range 20 to 3900°K. From a comparison of this curve with those of the different experiments, an estimate of the accuracy can be obtained. Except at extremely low temperatures, the differences between various measurements of the same grade of graphite appear to be about the same as the differences between different grades of graphite. It is concluded that, within the accuracy of the present measurements, the specific heat of all types of graphite is the same, except at very low temperatures and possibly for natural single-crystal graphite below room temperature.

The lattice specific heat at constant volume c_v has been obtained by subtracting the electronic specific heat c_e and the lattice $\Delta c = c_p - c_v$ correction from c_p. The electronic specific heat was recalculated from the most recent band parameters. In order to calculate Δc, it was necessary to make a brief literature survey of the coefficient of thermal expansion data at all temperatures and for different types of graphite and to estimate the temperature dependence of the bulk modulus from data on the change in the compressibility with pressure.

It is desirable to have an analytical representation of the specific heat c_v to use in theoretical calculations. Several functions were constructed of various combinations of Einstein, one-dimensional Debye, and two-dimensional Debye specific heat functions to represent the acoustical and optical modes of lattice vibrations. The best characteristic temperatures were obtained by a least-squares curve-fitting on a computer of the function to the experimental curve. Except at very low temperatures, a satisfactory analytical representation of the experimental curve was obtained. The very low temperature specific heat (below about 20°K) has not been considered. This region is very interesting theoretically but has been adequately treated in the recent literature.

3.2.2.6. Measurement of Thermal Conductivity at Elevated Temperatures

A technique has been developed for determining the thermal conductivity of small rod-like specimens under the perturbing influence of small transverse heat flows. It is these transverse heat flows, generally due to radiative heat exchange between the specimen and its surroundings, which cause the major error in the common "longitudinal heat flow" measurements of thermal conductivity* above room temperature. In most such measurements, the attempt is made to reduce the error to negligible proportions by use of a guard shield having a temperature distribution matched to that in the specimen. Although this approach can reduce the error somewhat if the specimen has a large diameter and conditions are mostly quite ideal, it is generally difficult to achieve the necessary precision in practice.** The present work is included in the Basic Studies Section of this report because of its important bearing on the development of a valid theory of lattice vibrations and heat conduction in graphite.

The present technique was devised with the intent of evading inherent limitations of the "guarded longitudinal heat flow method". Rather than attempting the difficult task of eliminating completely the transverse heat flow, the new method simply makes the transverse flow small and then measures its effect on the determination of the thermal conductivity. Thus, instead of requiring an enclosure whose temperature distribution is precisely matched to that in the specimen, one now requires an isothermal enclosure whose temperature can be controlled rather closely. This approach may be illustrated simply by reference to Figure 21. A specimen of perimeter p, cross-sectional area w, and length L, is inserted in an isothermal enclosed at temperature T_s.

The condition of interest here will be that in which the temperature difference between the specimen and the enclosure is everywhere sufficiently small that the heat exchange is a linear function of the temperature difference (Newton cooling); that is, the specimen loses (or gains) H watts/cm² from its surface for a 1°C difference in temperature between the two surfaces. The effect on the temperature of the specimen from this heat exchange with the enclosure will depend on the ratio of the perimeter to cross-sectional area and on the thermal conductivity κ of the specimen through the parameter μ, where $\mu^2 = \frac{Hp}{w\kappa}$. If the ends of the specimen are held at T_o and T_L, respectively, then the temperature at a distance x from the end at T_o is given by the following equation[38].

---

* One of the most careful investigations of thermal conductivity by this technique is described by L. D. Armstrong and T. M. Dauphinee, Can. J. Phys. 25, 357(1947). The precision achieved in that case was very high but would have been unattainable if a small specimen only had been available for study.

** Some basic limitations of the technique for small samples have been discussed by M. Bettman and J. E. Schneider in "Thermoelectricity" edited by Paul H. Egli, John Wiley (1960).

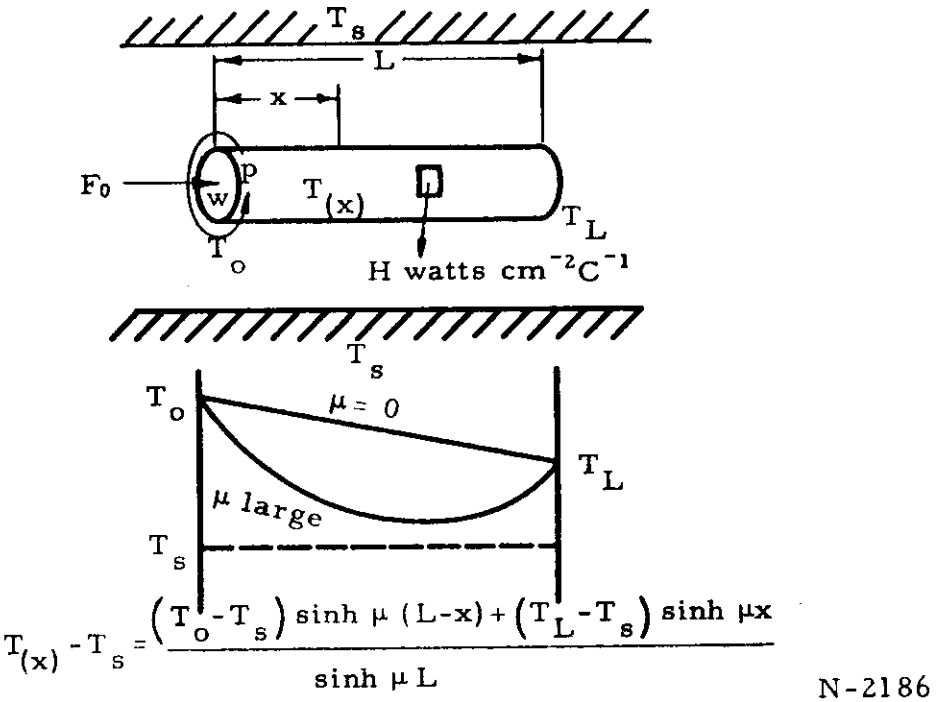

Figure 21. Specimen Environment in Thermal Conductivity Apparatus

$$T_{(x)} - T_s = \frac{(T_o - T_s)\sinh \mu (L-x) + (T_L - T_s)\sinh \mu x}{\sinh \mu L} \qquad (1)$$

or, in terms of the flux F_o injected at $x = 0$

$$T_{(x)} - T_s = (T_o - T_s)\cosh \mu x - \frac{F_o}{K\mu} \sinh \mu x \ . \qquad (2)$$

These two formulas suggest the approach which has been applied; for if one places three equally spaced thermocouples on the specimen at positions x, x + y, and x - y, then the parameter μ can be determined quite simply by holding the temperatures at $x \pm y$ fixed and measuring the change in temperature at the midpoint, x, while the temperature of the enclosure is varied.

It can be demonstrated quite simply that the slope of the curve of T(x) vs. T_s, with T (x+y) and T(x - y) held fixed, is given by

$$\frac{dT(x)}{dT_s} = 1 - \frac{1}{\cosh \mu y} \ . \qquad (3)$$

If thermocouples of the same material are used to measure T(x) and T_s, then, so long as the temperatures are close together, it is not even necessary to determine the temperature changes themselves but only the changes in thermocouple emfs, since

$$\frac{dT(x)}{dT_s} = \frac{dV(x)}{dV_s} \quad .$$

Having determined the parameter μ, it is then possible to determine the thermal conductivity κ from (2) by holding T_s and $T(x)$ fixed and measuring the temperature change at $x + y$ or at $x - y$ which results from a change in the flux injected at $x = 0$. Under these conditions, it is found that

$$\frac{dT(x-y)}{dF_o} = \frac{1}{\kappa \mu} \frac{\sinh \mu y}{\cosh \mu x} = \frac{-dT(x+y)}{dF_o} \quad , \qquad (4)$$

which can be rearranged in the form

$$\kappa = \kappa_o f(\mu y) \quad , \qquad (5)$$

where $\kappa_o = \frac{y}{dT(x-y)/dF_o}$ is the uncorrected thermal conductivity assuming no transverse heat losses and

$$f(z) = \frac{1}{z} \frac{\sinh z}{\cosh \gamma z} \quad , \text{ where } \gamma = x/y \quad . \qquad (6)$$

It will be noted that $dT(x)/dT_s$ and $f(\mu y)$ are related through the parametric equations (3) and (6). This relation is plotted in Figure 22 over most of the range of $dT(x)/dT_s$ for which the technique should be applicable.

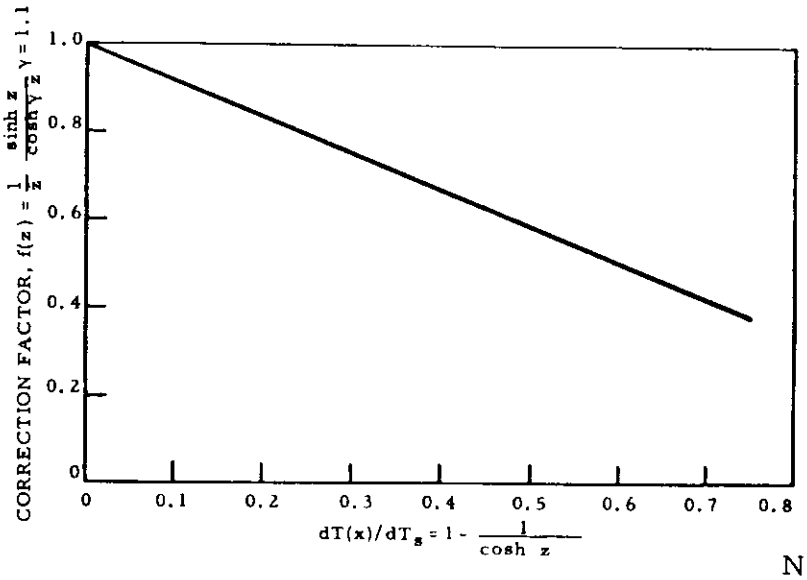

N-4108

Figure 22. Correction Factor for Thermal Conductivity

The principle of this method might be applied in various ways; one need not measure K_o in precisely the way described above. The approach chosen here is illustrated in Figure 23.

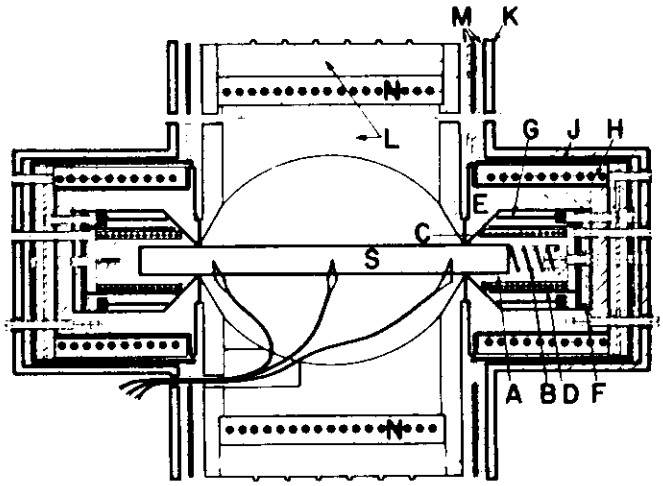

N-2185

Figure 23. Diagram of Thermal Conductivity Apparatus

S - the specimen, $\frac{1}{2}$-cm diameter
A - specimen mounting cup
B - graphite spring, in "cold end" cup only
C - specimen heater
D - outer mounting cup
E - guard
F - insulating disk
G - metal radiation shield
H - guard heater
J - mounting cups and radiation shield
K - " " " " "
L - three-section chamber
M - ceramic insulators and radiation shields
N - chamber heater

The assembled unit is shown (in the main furnace) in Figure 24.

The measurements are made by means of electronic equipment partially of commercial manufacture and partially designed and fabricated in this laboratory. Simplified schematic drawings of the circuit arrangements for the two measurements of $dT(x)/dT_s$ and of K_o, are given in Figures 25 and 26.

The method and equipment were tested first in a study of germanium, with quite satisfactory results near room temperature. At higher temperatures, an error appeared which increased with increasing temperature. To clarify the problem, supplementary measurements were made of the thermal diffusivity under identical conditions. The latter measurements agreed with

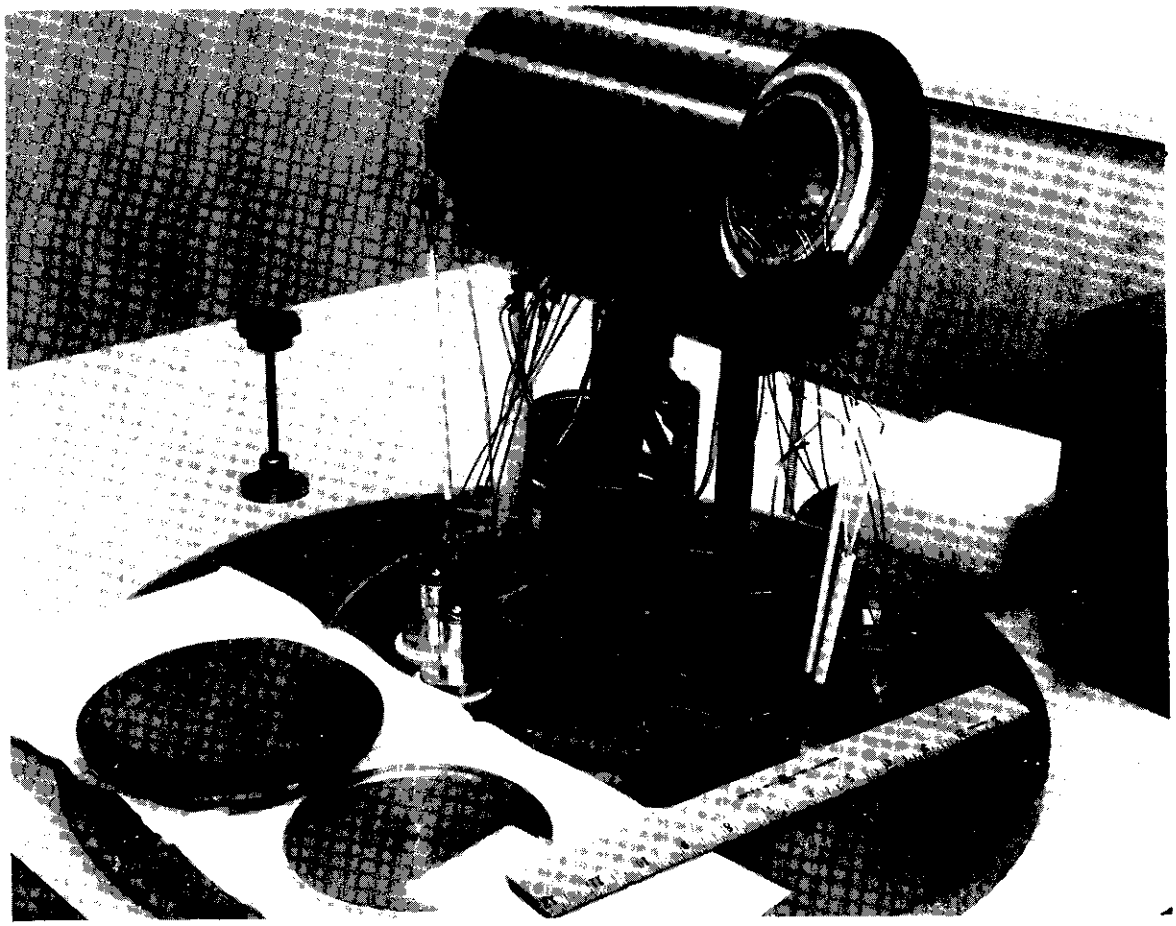

N-2271

Figure 24. Thermal Conductivity Apparatus Assembled in Vacuum Furnace

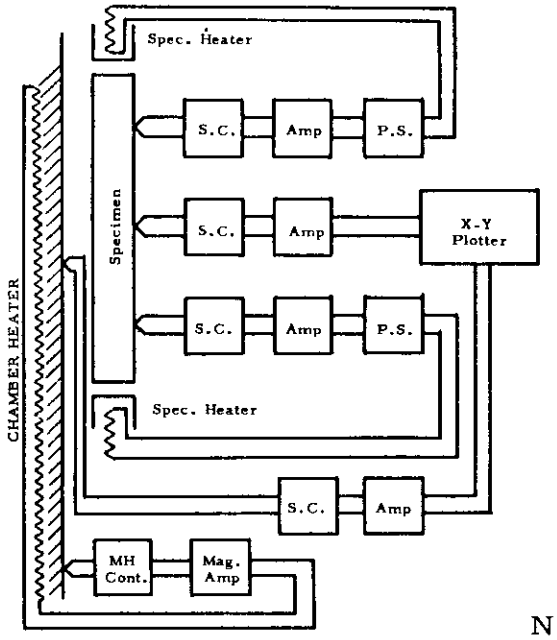

N-2363

Figure 25. Measurement of Effect of Transverse Heat Losses, i.e., Measurement of $dT(x)/dT_s$

S.C. = Thermocouple suppression circuit
Amp = d.c. amplifier
P.S. = Power supply for heaters
MH Cont. = Minneapolis-Honeywell temperature controller
Mag. Amp = Magnetic amplifier power supply for chamber heater.

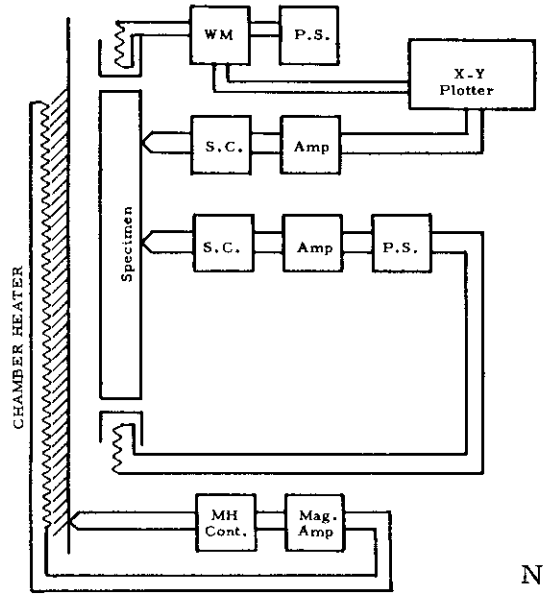

N-2362

Figure 26. Measurement of K_o, Uncorrected Thermal Conductivity. Symbols as before, except WM = Hall effect watt meter

the literature values, within experimental error, and suggested that an unexpected heat leak existed in the specimen mounting assembly. The apparatus has been modified to minimize this leak and now has been reassembled with an Armco Iron test specimen. No results are presently available to confirm whether this modification has corrected the problem.

3.3. Applied Research

This section of the report describes research examination of numerous properties of gross fabricated bodies of graphite which are important to engineering applications. Included are mechanical properties (creep, elasticity, and strength), thermal conductivity and radiant emissivity. Attention has been paid to the effect of high temperatures on these properties. Work is also reported on nondestructive testing for flaws by means of radiographic examination.

3.3.1. Studies of Creep of Graphite

Creep of graphite at high temperatures (2200 to 3000°C) has been investigated by means of flexural and tensile creep tests. Most of the data have been summarized in four reports [39-42]. A brief summary will be given of the contents of these reports as well as some additional results not included in the reports.

3.3.1.1. Flexural Creep Studies

WADD Technical Report 61-72, Volume V [39] presented an analysis of flexural creep data for ATJ graphite using several standard equations given in the literature. Emphasis was placed on an equation based on a simple model for a viscoelastic material An activation energy for the steady-state creep rate was determined to lie between 70 and 76 kcal/mole. Some deviations were detected between the actual behavior of the material and that predicted by the simple model which suggested some modifications in the simple model. Some experiments on recovery after creep were presented which gave good qualitative support to the model.

WADD Technical Report 61-72, Volume VI [40] contained flexural creep data for several standard and experimental National Carbon grades of graphite and for ZT grades of recrystallized graphite. The magnitude of the creep strain was found to decrease as the temperature of graphitization and the holding time at graphitization temperature increased. The activation energies which were determined from the steady-state creep rates were different for each grade of graphite and ranged from 23 to 92 kcal/mole. The manner in which the density, grain orientation, and crystallinity of the graphite influence the creep was discussed.

A few flexural creep measurements were made on pyrolytic graphite specimens. These results have been included along with other studies on pyrolytic graphite in WADD Technical Report 61-72, Volume XXXVII [42]. Annealing of pyrolytic specimens reduced the flexural creep rate, resulting in values below those for graphite grades ZTA and ATJ.

3.3.1.2. Tensile Creep Studies

WADD Technical Report 61-72, Volume XVIII[41] covers the high temperature tensile creep data of graphite. Several standard and experimental National Carbon grades of graphite and some ZTA graphite were tested. The temperature ranged from 2300°C to 2900°C. The data for ATJ graphite were fitted to several equations, the emphasis being placed again on the equation based on a simple model for a viscoelastic material. The steady-state creep rate of ATJ graphite was found to vary with the fourth power of the stress. An activation energy of 124 kcal/mole, based on the steady-state creep rates, was found for all of the graphites which were tested. The creep was found to be greater in the direction "against the grain" than in the direction "with the grain", and differences in creep strain and creep rate for the two orientations were found to increase as the anisotropy of the graphite increased. The creep in the direction "with the grain" was found to decrease as the density increased, but it was not very sensitive to differences in the proportions of filler and binder carbon.

3.3.1.3. Room Temperature Creep of Graphite

A room temperature creep fixture was used to follow the deformation of two bars of RVA graphite for six months. The bars, of width b and thickness d, were subjected to a constant force P under single point loading with a support distance L. The results are shown in Figure 27. There is no

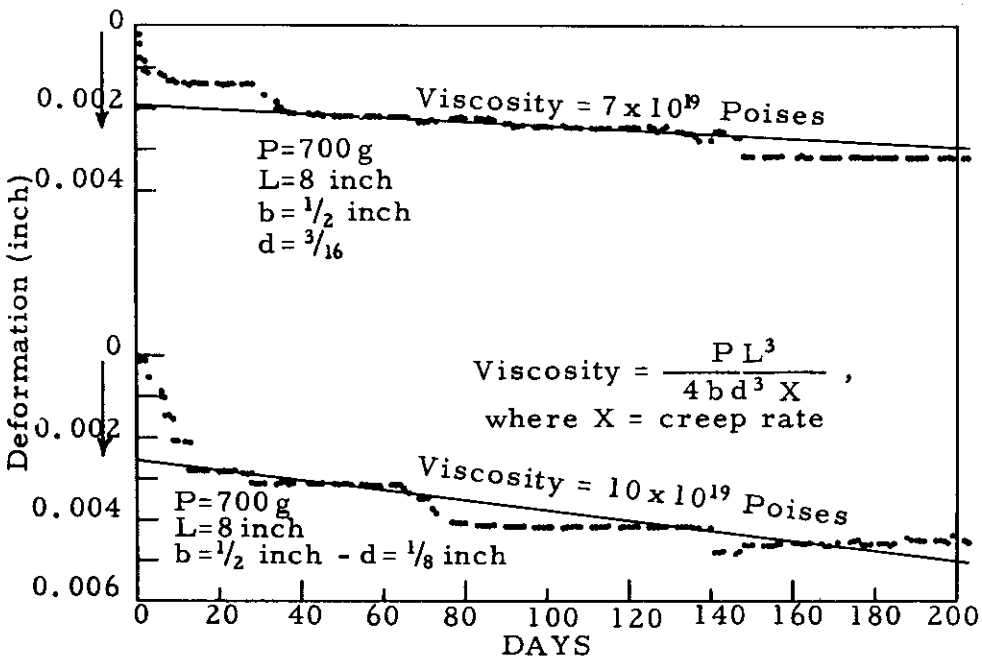

Figure 27. Flexural Creep of RVA Graphite at Room Temperature

are of the initial deflection introduced when the load was applied; the zero represents the position of the center of the graphite bar a few minutes after the load was applied. The two bars which were used were cut from the same block of graphite and had the same width, but different thicknesses. The distances between supports and the applied loads were the same for both bars. The deformation of the center of each bar was followed by a dial indicator.

The bars both exhibited creep, though the deformation as a function of time tended to be somewhat erratic. The deformation increased fairly rapidly the first few days, but it soon leveled off. The dial indicators recorded on occasion sizable jumps and then held constant sometimes for periods of weeks or months. The creep is definitely very slow. One can put a magnitude on it by following the example of Reiner[43] and calculating a viscosity, using the formula given in Figure 27. The room temperature "viscosity" of graphite, as obtained from these curves, is of the order of 7 to 10 x 10^{19} poise. These figures can be compared with those given by Reiner for concrete (3 x 10^{17} poise) and glass (6 x 10^{18} poise). Graphite, therefore, has a slower creep rate at room temperature than either concrete or glass.

3.3.2. Tensile Stress-Strain Behavior of Grade ATJ Graphite

An experimental investigation of the stress-strain behavior of grade ATJ graphite in a static tensile test at room temperature was undertaken. The strain was measured by strain gauges cemented to the center of the specimen. Tests were made on the Instron testing machine, and a brief account of the trials and some of the early data will be discussed.

The grade ATJ specimens were oriented "against the grain". One strain gauge was used to measure the longitudinal extension of the specimen and a second strain gauge was used to measure its transverse contraction. The gauges were Baldwin-Lima-Hamilton Type A-7 with a resistance of about 120 ohms, and they were cemented to the graphite with Duco cement. The X-Y recorder on the Instron and a Moseley X-Y recorder were used to simultaneously plot the stress-strain curves in the longitudinal and transverse directions. The load cell on the Instron was used for measuring the force. The Y axis input of the Moseley recorder was placed in parallel with that of the Instron recorder and both recorders were calibrated simultaneously. One strain gauge was used with the Instron strain gauge amplifier circuit to actuate a servo motor to drive the recorder chart by an amount proportional to the strain. The second strain gauge was used in conjunction with a Sanborn Transducer Amplier-Indicator to provide the signal for the X axis input to the Moseley recorder.

A cyclic stressing test was made. The rate of straining was 0.002 inch/min, which is the slowest rate possible on the Instron. In a typical test, as is shown in Figure 28, the stress was increased to 200 psi, reduced to zero, increased to 400 psi, reduced to zero again, and cycled in this manner while increasing the upper stress in increments of 200 psi up to a maximum stress of 1400 psi. This type of test is similar to that conducted by Andrew, Okada, and Wobschall[44] on carbon and graphite cantilever specimens and that

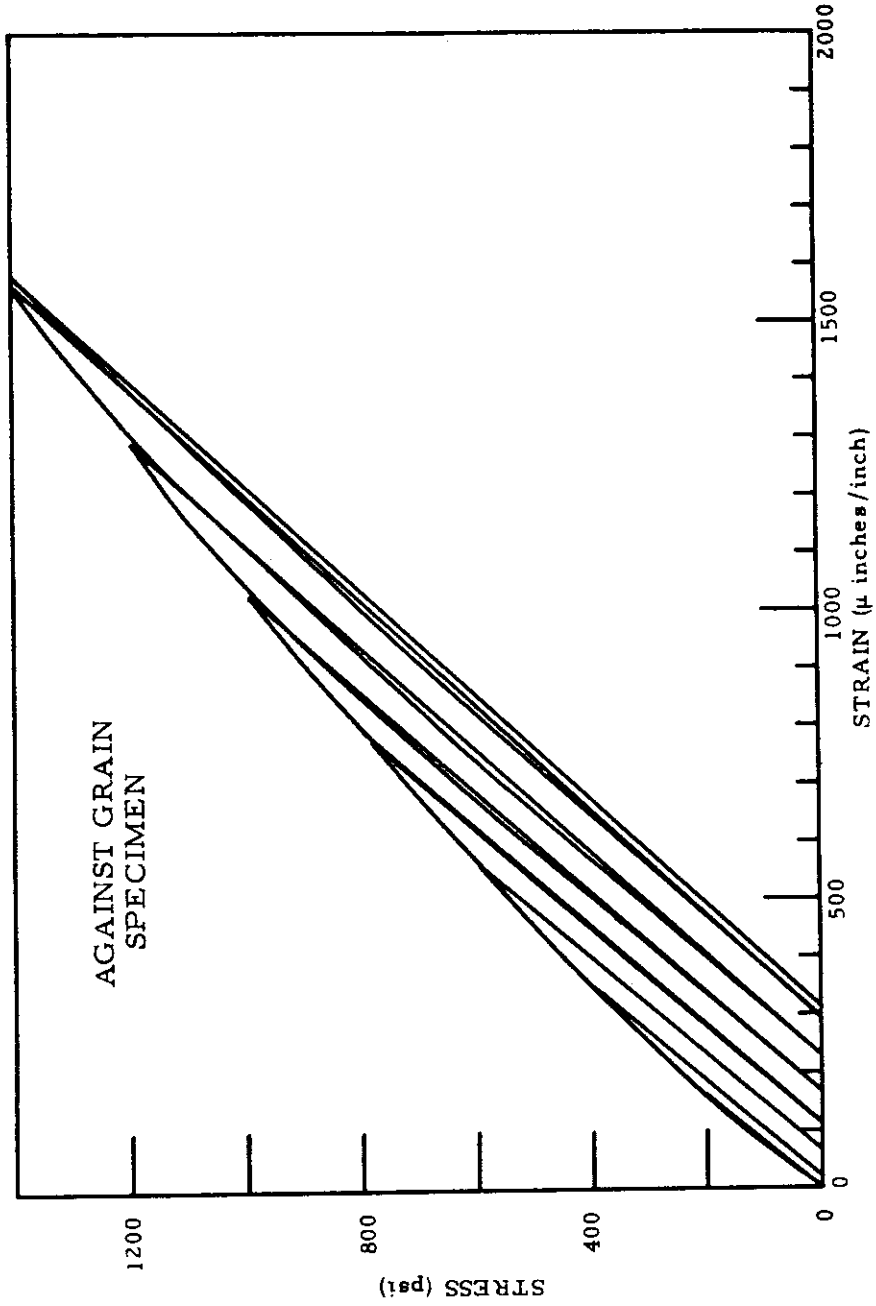

Figure 28. Stress-Strain Data for Grade ATJ Graphite

reported by Losty and Orchard[45] for specimens of graphite in tension and compression. The features of the stress-strain curves which have been obtained are in agreement, for the most part, with those observed by the above authors. The initial loading curve is not linear and there is a permanent set when the stress is removed. The curve obtained when the load is removed is linear or almost linear. As the stress is increased, the slope of the unloading curve tends to decrease and the permanent set increases. The unloading and reloading curves exhibit a hysteresis which increases as the maximum stress is increased. In the transverse direction, on the other hand, the strain in contraction appears to be proportional to the applied stress and little or no permanent set is found. Considerably more study will be required before meaningful interpretation can be attempted.

3.3.3. Thermal Stresses in Anisotropic Hollow Cylinders

Thermal stresses generated in anisotropic hollow cylinders have been investigated by quasi-static thermal elasticity theory and reported in WADD Technical Report 61-72, Volume XIX[46] and the results are summarized below.

The hollow cylinder was assumed to be transversely isotropic. The physical and thermal properties in the direction parallel with the basal planes are different from those in the direction normal to the basal planes or in the c-direction of the material. The c-axis of the material coincided with the axis of symmetry of the hollow cylinder.

The following three thermal boundary conditions were assumed on the bore of the hollow cylinder which is initially at zero or room temperature: (1) the bore temperature was suddenly increased to a finite value, (2) a constant heat flux was suddenly applied at the bore, or (3) heat flow by convection occurred at the bore. In all these cases the temperature of the outside surface was maintained at zero or initial temperature.

Based on these temperature distributions, the transient and steady-state thermal stresses in the hollow cylinder were calculated for a cylinder with a wall ratio of 2.0. Maximum tensile and compressive stresses generated were calculated for various values of Biot's moduli and wall ratios. The steady-state tensile stress at the outside surface proved to be also the maximum tensile stress. Maximum compressive stress always occurred at the bore. If Biot's modulus was small, the maximum compressive stress occurred at the steady-state condition. If Biot's modulus was large, the maximum compressive stress occurred during the transient period.

The maximum temperature which can be applied to the bore of the cylinder was calculated from the values of the maximum thermal tensile and compressive stresses and measured fracture stresses in uniaxial tension and compression.

Effects of anisotropy on thermal shock resistance of graphites were examined. Thermal shock resistance calculated by the isotropic formula and the properties in the with-grain direction was found to be too high. Calculation

based on the isotropic formula and the properties in the against-grain direction underestimated slightly the thermal shock resistance of graphite; however, it was sufficiently accurate for many practical engineering problems.

A problem of the sudden cooling of a hollow cylinder with a known initial temperature distribution was investigated in connection with the problem of the sudden forced cooling of rocket nozzles after test firing for early visual inspection. It was found that a high tensile stress is built up at the bore during cooling. The magnitude of this tensile stress is equal to the tensile stress at the outside surface but is not greater than the initial tensile stress which existed at the outside surface. It is possible that fracture might initiate at the bore due to rapid cooling if the bore surface were already damaged by ablation during the test firing.

3.3.4. Sonic Elastic Constants of Polycrystalline Graphite with Cylindrical Symmetry

The resonant bar technique has been used to study the sonic elastic constants of polycrystalline graphite. Five elastic constants are needed to describe properly the elastic properties of a molded or extruded graphite, but until recently essentially no work had been done on determining all five constants for any graphitic material. Therefore, the present work has centered on establishing the formulas needed in analyzing the data for round and rectangular bars and on determining the proper experimental techniques to yield the greatest accuracy. The work on longitudinal and torsional vibrations is fairly complete but work on the flexural vibrations of anisotropic bars has just started. The complete account of the work done to date has been placed in Appendix II of this report. Since the study is incomplete, some of the results are not conclusively established. Nevertheless, enough work has been done to give a rather clear picture of what can and cannot be done by the resonant bar method.

3.3.5. Study of High Temperature Tensile Properties of Grade ZTA Graphite

The above study was made by the Aeronutronic Division of Ford Motor Company with their apparatus and technical skills in this area, which were both fully available at the beginning of this activity. The study objective here was to determine the high temperature tensile strength properties for the highly anisotropic grade ZTA graphite and in particular to evaluate the effects of grain orientation, load rate, prior degassing treatment, and surrounding gas composition and pressure.

The results of this investigation have been reported in WADD Technical Report 61-72, Volume XIV [47] and are summarized as follows:

1. The grade ZTA graphite is moderately anisotropic in strength properties; the normal to mold (with-grain) direction is about three times that of the mold (across-grain) direction strength.

2. The strength of the graphite increases from about 4000 psi at room temperature to over 9000 psi near 2500°C (4500°F) for the with-grain oriented material.

3. The corresponding across-grain material over the same temperature range increases in strength from about 1500 psi to 2000 psi.

4. Above 2550°C (4600°F), the strength of ZTA grade graphite decreases in all cases.

5. The rate of change of stress with strain (Young's Modulus) increases from a relatively low value at low strain to higher values at higher stress.

6. No difference was found in the strength of ZTA graphite which had been annealed at 3000°C prior to testing and its unannealed counterpart.

7. The ultimate tensile strength of the ZTA graphite is load rate sensitive, with the slower rates resulting in the higher strength above 1650°C (3000°F).

8. The ultimate tensile strength is insensitive to a test atmosphere of nitrogen or carbon monoxide at all temperatures.

9. The strength of the across-grain oriented material decreases with increasing density within the density range examined.

10. Over the same density range, the strength of the with-grain oriented material is not significantly affected.

11. Between 1980°C (3600°F) and 2500°C (4500°F) the strength of the graphite is sensitive to external pressure, with an increase in pressure resulting in an increase in strength.

12. The removal of contained gases by heating in a vacuum increases the strength of the material below the outgassing temperature.

3.3.6. Radiographic Examination of Carbon and Graphite

Work performed under Subcontract by Picker X-Ray Corporation to determine the optimum conditions for obtaining maximum perceptibility of defects in high density carbon and graphite has been reported[48] in WADD Technical Report 61-72, Volume XVII. The use of grids and associated techniques has yielded a radiographic sensitivity of 0.5 per cent or better for 4- to 16-inch thicknesses of graphite. Sources evaluated included X-ray tube voltage from 110 to 270 KV, iridium-192, cesium-137 and cobalt-60.

3.3.7. Arc Image Furnace Studies

The carbon arc image furnace has proved to be a versatile and useful tool for high temperature studies. It has found numerous applications to the study of the properties of graphite and other materials of interest in this program. The studies, which have been reported[49] in WADD Technical Report 61-72, Volume XXI, are summarized below.

3.3.7.1. Reflectance and Emissivity of Carbon and Graphite

The arc image furnace[50] is ideally suited to the determination of spectral reflectance[51] and, by application of Kirchhoff's law to the spectral emissivity of opaque materials. Measurements on carbon and graphite have shown[49] that the spectral reflectance at 45° from the normal to the surface can range from values as large as 0.25 to 0.30 for highly polished materials to values of 0.05 and smaller for roughened surfaces. The observation of a slight increase in spectral reflectance with increasing wavelength through the visible portion of the spectrum is in general agreement with findings by other workers. Careful determinations of the spectral reflectance for various carbon and graphite materials from room temperature to more than 2000°K have shown no evidence of any temperature dependence[49]. Measurements by other workers,[52, 53] using direct radiation methods, have agreed on the temperature independence of the emissivity for polished surfaces of carbon and graphite but have indicated that roughened surfaces exhibit a decrease in spectral emissivity with increasing temperature equivalent to a reflectance increase of as much as 25 to 50 per cent from room temperature to 2000°K. Such large variations in reflectance could not have been overlooked by the arc image furnace. Analysis[49] indicates that the direct radiation methods for determination of spectral emissivity suffer from errors due to thermal gradients which become seriously large with roughened graphite materials at temperatures between 1000 and 2000°K.

Special optical techniques were developed[49] to measure the spectral reflectance of carbon and graphite at a surface temperature of 3800°K, the sublimation temperature in an electric arc. These measurements showed a spectral reflectance for the visible region in the range 0.01 to 0.03, with carbon showing higher reflectance values than graphite.

Measurements were made of the spectral reflectance and degree of polarization for highly oriented, high density pyrolytic graphite using three different orientations of the layer planes relative to the plane of incidence and to the polished reflecting surface. Good agreement was obtained with rough calculations of the reflectance and degree of polarization expected from single crystal graphite, using the known[54] indices of refraction and absorption coefficients.

3.3.7.2. Measurement of Thermal Conductivity

Solutions have been obtained for two mathematical problems related to the heating and cooling of homogeneous bodies in the carbon arc image furnace. One of these concerns the aperiodic cooling of the surface of the

material first heated to the steady-state value in the image furnace and then suddenly cooled by interrupting the furnace radiation. The other problem concerns the temperature variation of the surface of the material during the repetitive heating and cooling periods produced by a rapidly rotating shutter. Both mathematical solutions relate to the well-known cooling of a semi-infinite body in which the temperature change follows a square root of time dependence.

The rate of cooling has been measured for various carbon and graphite materials and used to calculate thermal conductivity at temperatures above 2000°K. The results have shown encouraging agreement with values obtained on the same material obtained by other methods. The arc image furnace method offers the following inherent advantages: (a) uses small specimens (< one cm dimension), (b) requires a short time of measurement (~ one minute), and (c) can be extended to temperatures above 3000°K.

3.3.7.3. Oxidation Studies of Graphite-Base Materials

The carbon arc image furnace has been used, as reported[55] in WADD Technical Report 61-72, Volume XXX, to study the oxidation behavior of graphite-refractory composite materials at high temperatures.

4. DEVELOPMENT

Development studies are classified as: (a) raw materials studies, (b) fabrication studies, and (c) material characterization and evaluation. These studies are outlined further as shown in Table 7.

Table 7. Organization of Development Program on Advanced Graphite Materials

Raw Materials	Fabrication	Material Characterization and Evaluation
1. Process studies in pilot coker.	1. High density recrystallized graphite.	1. Property measurements over a range of temperatures.
2. Binder systems for graphite.	2. Pressure-cured large size graphite.	2. Radiographic techniques.
3. Calcination of raw petroleum cokes.	3. Substrate graphite for coatings.	3. Photomicrographic techniques.
4. Preimpregnation of raw materials.	4. Oxidation resistant coatings and composites.	4. Environmental tests in subscale rocket motor.
	5. Liquid impregnation of graphite.	5. Applications technology.
	6. Fibrous carbon and graphite composites.	
	7. Graphite from pyrolytic processes.	
	8. Special extrusion techniques.	
	9. Carbon and graphite whiskers.	
	10. Carbon and graphite foams.	
	11. Cements for use with carbon and graphite.	

4.1. Raw Materials Studies

The principal development effort on raw materials has been centered on the design, construction, and operation of a pilot-scale delayed coker. The primary purpose of this coker is to carry out process studies and develop petroleum cokes with uniform and controllable properties for use in the fabrication of graphite with improved properties.

Other areas of raw materials investigation have included the study of binder systems, pressure and sulfur calcination of raw petroleum coke, and preimpregnation of raw cokes.

4.1.1. Process Studies in Pilot Coker

One of the biggest problems facing the graphite industry is the inability to control raw materials, especially petroleum cokes, used in the manufacture of carbon and graphite. There are two basic reasons for the lack of control on petroleum cokes. First, cokes are a by-product of petroleum refining and have held little interest for the oil companies. Second, a gap has existed between the smallest commercial coking unit and the laboratory

simulation of such a unit. This gap has made impossible the application of technology obtained from laboratory studies of commercial units. The pilot scale delayed coker, designed to fill this gap, and constructed adjacent to the Marathon Oil Company Refinery at Robinson, Illinois, is unique because it represents the first serious attempt to scale down a continuous coker to an experimental size and still retain the important features of the commercial size units.

A detailed report covering design development, operation, and study of materials from the experimental coker is contained in WADD Technical Report 61-72, Volume XXXVI[56]. This report discusses the engineering concepts of the experimental unit, problems encountered with respect to the design, and recommendations for engineering modifications. The effect of changes in operating conditions of the experimental coker, e.g., time, temperature, pressure, and recycle ratio,on the resultant cokes has been investigated with respect to the physical properties of graphitized, extruded and molded samples. Four basic charge stocks were studied: vacuum residuum, slurry (decant) oil, thermal tar, and a thermal residuum (low sulfur). Variations in bulk density as affected by changes in operating parameters, kerosene density, ash, and sulfur of the cokes are reported. Changes in bulk density, weight and volume losses of the extruded and molded test samples as they are processed from the formed through the baked to the graphitized state are presented. The CTE (coefficient of thermal expansion), specific resistance, and flexural strength of the graphitized plugs both in the with- and across-grain directions are reported as well as the same properties for the with-grain direction of the extruded rods. The variation of coke quality as a function of operating conditions and characteristics of the feed stock is explained.

High coke yields from cracked feed stocks were obtained by operating at high recycle ratios and higher than normal drum pressures. Thermally and catalytically cracked charge stocks have produced cokes yielding fabricated graphites exhibiting low CTE. Super-heated steam introduced into the hot oil stream between the furnace and the coking drum produced a marked effect on coke produced from vacuum residuum. The graphite formed using this coke as filler material was higher in CTE and more isotropic than conventional graphites.

4.1.2. Binder Systems for Graphite

Studies of modified or new binder systems represent another area of effort under the investigation of raw materials. Details of these studies are given in WADD Technical Report 61-72, Volume XXXII[57]. Binder systems were investigated with respect to their thermosetting characteristics both to replace pitch-sulfur combinations presently used in the pressure curing process[58] and to provide binders for development of new graphite grades. The binder systems included (a) prepolymerized furfural alcohol resin[59],

(b) pitch, furfural, furfuryl alcohol combinations, (c) pitch with Lewis Acid catalysts, and (d) pitch with oxidizers such as inorganic persulfates, chlorates, and oxides. Acenaphthylene pitch, a new binder, was investigated with regard to thermosetting properties when used in the pressure curing process.

These binder systems were used in the fabrication of graphite articles and property determinations were made on the finished graphites. The measurements[57] include strength, coefficient of thermal expansion, resistivity, and Young's modulus. Bulk densities are also reported for as-formed, baked, and graphitized blocks.

The binder modifications or systems investigated have produced no outstanding advantages over the pitch-sulfur system for use in the pressure curing process. The most promising of the new systems was pitch combined with oxidizing agents other than sulfur which produced a thermosetting binder of high coking value and which was comparable to the pitch-sulfur binder in other properties. The pitch-oxidizer system has the added advantage of eliminating sulfur, hydrogen sulfide, and sulfur dioxide fumes which are present during the curing of the pitch-sulfur system. The other combinations investigated generally resulted in a degradation of graphite properties when compared with pitch-sulfur binder, primarily due to the lack of thermosetting qualities. Some of these binder systems, however, should be investigated for use in processes other than pressure curing where thermosetting of the binder is not required.

4.1.3. Calcination of Raw Petroleum Cokes

Raw petroleum cokes were calcined (heat treated) to temperatures above 1000°C to remove the volatile hydrocarbon and to effect a shrinkage of the filler material before incorporation into the formed graphite article. Two methods of calcining raw petroleum cokes have been investigated and compared to standard calcination. These two methods were pressure calcination and sulfur calcination (the addition of elemental sulfur to the raw coke prior to calcining).

4.1.3.1. Pressure Calcination

The use of mechanically applied pressure during calcination of raw petroleum cokes effected a more ordered structure as evidenced by CTE and specific resistance measurements. Puffing of bulk graphites made from pressure calcined cokes was less than for those made from standard calcined cokes. Details of the pressure calcination trials are given in Appendix III.

4.1.3.2. Sulfur Calcination

The addition of sulfur to petroleum coke before calcination was effective in producing a needle-like structure and reducing the with-grain CTE and puffing characteristics of the coke. Sulfur calcination trials are reported in detail in Appendix III.

4.1.4. Preimpregnation of Raw Materials

Standard petroleum coke was pitch impregnated in the calcined or lump form followed by a recalcination to 450°C. The investigation was made in an effort to improve physical properties of bulk graphite using the impregnated coke as filler material and there were several reasons why improvement was expected. First, impregnation of the coke particles before using them as filler material in carbon mixes should be more effective than impregnation of the formed carbon or graphite block for increasing density. Second, calcination of the coke to 450°C after pitch impregnation and subsequent addition of raw or uncalcined pitch during the mixing operation should result in a higher effective binder concentration than can be attained by conventional processes. Third, mixes made from calcined impregnated cokes, in spite of their higher effective pitch level, have less volatile content because part of the volatile was driven off during the 450°C calcination of the coke. These coke mixes, because of the lower volatile content, might be successfully formed by the pressure curing process[58] which has been limited to the use of graphite filler materials.

Preliminary investigation of the preimpregnation of raw materials has been made and details are discussed in Appendix IV. The investigation was limited in scope; however, encouraging results were obtained using pitch impregnated coke filler material with the pressure curing process. These results indicated an increase in bulk density and flexural strength and a decrease in specific resistance of the graphitized piece.

4.2. Fabrication Studies

The areas of investigation concerning fabrication of bulk carbon and graphite materials were numerous. The field of application for these materials is being expanded and it is necessary to develop new and improved graphites to cover a wide range of physical properties. For example, there is a need for graphites that are relatively isotropic or extremely anisotropic, as well as a need to control density, thermal conductivity, thermal expansion, electrical resistivity, porosity, and permeability of graphites. When used as a structural and aerospace material, graphite is required to have increased resistance to thermal shock, erosion, and oxidation, as well as increased strength.

Some of the areas covered in these fabrication studies were hot forming techniques, pressure curing processes, impregnation investigations, oxidation resistant composites and coatings, and bulk graphite shapes made from carbon or graphite fibrous materials.

4.2.1. High Density Recrystallized Graphite (ZT Grades)

Three WADD Technical Reports 61-72, Volume VII[60], Supplement to Volume VII[61] and Volume XXXIII[62], describe the initial research and development work on ZT graphite, scale up from 14-inch to 30-inch diameter sizes, and investigations of the ZT processing effect on raw materials.

ZT graphites are high density materials formed by a hot working process which results in a highly oriented structure, intermediate in physical properties between premium quality graphites, such as Grade ATJ and pyrolytic. The ZT family of graphites, and more specifically Grade ZTA, has been tested in subscale solid fuel rocket motors and extensively evaluated for physical properties. ZT graphite can be produced with bulk densities up to 2.2 g/cc having impurity levels of less than 0.2 per cent.

4.2.2. Pressure-cured Large Size Graphite

A primary requirement for graphites used in aerospace applications is uniformity of properties both within a single piece and from piece-to-piece, and the ability to produce such materials in relatively large sizes without compromise of physical properties. The pressure curing produced materials with such improvements.

4.2.2.1. Large Diameter Fine-Grain Graphites

WADD Technical Report 61-72, Volume XII[58], describes the development of a pressure curing process, based on a thermosetting binder system, that produces a fine-grain graphite in sizes up to 30 inches in diameter. This graphite, designated Grade RVA, possesses one-half to one-third the physical property variation, both within a piece and from piece-to-piece, normally associated with quality industrial graphites such as Grade ATJ. Grade RVA is nominally characterized by a bulk density of 1.85 g/cc, room temperature with- and against-grain flexural strengths of 3,700 and 2,900 lbs/in^2, and elastic moduli of 1.7 and 1.3 x 10^6 lbs/in^2.

Another report, WADD Technical Report 61-72, Supplement to Volume XII[63], covers the continuation of development work on large diameter Grade RVA graphite.. The extension work consisted primarily of producing and evaluating raw materials for use as the inert filler in RVA blends. Significant properties of raw materials, as they affect the final properties of Grade RVA, were the total porosity and kerosene apparent density. The more porous and dense raw materials imparted higher strength and higher bulk density, respectively, to fully processed Grade RVA sections.

4.2.2.2. Ultra Fine-Grain Graphite of Large Diameter

The pressure curing process discussed in Section 4.2.2.1 has provided a large diameter fine-grain graphite (RVA) with better uniformity of properties than previously attained. This graphite, although of finer grain than materials heretofore produced in this size, incorporates some coke particles rather than all-coke flour in the filler blend. The coke particles (or graphite particles in the finished graphite) are of no concern in most applications considering the use of RVA grade; however, the particles can contribute to an erosion rate which is higher than desired in the throat of some specific rocket nozzles.

A program to develop and scale up a pressure-cured graphite grade of finer grain than RVA was undertaken and is reported in WADD Technical

Report 61-72, Volume XXXVIII[64]. This grade, designated RVD, is an extremely fine-grain graphite formed by the pressure curing of an all-flour blend and is characterized by a typical density of 1,87 g/cc and nominal flexural strengths of 4,700 and 3,100 lbs/in^2 with- and across-grain, respectively.

The development, fabrication, and physical properties of 18-inch diameter by 15-inch long Grade RVD graphite (development Grade RT-0008) and an attempted scale-up to 33-inch diameter sizes are covered in this report. Grade RVD graphite tested in the nozzle of a subscale rocket motor showed a relatively low erosion rate and high thermal shock resistance.

4.2.2.3. Induction Heating for Pressure Curing

The process for the fabrication of RVA grade graphite (as discussed in Section 4.2.2.1) is based on the use of a thermosetting binder and curing of this binder under heat and pressure. Heating to thermally set the binder is presently achieved by passing an electrical current through the mass. Resistance heating is readily adaptable to the pressure curing process for 30-inch diameter by 40-inch long graphite sections; however, as the diameter of the stock increases, the size and capacity of the electrical transformer required to supply the current necessarily increases. As size is increased, a point will be reached where resistance heating will not be feasible from a power requirement standpoint; therefore, another method must be employed to pressure cure very large sizes (e.g., approximately 100-inch diameter). In selecting an alternate heating method for pressure curing large diameters, one is restricted to a large bulk volume heating method. Under this requisite the only available heating method to be considered is low frequency induction heating. A program to develop methods of adapting induction heating to the pressure curing process was undertaken and the details are reported in Appendix V.

4.2.3. Substrate Graphite for Coatings

In some applications, the use of the unique high temperature properties of graphite is handicapped by oxidation which occurs at relatively low temperatures. The need for high temperature structural materials in the development of hypersonic aircraft, reentry vehicles, and other applications has resulted in considerable attention to means of protecting graphite from oxidation at relatively high temperatures. The differences between the thermal expansion characteristics of graphite and those of oxidation protective coatings have presented a major problem. A program was undertaken to tailor a graphite substrate material to match the thermal expansion of an oxidation resistant coating (silicon carbide) and to do this in useful sizes.

The work under this graphite substrate development program is reported in WADD Technical Report 61-72, Volume XIII[65], and in Supplement to Volume XIII[66]. The first report describes the development, fabrication, and physical properties of Grade RVC graphite (formerly designated as

experimental Grade RT-0029). Grade RVC has been fabricated in sizes up to 18 inches in diameter by 15 inches in length and is nominally characterized by a bulk density of 1.81 g/cc, an admittance to N_2 of 2×10^{-2} and 6×10^{-3} cm^2/second with- and against-grain, respectively, and a room temperature flexural strength with- and against-grain of 2,560 and 1,930 lbs/in^2. RVC is an excellent substrate material for silicon carbide coatings because its mean thermal expansion between 400° and 100°C is approximately 5×10^{-6}/°C in both grain directions. This expansion is in the same range as that for silicon carbide. Results are also presented on high temperature oxidation of silicon carbide coated RVC grade specimens. The unusually good oxidation protection afforded the graphite by the coating demonstrated the marked superiority of this substrate over other graphite materials which do not match the silicon carbide in thermal expansion.

Supplement to Volume XIII covers the characterization of Grade RVC graphite and describes process and blend variations which have been studied in the fabrication of substrate graphites since the writing of WADD Technical Report 61-72, Volume XIII. These trials indicated that a forming pressure of 900 lbs/in^2 instead of the 1,000 lbs/in^2 normally used increased the yield of Grade RVC and did not significantly change its characteristics. Studies also showed that various other blends produced a substrate graphite suitable for silicon carbide coating.

4.2.4. Oxidation Resistant Graphites

The effort to add oxidation resistance to the many other desirable high temperature properties of graphite has been extended beyond the tailoring of substrate materials as described in Section 4.2.3. The work in this category can be divided into two parts: (a) oxidation protection of graphite by coatings (in addition to silicon carbide), and (b) oxidation resistance afforded by various materials added to the graphite during fabrication.

4.2.4.1. Oxidation Resistant Coatings

The oxidation protection afforded graphite by different types of coatings applied by various methods is reported in WADD Technical Report 61-72, Volume XXXIV[67], which is composed of four sections as follows:

(a) Section 1 presents theoretical and general considerations of protective coatings for graphite.

The list of refractory materials which might be used for high temperature oxidation resistant coatings for graphite is reviewed. A coating applied to graphite must be able to withstand extreme chemical attack from both sides. The ability to resist the strongly reducing tendencies of carbon on one side and an oxidizing atmosphere on the other was not found in many refractory materials even at moderately high temperatures. Above 2000°C, one material, beryllium oxide, appeared to satisfy these requirements.

It was shown that several groups of materials such as the refractory metals, borides and carbides rendered a coating system thermodynamically

stable when placed between an oxidation-resistant outer coating and the graphite substrate. This multiple layer coating scheme theoretically allows graphite to be used in oxidizing environments at very high temperatures. Calculations were made showing that with properly selected intermediate reaction barriers many very refractory oxides, such as thoria, can be used as coatings at temperatures up to their melting points.

The methods of applying coatings to graphite are also discussed.

(b) Section 2 describes plasma arc deposition of coatings for graphite.

Titanium diboride, hexaboron silicide, and the zirconates of magnesium and calcium were plasma-sprayed on graphite to evaluate their effectiveness in providing oxidation resistant coatings.

All coatings were tested at temperatures between 1200 and 2200°C. TiB_2 at these temperatures readily converted to TiO_2 which reacted with the graphite to form CO. The pressure of the CO combined with the volumetric change which took place with the reaction, created stresses that ruptured the coating; the protection afforded by TiB_2 was limited to a few minutes above 1200°C.

B_6Si as sprayed on graphite offered very poor oxidation resistance. When heat treatment of the coated sample was employed prior to oxidation, a mixture of B_4C and βSiC was formed. Heat treated B_6Si then afforded essentially the same protection as SiC coatings prepared by vapor deposition through diffusion.

Calcium zirconate sprayed over an intermediate layer of tungsten provided oxidation protection for graphite up to 20 minutes at 1900°C but, because of the large CTE differential existing between the graphite and zirconates, both the calcium and magnesium zirconate coatings invariably ruptured during cooling.

(c) Section 3 describes protective coatings applied on graphite by a vapor deposition process.

The coating systems which showed the best oxidation resistance at high temperatures were TiC-TiN and SiC-Si. Oxidation resistance of a 0.95 mm coating of TiC-TiN was shown to protect graphite from oxidation for 41 hours at 1000°C and 9.4 hours at 1200°C when the test specimen was heated externally. A 0.34 mm thickness provided protection for 1.4 hours at 1600°C under the same conditions. Effective protection by these coatings was substantially less at each test temperature when the test specimen was resistance heated.

SiC-Si coatings provided oxidation protection for graphite to higher temperatures for longer times than coatings heretofore reported. The mechanism of protection, formation of an SiO_2 surface, is identical to that offered by silicon carbide coatings but the oxidation protection was greater. Oxidation tests by electric resistance heating showed that graphite articles coated

with SiC-Si were unattacked at 1700°C during standard 5-hour exposures; several specimens exhibited similar protection at 1750° and 1800°C. Above 1700°C, however, a few samples showed a tendency toward rapid coating disintegration. These failures were prevented to a large extent by preoxidizing the samples at lower temperatures.

(d) Section 4 describes the protective coatings for graphite applied by vapor deposition through pack diffusion.

Vapor diffusion is a simple method of providing graphite with an oxidation resistant SiC coating. The process consists of enclosing the graphite article in a pack composed of a powdered blend of silicon and filler material and heating the pack to a temperature near 2000°C.

The filler permits removal of the graphite article from the pack after processing since it separates the regions of molten silicon representing the vapor source. The filler must not melt at the process temperature and must neither react with nor be wetted by molten silicon. SiC appeared to be the most economical and most suitable choice of a number of materials evaluated as fillers.

4.2.4.2. Oxidation Resistant Composites

Hot pressing techniques have been used for fabricating composites of graphite and the refractory hard metals. Development of an oxidation resistant graphite base body was the immediate objective of this work. This family of materials should offer promise for such applications as nozzles for use with the more oxidizing fuels and as airframe components, such as leading edges and nose cones.

The work performed with regard to these composites is covered in WADD Technical Report 61-72, Volume XXX[68], which describes certain graphite-base composites capable of resisting oxidation by forming a protective coating from their oxidation products. When first exposed to oxidizing conditions, the additives or graphite-additive reactants oxidize and form a coating which protects the composite against further oxidation. These composites have an advantage over coatings applied to graphite surfaces, since the former are homogeneous materials and can be machined without destroying their oxidation resistant characteristics. The composites under conditions of erosion continuously re-form the protective coating.

The most effective additives investigated were combinations of ZrB_2, Si, B, Nb, and Th. The report also describes the equipment required to fabricate graphite-refractory composites by hot pressing at temperatures up to 3100°C. Oxidation test methods employed indirect induction heating, resistance heating, arc image furnace techniques, and electromagnetic levitation.

4.2.5. Liquid Impregnation of Graphite

Impregnation of carbon and graphite bodies with a carbonaceous material (such as coal tar pitch) as a means of increasing density and strength, and reducing permeability has been a standard practice in industry for years. Considerable effort has been expended recently on impregnation of graphite with materials other than tar or pitch for the purpose of obtaining very low permeability. These materials are primarily thermosetting resin systems which deposit a high percentage of carbon upon heat treatment to at least 800 °C.

Development work covering liquid impregnation of graphites is reported in WADD Technical Report 61-72, Volume XXXI[69], which discusses various materials used as impregnants, techniques for impregnating and subsequent heat treatment to convert these liquids to coke or graphite within the pores of the base stock. Impregnation procedures and base stock structure affect the physical properties, particularly the density, strength, and porosity of impregnated graphite. These physical properties are related to the performance of nozzle inserts in solid propellant rocket motors, e.g., density and strength influence mechanical erosion (Section 4.3.4) and porosity influences chemical erosion (Section 4.3.5.2).

4.2.6. Fibrous Carbon and Graphite Composites

National Carbon Company introduced graphite cloth to the field of commercially available graphites several years ago. More recently carbon cloths, as well as carbon and graphite felts and yarns were introduced. The individual fibers of these materials are of high purity, quite flexible and have tensile strengths up to 150 times those of standard commercial graphites. The fibrous materials form the basis for a new series of bulk graphite bodies fabricated by laminating layers of cloth or felt with a graphitizable binder or by macerating the cloth or felt and using this as the filler material with a suitable binder. The development of bulk fibrous composites was divided into three work areas:

1. Determination of the forming variables and processing parameters;
2. Characterization of these materials, and
3. Fabrication of subscale and prototype hardware for testing.

The development of fibrous carbonaceous composites and laminates has been described in WADD Technical Report 61-72, Volume IX[70], in which the evaluation of graphite, carbon, and heat treated cloth as well as graphite and carbon felts as filler materials is discussed. Physical properties of the carbonized and graphitized forms of these composites are tabulated. Potential applications and results of the testing of these materials in missile components are presented.

4.2.7. Graphite from Pyrolytic Processes

Work on pyrolytic or vapor-deposited graphites under this contract has been limited to mechanism studies and is reported in WADD Technical Report

61-72, Volume XXXVII[71]. Methods of depositing high quality pyrolytic graphite are described with evidence as to the cause of conical growths and delaminations within the structure of the material. Results are presented on the use of hydrogen, helium, and argon as diluents, and on the use of chlorine as an additive in the pyrolytic process. The mean deposition rate is shown to be a function of hydrocarbon concentration, gas velocity, temperature, and pressure. Theoretical studies of the equilibrium composition of methane as affected by changes in temperature and pressure are presented along with cracking temperature curves for various fluoromethanes.

Feasibility studies on the production of graphite by carbon vapor deposition were conducted which indicate that nonlamellar graphite with a predetermined degree of anisotropy can be produced by this method.

Room temperature pull strength of graphite yarn has been increased as much as 360 per cent by reinforcement of the yarn with thin coatings of pyrolytic carbon; both single and multiple strand yarns have been coated.

4.2.8. Special Extrusion Techniques

A method (described in Appendix VI) was investigated for fabricating graphite by extrusion through an expansion-reduction die section and a mechanical back pressure was applied to the carbon mix as it was being forced through the die. The objective of the experiment was to form bulk graphite by extrusion which would have the grain orientation typical of molded grades; i.e., the layer planes normal to the direction of extrusion. The studies indicated that it should be possible to form graphite sections larger than the diameter of the extrusion equipment mix chamber and to produce the desired grain orientation.

4.2.9. Carbon and Graphite Whiskers

Carbon and graphite whiskers have been produced under two conditions: (a) during the hot working process[62], and (b) during the calcination of coke from the experimental delayed coker[56]. Although in both cases the whiskers were "discovered" they have since been reproduced several times. Tensile strengths of these whiskers have been measured to almost 200,000 lbs/in^2. Details of the "discovery" and fabrication of these whiskers are given in Appendix VII.

4.2.10. Carbon and Graphite Foams

A limited investigation was made regarding the feasibility of fabricating carbon and graphite foamed materials. Foams would provide a solid form of insulating material having low density, low thermal conductivity, and high temperature stability. Urethane base foams were both carbonized and graphitized in relatively small sizes with a bulk density of approximately 0.3 g/cc and flexural strengths up to 700 lbs/in^2. A detailed discussion of these feasibility studies is contained in Appendix VIII.

4.2.11. Cements for Use with Carbon and Graphite

Many of the aerospace applications for carbon and graphite require special sizes or configurations which cannot be obtained from a monolithic piece of material. A limited effort was applied to the development of a cement to be used with graphite. A standard carbonaceous cement (National Carbon Company C-9 grade) was compared with an experimental cement (TS-341) made from finely divided titanium diboride and a binder. The TS-341 produced superior strengths at temperatures above 1650°C. Details of the investigation are given in Appendix IX.

4.3. Material Characterization and Evaluation

The use of carbon and graphite in the aerospace industry has brought about the need for extensive characterization and evaluation. It has become necessary to measure physical properties of graphite over a wide range of temperatures in order to supply engineering data. Other information, in addition to the commonly measured physical properties, is required for predicting the performance and design of graphite for use in aerospace applications. The latter information includes resistance to mechanical and chemical erosion by exhaust gases under conditions of use in a rocket nozzle throat, compatibility with other materials, such as insulations, metals, and plastics, and with propellant combustion products. Nondestructive methods of determining the structural integrity of graphites are essential for establishing reliability figures.

The areas covered under this section are: (a) a survey of physical properties of new graphite materials measured over a range of temperatures, (b) radiographic examination for locating flaws in graphite, (c) special techniques required for micrographic studies, and (d) evaluation of graphites in a subscale solid propellant rocket motor. Each of these areas is the topic for one or more WADD Technical Reports and consequently details are not given here.

Applications Technology contact has been maintained with many of the principal governmental agencies and contractors in the aerospace field and a discussion of these contacts is presented in this section.

4.3.1. Graphite Properties over a Range of Temperatures

The characterization of materials developed under this advanced graphite materials program is presented in WADD Technical Report 61-72, Volume XXVI[72]. The physical properties are presented for eighteen new graphite grades, developed or evaluated under this program, which include seven high density, recrystallized graphites designated at ZT grades[60, 61]; six graphites in which the fillers are shredded or woven carbonized cloths designated as PT grades[70]; and five pressure-cured and/or impregnated grades identified as RVA[58, 63], RVC[65, 66], CFZ[69], CFW[69], and RVD[64]. Similar properties of ATJ graphite are presented as a basis for comparing the newly developed grades with one well-known grade.

Properties measured only at room temperature include bulk density, electrical resistivity, thermal conductivity, flexural strength (modulus of rupture) and permeability or admittance, whichever is applicable; per cent ash and representative pore size spectra are included. Density profiles are shown for ZTA and RVA grades. Short-time ultimate compressive strength data are presented for all grades at room temperature and for several grades at elevated temperatures. Short-time ultimate tensile and shear (clevis method) strengths and representative stress-strain curves in tension, compression and shear at room and elevated temperatures are presented for a number of grades. Young's modulus of elasticity (sonic method) and thermal expansion data at room and elevated temperatures are given for all grades.

Methods and equipment for measuring physical properties at elevated temperatures are discussed in two technical reports, WADD Technical Report 61-72, Volumes XXXV[73] and XXIII[74]. The first of these reports describes procedures and equipment for the measurement of various mechanical properties of graphite in the temperature range from 20° to 2700°C. Measured properties include the short-time ultimate tensile, compressive and shear strengths of graphite and the stress-strain relationship in tension, compression and shear. A method for the measurement of Poisson's ratio at room and elevated temperatures is also discussed. The second of these two reports presents a vibrational or sonic method for determining the elastic modulus of graphite to temperatures of 3000°C. The theory as well as working equations are provided and limitations and assumptions are discussed with reference to other methods of measurement. The apparatus and procedures are described in detail.

4.3.2. Radiographic Techniques for Examination of Graphite

Nondestructive examination of graphite to determine its structural integrity is imperative to aerospace applications for both reliability and economic considerations. X-ray radiographic examination appears to be the most useful of several available methods. The development of special equipment and techniques for the radiographic inspection of large size graphite blocks as well as for multi-thickness shapes are described in WADD Technical Report 61-72, Volumes IV[75] and XVII[48]. These reports discuss radiation characteristics of industrial X-ray units, intensifying action of fluorescent screens, scanning techniques, radiographic sensitivity and the preparation of X-ray exposure charts for use with graphite.

4.3.3. Photomicrographic Techniques for Examination of Graphite

Investigation of the microstructure of formed carbon and graphite materials is essential not only to the development of new grades but also to understanding the behavior of the materials in various applications. Standard metallographic equipment can be used for such studies; however, carbon and graphite materials require special preparation for photomicrographic examination. Vacuum impregnation of the sample with monomeric styrene followed by polymerization at elevated temperature prevents smearing during grinding and polishing. Mounting the sample in Lucite after polymerization of the styrene prevents the latter from cracking during final sample preparation.

Samples are ground on 100, 320 and 500 grit diamond wheels and successively polished with Beuhler microcloth saturated with aqueous suspensions of silicon carbide, Linde Grade A alumina and Linde Grade B alumina.

Filtered bright-field, polarized light, sensitive tint, and dark-field illuminations are all useful in revealing and interpreting microstructure. The selection of proper photographic film and plates, developer and printing paper is important in providing pertinent details in the final photomicrograph.

The special techniques required for effective photomicrographic examination of carbon and graphite materials are described in detail in WADD Technical Report 61-72, Volume XXII[76].

4.3.4. Environmental Tests in Subscale Rocket Motors

Full-scale static tests of large solid propellant rocket motors are extremely expensive. Carbon and graphite materials, therefore, must be tested under subscale environmental conditions before they can be accepted for these full-scale static tests. The subscale tests are also useful in delineating graphite development programs. A solid propellant rocket motor was installed by National Carbon Company to perform these subscale tests. The motor and various propellants used were designed and fabricated by the Atlantic Research Corporation.

A detailed discussion of the subscale rocket motor is contained in WADD Technical Report 61-72, Volume XXIX[77] and Supplement to Volume XXIX[78]. These two reports present the propellant type, firing conditions, and materials performance characteristics for each of sixty-six static test firings. Each firing report is complete with photographs of the nozzle materials after firing and shadowgraphs showing the throat size and configuration before and after testing. All types of graphitic materials were tested, including standard grades, high density graphites, impregnated grades, fibrous composites, and oxidation resistant graphite-base composites. These materials were evaluated in nozzle insert, insert backup, entrance cap, exit cone and blast tube applications. In many instances the information was valuable in guiding the next logical step in a graphite improvement program.

The subscale firings indicated that erosion of the graphite decreased as the graphite bulk density increased. Various types of impregnations also decreased erosion without drastically increasing density, especially with the carbon or graphite cloth composites. The erosion pattern of graphite was affected by the maximum particle size of the filler material, with the fine-grain graphites presenting the more smoothly eroded surface. Graphites of somewhat coarser grain were less subject to thermal stress failure.

4.3.5. Applications Technology

A research and development program such as this is more effective when there is good communication between the laboratories performing the research and development work and the agencies or contractors expecting to use the materials and knowledge from the program.

The objective of the Applications Technology effort has been to maintain contact with interested elements of the Department of Defense and other governmental agencies and their contractors so as to (a) provide guidance for the research and development program in developing graphitic materials tailored to meet future requirements, (b) expedite awareness of improved materials developed under this program, and (c) coordinate the evaluation of materials from this program at other locations.

4.3.5.1. Cooperative Programs

A program of continuous technical consultation has been carried out with the principal contractors and governmental agencies involved in solid propellant propulsion and space vehicle systems. Technical consultation has been maintained not only with agencies and contractors within the Air Force program, but also with Navy, Army, and NASA programs on an equal interest basis.

Oral reviews of the progress of this program have been given to interested parties. To assist in the overall guidance of the program, personnel responsible for materials development and hardware design have been encouraged to define their graphite requirements in terms of specific properties.

Cooperative programs for evaluation of materials have been arranged with numerous contractors and agencies in line with their interests and requirements. All available data required for design and test have been provided, and although a large amount of evaluation is still in progress, in many cases the required evaluation is available in the progress reports regarding the individual projects. Fifteen hundred samples of various types of material have been provided to seventy-two contractors and agencies. Changing objectives and requirements, personnel changes, project scheduling and individual company interests among the contractors and agencies, in many cases, have made it difficult to obtain test and evaluation information from those receiving sample materials. In spite of prior arrangements for return of information in all cases, complete meaningful data was received for less than fifty per cent of the specific evaulations. Detailed reports giving all test conditions, comparison of sample material performance versus other candidate materials, and recommendations for future needs were available in relatively few cases. For these reasons as well as the slightly different conditions of test and evaluation from one location to another, a rigorous analysis of data received is not possible. The information obtained was quite valuable however in establishing the general guidelines for direction of the research and development effort.

5. LIST OF REFERENCES

1. WADD Technical Report 61-72, Volume X and Supplement to Volume X, Thermal Reactivity of Aromatic Hydrocarbons, by I. C. Lewis and T. Edstrom.

2. Boersma, S. L., J. Amer. Ceramic Soc. 38, 8, 281-284 (1955).

3. WADD Technical Report 61-72, Volume XVI, An Electron Spin Resonance Study of Thermal Decomposition Reactions of Organic Compounds, by L. S. Singer and I. C. Lewis.

4. L. S. Singer and G. Wagoner, J. Chem. Phys. 37, 1812 (1962).

5. WADD Technical Report 61-72, Volume XXVII, Carbonization Studies of Aromatic Hydrocarbons, by I. C. Lewis and T. Edstrom.

6. WADD Technical Report 61-72, Volume XXVIII, Polarographic Reduction of Polynuclear Aromatics, by I. C. Lewis, H. Leibecki, and S. L. Bushong.

7. WADD Technical Report 61-72, Volume XI, Characterization of Binders Used in the Fabrication of Graphite Bodies, by E. de Ruiter, A. Halleux, V. Sandor, and H. Tschamler, and Supplement to Volume XI, by E. de Ruiter, J. F. M. Oth, V. Sandor, and H. Tschamler.

8. WADD Technical Report 61-72, Volume XV, Alumina-Condensed Furfuryl Alcohol Resins, by C. W. Boquist, E. R. Nielsen, H. J. O'Neil, and R. E. Putcher.

9. WADD Technical Report 61-72, Volume XL, Bonding Characteristics of Certain Synthetic Binders, C. W. Boquist, H. J. O'Neil, R. E. Putcher, and A. Dynako.

10. WADD Technical Report 61-72, Volume XXXII, Studies of Binder Systems for Graphite, by T. Edstrom, I. C. Lewis, R. L. Racicot, and C. F. Stout.

11. G. R. Hennig, "Interstitial Compounds of Graphite", Progress in Inorganic Chemistry, Volume 1, Interscience Publishers, New York (1959).

12. W. Rudorff, "Graphite Intercalation Compounds", Advances in Inorganic Chemistry and Radiochemistry, Volume I, Academic Press, New York (1959).

13. F. M. Collins, "Dimensional Changes During Heat-Treatment and Thermal Expansion of Polycrystalline Carbons and Graphite",

Proceedings of the First and Second Conference on Carbon, University of Buffalo, The Waverly Press, Inc. (1956).

14. C. Baraniecki, H. L. Riley and E. Streeter, "The Solid Complexes of Carbon with Oxygen, Nitrogen, and Sulfur", Report of the Conference on Industrial Carbon and Graphite held in London, September 24-26, 1957, published by Society of Chemical Industry (1958).

15. WADD Technical Report 61-72, Volume XXV, Lamellar Compounds of Non-Graphitized Petroleum Coke, by H. F. Volk.

16. G. Wagoner, Phys. Rev. 118, 647 (1960).

17. J. W. McClure and Y. Yafet, "Theory of the g-Factor of the Current Carriers in Graphite Single Crystals", Proc. Fifth Carbon Conf., Volume 1, Pergamon Press (1962), p. 22.

18. WADD Technical Report 61-72, Volume VIII, Electron Spin Resonance in Polycrystalline Graphite, by L. S. Singer and G. Wagoner.

19. A. R. Ubbelohde, Nature 180, 380 (1957).

20. WADD Technical Report 61-72, Volume XXXIX, Diamagnetic Susceptibility of Graphite by the Faraday Method, by D. E. Soule and C. W. Nezbeda.

21. WADD Technical Report 61-72, Volume XX, The Electric and Magnetic Properties of Pyrolytic Graphite, by G. Wagoner and B. H. Eckstein.

22. J. W. McClure, Phys, Rev. 104 666 (1956).

23. J. W. McClure, Private communication.

24. D. E. Soule, "The Effect of Boron on the Electronic Properties of Graphite". Proc. Fifth Carbon Conf., Volume 1, Pergamon Press (1962), p. 13.

25. M. L. Dzurus and G. R. Hennig, J. Chem. Phys. 27, 275 (1957).

26. WADD Technical Report 61-72, Volume I, Observations by Electron Microscopy of Dislocations, by R. Sprague.

27. WADD Technical Report 61-72, Volume III, Decoration of Dislocations and Low Angle Grain Boundaries in Graphite Single Crystals, by R. Bacon and R. Sprague.

28. J. D. Eshelby, W. T. Read, and W. Schockley, Acta Met. 1, 251 (1953).

29. WADD Technical Report 61-72, Volume II, Applications of Anisotropic Elastic Continuum Theory to Dislocations in Graphite, by G. B. Spence.

30. Reference 29, pp. 13-15.

31. I. M. Dawson and E. A. C. Follett, Proc. Roy. Soc. A253, 390 (1959).

32. Private communication.

33. E. Kováts, H. H. Günthard, and P. A. Plattner, Helv. Chim. Acta 38, 1912 (1955).

34. C. E. Lowell, unpublished results.

35. See for example W. L. Miller and A. R. Gordon, J. Phys. Chem. 35, 2785 (1931) or B. Lohmander and S. Rittsten, Kgl, Fysiograf. Sällskap. i Lund, Förh 28, 45 (1958).

36. WADD Technical Report 61-72, Volume XXIV, The Thermal Expansion of Graphite in the c-Direction, by C. E. Lowell.

37. WADD Technical Report 61-72, Volume XLI, Survey and Analytical Representation of the Measurements of the Specific Heat of Graphite, by G. B. Spence.

38. H. S. Carslaw and J. C. Jaeger, 2nd, Edition, "Conduction of Heat in Solids," Oxford University Press (1959).

39. WADD Technical Report 61-72, Volume V, Analysis of Creep and Recovery Curves for ATJ Graphite, by E. J. Seldin and R. N. Draper.

40. WADD Technical Report 61-72, Volume VI, Creep of Carbons and Graphites in Flexure at High Temperatures, by E. J. Seldin.

41. WADD Technical Report 61-72, Volume XVIII, High Temperature Tensile Creep of Graphite, by E. J. Seldin.

42. WADD Technical Report 61-72, Volume XXXVII, Studies of Graphite Deposited by Pyrolytic Processes, by P. H. Higgs, R. L. Finicle, R. J. Bobka, E. J. Seldin, and K. J. Zeitsch.

43. M. Reiner, Deformation and Flow, H. K. Lewis and Co. Ltd., London, (1949).

44. J. F. Andrew, J. Okada, and D. C. Wobschall, Elastic Constants and Permanent Set in Carbons and Graphite at Room Temperature, Proceedings of the Fourth Conference on Carbon, pp. 559-575, Pergamon Press (1960).

45. H. H. W. Losty and J. S. Orchard, The Strength of Graphite, Proceedings of the Fifth Conference on Carbon, Volume I, p. 519-532, Pergamon Press (1962).

46. WADD Technical Report 61-72, Volume XIX, Thermal Stresses in Anisotropic Hollow Cylinders, by Tu-Lung Weng.

47. WADD Technical Report 61-72, Volume XIV, Study of High Temperature Tensile Properties of ZTA Grade Graphite, by R. M. Hale and W. M. Fassell, Jr.

48. WADD Technical Report 61-72, Volume XVII, Radiography of Carbon and Graphite, by T. C. Furnas, Jr. and M. R. Rosumny.

49. WADD Technical Report 61-72, Volume XXI, Arc Image Furnace Studies on Carbon and Graphite Materials, by M. R. Null and W. W. Lozier.

50. M. R. Null and W. W. Lozier, Rev. Sci. Instr. 29, 163 (1958).

51. WADC Technical Report 59-789, Development of Graphite and Graphite-Base Multicomponent Materials for High Temperature Service, by W. W. Lozier.

52. J. D. Plunkett and W. D. Kingery, Proceedings of the Fourth Conference on Carbon (Pergamon Press) New York, (1960), pp. 457-472.

53. A. F. Grenis and A. P. Levitt, Watertown Arsenal Technical Report No. WAL TR 851.2/1, May (1962).

54. J. T. McCartney and S. Ergun, Fuel 37, 272 (1958).

55. WADD Technical Report 61-72, Volume XXX, Oxidation-Resistant Graphite-Base Composites, by K. J. Zeitsch and J. Criscione.

56. WADD Technical Report 61-72, Volume XXXVI, Studies of the Quality of Petroleum Coke from a Pilot Scale Delayed Coker, by C. F. Stout, M. Janes and J. A. Biehl.

57. WADD Technical Report 61-72, Volume XXXII, Studies of Binder Systems for Graphite, by T. Edstrom, I. C. Lewis, R. L. Racicot and C. F. Stout.

58. WADD Technical Report 61-72, Volume XII, Development of an Improved Large Diameter Fine-Grain Graphite for Aerospace Applications, by C. W. Waters and E. L. Piper.

59. WADD Technical Report 61-72, Volume XV, Alumina Condensed Furfuryl Alcohol Resins by C. W. Boquist, E. R. Neilsen, H. J. O'Neil and R. E. Putcher.

60. WADD Technical Report 61-72, Volume VII, High Density Recrystallized Graphite by Hot Forming, by E. A. Neel, A. A. Kellar and K. J. Zeitsch.

61. WADD Technical Report 61-72, Supplement to Volume VII, High Density Recrystallized Graphite by Hot Forming, by G. L. Rowe and M. B. Carter.

62. WADD Technical Report 61-72, Volume XXXIII, Investigation of Hot Worked, Recrystallized Graphites, by J. H. Turner and M. B. Carter.

63. WADD Technical Report 61-72, Supplement to Volume XII, Development of an Improved Large Diameter Fine-Grain Graphite for Aerospace Applications, by R. L. Racicot and C. W. Waters.

64. WADD Technical Report 61-72, Volume XXXVIII, Development of an Improved Large Diameter Ultra Fine-Grain Graphite, by R.A. Howard and R. L. Racicot.

65. WADD Technical Report 61-72, Volume XIII, Development of a Fine-Grain Isotropic Graphite for Structural and Substrate Applications, by R. A. Howard and E. L. Piper.

66. WADD Technical Report 61-72, Supplement to Volume XIII, Development of a Fine-Grain Isotropic Graphite for Structural and Substrate Applications, by R. A. Howard and R. L. Racicot.

67. WADD Technical Report 61-72, Volume XXXIV, Oxidation Resistant Coatings for Graphite, by D. A. Schulz, P. H. Higgs, and J.D. Cannon.

68. WADD Technical Report 61-72, Volume XXX, Oxidation Resistant Graphite-Base Composites, by K. J. Zeitsch and J. Criscione.

69. WADD Technical Report 61-72, Volume XXXI, High Performance Graphite by Liquid Impregnation, by C. E. Waylett, M. A. Spring and M. B. Carter.

70. WADD Technical Report 61-72, Volume IX, Fabrication and Properties of Carbonized Cloth Composites, by W. C. Beasley and E. L. Piper.

71. WADD Technical Report 61-72, Volume XXXVII, Studies of Graphites Deposited by Pyrolytic Processes, by P. H. Higgs, R. L. Finicle, R. J. Bobka, E. J. Seldin and K. J. Zeitsch.

72. WADD Technical Report 61-72, Volume XXVI, Physical Properties of Some Newly Developed Graphite Grades, by R. B. Dull.

73. WADD Technical Report 61-72, Volume XXXV, Methods of Measuring Mechanical Properties of Graphite in the 20° to 2700°C Temperature Range, by M. B. Manofsky and R. B. Dull.

74. WADD Technical Report 61-72, Volume XXIII, A Method for Determining Young's Modulus of Graphite at Elevated Temperatures, by S. O. Johnson and R. B. Dull.

75. WADD Technical Report 61-72, Volume IV, Adaptation of Radiographic Principles to the Quality Control of Graphite, by R. W. Wallouch.

76. WADD Technical Report 61-72, Volume XXII, Photomicrographic Techniques for Carbon and Graphite, by G. L. Peters and H. D. Shade.

77. WADD Technical Report 61-72, Volume XXIX, Evaluation of Graphite Materials in a Subscale Solid Propellant Rocket Motor, by D.C. Hiler and R. B. Dull.

78. WADD Technical Report 61-72, Supplement to Volume XXIX, Evaluation of Graphite Materials in a Subscale Solid Propellant Rocket Motor, by S. O. Johnson and R. B. Dull.

6. GLOSSARY

6.1. Abbreviations

AG - Across grain or against grain.
WG - With grain.
ARF - Armour Research Foundation of Illinois Institute of Technology.
CFH - Cubic feet per hour.
CTE - Coefficient of thermal expansion.
DTA - Differential thermal analysis.
ERA - Union Carbide European Research Associates.
ESR - Electron spin resonance.
BP - Boiling point.
MP - Melting point.
NMR - Nuclear magnetic resonance.
PPH - Parts per hundred

6.2. National Carbon Company Grades

AGKSP and L113SP - Extruded spectroscopic graphite.
ATJ - Fine-grain molded graphite.
ATL - Medium-grain molded graphite.
CEP - Lampblack base molded graphite.
CFW and CFZ - Molded graphites, impregnated.
JT - Oxidation resistant graphite base composites.
PT - Fibrous carbon and graphite composites.
RVA - Pressure cured fine-grain graphite.
RVC - Substrate graphite for coatings.
RVD - Pressure cured ultra fine-grain graphite.
ZT, ZTA, ZTE - High density hot formed graphites.
C-9 - Carbonaceous cement.
TS-341 - Experimental titanium diboride cement.

6.3. Terms

Apparent Density or Kerosene Apparent Density - Density measured by Kerosene Displacement.

Bulk Density - Ratio of mass to bulk volume.

Filler Material - Carbonaceous particles used in a carbon mix with binder.

45 Flour - Filler material milled to 45 per cent through 200 mesh screen.

60 Flour - Filler material milled to 60 per cent through 200 mesh screen.

Plugs - Carbonaceous shapes formed by molding.

Rods - Carbonaceous shapes formed by extrusion.

Green - Filler and binder mixture before carbonization of the binder.

Baked - Filler and binder mixture after carbonization of the binder.

Graphitized - Filler and binder mixture after heating to the 2600-3000°C range.

APPENDIXES I THROUGH IX

APPENDIX I

MECHANICAL PROPERTIES OF GRAPHITE WHISKERS AT HIGH TEMPERATURE

I. 1. Purpose

A project was undertaken to measure the strength and elastic modulus of graphite whiskers as a function of temperature in a controlled atmosphere. Previous studies* had shown that these whiskers possessed a unique structure consisting of graphite single crystal layer planes running continuously along the length of the whisker. It was further shown that the graphite layers were rolled up into a scroll form so that the external cylindrical surface was essentially identical to the hexagonal layer surfaces of a graphite single crystal. Since the covalent carbon-carbon bonds within layers are very strong whereas the bonding between layers is relatively weak, graphite whiskers are ideal specimens for the measurement of mechanical properties of graphite in a direction parallel to the layer planes. Tensile strengths as high as 3,000,000 lbs/in.^{2} were measured on whiskers with a diameter less than 1 micron. Such values are nearly 1000 times those commonly observed for commercial graphites.

The primary purpose of this project was to measure the mechanical properties along the layer planes at high temperatures. This result would provide one important piece of information required to explain the high temperature behavior of polycrystalline graphite, which exhibits increased mechanical strength with increasing temperature up to about 2500°C. If the strength of graphite is limited by the shear strength between graphite layers, then one should look for a mechanism to increase the shear strength at high temperatures in order to explain this behavior. On the other hand, if the strength of graphite is determined to some degree by the intrinsic tensile strength within graphite layers then it becomes of obvious interest to investigate the effect of high temperatures on this tensile strength.

Unfortunately, it is not possible to apply a pure tensile stress to a graphite whisker in the region of each tensile grip, which is a hard cement applied to the end of the whisker. There is necessarily a shear component in the total stress which is maximum at the surface and drops off toward the interior of the whisker. Because of the extremely high anisotropy in the elastic properties of graphite, this problem is severe. Therefore, a measurement of the tensile properties within the layer planes always includes to some degree the shear properties between layer planes. In order to separate the two, it is necessary to do experiments on whiskers with a range of sizes. As one goes to smaller diameters, the shear effect becomes less important, but the experimental difficulties become greater.

---

* R. Bacon, J. Appl. Phys. 31, 283 (1960).

I.2. Technique and Apparatus

The study of the mechanical properties of graphite whiskers required:

a. The development of a technique for removing long (1-2 cm) graphite whiskers from the matrix of the boule in which they were grown without damaging them.

b. The development of a rigid, reliable high temperature tensile grip for graphite whiskers capable of withstanding temperatures ranging up to 2800°C.

c. The design of a high temperature stress-strain apparatus which would be capable of making and recording direct measurements of whisker tension as a function of elongation at temperatures varying from 25 to 2800°C in a vacuum or controlled atmosphere.

These techniques and equipment are described in detail as follows:

I.2.1. Technique for Removing Graphite Whiskers from Matrix of Boule

The graphite whiskers used in this study were grown in a d.c. carbon arc under high pressures.* The whiskers are embedded in solid graphite "boules" which resemble stalagmites. They are recovered by cracking the boule longitudinally, thereby exposing the center of the boule where they are found in greatest number.

Several techniques for removing whiskers undamaged from the matrix of the boule have been investigated. Initially, selective oxidation was tried in which the matrix material was oxidized selectively, thus leaving the whisker intact.** However, whiskers obtained in this manner were brittle and it was difficult to obtain whiskers longer than 1 cm. Removal of whiskers by cathodic etching was investigated but it was found that the exposed ends of these whiskers would become attracted toward the anode of the cell, serving as a current path to the boule. The most reliable technique was that of carefully removing the whisker from a cracked boule submerged in distilled water by gripping the ends of the whisker with micromanipulators and forceps and cleaving the matrix material away with a scalpel. Although the procedure is tedious, several apparently undamaged whiskers approximately 3.5 cm long have been obtained in this fashion.

I.2.2 The Development of a High Temperature Tensile Grip for Graphite Whiskers

In order to make stress-strain measurement on graphite whiskers at temperatures up to 2800°C, the development of a rigid, reliable high temperature

---

* R. Bacon, op. cit.

** P. J. Bryant, Midwest Research Institute, WADD TR60-529 (May, 1960).

gripping technique was required. Two spectroscopically pure graphite rods of $^1/_{16}$-inch diameter each with a rectangular slot in one end were used as whisker holders (see Figure I. 1.). The whiskers were cemented in place with cement composed of about 70 per cent powdered graphite with an average particle size of ~0. 1μ, 15 per cent dextrose to serve as a binder when subsequently charred, 15 per cent water to dissolve the dextrose, plus a small fraction of a per cent of detergent to insure wetting of the contact surfaces. The cement was then baked out at 350°C, and was found to withstand subsequent temperatures as high as 2800°C. This cement has been more satisfactory even at room temperature than any of the many conventional cements previously tried. It apparently bonds chemically to the whisker surfaces, but in addition it may actually exert an inward pressure on the whisker due to a volume contraction which occurs after the cement has thermally set.

I. 2. 3. The Design of a High Temperature Stress-Strain Device

An apparatus was designed to measure and record the force applied to a whisker as a function of elongation. Graphite whiskers are mounted between the ends of two graphite rods and placed in the heater of the tensile testing apparatus as shown in Figure I. 2. The upper rod transmits the applied force to a differential transformer-type dynamometer which translates mechanical force into an electrical output. The amplified output is recorded on the "y" axis of an xy recorder. The lower support is rigidly coupled to a permanent magnet whose vertical movement is controlled by a solenoid. A linear variable differential transformer attached to the magnet detects the movement of the lower support, which is equal to the whisker elongation. The output from the differential transformer is amplified and fed into the x-axis of the xy recorder. The micrometer head attached to the dynamometer varies the distance between the grips to compensate for differences in lengths of the samples. A photograph of the tensile apparatus is shown in Figure I. 3. Atmospheric studies and high temperature measurements are made with the apparatus mounted inside a bell jar on a vacuum pumping station as shown in Figure I. 4. The entire system is mounted on a concrete isolation column, free from building vibrations.

I. 3. Results

I. 3. 1. Room Temperature Behavior

Room temperature stress-strain measurements on graphite whiskers have yielded interesting results. A typical plot of whisker tension vs elongation is shown in Figure I. 5. The curve is fairly linear up to the yield point, beyond which continued stretching of the whisker took place at substantially constant tension. This plastic yield is recorded as a series of small peaks and dips in the force as the whisker elongates as much as 20 per cent.

A study of the elastic portion of the stress-strain curve appears in Figure I. 6. A hysteresis loop results from increasing the applied force up to slightly below the yield point and subsequently returning to a state of zero

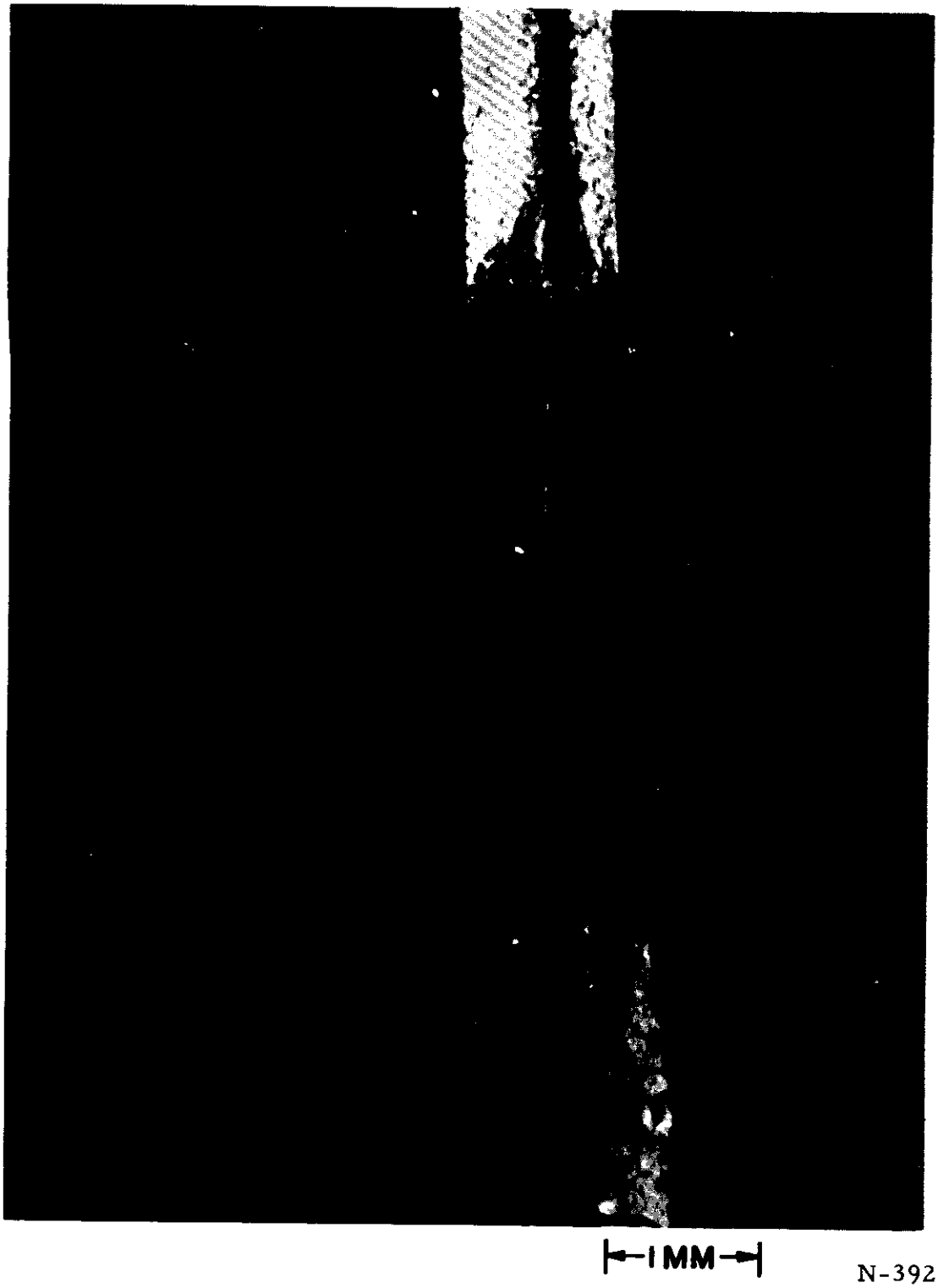

Figure I.1. Graphite Whisker of 4-mm Length Mounted Between Two Graphite Rod Tensile Grips

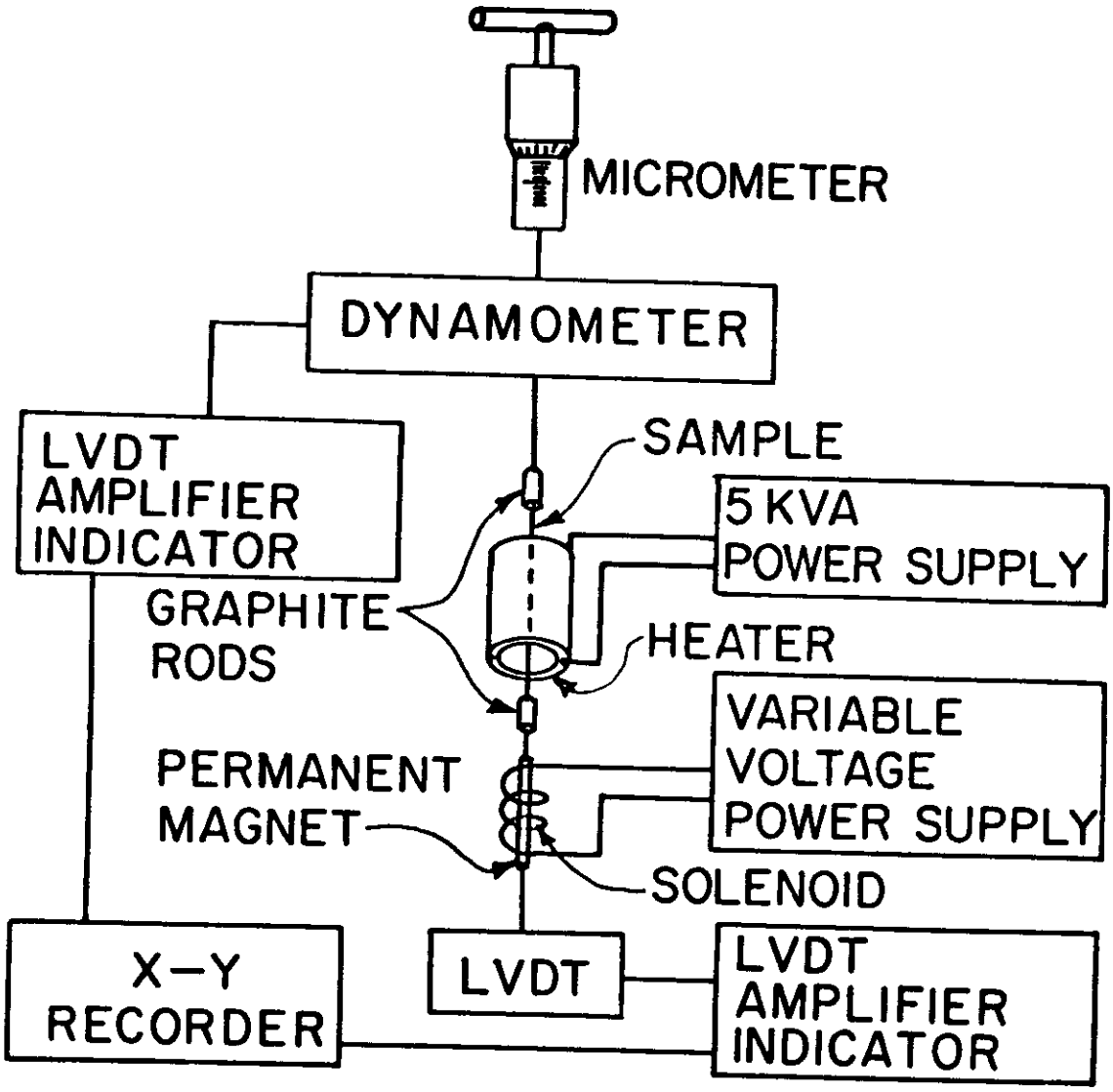

Figure I. 2. Diagram of Tensile Apparatus N-3912

N- 2314

Figure I. 3. Photograph of High Temperature Tensile Apparatus

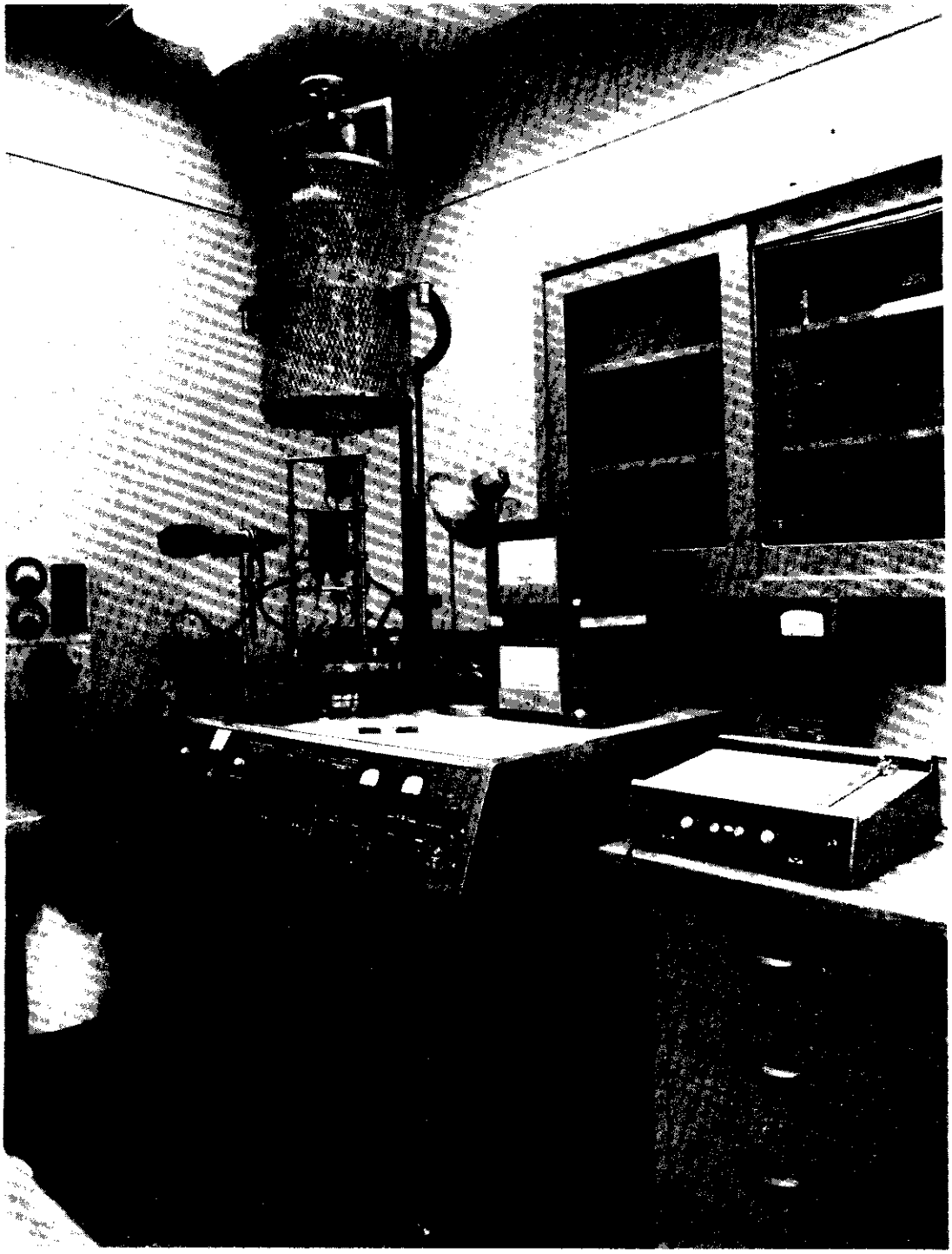

N-3689

Figure I.4. Tensile Apparatus Shown with Pumping Station and Recording Equipment

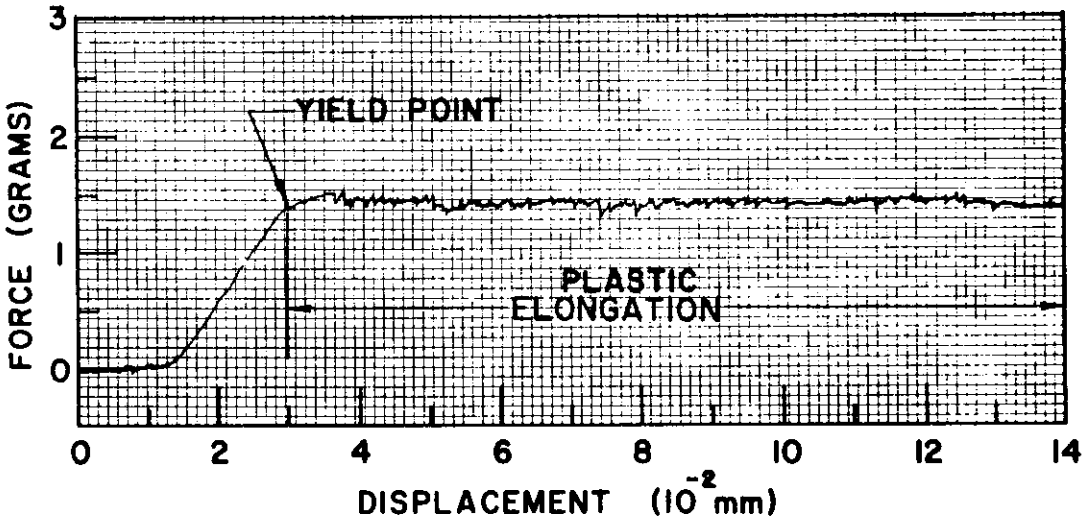

N-3913

Figure I.5. Typical Tension-Elongation Curve for a Graphite Whisker at Room Temperature

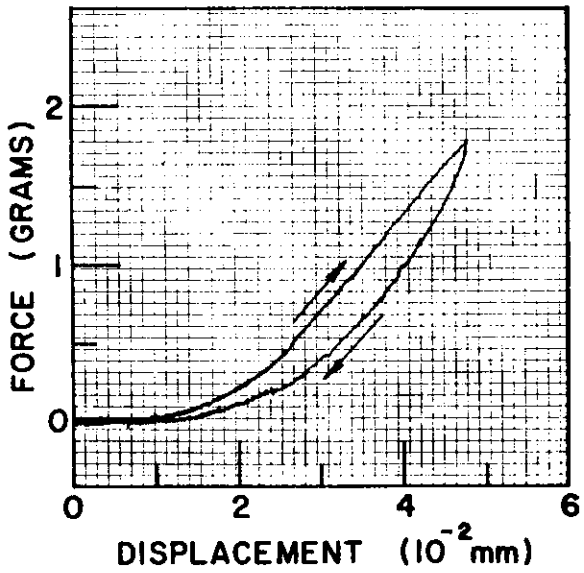

N-4113

Figure I.6. Hysteresis Loop Resulting from Application and Subsequent Release of Force on a Whisker

tension. The observation of a hysteresis behavior shows that the linear portion of the stress-strain curve represents a combination of elastic and anelastic strain, the latter being recoverable.

Since a whisker can be cycled many times between zero tension and its yield point, with nearly the same results each time, it is possible to make many measurements of "elastic" modulus and yield point on the same whisker while varying the conditions of test, e.g., the temperature or the surrounding atmosphere.

Results of complete sets of measurements on nine whiskers at room temperature are shown in Table I.1. The highest tensile strength measured in previous studies is included in this table for comparison. That measurement was made on an extremely small diameter whisker, and the relatively low yield stresses reported for the whiskers in the present work are the result of their large size. Similarly, the low values for Young's modulus are the result of large size as well as the static nature of the tests. Previous studies* by a dynamic method indicated that the true modulus was at least as high as 100 x 10^6 psi.

Table I.1. Tensile Test Results on Graphite Whiskers at Room Temperature

Test No.	Gauge Length (mm)	Diameter (μ)	"Elastic" Strain Per Cent	Plastic Strain Per Cent	Ultimate Stress (10^3 lb/in.^{2})	Young's Modulus (10^6 lb/in.^{2})
61-1	8.86	5.1	.08	---	75	81
-2	4.76	3.9	.15	2.0	104	51
-3	6.95	4.5	.22	0.7	128	54
-4	6.17	4.2	.23	1.5	95	41
-5	6.00	2.7	.20	1.3	176	81
-9	5.12	4.5	.19	1.7	88	46
-12	6.99	5.1	.11	8.6	58	51
-13	6.99	4.8	.17	---	67	36
-14	6.99	4.8	.13	17.2	45	59
Previous Study		0.3	---	---	3000	100

I.3.2. High Temperature Behavior

Tests at high temperature have been confined so far to the range between 800 and 1500°C. The normal procedure has been to stress a whisker to its yield point and back to zero again at room temperature, then heat it to a high

* R. Bacon, op. cit.

temperature and repeat the test, looking for changes in yield point and in the slope of the linear portion of the curve, i.e., the "elastic" modulus. The whisker was frequently returned to room temperature for a retest, since the room temperature strength was found to decrease with the number of tests performed, owing to a slight alteration or weakening of structure resulting from each test. There was no evidence that more weakening resulted from a high temperature test than from a room temperature test.

In order to take into account the weakening effect of each successive test, the results of a series of tests on one whisker were displayed by plotting relative yield stress against the number of tests performed. Results for two whiskers on which a large number of tests were performed are plotted in Figures I.7. and I.8. The room temperature measurements are shown as squares while the high temperature tests are shown as circles, with the temperature of the test labeled for each point. There is a clear trend of decreasing room temperature yield stress with the number of tests performed. The yield stress at high temperature is consistently below that at room temperature, but no more explicit dependence upon temperature has been found. An apparent temperature dependence is evident in Figure I.7., but the same trend was not observed in other whiskers, and to date we can say only that the yield point between 800 and 1500°C is significantly lower than that at room temperature.

Measurements of the slopes of the linear portions of the stress-strain curves have yielded a great deal of data, again with no consistent dependence upon temperature, except for the fact that the slope is always less at high temperature (between 800 and 1500°C) than at room temperature. The amount of the decrease in slope may be as much as 50 per cent, and in a few exceptional cases we have noted even larger changes.

Initial studies of atmospheric effects on the mechanical behavior of whiskers have shown that there is no difference between testing in air and in a vacuum below 10^{-6} torr. "Degassing" in a vacuum at high temperature has failed to produce an effect. However, there is some evidence that very long term degassing may affect the properties.

I.4. Interpretation and Discussion of Experimental Results

I.4.1. Room Temperature Behavior

The stress-strain curve of a graphite whisker at room temperature consists of two distinct portions: a linear increase of stress with increasing strain up to the yield point followed by a long region of plastic flow with slowly decreasing stress up to maximum strains as high as 20 per cent or more. Within the linear region the strain is recoverable, but the stress-strain diagram exhibits a small hysteresis loop. Furthermore, the slope of the curve is variable, occasionally showing a drastic decrease at temperatures above 1000°C. The slope of the linear portion of the stress-strain curve, therefore, does not represent purely elastic behavior, but is a mixture of elastic deformation and a recoverable anelastic deformation.

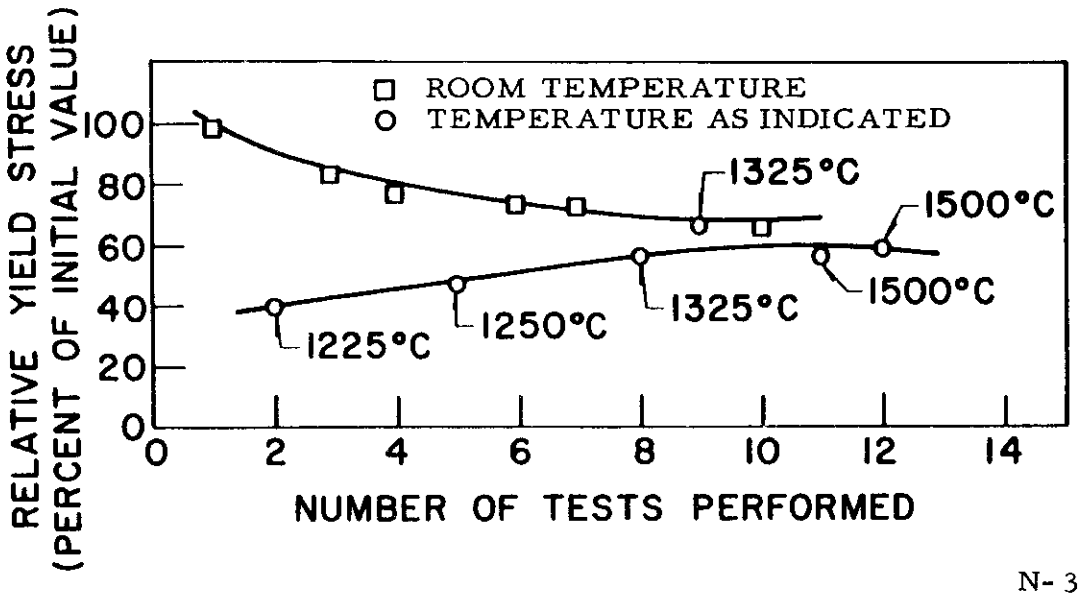

N-3914

Figure I.7. Relative Yield Stress at Room and High Temperatures on Whisker 7B

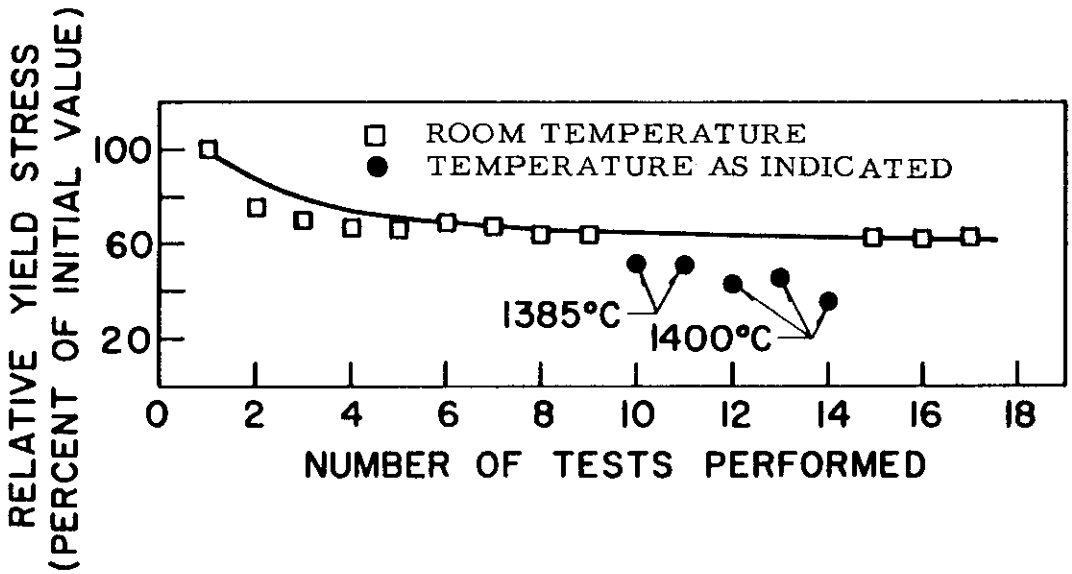

N-3914

Figure I.8. Relative Yield Stress at Room and High Temperatures on Whisker 19.

The room temperature stress-strain behavior can be explained in a general way in terms of the graphite whisker structure. This structure has been described in the article* published in 1960. The whisker consists of a number of concentric tubes. Each tube has a form obtained by rolling up a thin layer of graphite into a scroll of several turns. Successive turns of a perfect cylindrical scroll necessarily maintain a constant orientation of the hexagonal graphite layers. However, from one concentric tube to the next there occurs a random change in orientation.

Recent electron microscope observations of graphite whiskers which had been treated with bromine indicate that the bromine penetrated into inter-layer spaces which extended over great distances along the whisker. Since there was no evidence of any sort of helical or "soda-straw" structure, it is concluded that the scroll structure is continuous over essentially the entire length of the whisker.

Direct evidence for the existence of a scroll consisting of several turns was obtained when a whisker was exploded by passage of a large electrical current. Recent experiments of this sort were carried out inside the electron microscope without any supporting film substrate. Figures I.9A. and I.9B. show a large wrinkled sheet of graphite exfoliated from the whisker during such an explosion. Its width is nearly ten times the diameter of the whisker from which it came, even in its wrinkled condition. Selected area diffraction of this sheet showed that it was a highly crystalline layer of graphite. Figure I.10. shows the appearance of the tip of the whisker at the point of burn-out. The inner core of this whisker is clearly a hollow tube.

The anelastic stress-strain behavior of a graphite whisker is interpreted as resulting from the slip between graphite layers. It appears that two rather distinct kinds of slip can occur: slip between concentric tubes and slip within a tube of one turn of the scroll relative to the next. Slip between tubes merely consists of the sliding of one tube over the next, and would not be expected to be recoverable. On the other hand, slip within a tube of one turn of the scroll relative to the next would involve a certain amount of elastic deformation and therefore should be in part recoverable. This "scroll stretching" process may account for the linear portion of the stress-strain curve. The process of slip between concentric tubes accounts for the long region of plastic flow beyond the yield point, as observations of the two halves of a whisker tested to failure have repeatedly suggested.

This explanation for the anelastic behavior of graphite whiskers is partly speculative. We have no direct experimental evidence that scroll stretching is responsible for the linear region of the stress-strain curve and that tube sliding alone is responsible for the plastic flow. It is entirely possible that both processes contribute to both the linear and the plastic flow region. In fact, one interesting observation was made which suggests that scroll stretching plays a part in permanent plastic deformation. A whisker whose outer

---

* R. Bacon, op. cit.

A. Opaque Whisker is Shown Along With Exfoliated Scroll
N-3955

B. Higher Magnification of Wrinkled Sheet Shown in A
N-3956

Figure I.9. Graphite Whisker Exploded Inside the Electron Microscope

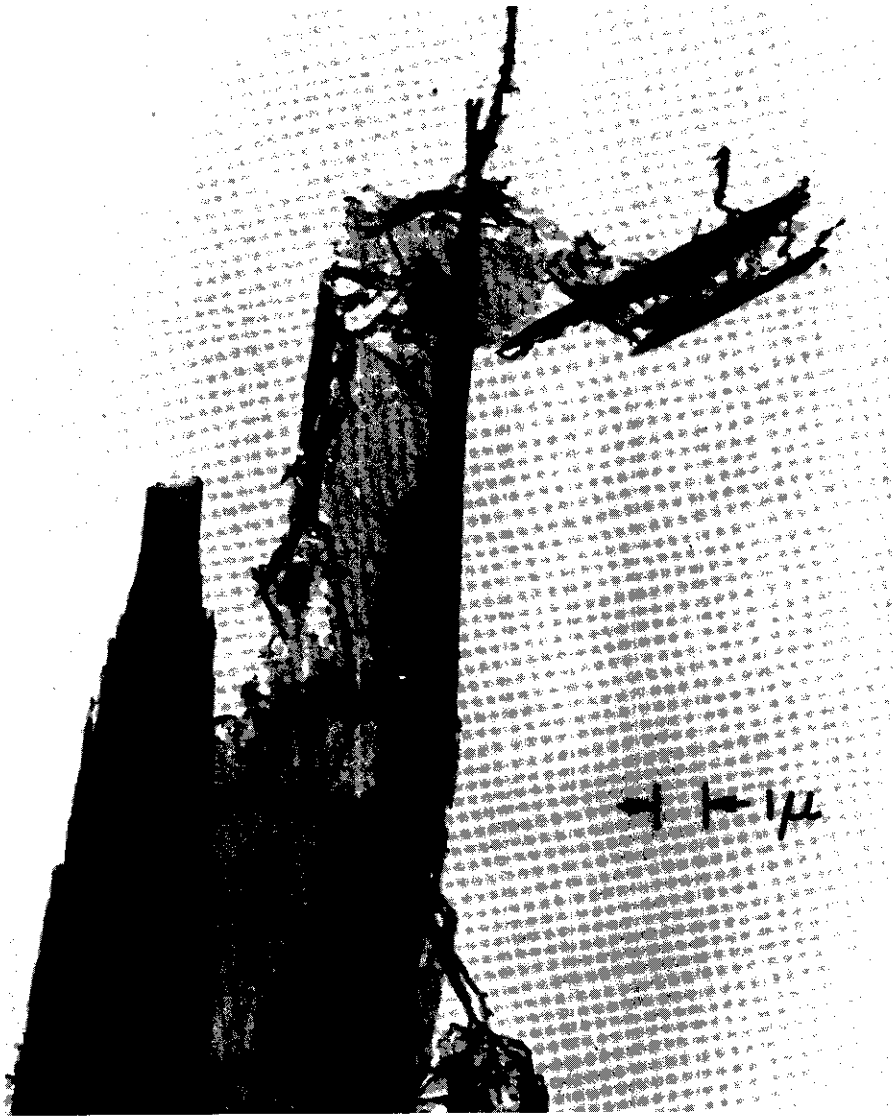

N-3954

Figure I. 10. Tip of an Exploded Whisker Showing Hollow Inner Core

N-4070

Figure I. 11. Twisted Section of a Plastically Deformed Inner Core

layers were removed by exfoliation under bromine treatment was plastically deformed in tension. The deformed section of the whisker when photographed optically showed an obviously twisted structure as seen in Figure I. 11. It is reasonable to guess that this resulted from a scroll stretching phenomenon.

I. 4. 2. High Temperature Behavior

The character of the stress-strain curve of a graphite whisker obtained at high temperatures is not essentially different from that at room temperature. The only difference is that the yield point is usually lower and the slope of the linear region of this stress-strain curve is usually lower also. Reproducibility is poor and no consistent pattern in the dependence of these properties on temperature has been uncovered. The yield point and the slope of the linear portion are functions of the slip behavior of the whisker and at present we can only say that slip occurs more easily between 1000 and 1500°C than it does at room temperature. This may be due to a higher dislocation mobility at these temperatures.

I. 4. 3. Conclusions

In the light of the foregoing discussions, the following conclusions can be made:

a. The interesting anelastic behavior of graphite whiskers shown in their stress-strain diagrams can be explained in terms of slip processes.

b. The separation of anelastic deformation from elastic deformation can be accomplished only by studying whiskers of successively smaller diameters.

c. Graphite whiskers are not suitable specimens for a quantitative study of anelastic properties of graphite in view of their inconsistent behavior at high temperature.

d. Graphite whiskers still represent the most promising specimens for studying the mechanical properties of graphite along the layer plane direction, provided specimens of very small diameter can be measured in order to separate the effects of shear deformation between layers. It is hoped that recent progress in stripping off outer layers to get to the inner core material will enable us to come much closer to measuring the true tensile strength and elastic modulus along graphite layer planes as a function of temperature up to 2800°C.

APPENDIX II

SONIC ELASTIC CONSTANTS OF POLYCRYSTALLINE GRAPHITES

II.1. Introduction

With the increasing use of graphite as a structural material there has arisen a pressing need for an accurate and complete characterization of the elastic properties. Engineering applications usually require the static elastic constants for large strains. However, compared to sonic elastic constants, the static constants are more difficult to measure and are more complicated due to the nonlinearity of the stress-strain curve of graphite. From the results shown in Figure 28 of Section 3.3.2, it appears that the sonic elastic constants may be very close to the average static elastic constants of prestressed graphite. A program on measuring the sonic and static constants on the same samples has recently been initiated to establish more exactly the relation of the sonic to the static elastic constants. Thus, the sonic elastic constants may be the cheapest and easiest means of estimating the static constants. In addition, the sonic constants are of greater scientific interest because they are more simply and directly related to the elastic constants of the individual crystallites of the polycrystalline material.

The study of the sonic elastic constants was begun rather late in this work period and the following report must be considered as preliminary. The resonant bar technique was selected because this method has long been used to determine with-grain and against-grain Young's moduli. Both molded and extruded graphite have, to a reasonable approximation, an axis of cylindrical symmetry; and, except for a skin effect, both are elastically isotropic in a plane perpendicular to the symmetry axis. Consequently, both molded and extruded graphites have the same elastic symmetry as a hexagonal crystal. Five elastic constants are required to characterize completely the elastic properties of materials with this symmetry. Work done up to the present has centered on (a) collecting from the literature the formulas to be used in relating the five elastic constants to the resonant frequencies; (b) determining the best methods of measurement; and(c) determining the accuracy with which the elastic constants can be obtained on graphite that is always somewhat inhomogeneous. This initial work has been restricted to longitudinal and torsional vibrations because the theory of the flexural vibrations of an anisotropic bar is very much more complicated than that of the other two types of vibrations.

II.2. Theory

II.2.1. Frequency Corrections

The theories which relate the elastic constants to the resonant vibrations of bars are based on the assumption that the width to length ratio of the bar

is infinitesimally small. Under this condition the frequencies of harmonics for both longitudinal and torsional vibrations are integral multiples of the fundamental. For bars with finite width to length ratios, all the frequencies are slightly perturbed. Let

f_0 = fundamental (longitudinal or torsional) frequency for an infinitesimal width to length ratio,

f_1 = fundamental frequency for a finite width to length ratio,

f_n = harmonic frequency for a finite width to length ratio, where n = 1 for the fundamental, n = 2 for the first harmonic, etc.

For isotropic bars with a finite width to length ratio, f_n is related* to f_0 by

$$\frac{n^2}{f_n^2} = \frac{1}{f_0^2} \left(1 + C\, n^2 \right),$$

where C is a positive constant. Note that f_1 is not equal to f_0. For longitudinal vibrations C depends on Poisson's ratio and the square of the width to length ratio. For torsional vibrations C depends only on the cross-sectional shape and is zero for circular cross sections. From the nature of the derivation of this formula it is clear that the same formula will apply to an anisotropic bar with C still being a positive constant.

The finite cross section correction is expected to be important for measurements on coarse-grained graphites and samples cut perpendicular to the extrusion axis where the width to length ratio may have to be greater than 0.2. The correction can be obtained without knowing the value of C for an anisotropic bar by plotting n^2/f_n^2 against n^2. A straight line through the experimental points has an intercept on the vertical axis at $1/f_0^2$. This procedure was attempted on twenty longitudinal and torsional vibrations of ATJ graphite. In no case was a linear relation found and in the majority of cases n^2/f_n^2 decreased instead of increased as n increased. Consequently, it is felt that at present it is best to set $f_0 = f_1$. From the difference between f_1^2 and $f_2^2/4$ the uncertainty in f_0^2 appears to be about ± 1 per cent, which is five or ten times larger than the experimental error in measuring the frequencies. The error in f_0^2 causes an uncertainty of about ± 1 per cent in the compliance constants s_{11}, s_{33} (or Young's moduli), and s_{44} (or torsion modulus). Although an error of ± 1 per cent in these constants is not serious, this uncertainty causes an error in the constants s_{12} and s_{13} (or Poisson's ratios) of up to about ± 30 per cent. At the present time the complete lack of understanding of the variation in the harmonic series and of how to obtain an accurate value of f_0 is the major source of error in the use of the resonant bar technique to obtain accurate values of all five elastic constants. More theoretical and experimental work must be done on this problem.

*See, for example, A. E. H. Love, Mathematical Theory of Elasticity, Fourth Ed., New York:Dover (1944), pp. 428-429.

II.2.2 Formulas for Round Bars

Formulas relating the elastic compliance constants s_{ij} to the resonant frequencies are given at various places in the literature.* In the following the formulas are collected together and put in a form which is useful for practical applications. The formulas of this section only apply to bars of circular cross section. Let

θ = angle between the axis of the bar and the symmetry axis of the material

ρ = density of the bar

ℓ = length of the bar

f_{0L} = fundamental frequency of longitudinal vibration of a bar of infinitesimal width to length ratio

f_{0T} = fundamental frequency of torsional vibration of a bar of infinitesimal width to length ratio.

The effective Young's moduli are given by

$$E_{\parallel} = 4\rho\ell^2 f_{0L}^2 \qquad \text{for} \qquad \theta = 0°$$

$$E_{\theta} = 4\rho\ell^2 f_{0L}^2 \qquad \text{for} \qquad 0° < \theta < 90°$$

$$E_{\perp} = 4\rho\ell^2 f_{0L}^2 \qquad \text{for} \qquad \theta = 90°,$$

and the effective torsional moduli are given by

$$G_{\parallel} = 4\rho\ell^2 f_{0T}^2 \qquad \text{for} \qquad \theta = 0°$$

$$G_{\theta} = 4\rho\ell^2 f_{0T}^2 \qquad \text{for} \qquad 0° < \theta < 90°$$

$$G_{\perp} = 4\rho\ell^2 f_{0T}^2 \qquad \text{for} \qquad \theta = 90°.$$

Three of these moduli are of fundamental significance and their reciprocals are elastic compliance constants:

$$s_{11} = E_{\perp}^{-1}$$

$$s_{33} = E_{\parallel}^{-1}$$

$$s_{44} = G_{\parallel}^{-1} \quad .$$

*See, for example, R. F. S. Hearmon, An Introduction to Applied Anisotropic Elasticity, Oxford Univ. Press (1961), Chapt. IV.

The modulus $G_\perp$ is related to the s_{ij} by

$$\tfrac{1}{2}[\,2(s_{11} - s_{12}) + s_{44}] = G_\perp^{-1} .$$

The reciprocal of the modulus for shear of (not between) a basal plane is given by

$$2(s_{11} - s_{12}) = 2G_\perp^{-1} - G_\parallel^{-1} ,$$

from which it follows that

$$s_{12} = - G_\perp^{-1} + \tfrac{1}{2} G_\parallel^{-1} + E_\perp^{-1} .$$

Note that $G_\perp$, which for a molded sample would be called the with-grain torsional modulus, is not a fundamental quantity and in fact is relatively useless unless it can be combined with $G_\parallel$ obtained from another bar of the same material. Normally, s_{12} is about a factor of 10 smaller than the reciprocals of the E's and G's, so that roughly one significant figure is lost in calculating s_{12}. A useful value of s_{12} cannot be obtained unless the fundamental frequencies are accurate to within one per cent and unless density corrections can be applied to moduli obtained from two different bars to reduce them to a common density.

The effective Young's modulus E_θ for a bar cut at an arbitrary angle θ with the symmetry axis is related to all five elastic constants. For the purpose of calculating s_{13} the formula can be put in the form

$$s_{13_L} = -\tfrac{1}{2}\left[\frac{1 - \gamma^2}{\gamma^2} E_\perp^{-1} + \frac{\gamma^2}{1 - \gamma^2} E_\parallel^{-1} - \frac{1}{\gamma^2(1 - \gamma^2)} E_\theta^{-1} + G_\parallel^{-1}\right] ,$$

where

$$\gamma = \cos \theta$$

and the subscript L has been added to denote a value calculated from the frequency of longitudinal vibrations. At $\theta = 45°$

$$s_{13_L} = -\tfrac{1}{2}(E_\perp^{-1} + E_\parallel^{-1} + G_\parallel^{-1}) + 2E_{45}^{-1} .$$

The theory of the torsional vibrations of a bar cut at an angle between 0 and 90° is complicated by a coupling between torsional and flexural motion. A twist of the bar about the long axis of the bar produces a bending of the bar about an axis at right angles to the bar axis. If this bending is permitted, the bar is said to be in "free torsion"; if this bending is restrained so that only a twisting motion occurs, the bar is said to be in "pure torsion." The bar acts as if it were stiffer in pure torsion than in free torsion, so the relation between the resonant frequency and the elastic constants is different in the two cases. Solving these relations for s_{13}, one obtains

For Free Torsion

$$s_{13FT} = -\frac{1}{2}\left[\frac{G^{-1} - G_{\parallel}^{-1}}{2\gamma^2(1-\gamma^2)} + G_{\parallel}^{-1} - E_{\perp}^{-1} - E_{\parallel}^{-1}\right]$$

and

For Pure Torsion

$$s_{13PT} = -\frac{1}{2}\left[G^{-1} - \sqrt{(E_1^{-1} - G^{-1})^2 - (E_2^{-1})^2}\right],$$

where

$$G^{-1} = G_{\theta}^{-1} + (1-\gamma^2)(G_{\parallel}^{-1} - G_{\perp}^{-1})$$

$$E_1^{-1} = \frac{1-\gamma^2}{\gamma^2} E_{\perp}^{-1} + \frac{\gamma^2}{1-\gamma^2} E_{\parallel}^{-1} + G_{\parallel}^{-1}$$

$$E_2^{-1} = \frac{1-\gamma^2}{\gamma^2} E_{\perp}^{-1} - \frac{\gamma^2}{1-\gamma^2} E_{\parallel}^{-1} .$$

In this notation

$$s_{13L} = -\frac{1}{2}\left[E_1^{-1} - \frac{E_{\theta}^{-1}}{\gamma^2(1-\gamma^2)}\right]$$

At $\theta = 45°$ these formulas simplify to

$$s_{13L} = -\frac{1}{2}(E_{\perp}^{-1} + E_{\parallel}^{-1} + G_{\parallel}^{-1}) + 2E_{45}^{-1}$$

$$s_{13FT} = -G_{45}^{-1} + \frac{1}{2}(E_{\perp}^{-1} + E_{\parallel}^{-1} + G_{\perp}^{-1})$$

$$s_{13PT} = -\frac{1}{2}\left[G^{-1} - \sqrt{(E_1^{-1} - G^{-1})^2 - (E_{\perp}^{-1} - E_{\parallel}^{-1})^2}\right],$$

where

$$G^{-1} = G_{45}^{-1} + \frac{1}{2}(G_{\parallel}^{-1} - G_{\perp}^{-1})$$

$$E_1^{-1} = E_{\perp}^{-1} + E_{\parallel}^{-1} + G_{\parallel}^{-1} .$$

Normally, s_{13} is about a factor of 10 smaller than the reciprocals of the E's and G's. Furthermore, moduli obtained from bars cut at three different angles must be used in calculating s_{13}; so the requirement of being able to

reduce all the data to a common density is even more important than in the case of s_{12}.

In a resonant bar experiment the bar is free to bend at the same time that it is in torsion. However, Brown* cites both experimental and theoretical evidence that bars of normal length undergo pure torsion provided the flexural and torsional resonant frequencies do not approximately coincide. Experiments on bars of graphite cut at 45° have been made to try to detect any flexural vibration occurring at the torsional resonant frequency. If any flexural motion occurs at all, its amplitude is smaller by at least a factor of 10 from the amplitude which would occur at the flexural resonant frequency. Although further experimental work on this problem should be done, it appears at present that the bar is in pure torsion.

II.2.3. Formulas for Rectangular Bars

The formulas relating the resonant vibrations of rectangular bars to the elastic constants are considerably more complicated than those for round bars. Although a search of the literature has not been completed, formulas for the torsional vibrations of a rectangular bar cut at an angle between 0 and 90° have not been found. Formulas for rectangular bars are needed for joint sonic and static testing of the same samples. Static testing requires rectangular or at least square bars on which to put three perpendicular strain gages.

Certain of the formulas are expressed in terms of a function F(c), which will be discussed first. This function, derived in Love** and quoted in Hearmon,*** is defined by

$$F(c) = \frac{1}{3}\left[1 - \frac{192}{c\pi^5}\sum_{n=0}^{\infty}\frac{\tanh(2n+1)\pi c/2}{(2n+1)^5}\right],$$

where the relation of c to the elastic constants and physical dimensions depends on the problem under investigation. Alternatively, a derivation given

---

*W. F. Brown, Jr., Phys. Rev. 58, 998 (1940).
**A. E. H. Love, op. cit., p. 325.
***R. F. S. Hearmon, loc. cit.

by Sokolnikoff* for isotropic materials can be generalized to anisotropic materials to obtain the new form

$$F(c) = \frac{c^2}{3}\left[1 - \frac{192c}{\pi^5}\sum_{n=0}^{\infty}\frac{\tanh(2n+1)\pi/2c}{(2n+1)^5}\right].$$

Equating these two expressions gives the useful new relation that

$$F(c) = c^2\,F(1/c).$$

For $c \geq 1$ one can to a high approximation set $\tanh(2n+1)\pi c/2$ equal to unity in the third and subsequent terms and sum the series in terms of the Riemann Zeta function. One obtains for $c \geq 1$

$$F(c) \simeq \frac{1}{3}\left[1 - \frac{0.6274106190}{c}\left(\tanh \pi c/2 - \frac{1 - \tanh 3\pi c/2}{243} + 0.004\,523\,763\right)\right],$$

which is accurate to better than one part in 10^8. This formula together with the relation $F(c) = c^2\,F(1/c)$ provides a simple means of computing $F(c)$ for all values of c $(0 < c < \infty)$.

For $\theta \neq 0$, let

$a_{\parallel}$ = length of the cross-sectional edge which is parallel to the plane containing the symmetry axis and the bar axis

$a_{\perp}$ = length of the cross-sectional edge which is perpendicular to the symmetry axis.

For $\theta = 0$, $a_{\parallel}$ may denote the length of either edge and $a_{\perp}$ that of the other. The longitudinal vibrations are independent of the cross-sectional shape for very small width to length ratios. Therefore the formulas for $E_{\parallel}$, E_{θ}, $E_{\perp}$, s_{11}, s_{33}, and s_{13} are the same as in the previous section. The expressions relating $G_{\perp}$ and $G_{\parallel}$ to the frequencies are different.

For $\theta = 0°$ (bar axis parallel to symmetry axis): Let

$$c = a_{\parallel}/a_{\perp}\ .$$

Then

$$G_{\parallel} = \frac{1 + c^2}{3\,F(c)}\,\rho\ell^2\,f_{0T}^2$$

and

$$s_{44} = G_{\parallel}^{-1}\ .$$

*I. S. Sokolnikoff, Mathematical Theory of Elasticity, 2nd Ed., McGraw-Hill (1956), Section 38.

Because of the elastic isotropy within a plane perpendicular to the symmetry axis, the formula for $G_{\parallel}$ is the same as that for an isotropic material; that is, the torsional modulus of a rectangular bar of an isotropic material is given by

$$G = \frac{1 + c^2}{3\,F(c)}\ \rho \ell^2 f_{0T}^2 \quad ,$$

where c is the ratio of the two cross-sectional dimensions.

For $\theta = 90°$ (bar axis perpendicular to symmetry axis): The data can be handled in various ways but for the present purposes it is assumed that $s_{44} = G_{\parallel}^{-1}$ has already been determined. The value of the function F(c) is calculated from the resonant frequency for $\theta = 90°$ by the formula

$$F(c) = \tfrac{1}{3}\ (1 + a_{\parallel}^2 / a_{\perp}^2)\, G_{\parallel}^{-1}\ \rho \ell^2 f_{0T}^2 \ .$$

The value of c is obtained by inverse interpolation in a table of F(c) as a function of c. Then,

$$2(s_{11} - s_{12}) = (a_{\parallel}^2 / a_{\perp}^2 c^2)\ G_{\parallel}^{-1}$$

and

$$s_{12} = -\ (a_{\parallel}^2 / 2a_{\perp}^2 c^2)\, G_{\parallel}^{-1} + E_{\perp}^{-1} \ .$$

Also,

$$G_{\perp} = 2\, G_{\parallel}\ /(1 + a_{\parallel}^2\ /a_{\perp}^2\, c^2).$$

The formulas relating $G_{\perp}$ to the elastic constants are the same as in the previous section. The requirements of high accuracy in measuring f_0 and of making density corrections are, of course, the same as for round bars. Experimental evidence presented later shows that this complicated method of calculating $G_{\perp}$ is unnecessary in materials which are only slightly anisotropic. For such materials the isotropic formula is surprisingly accurate.

II.3. Results on Grade ATJ Graphite

An extensive series of measurements has been made on a large block of grade ATJ graphite as a preliminary step in establishing the best methods to be used and the possible accuracy which may be attained by the resonant bar technique. Phonograph cartridges were used for both the driver and receiver. A Beckman Universal EPUT and Timer, Model 7350, was used to measure frequencies and an oscilloscope was used to aid in correctly identifying the modes of vibration.

II.3.1. Variation of Moduli with Density

A large number of bars approximately six inches long by 0.6-inch square were cut from the block at various places, some parallel to the symmetry (molding) direction and some perpendicular. The longitudinal and torsional resonant frequencies and the densities were measured. From these data graphs of $E_{\parallel}$, $E_{\perp}$, $G_{\parallel}$, and $G_{\perp}$ against density were plotted. Figures II.1 and II.2 show typical results for $E_{\parallel}$ and $G_{\parallel}$. Although there is a high

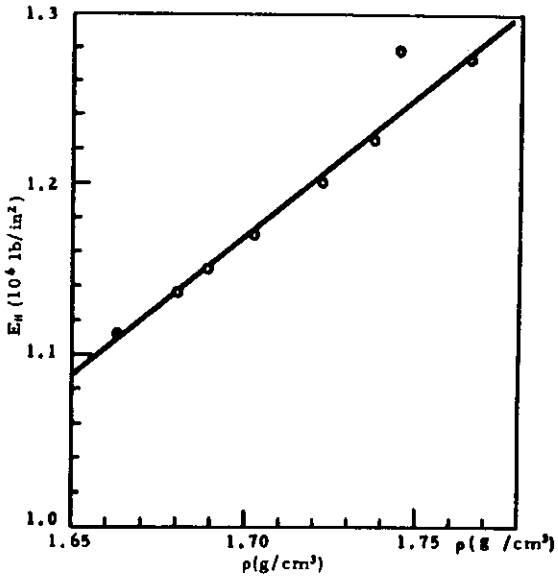

N-3755

Figure II.1. Sonic Young's Modulus for Grade ATJ Graphite Parallel to the Molding Direction Versus Density

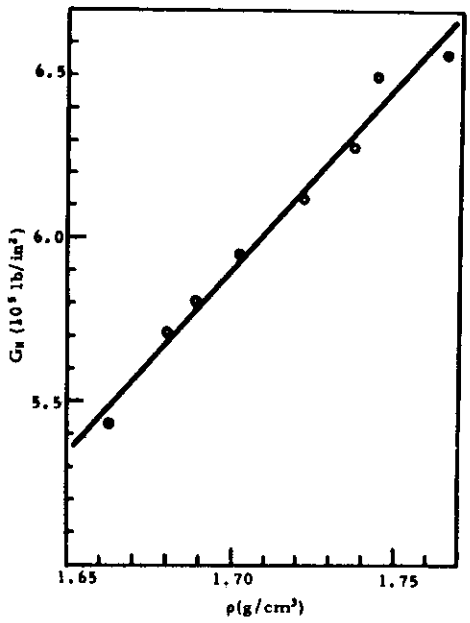

N-3758

Figure II.2. Sonic Torsion Modulus for Grade ATJ Graphite Parallel to the Molding Direction Versus Density

correlation between modulus and density, the scatter in the data is sufficiently large and the data cover such a narrow density range that it is impossible to determine the exact functional dependence on density. Therefore, a straight line has been fitted to the experimental points. The equations of these lines are

$$E_{\parallel} = 1.640\ (\rho - 0.9874) \times 10^6\ \text{lb/in}^2$$

$$= 1.131\ (\rho - 0.9874) \times 10^{11}\ \text{d/cm}^2$$

$$E_{\perp} = 3.153\ (\rho - 1.204) \times 10^6\ \text{lb/in}^2$$

$$= 2.174\ (\rho - 1.204) \times 10^{11}\ \text{d/cm}^2$$

$$G_{\parallel} = 1.130\ (\rho - 1.177) \times 10^6\ \text{lb/in}^2$$

$$= 0.7791\ (\rho - 1.177) \times 10^{11}\ \text{d/cm}^2$$

$$G_{\perp} = 1.168\ (\rho - 1.150) \times 10^6\ \text{lb/in}^2$$

$$= 0.8053\ (\rho - 1.150) \times 10^{11}\ \text{d/cm}^2\ ,$$

where ρ must be in grams per cubic centimeter in all formulas. It is to be emphasized that these formulas are not expected to be valid outside the density range for which they were derived. Comparison of these results with data taken on other blocks of grade ATJ graphite indicates that for samples with the same density the variation from block to block is considerably greater than the variation within one block. Therefore, the formulas are only representative of the type of data that can be obtained for one block and are not necessarily valid for other blocks. Nevertheless, preliminary evidence suggests that the slopes, which are the only quantities needed for density corrections, are approximately constant from block to block. This would be a very helpful result, but further experimental work must be done to establish this point.

II.3.2. Elastic Constants of Grade ATJ Graphite

Twelve bars were cut from near the center of the same block of grade ATJ graphite discussed in the previous section. The relative sizes and positions of these bars are shown in Figure II.3. The bars labelled with an "A" were located directly behind the bars shown but were not exactly the same length. All bars were about 0.5 inch in width and the longest bar was about 4.5 inches in length. Some were round, some square, as indicated in Table II.1.

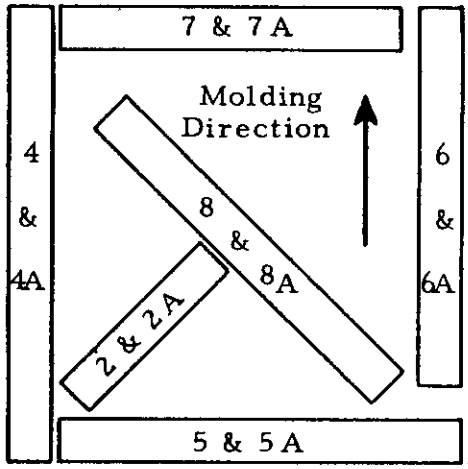

N-4118

Figure II.3. Orientation of Samples of Grade ATJ Graphite for Sonic Modulus Testing

Table II.1. Young's and Torsional Moduli for Grade ATJ Samples

Sample	Shape*	θ Deg.	ρ g/cm^3	E 10^{11} d/cm^2	G 10^{11} d/cm^2
4	R	0	1.680	.774	.387
4A	S	0	1.684	.779	.390
6	R	0	1.664	.758	.377
6A	S	0	1.674	.773	.386
2	S	45	1.674	.880	.403**
2A	S	45	1.675	.889	.404**
8	R	45	1.675	.887	.402
8A	R	45	1.679	.896	.409
5	R	90	1.688	1.068	.426
5A	S	90	1.694	1.093	.438
7	S	90	1.671	.994	.411
7A	S	90	1.677	1.004	.415

*R = Round, S = Square
**Based on formulas for an isotropic bar.

The crystallite orientation dependence was obtained by X-rays from several disk-shaped samples cut in three perpendicular directions. The X-ray method determines the relative number of crystallographic planes

whose c-axis is in the plane of the disk and at an angle ϕ with respect to a reference line in the disk. For the two disks cut with their planes parallel to that of Figure II.3, the direction of peak intensity coincided with the molding direction to within the limits of ±3° of the measurements. For the two disks cut with their planes perpendicular to that of Figure II.3, one gave the symmetry axis at 3°±3° on one side of the molding direction and the other at 4°±3° on the other side of the molding direction. These two disks were taken from positions directly above and below one another and about 1.5 inches between centers. Other disks cut perpendicular to the plane of Figure II.3 and below samples 5 and 5A also showed a deviation of several degrees between the symmetry axis and the molding direction. The valley to peak intensity ratios of all these samples were within the range 0.65 ± .02. For the two disks cut with their plane perpendicular to the molding direction, the valley to peak intensity ratios were 0.89 and 0.94. The tentative conclusions to be drawn from this first study are (a) within a small (one-half inch) region the symmetry axis may vary by up to five degrees from the molding direction but usually is within three degrees; and (b) the distribution of crystallites deviates from cylindrical symmetry by about 10 per cent. Further studies of the orientation dependence are needed both in other blocks of ATJ graphite and in other materials.

The density and the Young's and torsional moduli are given in Table II.1. For the square samples 5A, 7, and 7A at $\theta = 90°$, $G_\perp$ was calculated by the procedure outlined in Section II.2.3, which necessitated estimating the value of $G_\parallel$ for the densities of samples 5A, 7, and 7A. This complicated procedure was found unnecessary for ATJ graphite. For example, for sample 7A the formula for an isotropic bar gave 0.4151 compared to 0.4150 obtained by the method for anisotropic bars. Because of the success of the isotropic formula for bars at $\theta = 90°$, the isotropic formula has been used for the square bars 2 and 2A at $\theta = 45°$, for which no exact formula exists.

The elastic compliance constants for some of the samples of ATJ graphite are given in Table II.2. The values of the moduli $E_\parallel$, $E_\perp$, $G_\parallel$, and $G_\perp$ needed at different densities were obtained from graphs of moduli versus density by fitting straight lines with the slopes given in the previous section to the experimental points of bars 4 through 7A. The elastic compliance constants calculated from these smooth moduli versus density curves are indicated by asterisks in Table II.2. The experimental values of s_{12} show no systematic dependence on density and a scatter of only about ±10 per cent instead of the ±30 to 50 per cent which was expected. This non-dependence of s_{12} on density is also indicated by values of s_{12} calculated from the smooth moduli versus density curves of the previous section: this gave -1.30, -1.36, -1.32×10^{-12} cm^2/d at densities of 1.6, 1.7, and 1.8 g/cm^3, respectively.

Table II.2 shows that the values of s_{13} calculated from longitudinal vibrations are some 30 per cent more negative than the values obtained by assuming either pure torsion or free torsion. The reason for this is not known at present. One possibility is not knowing the true angle θ between the symmetry axis and the bar axis. The values in Table II.2 assume that

Table II.2. Elastic Compliance Constants for Grade ATJ Samples

Sample	ρ g/cm³	s_{11}	s_{33}	s_{44}	s_{12}	s_{13L}	s_{13PT}	s_{13FT}
				— 10^{-12} cm²/d —				
5	1.688	9.36		25.33*	-1.46			
5A	1.694	9.15		25.01*	-1.20			
7	1.671	10.06		26.20*	-1.18			
7A	1.677	9.96		25.90*	-1.19			
2	1.674	9.73*	13.00*	26.06*	-1.36*	-1.68	-1.51	-1.40
2A	1.675	9.70*	12.97*	25.99*	-1.36*	-1.85	-1.50	-1.39
8	1.675	9.71*	12.98*	26.01*	-1.36*	-1.81	-1.60	-1.48
8A	1.679	9.62*	12.89*	25.77*	-1.36*	-1.83	-1.35	-1.23

*Value calculated from linear moduli vs density curves.

$\theta = 45°$. Figure II.4 shows the calculated values of s_{13L}, s_{13PT}, and s_{13FT} for values of θ from 40 to 50° for sample 2A. Almost identical figures are obtained for samples 2, 8, and 8A. If the symmetry axis were inclined to the plane of Figure II.3, then it could make an angle of about 48° with all samples. The study of crystallite orientations showed that this variation is easily possible. It has consistently been found that s_{13L} varies much more rapidly with θ than does s_{13PT} or s_{13FT}. Therefore, since there will always be an uncertainty in the value of θ, s_{13PT} and s_{13FT} are more reliable estimates of the true s_{13} than is s_{13L}. There seems to be little hope of attaining sufficient accuracy to choose between s_{13PT} and s_{13FT} and this point will have to be settled by other methods.

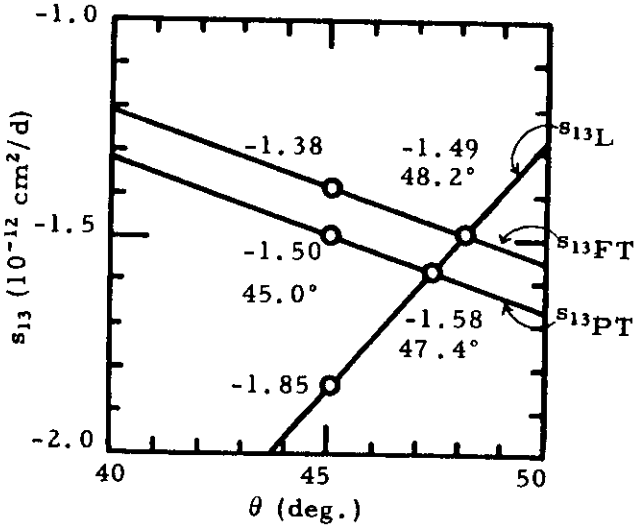

N-4119

Figure II.4. Calculated Values of s_{13} as a Function of Orientation for Grade ATJ Sample 2A

II.4. Preliminary Results on Other Materials

Several minor investigations have been made which are of some interest. Measurements were made on a rectangular bar of ATJ graphite cut parallel to the molding direction. The bar was about 6.5 inches long, one inch wide, and 0.5 inch thick. The bar was cut lengthwise and measurements made on the two parts of almost square cross section. Except for a slight but correctly predicted density variation, the three values of the torsional modulus agreed within about +0.5 per cent. This confirms the correctness of the theory for rectangular bars.

Three samples cut at 0°, 45°, and 90°, of grade ATJ, of grade RVA, and of grade RT 0029 graphite were measured at the Advanced Materials Laboratory and at the Parma Research Center. The resonant frequencies obtained under routine conditions by different operators agreed to within 0.2 per cent. This agreement is due in part to the use of frequency counters. All samples were about five inches long and one inch in diameter. All five compliance constants were calculated without making density corrections, but the results for s_{12} and s_{13} were unsatisfactory. A density correction to the ATJ results gave $s_{12} = -1.8$, $s_{13L} = -2.8$, $s_{13PT} = -1.5$, and $s_{13ET} = -1.3 \times 10^{-12}$ cm^2/d. The value of s_{12} is different from those previously measured but that of s_{13PT} is the same. The large difference between s_{13L} and s_{13PT} is probably due in part to an error in θ and in part to a slight variation in properties (in addition to those caused by a density variation) over the large region from which these samples were cut. It seems desirable to cut samples from as small a region as possible to obtain the maximum homogeneity. Experimental work is being done to determine the smallest practical sample size.

APPENDIX III

CALCINATION OF RAW PETROLEUM COKES

III. 1. Pressure Calcination

Pressure calcination of raw petroleum cokes has been shown to produce a needle-like or ordered structure usually indicative of a low with-grain CTE. An example of this needle-like structure is shown in Figure III. 1 and may be compared to the structure produced by standard calcination shown in Figure III. 2.

Five petroleum cokes were used in the pressure calcination trials and included (a) VT coke; (b) TA coke; (c) DK coke; (d) NA coke, and (e) AX coke. * Each coke was calcined both in lump form and after milling to a 60-flour size. The experiments were made in a four-inch vertical tube furnace and a hydraulic ram exerted a constant pressure on each end of the coke packed in a graphite liner. The furnace temperature was increased, while holding the pressure constant, until the coke pack reached a selected temperature in the range from 1000°-1400°C. The pressure was released after the temperature had been maintained for twenty minutes and the coke was allowed to cool. Oxidation protection was afforded by an argon atmosphere inside the furnace.

The calcined coke was milled to a flour, 60 per cent through 200-mesh, hot mixed with coal tar pitch and pressure molded into plugs. The plugs were baked and graphitized by conventional techniques and used for determination of physical properties as shown in Tables III. 1 through III. 5. Plugs were also made from the same calcined coke using a particle mix, baked to 1000°C and carefully measured before and periodically during the graphitizing cycle for indications of abnormal thermal expansion, commonly referred to as puffing.

Figures III. 3, III. 4 and III. 5 show puffing comparisons between standard and pressure calcination for TA coke flour, AX coke flour, and lump AX coke, respectively. Pressure calcination reduced puffing of coke flours (Figures III. 3 and III. 4), but was not effective with lump coke (Figure III. 5). There are two factors which may explain this behavior. First, there may be a rearrangement of the sulfur-carbon complex facilitated by the increased surface area of the milled material. Second, the pressure is not distributed uniformly through the lumps of coke.

CTE and specific resistance measurements given in Tables III. 1 through III. 5 also show that pressure calcination is more effective on the 60-flour than on the lump coke. There is a general increase in across-grain CTE which indicates a decrease in the with-grain CTE. The specific resistance in the with-grain direction is decreased by pressure calcination. The effect on both of these properties is consistent with the greater orientation shown in Figure III. 1.

* Commercially prepared petroleum cokes.

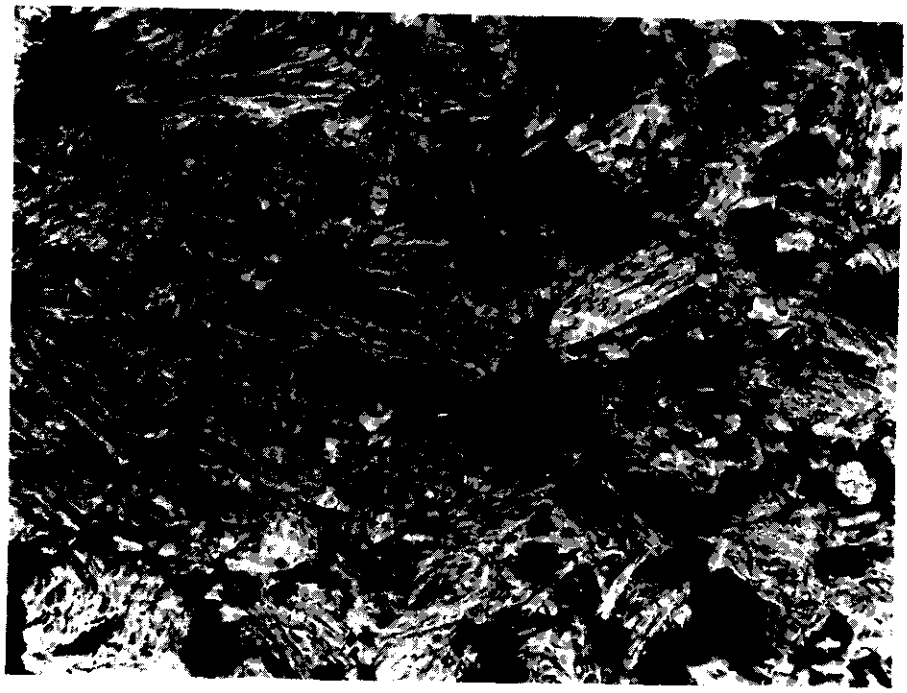

Figure III. 1. Photomicrograph of Petroleum Coke 60-Flour, Pressure Calcined at 1350°C, 150X. N-4510

Figure III. 2. Photomicrograph of Petroleum Coke 60-Flour Control Calcined at 1350°C, 150X. N-4511

Table III. 1

Effect of Pressure Calcination on VT Coke

Description	Calcine Temperature °C	Calcine Wt. Loss per cent	Sulfur Content per cent	Kerosene Apparent Density g/cc	Properties of Graphitized Plugs: Specific Resistance 10^{-4} ohm-cm wg	Properties of Graphitized Plugs: CTE 10^{-6}/°C 25°-2000°C ag	Properties of Graphitized Plugs: Bulk Density g/cc
Lump Coke	1000	9.6	1.14	2.10	45	5.5	1.34
Control	1100	8.8	1.33	2.11	22	5.8	1.33
Calcine	1200	9.8	1.35	2.15	17	5.5	1.35
(atm pressure)	1300	10.2	1.28	2.14	18	5.2	1.38
	1350	10.2	1.30	2.11	19	4.5	1.34
	1400	10.0	1.31	2.12	22	5.8	1.36
Lump Coke	1000	10.0	1.31	2.11	15	6.9	1.36
Pressure	1100	11.5	1.37	2.11	16	6.1	1.35
Calcine	1200	10.4	1.30	2.10	35	6.7	1.39
(2,000 psig)	1300	9.2	1.37	2.12	13	5.6	1.42
	1350	9.2	1.28	--	--	--	1.36
	1400	10.0	1.30	2.15	15	6.4	1.30
60-Flour Coke	1000	10.2	1.13	--	32	5.5	1.45
Control	1100	10.8	1.19	2.11	48	5.1	1.39
Calcine	1200	10.0	0.85	2.11	51	4.7	1.38
(atm pressure)	1300	10.2	1.21	2.14	50	6.0	1.39
	1350	11.0	1.18	2.11	55	5.0	1.37
	1400	10.4	1.19	2.11	36	4.5	1.39
60-Flour Coke	1000	11.7	1.21	2.14	17	5.6	1.37
Pressure	1100	11.2	1.31	2.17	13	6.7	1.39
Calcine	1200	10.8	1.26	2.15	42	6.8	1.41
(2,000 psig)	1300	11.2	1.15	2.14	20	6.3	1.26
	1350	10.8	1.18	2.15	20	7.0	1.27
	1400	11.2	1.23	2.16	21	6.7	1.27

Table III. 2

Effect of Pressure Calcination on TA Coke

Description	Calcine Temperature °C	Calcine Wt. Loss per cent	Sulfur Content per cent	Kerosene Apparent Density g/cc	Properties of Graphitized Plugs: Specific Resistance 10^{-4} ohm-cm wg	Properties of Graphitized Plugs: CTE 10^{-6}/°C 25°-2000°C ag	Properties of Graphitized Plugs: Bulk Density g/cc
Lump Coke Control Calcine (atm pressure)	1000	10.2	1.30	2.08	16	6.5	1.34
	1100	10.0	1.49	2.10	17	4.7	1.31
	1200	10.8	1.34	2.14	13	5.4	1.37
	1300	11.2	1.69	2.06	16	6.1	1.32
	1350	10.6	1.42	2.12	17	5.6	1.39
	1400	11.2	1.44	2.12	21	5.6	1.39
Lump Coke Pressure Calcine (2,000 psig)	1000	--	1.28	2.12	19	5.5	1.36
	1100	10.3	1.61	2.09	20	4.6	1.32
	1200	11.2	1.37	2.24	19	6.2	1.33
	1300	12.9	1.31	2.16	15	5.3	--
	1350	14.2	1.41	2.10	19	6.3	1.26
	1400	12.1	1.32	2.08	21	5.9	1.21
60-Flour Coke Control Calcine (atm pressure)	1000	11.0	1.29	2.14	23	6.2	1.31
	1100	10.8	1.23	2.12	40	4.5	1.34
	1200	11.2	1.20	2.09	46	5.9	1.27
	1300	11.6	1.48	2.11	47	4.0	1.24
	1350	11.2	1.25	2.12	54	4.4	1.36
	1400	11.4	1.18	2.10	42	5.4	1.33
60-Flour Coke Pressure Calcine (2,000 psig)	1000	--	1.26	2.16	17	6.5	1.39
	1100	10.4	1.26	2.07	19	6.1	1.39
	1200	14.2	1.30	2.13	15	5.6	1.39
	1300	12.9	1.26	2.16	17	8.3	1.43
	1350	9.2	1.23	2.11	18	4.9	1.38
	1400	12.9	1.28	2.13	16	6.7	1.39

Table III. 3

Effect of Pressure Calcination on DK Coke

Description	Calcine Temperature °C	Calcine Wt. Loss per cent	Sulfur Content per cent	Kerosene Apparent Density g/cc	Properties of Graphitized Plugs: Specific Resistance 10^{-4} ohm-cm wg	Properties of Graphitized Plugs: CTE 10^{-6}/°C 25°-2000°C ag	Properties of Graphitized Plugs: Bulk Density g/cc
Lump Coke	1000	10.8	1.44	2.09	13	4.6	1.37
Control	1100	11.6	1.51	2.06	18	4.2	1.27
Calcine	1200	11.0	1.52	2.12	31	6.0	1.38
(atm pressure)	1300	10.8	1.52	2.11	19	5.2	1.32
	1350	11.0	1.59	2.11	17	4.6	1.38
	1400	11.0	1.51	2.13	22	5.5	1.33
Lump Coke	1000	10.4	1.48	2.10	18	6.1	1.30
Pressure	1100	11.5	1.54	2.15	16	6.0	1.36
Calcine	1200	10.4	1.52	2.13	17	5.4	1.39
(2,000 psig)	1300	10.0	1.62	2.08	38	6.8	1.39
	1350	10.8	1.53	2.13	15	5.4	1.31
	1400	11.7	1.53	2.16	16	5.4	1.30
60-Flour Coke	1000	11.6	1.38	2.11	39	6.2	1.39
Control	1100	10.8	1.36	2.11	41	6.5	1.42
Calcine	1200	11.0	1.37	2.11	37	4.2	1.40
(atm pressure)	1300	11.2	1.36	2.11	43	6.1	1.40
	1350	11.8	1.39	2.12	40	5.2	1.40
	1400	11.4	1.38	2.10	44	4.0	1.38
60-Flour Coke	1000	14.2	1.35	2.13	18	7.4	1.40
Pressure	1100	11.5	1.43	2.10	15	7.1	1.36
Calcine	1200	11.5	1.40	2.11	43	6.1	1.39
(2,000 psig)	1300	11.7	1.42	2.16	17	4.9	1.37
	1350	12.1	1.38	2.15	17	6.8	1.29
	1400	12.2	1.36	2.14	25	5.4	1.26

Table III. 4

Effect of Pressure Calcination on NA Coke

Description	Calcine Temperature °C	Calcine Wt. Loss per cent	Sulfur Content per cent	Kerosene Apparent Density g/cc	Properties of Graphitized Plugs: Specific Resistance 10^{-4} ohm-cm wg	Properties of Graphitized Plugs: CTE 10^{-6}/°C 25°-2000°C ag	Properties of Graphitized Plugs: Bulk Density g/cc
Lump Coke	1000	9.4	1.69	2.09	18	4.1	1.30
Control	1100	8.3	1.83	2.12	16	4.5	1.36
Calcine	1200	8.5	1.68	2.04	19	6.0	1.30
(atm pressure)	1300	9.2	1.39	2.14	18	5.5	1.40
	1350	10.2	1.84	2.07	18	4.5	1.33
	1400	9.0	1.61	2.10	24	6.5	1.30
Lump Coke	1000	11.7	1.62	2.08	16	7.9	1.38
Pressure	1100	10.0	1.29	2.11	15	6.4	1.33
Calcine	1200	10.0	1.56	2.05	17	5.0	1.32
(2,000 psig)	1300	10.0	0.86	2.19	18	6.2	1.40
	1350	11.2	0.88	2.19	16	5.7	1.41
	1400	--	0.81	2.19	17	6.2	1.42
60-Flour Coke	1000	8.4	1.49	2.10	27	4.9	1.38
Control	1100	8.4	1.55	2.05	34	5.3	1.32
Calcine	1200	9.0	1.46	2.05	32	4.1	1.38
(atm pressure)	1300	9.6	1.52	2.05	39	4.1	1.35
	1350	9.0	1.52	2.07	47	4.4	1.37
	1400	9.2	1.47	2.07	41	4.4	1.35
60-Flour Coke	1000	8.8	1.44	2.13	24	7.2	1.37
Pressure	1100	10.4	1.48	2.08	18	6.4	1.34
Calcine	1200	9.6	1.45	2.14	19	5.7	1.36
(2,000 psig)	1300	11.7	1.46	2.07	16	5.3	1.42
	1350	13.7	1.47	2.05	18	6.2	1.32
	1400	--	1.49	2.04	24	4.9	1.25

Table III. 5

Effect of Pressure Calcination on AX Coke

Description	Calcine Temperature °C	Calcine Wt. Loss per cent	Sulfur Content per cent	Kerosene Apparent Density g/cc	Properties of Graphitized Plugs: Specific Resistance 10^{-4} ohm-cm wg	Properties of Graphitized Plugs: CTE 10^{-6}/°C 25°-2000°C ag	Properties of Graphitized Plugs: Bulk Density g/cc
Lump Coke Control Calcine (atm pressure)	1000	10.6	0.96	2.20	19	4.7	1.39
	1100	10.0	0.94	2.19	19	4.7	1.39
	1200	10.6	0.93	2.18	18	5.6	1.41
	1300	9.8	0.98	2.20	20	3.9	1.43
	1350	10.4	1.03	2.17	21	4.8	1.40
	1400	10.2	0.95	2.18	23	4.0	1.39
Lump Coke Pressure Calcine (2,000 psig)	1000	6.3	0.90	2.13	22	6.1	1.38
	1100	6.7	0.91	2.21	17	5.6	1.39
	1200	6.3	0.91	2.18	17	4.6	1.40
	1300	7.5	0.87	2.18	17	6.1	1.42
	1350	3.8	0.97	2.19	19	4.4	1.41
	1400	4.2	0.92	2.17	21	5.1	1.38
60-Flour Coke Control Calcine (atm pressure)	1000	9.4	0.80	2.17	42	5.0	1.32
	1100	9.4	0.84	2.20	41	4.0	1.34
	1200	10.6	0.78	2.19	44	4.1	1.34
	1300	8.4	0.85	2.16	47	4.8	1.37
	1350	7.7	0.89	2.17	48	4.4	1.38
	1400	7.3	0.87	2.15	53	4.3	1.38
60-Flour Coke Pressure Calcine (2,000 psig)	1000	10.8	0.82	2.18	20	7.2	1.42
	1100	12.5	0.84	2.22	19	5.8	1.45
	1200	16.7	0.79	2.22	21	5.8	1.45
	1300	10.8	0.85	2.22	17	6.3	1.43
	1350	13.3	0.82	2.18	22	6.2	1.43
	1400	13.3	0.87	2.20	21	4.7	1.40

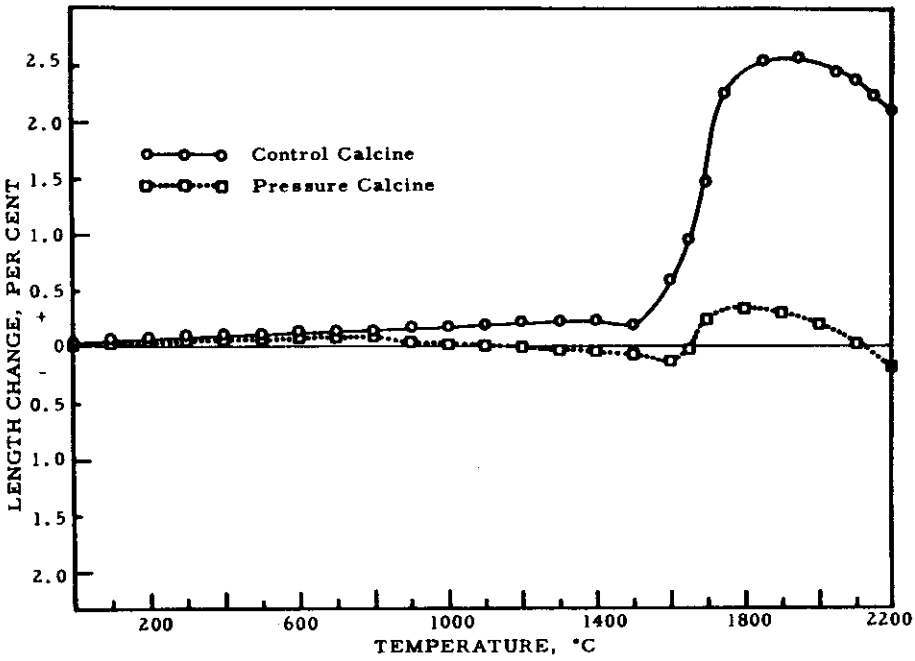

Figure III. 3. Puffing Diagram of Plugs Made from TA Coke Calcined to 1350°C as 60-Flour. N-4512

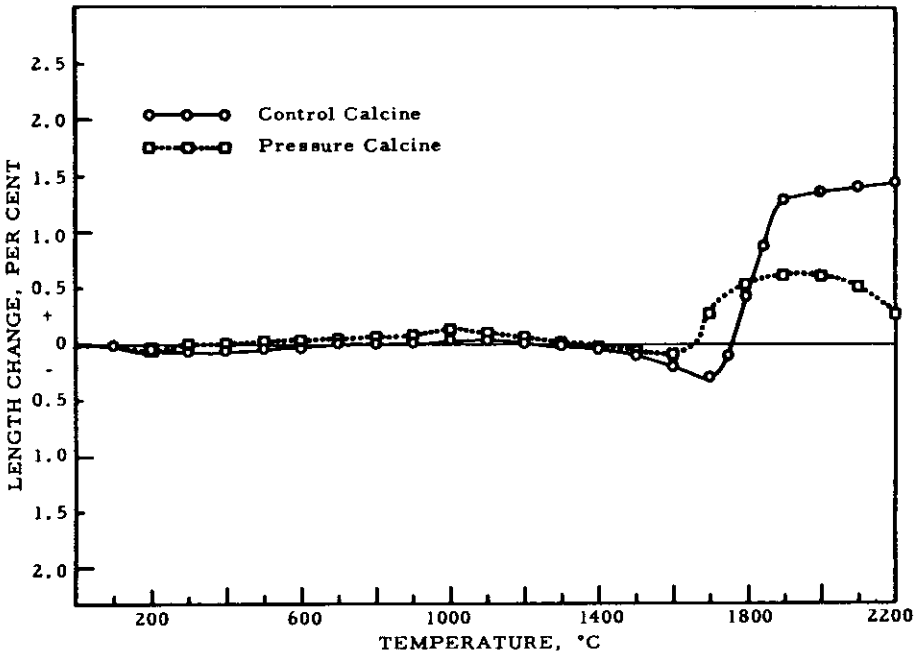

Figure III. 4. Puffing Diagram of Plugs Made from AX Coke Calcined to 1350°C as 60-Flour. N-4513

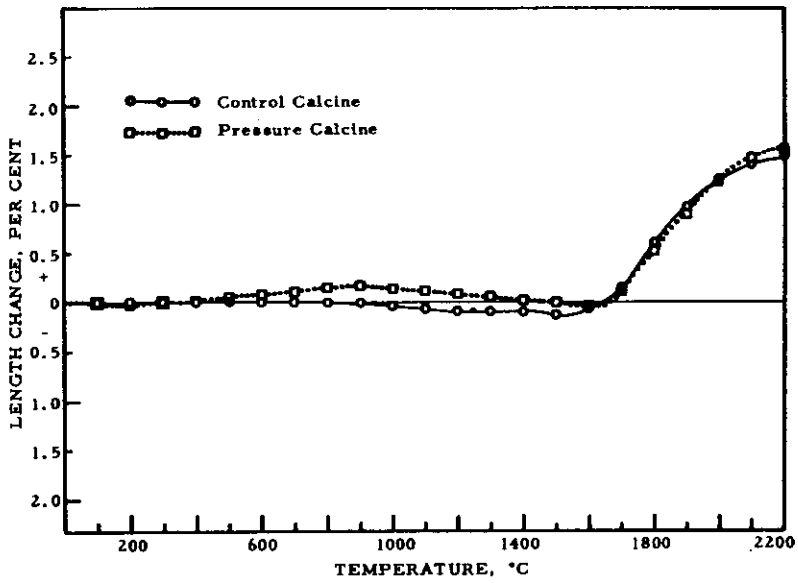

N-4514

Figure III.5. Puffing Diagram of Plugs Made from AX Coke Calcined to 1350°C in Lump Form

The five cokes selected for testing show some differences in (a) volatile content, (b) sulfur content, and (c) crystallinity as shown by the CTE. All five cokes, nevertheless, responded similarly to pressure calcination.

III.2. Sulfur Calcination

Sulfur is known to be a useful oxidizing agent for aromatic compounds to increase the yield of carbon and reduce the amount of condensable volatiles. A study was made of the effect on coke properties by the addition of sulfur prior to calcination. The preliminary trials were made with raw coke milled to a 60-flour, blended with 33 per cent by weight of powdered sulfur and calcined to 1350°C. Plugs were molded from the coke (as with pressure calcined cokes) and used to measure puffing and CTE. The results indicated that not only was the puffing tendency of the final article suppressed but also there was a reduction of the with-grain CTE. Sulfur calcination of both TA and HT cokes produced a more oriented structure as shown in Figures III.6 and III.8, compared to the standard calcination (Figures III.7 and III.9). The sulfur calcined cokes were lighter in weight, the binder requirement was increased about 5 pph by weight and there was an agglomeration effect as shown by differences in screen analyses before and after calcination.

The effects obtained from the above preliminary trials were significant enough to warrant further investigation. The variables studied included types of cokes, calcining methods, rates and temperatures, and amount of sulfur added. The calcined coke was milled to flour, mixed with pitch binder

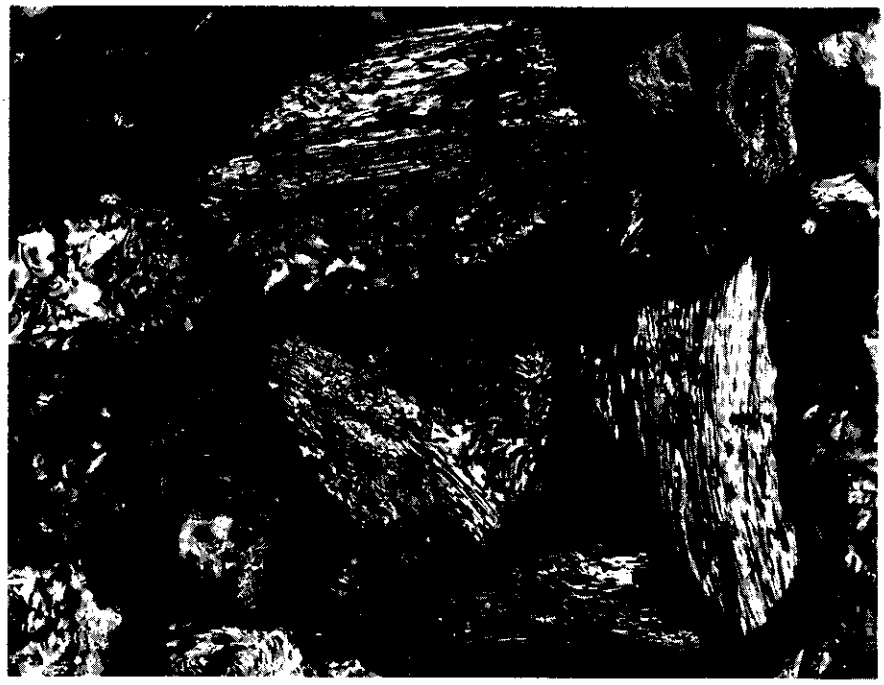

N-4515

Figure III. 6. Photomicrograph of TA Coke, Sulfur Calcined, 100X

Figure III. 7. Photomicrograph of TA Coke, Standard Calcined, 100X

N-4516

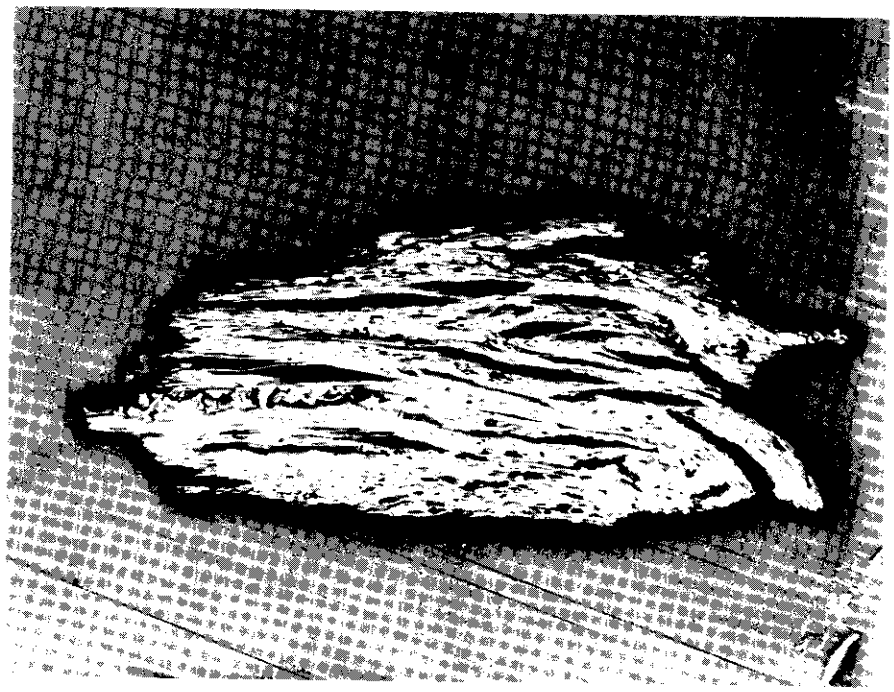

N-4517
Figure III. 8. Photomicrograph of HT Coke, Sulfur Calcined, 100X.

Figure III. 9. Photomicrograph of HT Coke, Standard Calcined, 100X.
N-4518

and extruded into rods which were baked and graphitized. Physical properties were measured on the calcined cokes and the extruded rods.

Table III. 6 and Figure III. 10 show that different samples of TA coke calcined under similar conditions yielded different reductions in CTE. Table III. 7 and Figure III. 11 show that the addition of sulfur to HK coke consistently reduced the CTE but the level of CTE was raised by increased volatile content and calcination rate. The higher volatile content was also responsible for agglomeration as noted in Table III. 7. Differences in volatile were probably the cause of the different behavior of TA No. 1 and No. 2 cokes described in Table III. 6 and Figure III. 10. Table III. 8 and Figure III. 12 demonstrate that the reduction of CTE due to the addition of sulfur to TA coke steadily decreased as the calcining temperature increased. Table III. 9 and Figure III. 13 indicate that, at least with DK coke, additions of sulfur up to 33 per cent were effective in reducing CTE, but 66 per cent sulfur gave a slightly higher CTE. The calcination of DK coke without sulfur (Table III. 10 and Figure III. 14) in an induction heated furnace resulted in much lower CTE than in a resistance heated furnace, but the addition of 33 per cent sulfur eliminated the furnace effect on CTE.

The explanations for the above effects are not obvious but the kinetics of the sulfur-hydrogen reactions contribute importantly since the CTE is markedly affected by volatile content.

Sulfur calcining, similar to pressure calcining, yields a coke in which the puffing is materially reduced. Figures III. 15, III. 16 and III. 17 give puffing diagrams for TA cokes calcined at 1200°, 1350°, and 1600°C, respectively, and show that the puffing is much more severe for the 1200°C calcination. This effect is undoubtedly related to the retention of sulfur at the lower calcining temperature, as shown in Table III. 8.

Table III.6. Effect of Sulfur Calcination on TA Coke

Coke Source	Added Sulfur per cent	Calcining Temperature °C	Calcining Rate °C/hr	Apparent Density g/cc	Sulfur per cent	Extruded Rod Properties: Pitch Level pph	Green Bulk Density g/cc	Baked Bulk Density g/cc	Graphite Bulk Density g/cc	CTE 10^{-6}/°C 30°-100°C wg	Agglomeration
TA-1	0	1350	400	2.053	1.06	34	1.631	1.430	1.454	0.64	No
	5	1350	400	2.016	.68	37	1.536	1.385	1.390	0.76	No
	10	1350	400	1.947	.73	37	1.444	1.343	1.354	0.62	No
	33	1350	400	1.844	.70	39.5	1.369	1.258	1.281	0.55	No
TA-2	0	1350	400	2.117	1.62	34	1.630	1.46	1.423	1.48	Yes
	5	1350	400	1.916	1.78	34	1.499	1.401	1.401	1.18	Yes
	10	1350	400	1.788	1.52	34	1.369	1.292	1.319	--	Yes
	33	1350	400	1.727	1.34	35.5	1.313	1.266	1.27	0.88	Yes

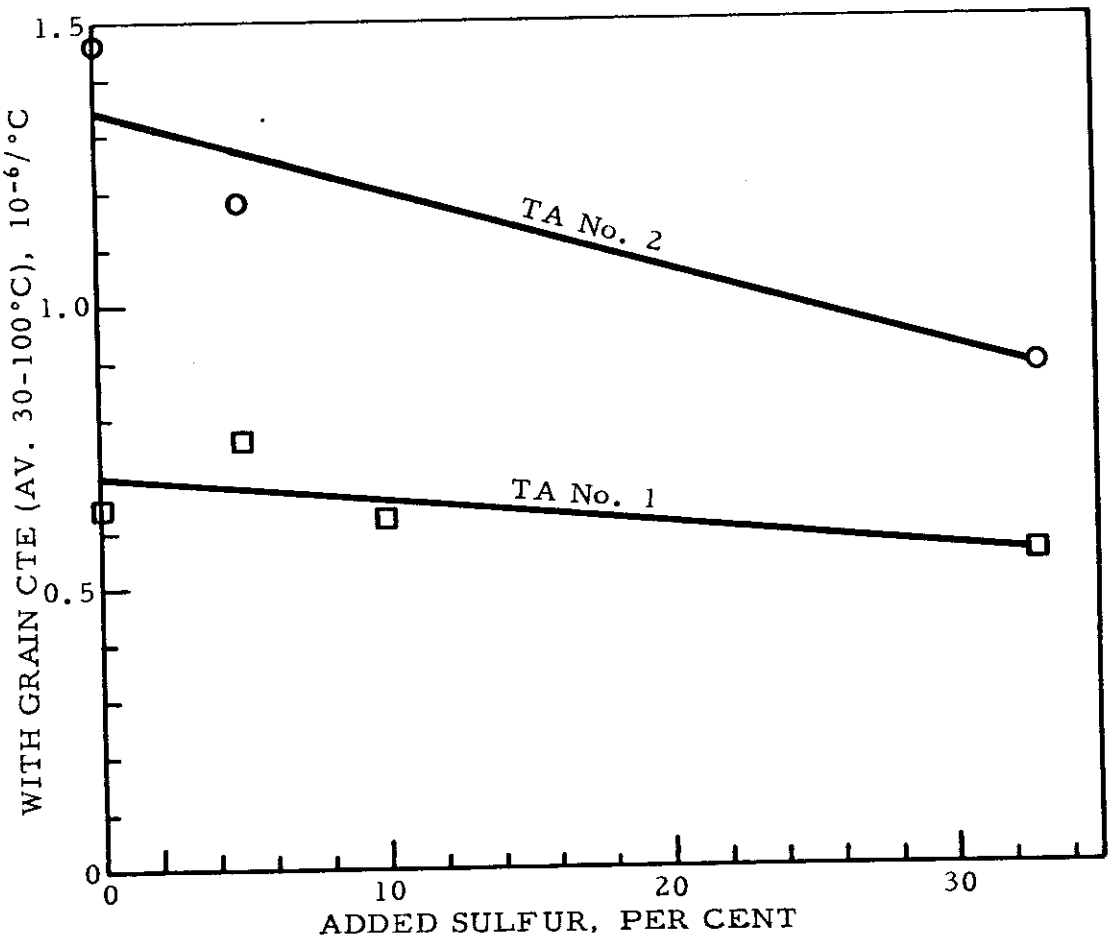

N-4519

Figure III.10. Sulfur Calcination of Different TA Coke Samples, Calcined to 1350°C.

Table III. 7. Effect of Sulfur Calcination on HK Coke as Related to Initial Volatile Content and Calcining Rate

Coke Source	Added Sulfur per cent	Calcining Temperature °C	Calcining Rate °C/hr	Apparent Density g/cc	Sulfur per cent	Extruded Rod Properties: Pitch Level pph	Green Bulk Density g/cc	Baked Bulk Density g/cc	Graphite Bulk Density g/cc	CTE 10^{-6}/°C 30°-100°C wg	Agglomeration
HK-1*	0	1350	400	2.102	0.44	34	1.708	1.541	1.527	0.70	No
	33	1350	400	1.823	2.80	34	1.431	1.343	1.329	0.52	No
	0	1350	1100	2.092	0.36	38	1.720	1.459	1.474	0.97	No
	33	1350	1100	1.984	3.46	37	1.624	1.421	1.394	0.88	No
HK-2**	0	1350	400	2.066	0.42	34	1.652	1.566	1.612	1.55	Yes
	33	1350	400	1.931	4.84	34	1.461	1.437	1.388	1.27	Yes
	0	1350	1100	2.045	0.22	38	1.680	1.563	1.607	1.87	Yes
	33	1350	1100	1.963	4.24	37	1.605	1.425	1.414	1.48	Yes

* Volatile Content = 8.2 per cent
** Volatile Content = 13.8 per cent

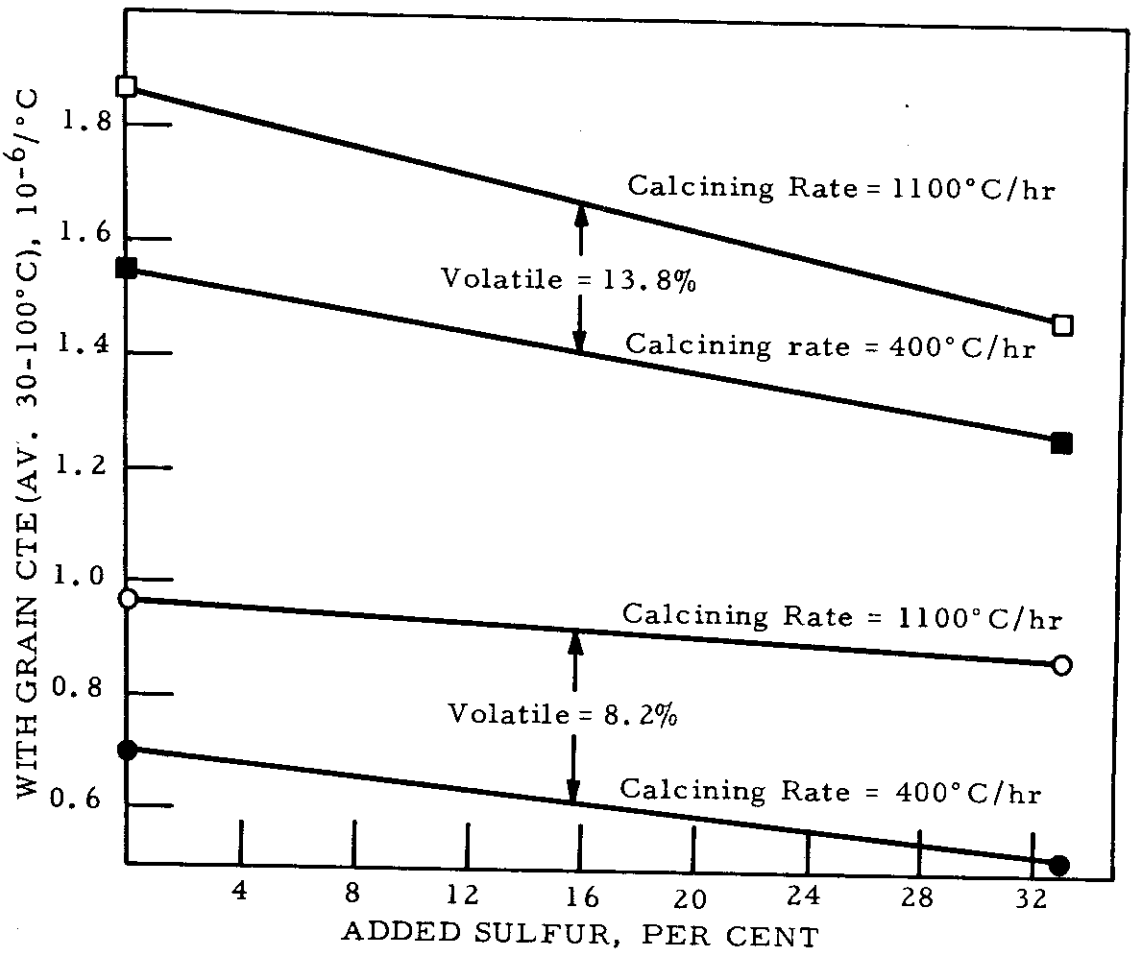

Figure III. 11. Effect of Volatile Content and Calcining Rate on Sulfur Calcination of HK Coke, Calcined to 1350°C. N-4520

Table III. 8. Effect of Temperature on Sulfur Calcination of TA Coke

Added Sulfur per cent	Calcining Temperature °C	Calcining Rate °C/hr	Apparent Density g/cc	Sulfur per cent	Extruded Rod Properties: Pitch Level pph	Green Bulk Density g/cc	Baked Bulk Density g/cc	Graphite Bulk Density g/cc	CTE 10^{-6}/°C 30°-100°C wg
0	1000	400	1.940	1.58	32.0	1.633	1.490	1.530	1.69
33	1000	400	1.956	4.12	36.5	1.627	1.436	1.370	0.86
0	1200	400	2.000	1.68	35.0	1.690	1.504	1.520	1.67
33	1200	400	2.050	5.70	37.0	1.743	1.552	1.470	1.00
0	1350	400	2.117	1.62	34.0	1.630	1.462	1.423	1.48
33	1350	400	1.727	1.34	35.5	1.313	1.266	1.277	0.88
0	1600	400	2.006	0.40	44.0	1.612	1.384	1.384	0.93
33	1600	400	1.911	0.34	44.0	1.418	1.234	1.234	0.66

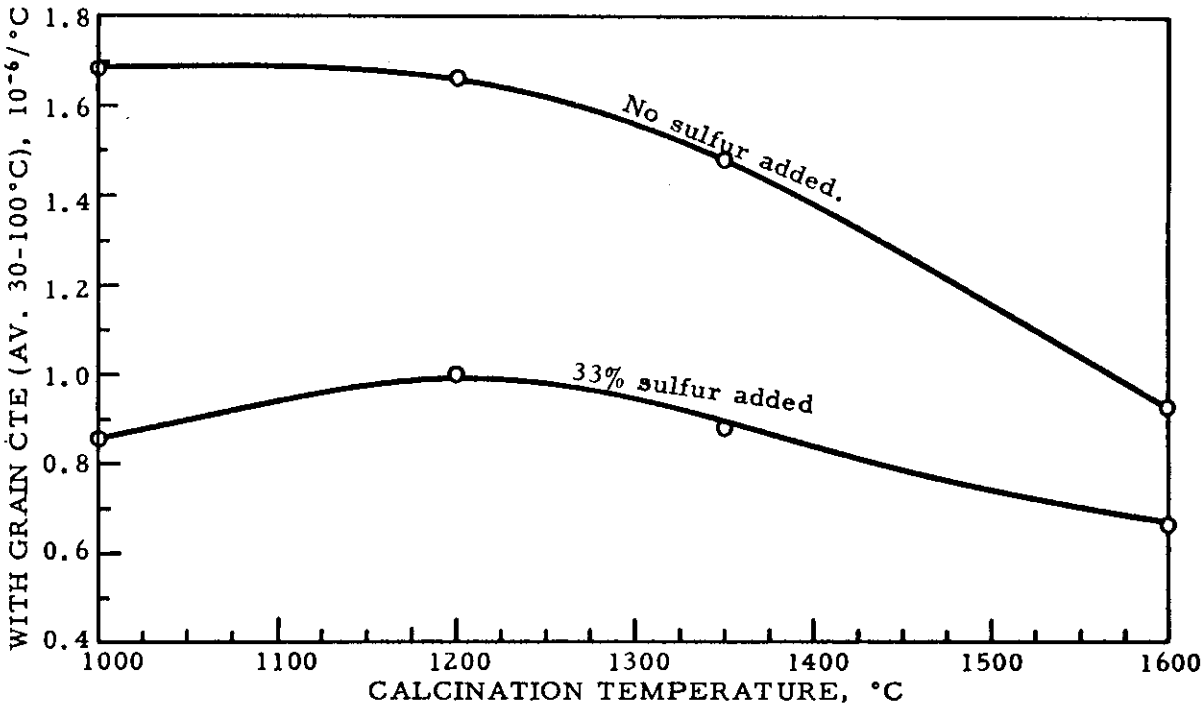

N-4521

Figure III. 12. Effect of Temperature on Sulfur Calcination of TA Coke

Table III. 9. Effect of Sulfur Concentration on Calcination of DK Coke

Added Sulfur per cent	Calcining Temperature °C	Calcining Rate °C/hr	Apparent Density g/cc	Sulfur per cent	Extruded Rod Properties: Pitch Level pph	Green Bulk Density g/cc	Baked Bulk Density g/cc	Graphite Bulk Density g/cc	CTE 10^{-6}/°C 30°-100°C wg
0	1350	1100	1.958	1.68	36	1.678	1.422	1.387	2.34
33	1350	1100	1.994	5.44	36	1.623	1.391	1.319	1.00
66	1350	1100	1.893	3.2	36	1.562	1.383	1.329	1.34

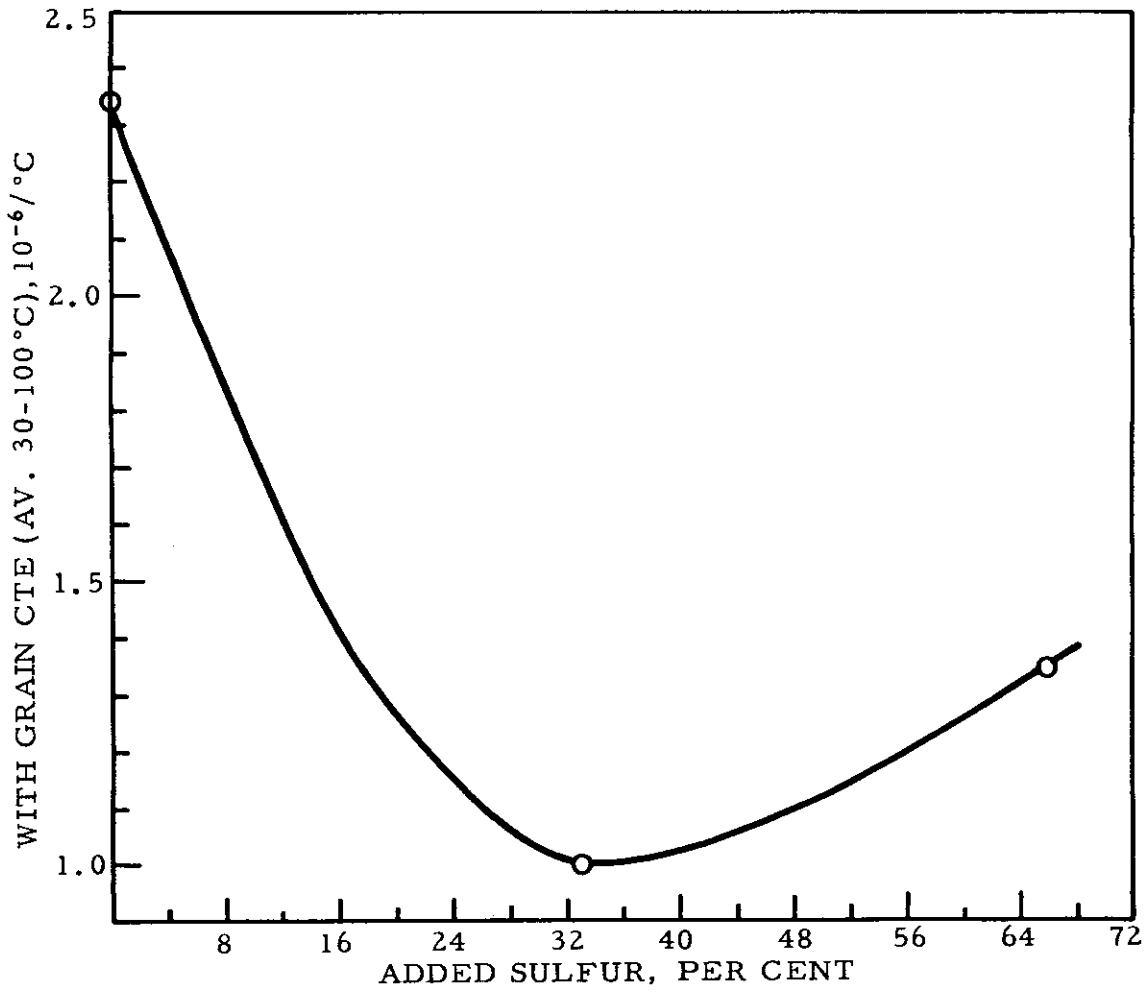

N-4522

Figure III. 13. Effect of Sulfur Concentration on Calcination of DK Coke, Calcined to 1350°C

Table III. 10. Effect of Furnace Type Sulfur Calcination of DK Coke

Furnace Type	Added Sulfur per cent	Calcining Temperature °C	Calcining Rate °C/hr	Apparent Density g/cc	Sulfur per cent	Extruded Rod Properties: Pitch Level pph	Green Bulk Density g/cc	Baked Bulk Density g/cc	Graphite Bulk Density g/cc	CTE 10^{-6}/°C 30°-100°C wg
Resistance	0	1350	1100	1.958	1.68	36	1.678	1.422	1.387	2.34
Resistance	33	1350	1100	1.944	5.88	36	1.623	1.391	1.319	1.00
Induction	0	1350	1100	2.042	1.56	36	1.640	1.451	1.519	1.45
Induction	33	1350	1100	1.885	3.54	36	1.756	1.528	1.424	1.12

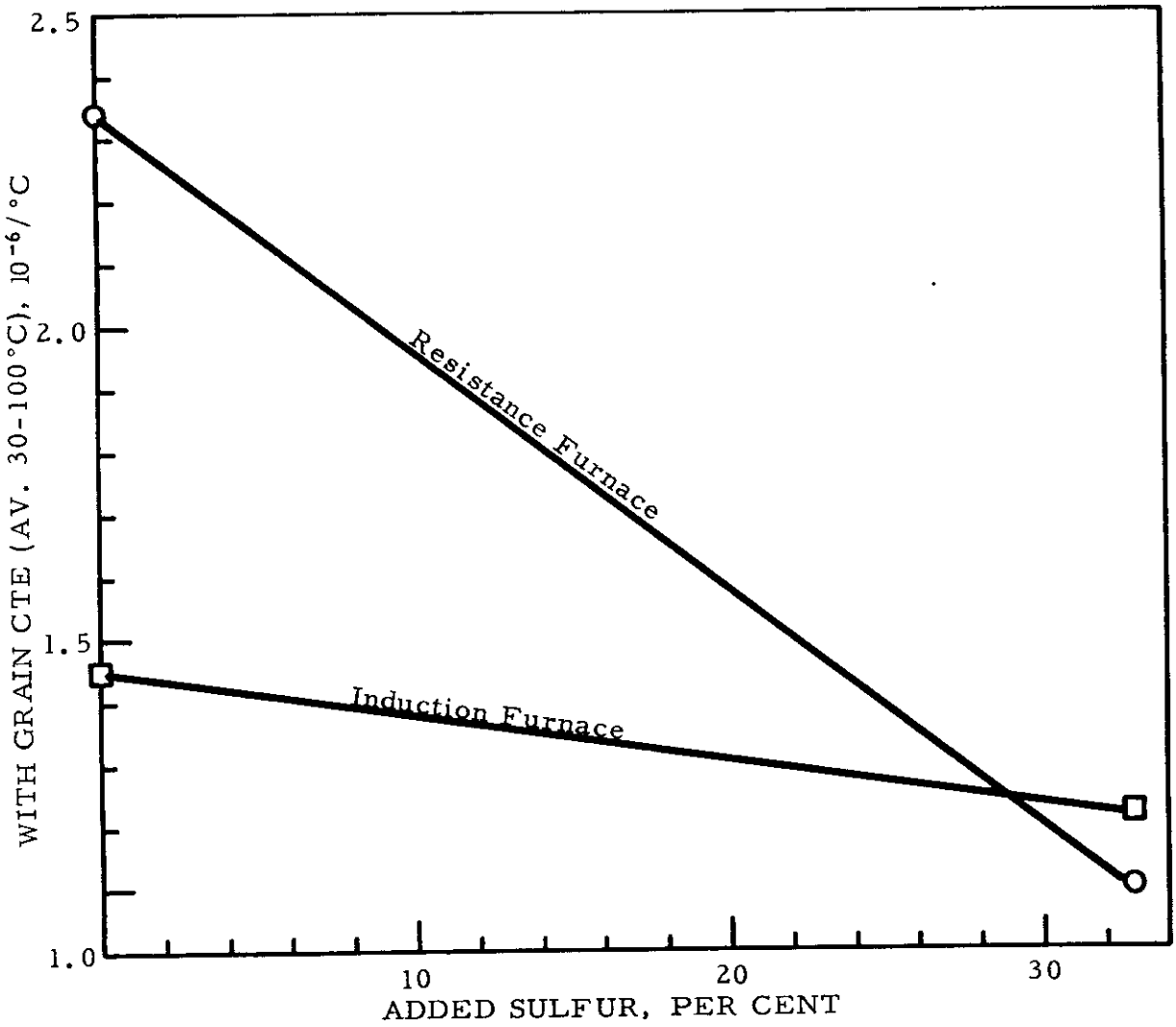

N-4523

Figure III. 14. Effect of Furnace Type on Sulfur Calcination of DK Coke, Calcined to 1350°C

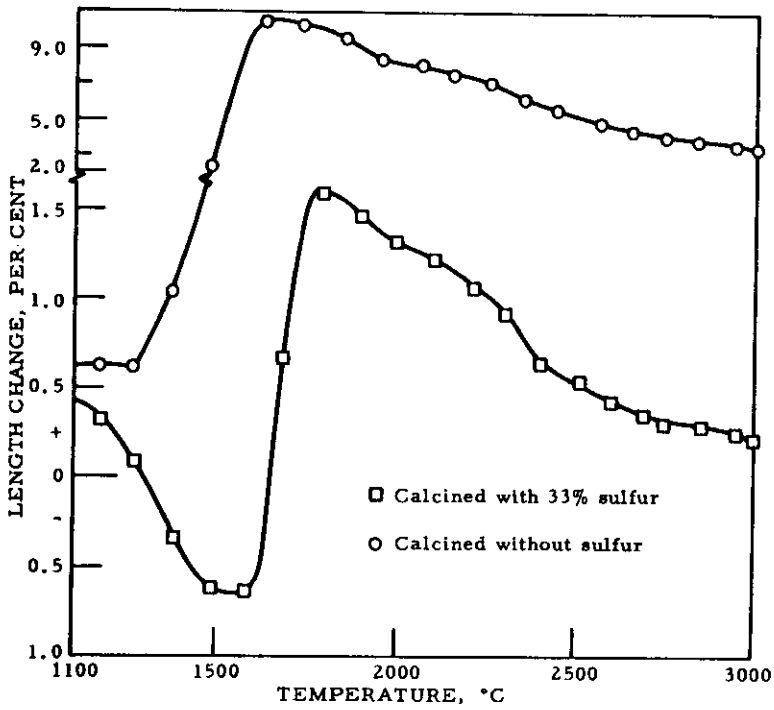

N-4524

Figure III. 15. Puffing Diagrams of Plugs Made from TA Coke, Calcined to 1200°C

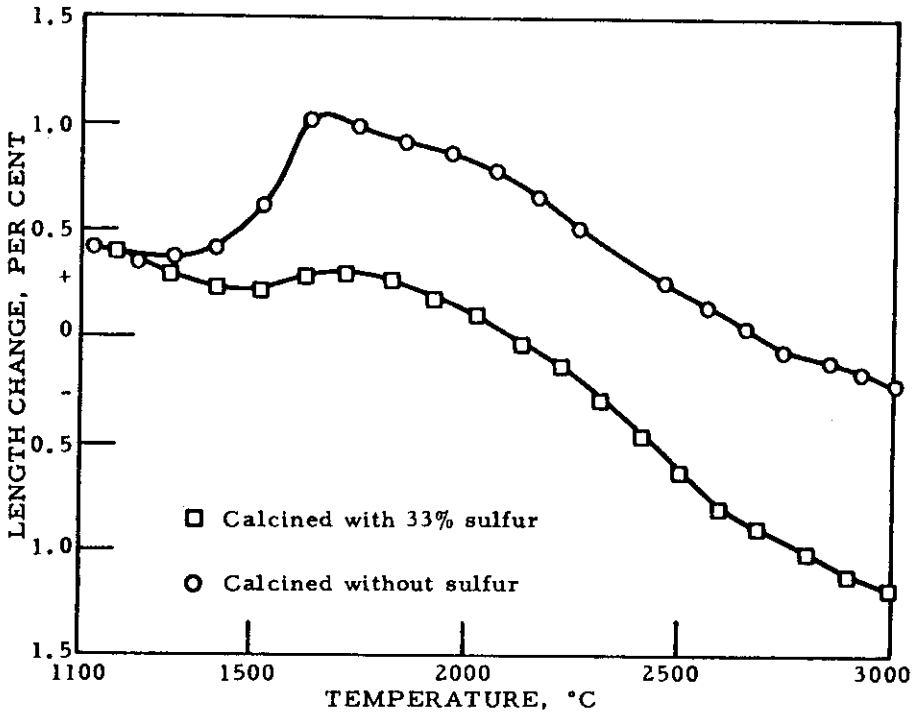

Figure III. 16. Puffing Diagrams of Plugs Made from TA Coke, Calcined to 1350°C

N-4525

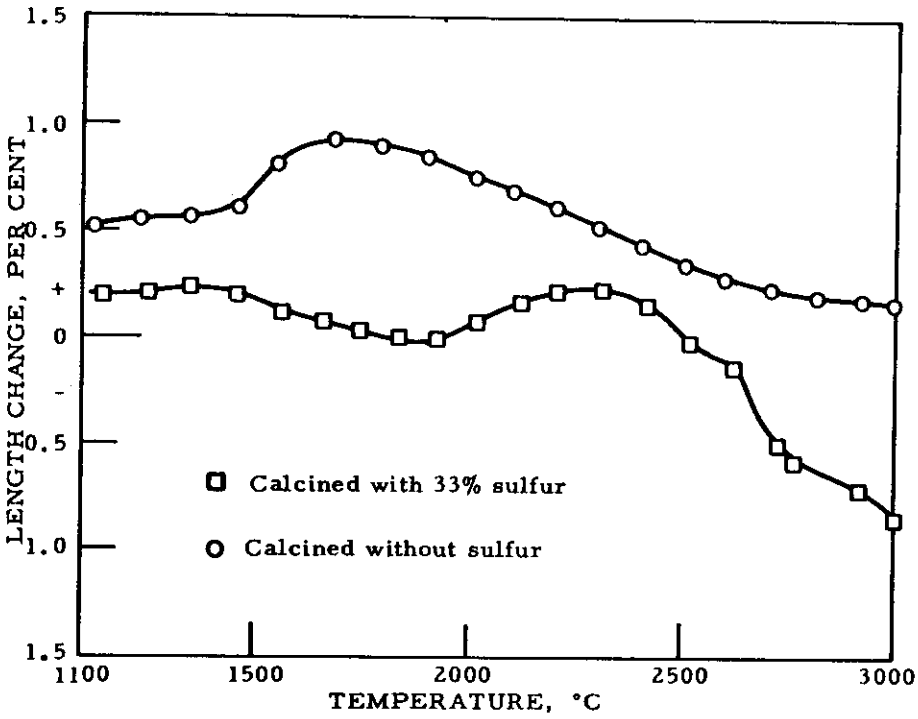

N-4526

Figure III. 17. Puffing Diagram of Plugs Made from TA Coke, Calcined to 1600°C

APPENDIX IV

IMPROVEMENT OF GRAPHITE PROPERTIES BY PREIMPREGNATION OF RAW MATERIALS

IV. 1. Objective

The objective of this investigation was to determine what effect impregnation of petroleum coke, prior to its use as filler material in carbon mixes, would have on the final graphite physical properties.

IV. 2. Raw Materials Impregnation

AX petroleum coke calcined to 1350°C was selected as the material for the initial trial of raw material impregnation. For ease of handling, the coke used for this trial was screened to maintain a particle size of not less than 3/16-inch diameter. The material was loaded into a wire basket, preheated to 125°C and held at this temperature for one hour under vacuum in an autoclave. Melted coal tar pitch was then admitted to the autoclave and a pressure of 100 lbs/in^2 applied for four hours at 125°C. The amount of pitch retention was calculated to be 28 per cent of the weight of the coke. The impregnated coke was then calcined to 450°C. During the 450°C calcination of the impregnated raw materials, approximately 48 per cent of the pitch volatiles was expelled. The coke retained the remaining 52 per cent as a high melting point impregnant having a coking value of about 90 per cent. These values were calculated by measuring the residual volatile of the impregnated coke. The polymerized impregnant was partially soluble in the raw pitch binder added during subsequent processing. Higher effective binder concentrations were achieved in this manner than had before been possible without impairing the structural qualities of the product. The results of this initial trial indicated that further investigation was warranted.

The proper calcination temperature was determined by the amount of binder required to produce bulk articles from impregnated coke calcined to various temperatures. Six calcination temperatures were evaluated at 25°C intervals over the temperature range of 400-550°C. Figures IV. 1 through IV. 8 show the original AX coke before and after pitch impregnation and after calcination to each of the above temperatures. The pitch or pitch coke deposits are indicated by arrows on the photomicrographs. The amount of pitch retained was determined by the structure of the coke as can be seen in these figures. Residual volatile, specific resistance, and kerosene apparent density were determined after each test bake. The preliminary lots of calcine were milled to a 45-flour, subdivided into 500 gram lots and used for determination of binder requirements. Binder levels (100°C melting point coal tar pitch) were evaluated in two-pound increments from 32 to 40 pounds of pitch per 100 pounds of flour. Mixes were made at each binder level, manually formed into two-inch diameter balls and baked to 750°C. The amount of coke sticking to the balls after baking was considered as a measure of the binder required for a given flour or calcine, with excessive coke sticking indicating too much binder. A calcination temperature of 450°C was selected for further investigations discussed in this report, the selection being based on the results of the calcination test bakes and subsequent mixing and baking trials.

N-4527
Figure IV.1. AX Coke, Calcined to 1350°C, 100X

Figure IV.2. AX Coke, Calcined to 1350°C, Pitch Impregnated, 100X
N-4528

Figure IV.3. AX Coke, Calcined to 1350°C, Pitch Treated and Recalcined to 425°C, 100X N-4529

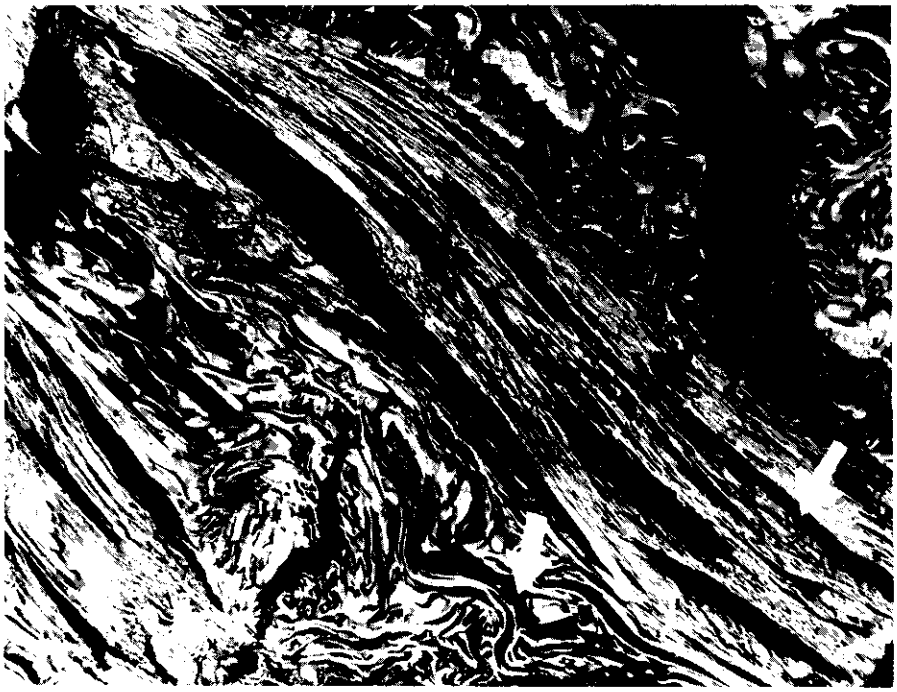

Figure IV.4. AX Coke, Calcined to 1350°C, Pitch Treated and Recalcined to 450°C, 100X N-4530

Figure IV.5. AX Coke, Calcined to 1350°C, Pitch Treated and Recalcined to 475°C, 100X N-4531

Figure IV.6. AX Coke, Calcined to 1350°C, Pitch Treated and Recalcined to 500°C, 100X N-4532

Figure IV.7. AX Coke, Calcined to 1350°C, Pitch Treated and Recalcined to 525°C, 100X N-4533

Figure IV.8. AX Coke, Calcined to 1350°C, Pitch Treated and Recalcined to 550°C, 100X N-4534

IV. 3. Preimpregnated Coke as a Raw Material in the Pressure Curing Process

Several grades of graphite are produced using pressure curing[58] as one of the initial processing steps. This pressure curing process permits successful baking of larger cross sections of fine-grain graphite than can be baked when using conventional processing methods. The pressure curing process has been successful for fabricating grades incorporating graphite filler materials but not for grades using coke filler materials. Experience in conventional processing suggests that a strength improvement would result if a coke base pressure cured graphite could be developed.

The volume shrinkage which takes place during the final heating or graphitizing (above 2450°C) of bulk graphites produced from petroleum cokes is one factor contributing to their relatively high strength; however, shrinkage is virtually nonexistent when graphite filler materials are produced through the pressure curing process. The strength of the material produced in this manner is lower than would be expected with coke filler material. Three rather serious problems encountered in development trials using coke filler in the pressure curing are:

1. The electrical resistance of 1350°C petroleum coke is higher than graphitized coke by a factor of 3. Current channeling caused by this high resistance results in nonuniform thermosetting of the binder systems.

2. Higher pressures are generally required to eject the cured compacts from the die cavity than employed for curing, causing the compact to crack.

3. Coke-base pressured cured compacts are more difficult to bake than the graphite-base compositions.

Preimpregnated cokes, as discussed in Section IV. 2, were considered as a possibility for filler material in the pressure curing process. Due to the 450°C calcination and subsequent additions of raw pitch at lower concentrations, the mixes made with preimpregnated petroleum coke contain fewer volatiles than do mixes made with standard coke fillers. It was reasoned that the expulsion of less volatile during pressure curing would alleviate some of the above listed processing problems. A pressure curing trial was made in order to test this possibility.

The initial trial was made with 1350°C calcined AX petroleum coke as the primary base material. This AX coke, pitch treated and calcined to 450°C in the same manner as described in Section IV. 2, was crushed and milled to pass one hundred per cent through a 20-mesh screen. The milled 450°C calcine was blended with 175°C melting point pitch for 45 minutes in a Patterson-Kelley twin-shell blender. A reference blend having unimpregnated 1350°C calcined AX coke flour, one hundred per cent through 20-mesh, was made in the same manner. Blend compositions were:

Ingredients	Test Lot	Reference
Preimpregnated AX Coke Flour - lbs	400	-
Standard AX Coke Flour - lbs	-	400
175°C Coal Tar Pitch - lbs	72.0	80.0
Sulfur, Screen through 35-mesh - lbs	14.4	16.0

The 450°C calcined coke in the test lot contained a calculated 9.9 pounds 450°C semipitch coke per 100 pounds base petroleum coke. The total binder concentration, including the pitch added to the blend, was 27.9 pounds of pitch per 100 pounds of coke. Binder level for the reference blend was 20 pounds of pitch per 100 pounds of coke.

Each mix was precompacted into a 22-inch diameter x 20-inch long cylinder and pressure cured at 1,000 lbs/in^2. Pressures as high as 2,000 lbs/in^2 were required to eject the plugs from the die cavity which resulted in two peripheral cracks.

Baking of the plug from the test lot to 750°C produced no increase in the two cracks observed after precompaction; however, the peripheral cracks in the reference sample were increased by 2 or 3 inches and a vertical flaw extending over the entire length of the plug was also observed. Since these results represent the initial test for only one block of each type, one cannot positively conclude that the test sample was more "bakeable" than the reference sample.

Evaluation of the physical and electrical properties of the test specimens at the various processing levels present more conclusive results. After the initial 750°C bake the blocks were subdivided into three pieces:

1. Each block was sawed through the length into two approximately equal parts. One-half of each block was pitch treated, rebaked to 750°C and graphitized to 3000°C.

2. The other half of each block was sawed ninety degrees to produce two 10-inch long quarter-round pieces. One sample of each type was graphitized to 3000°C.

3. The remaining two quarter sections were given no further treatment.

The blocks representing each of the above three processing steps were sawed into with- and against-the-grain samples on which physical and electrical properties were determined as shown in Table IV.1.

Bulk density versus processing temperature is plotted in Figure IV.9. The density of the 750°C baked test samples averaged 0.19 g/cc higher than the reference samples and after 3000°C graphitization, with no added pitch treatment, the test samples were 0.16 g/cc higher than the reference samples. The differences in bulk density after one pitch treatment and 3000°C bake were not quite as large but were still significant.

Table IV. 1. Property Comparison of Pressure Cured Blocks, Preimpregnated AX Coke Base vs Standard AX Coke Base.

	Preimpregnated AX Coke Base		Standard AX Coke Base	
Bulk Density, g/cc				
Precompacted (22" dia x 20" long Plug)	1.612		1.43	
Pressure-cured (20" dia x 18" long Machined Plug)	1.738		1.565	
	With Grain	Against Grain	With Grain	Against Grain
750°C Bake* (1/2" x 1/2" x 5" long Sawed Samples)	1.674	1.661	1.476	1.476
Number of samples	10	9	14	12
3000°C Bake	1.597	1.597	1.44	1.42
Number of samples	18	18	18	18
Pitch Treat + 3000°C Bake	1.69	1.69	1.64	1.63
Number of samples	18	18	18	18
Sonic Modulus x 10^6				
750°C Bake	1.15	0.294	0.660	0.063
Number of samples	10	9	14	12
3000°C Bake	0.80	0.16	0.46	0.08
Pitch Treat + 3000°C Bake	1.64	0.50	1.47	0.44
Specific Resistance x 10^{-4}				
700°C Bake	156.2	381.6	363.6	944.0
3000°C Bake	13.87	40.88	28.31	142.52
Pitch Treat + 3000°C Bake	12.76	27.19	17.27	46.28
Flexural Strength, lbs/in^2				
750°C Bake	1,082	482	821	151
Number of Samples	10	9	14	12
3000°C Bake	1,133	219	364	68
Pitch Treat + 3000°C Bake	2,773	1,174	2,316	812

* The remainder of the samples were 1/2" x 1/2" x 5" long, sawed.

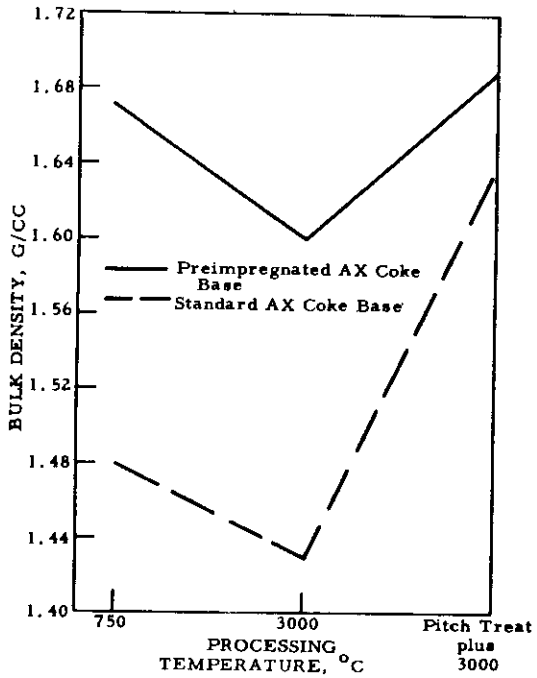

Figure IV. 9. Density Comparison, Pressure Cured Blocks, Preimpregnated AX Coke Base and Standard AX Coke Base.

N-4535

Specific resistance versus temperature is plotted in Figure IV. 10 for both with- and against-grain directions. The 750°C baked samples show the test lot material was much lower in resistance than the reference material. The differences in the resistance values between the two processes were reduced by baking to 3000°C and still further by pitch treating and rebaking to 3000°C; however, in each case, the lower resistance of the test lot was quite significant.

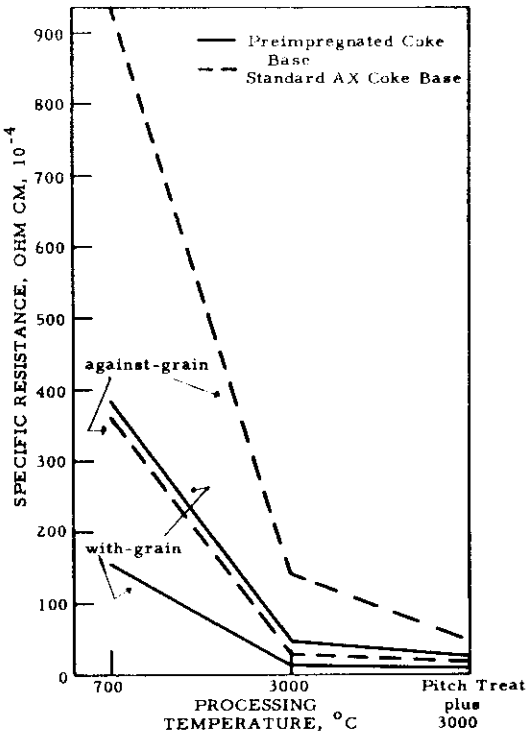

N-4536

Figure IV. 10. Resistance Comparison, Pressure Cured Blocks Preimpregnated AX Coke Base and Standard AX Coke Base.

Flexural strength values with- and against-grain versus temperature are given in Figure VI. 11. The test lot displayed superior strength performances at all three points of processing.

The data from this trial were not enough to permit drawing definite conclusions. The results were encouraging, however, and indicate strongly that the objectives of this study hold considerable merit. Areas warranting further investigation include:

1. Preimpregnation of artificial graphites for evaluation in the pressure curing process;
2. Evaluation of the adaptability of preimpregnated artificial graphites as the base material for other fabrication methods;
3. Investigation of pressure cured stocks made from preimpregnated cokes and graphites for hot working [60] applications.

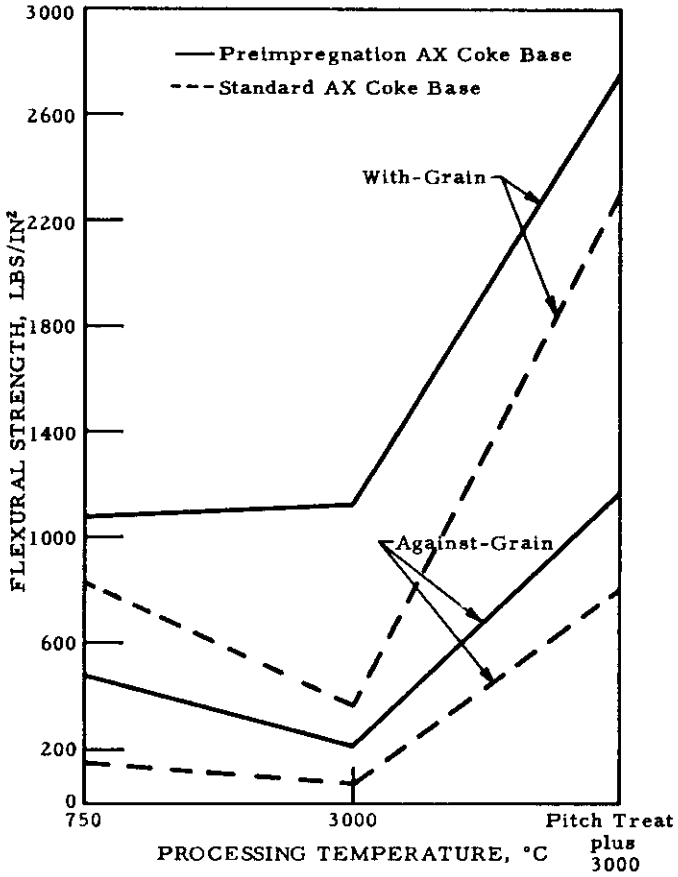

N-4537

Figure IV.11. Flexural Strength Comparison, Pressure Cured Blocks, Preimpregnated AX Coke Base and Standard AX Coke Base.

APPENDIX V

INDUCTION HEATING FOR PRESSURE CURING

V.1. Description of Development Program

A program was undertaken to check the feasibility of scaling up the pressure curing process to large size graphite (e.g., 60 inch diameter or larger). The use of resistance heating in the pressure curing process will become economically impractical for very large sizes of graphite and beyond this point induction heating becomes more feasible. It is estimated that this point is in the neighborhood of 60 inch diameter. The development program to adapt induction heating to pressure curing was divided into three phases as follows:

Phase I was concerned with the heating patterns produced by induction heating during pressure curing of a green RVA plug.

Phase II involved the selection of engineering materials for use in the design of mold and pressure ram tooling.

Phase III coordinated the information obtained from Phases I and II into a process permitting successful pressure curing of RVA grade graphite utilizing induction heating.

V.2. Phase I - Induction Heating Studies

Uniform heating is essential in the plugging and curing cycles of the RVA process, so it was necessary to determine the degree of temperature uniformity that could be realized using induction heating.

The heating of a cylindrical charge in an induction furnace is accomplished by I_w^2R heating; i.e., the square of the work current induced in the cylindrical block is multiplied by the electrical resistance of the charge. The uniformity of heating will then be determined by the depth of penetration of the effective work current in the cylindrical stock. The depth of penetration of the current, I_w, in the cylindrical charge can be expressed by the following equation:

$$\Delta = 3,565 \sqrt{\rho/\mu f}$$

where Δ = effective depth of work current penetration in centimeters; ρ = electrical resistivity in ohm-cm; μ = effective magnetic permeability (in this case $\mu = 1$); and f = frequency in cycles per second. An existing 500 kw, 180 cycles per second Multiductor unit was used for all the induction curing trials.

The equation previously discussed shows that as the resistivity of the charge decreases the effective depth of current penetration also decreases.

Calculations show that as a green RVA plug is heated from ambient temperature to 335°C, the resistivity will change from approximately 2000×10^{-4} to 300×10^{-4} ohm-cm. The depth of penetration of the work current is reduced from 46.6 inches to 18.1 inches which produces a change in the work current density. The calculations indicate that the 180 cycles per second unit would be marginal for 30-inch diameter RVA, but heating trials subsequently proved the system satisfactory for this size charge. The calculations also showed that the 180-cycle per second power source would operate more efficiently with larger diameter plugs. A 46-inch diameter by 60-inch long induction coil was used for the initial heating trials, and although it was not specifically designed for a high resistance work load, the coil proved to be adequate.

A green RVA plug, 32 inches in diameter by 38 inches in length, having a resistivity of approximately 2000×10^{-4} ohm-cm, was heated to 130°C for the first trial, Run No. 1-X. Figure V.1 is a graphical representation of

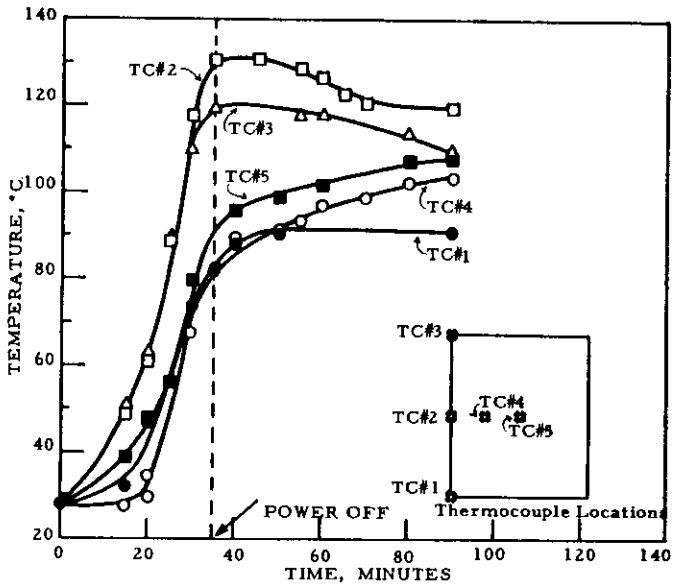

N-4128

Figure V.1. Run No. 1-X, Induction Heating Trial, Green RVA Plug

the heating cycle for this trial. Although the plug was not heated as uniformly as desired, trial No. 1-X definitely established that induction curing of RVA was quite possible using a 180-cycle power source with the proper induction coil. The temperature gradient in this plug was minimized by cycling the power source on and off.

The second trial, Run No. 2-X, utilized a cured RVA plug 32 inches O.D. by 10 inches I.D. by 37 inches in length, with a resistivity of approximately 300×10^{-4} ohm-cm; this plug was heated to 300°C. A graphical representation of the heating cycle for this trial is given in Figure V.2. The

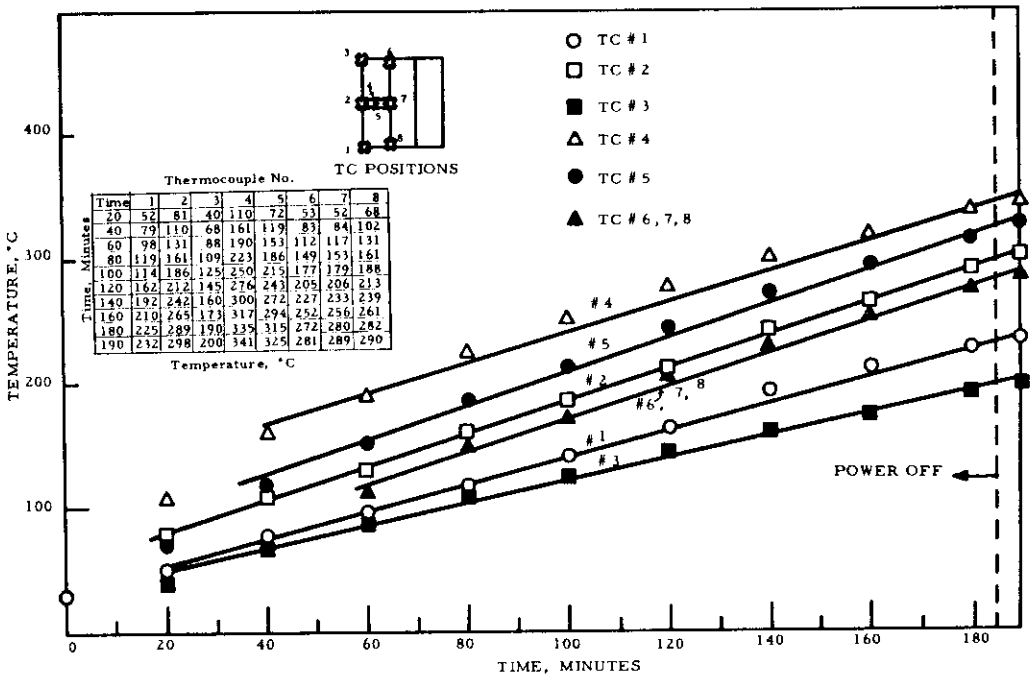

Time	1	2	3	4	5	6	7	8
20	52	81	40	110	72	53	52	68
40	79	110	68	161	119	83	84	102
60	98	131	88	190	153	112	117	131
80	119	161	109	223	186	149	153	161
100	114	186	125	250	215	177	179	188
120	162	212	145	276	243	205	206	213
140	192	242	160	300	272	227	233	239
160	210	265	173	317	294	252	256	261
180	225	289	190	335	315	272	280	282
190	232	298	200	341	325	281	289	290

N-4129

Figure V.2. Run No. 2-X, Induction Heating Trial, Cured RVA Plug

extremely wide temperature differential at the time the power was turned off (198-340°C) was undoubtedly in error because of inaccurate measurements by the thermometry used in this trial. Induction heating does not heat from the inside out, contrary to the indications of thermocouples Nos. 2, 4, and 5, Figure V.2. Therefore, either thermocouple No. 2 was indicating a lower temperature than actually existed or thermocouples Nos. 4 and 5 were indicating a higher temperature than actually existed.

For the third trial, Run No. 3-X, an RVA plug 32 inches O.D. by 12 inches I.D. by 36 inches in length with an approximate resistivity of 2000 x 10^{-4} ohm-cm was heated to 100°C. Figure V.3 is a graphical representation of the heating cycle for this trial. The maximum temperature differential for the trial at the above temperature was 20°C and was maintained by turning the power source on and off throughout the cycle. The various heating curves have approximately the same slope at the end of the heating cycle and it is reasonable to believe that they could be extended to 350°C without increasing the gradient.

The evidence obtained from these three trials established the fact that induction heating could adequately supply the heat necessary for pressure curing. The design characteristics for a specific induction coil to be used in pressure curing 30-inch RVA were also established and are as follows: 46-inch diameter by 24-inch length; 21 mechanical turns and seven electrical turns (three electrically parallel sections of seven mechanical turns).

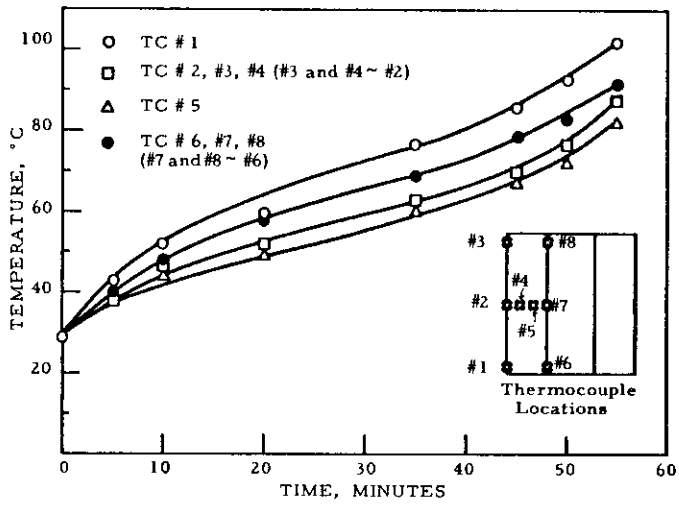

N-4130

Figure V.3. Run No. 3-X, Induction Heating Trial, Green RVA Plug

V.3. Phase II - Engineering Materials for Tooling

Selection of mold and ram design and materials presented a problem in the induction heated-pressure curing program because electrical non-conductors have to be used within the magnetic field.

Material for a mold had to satisfy three basic requirements. First, the material had to be an electrical insulator. Second, the material had to have sufficient strength to withstand the pressures used in the pressure curing process. Third, the material had to retain physical integrity at a temperature of 340°C.

Fiber glass was selected as a material which might be used to meet all three requirements. This material had the strength and was a non-conductor but was limited to a maximum use temperature of 200°C. The pressure curing application required a temperature of 330-340°C which meant that some form of insulation and/or heat transfer mechanism had to be installed between the fiber glass mold and heated charge stock. A two-inch thick liner of refractory castable* was placed on the inner surface of the mold. Vertical heat exchangers, in the form of 3/8-inch diameter copper tubing, were placed at the interface of the fiber glass mold and castable liner to further aid in heat dissipation. This arrangement was expected to keep the temperature of the fiber glass mold below the critical temperature of 200°C.

*Hot Top Moldit--a refractory castable manufactured by Refractory and Insulation Corporation.

Figure V.4 illustrates the mold and liner that was utilized in the induction heating-pressure curing system.

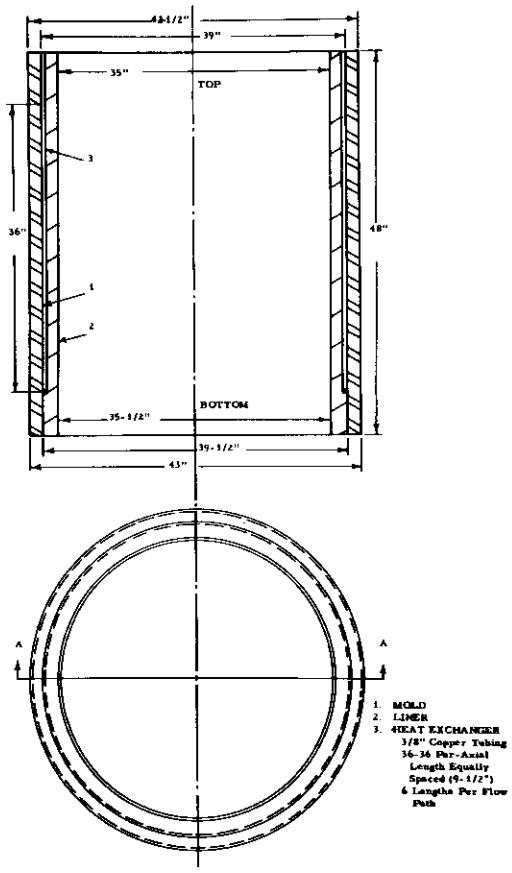

N-4131

Figure V.4. Fiber Glass Mold, Refractory Liner and Heat Exchanger Assembly for Induction Heating-Pressure Curing Process

The pressure ram material selection was restricted by the same basic requirements as listed for the mold. However, the strength requirement for the pressure rams is quite different. The mold is subjected to a load that will result in a "hoop" stress, whereas the pressure rams are subjected to a compressive stress.

The material selected for the construction of the pressure rams was the same "hydraulic set" refractory castable used for the mold liners. This castable material in the cured state (all excess water removed) possesses a crushing strength of 2500 lbs/in^2 which exceeds the 1000 lbs/in^2 required in the pressure curing process. The two pressure rams fabricated for the

induction heating-pressure curing system are illustrated in Figure V.5 with their respective casting conditions.

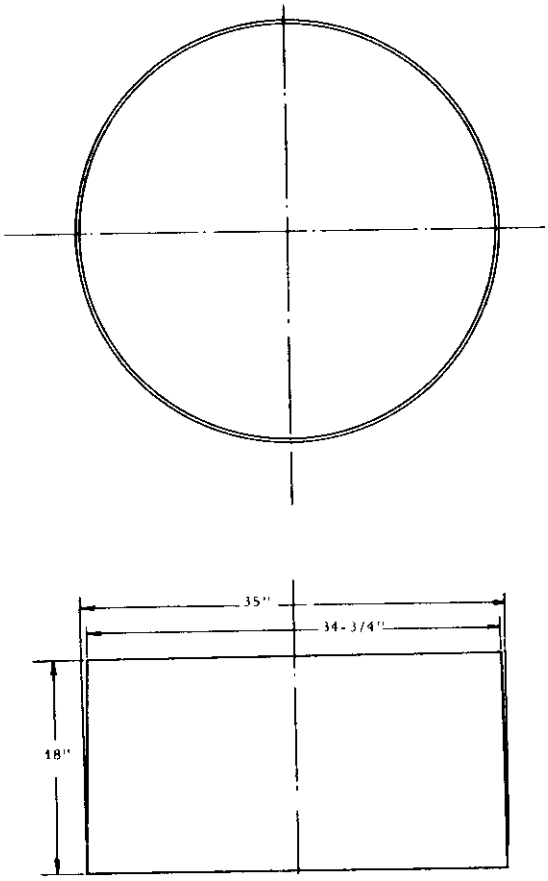

CASTING CONDITIONS

	Ram #1	Ram #2
Mix Ratio		
Refractory Castable	100 parts	100 parts
Water	14 parts	14 parts
Mix Weights		
Hot Top Moldit	1500 #	1500 #
Water	210 #	210 #
Mixing Time (Rotary Mixer)	15 Minutes	15 Minutes
Vibration Time (5 Kc)	5 Minutes	8 Minutes
Weight After Set	1379 #	1376 #
Weight After Cure	1308 #	1320 #
% Weight Loss	5.15%	4.23%
Cured Density lb/cubic ft.	131	132.2

Curing Schedule for Both Rams

25°C to 110°C in 48 Hours.
Hold at 110°C for 336 Hours.

N-4132

Figure V.5. Cast Refractory Pressure Rams for Induction Heating-Pressure Curing Process

V.4. Phase III - Induction Heating-Pressure Curing

The induction heated-pressure curing equipment was assembled, as shown schematically in Figure V.6 and pictured in Figures V.7 and V.8, using the design and fabrication of the induction coil, mold,and pressure rams previously described. The charge stock used for all the induction heating-pressure curing trials discussed in this report was pre-compacted 31-inch diameter by 15-inch long RVA grade.

The induction curing assembly illustrated in Figure V.6 was used for trial No. 11-R except that a layer of carbon felt was placed between the castable pressure ram and the coke envelope. This felt trapped the coke particles within the charge cavity and permitted easy escape of the volatiles.

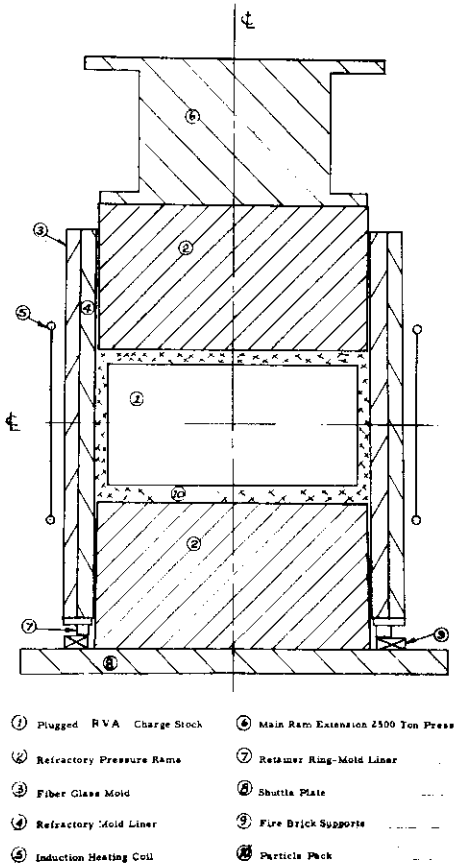

N-4133

Figure V.6. Induction Heating-Pressure Curing Assembly

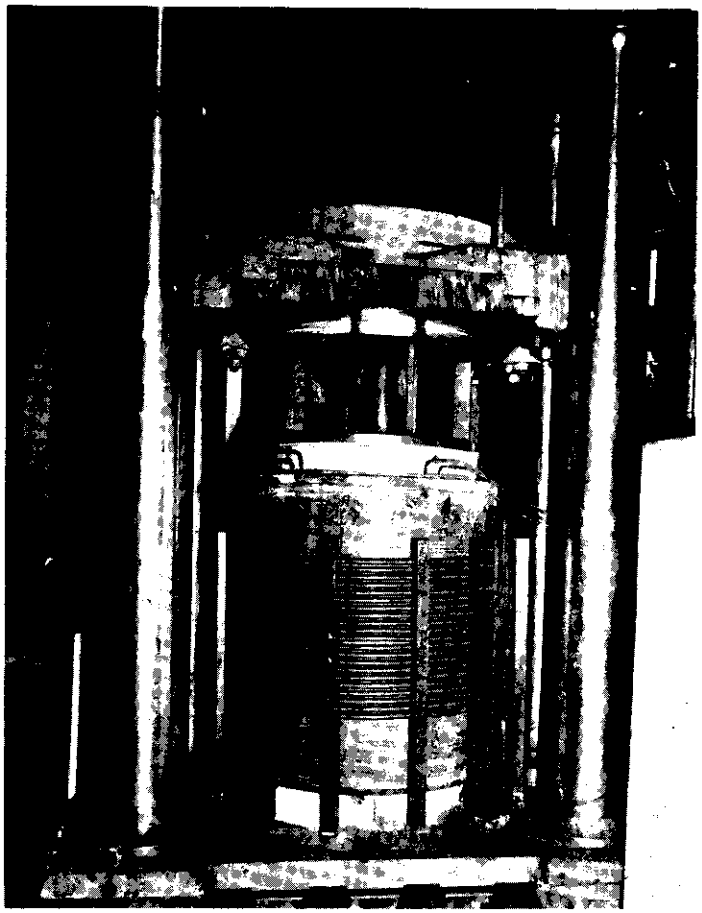

N-3134

Figure V.7. Induction Heating-Pressure Curing Assembly, Front View

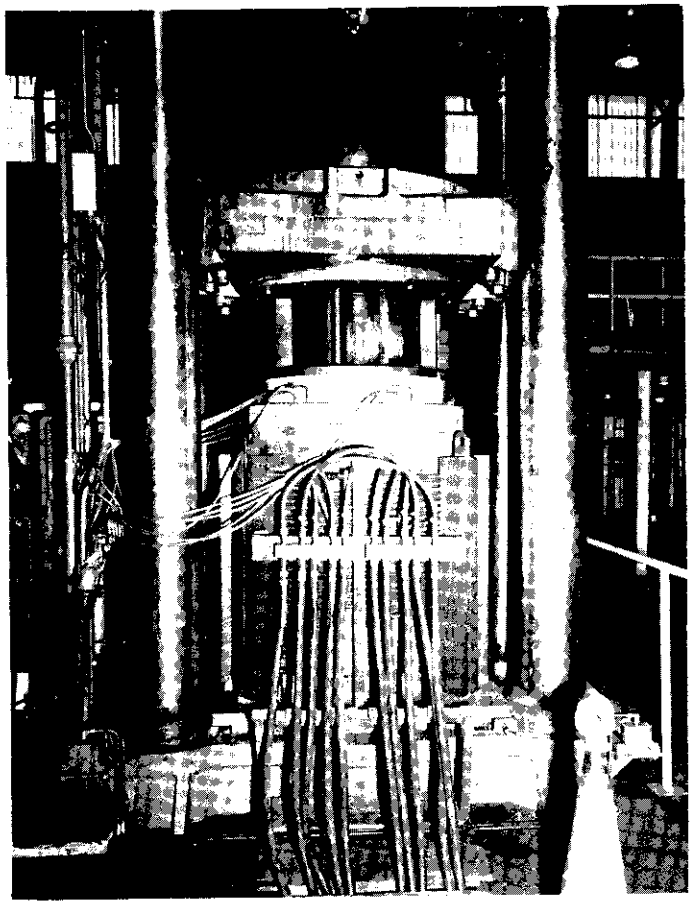

N-4135

Figure V.8. Induction Heating-Pressure Curing Assembly, Rear View

Figure V.9 is a graphical presentation of the pressure curing conditions and results for trial No. 11-R. The unexpected length of the heating cycle (874 minutes) was the most unusual feature of this trial. This time interval was governed by the maximum desirable temperature gradient which was arbitrarily set at 40°C. Curves 1 and 2 in Figure V.9 represent the maximum and minimum temperatures of the plug throughout the heating cycle and show that the temperature gradient of the product varied between 20 and 40°C over most of the cycle. The 20 to 40°C gradient was maintained only by turning the induction heating power source on and off 35 times during the curing cycle. The temperature gradient from top to bottom of the charge was not nearly as pronounced as the outside to inside gradient.

The performance of the combination fiber glass-castable mold was a most encouraging feature of this induction curing trial. Temperature measurements recorded by thermocouples placed at the fiber glass-castable interface are presented graphically in Figure V.10. The maximum indicated temperature of any of these seven thermocouples during the entire cycle was 119°C (thermocouple No. 3) which, while it was a correct reading, was not measuring the temperature at the liner-mold interface. Actually neither thermocouple No. 3 nor thermocouple No. 7 were measuring the interface temperature. Thermocouple No. 3 apparently shifted when the liner was poured and was measuring the temperature of the castable. Thermocouple No. 7 came into contact with part of the heat exchanger and actually measured the cooling water temperature over the entire cycle. Therefore, it is safe to assume that the maximum temperature at the interface was 81°C as indicated by thermocouple No. 4. The results of this trial show that the fiber glass-castable mold is a practical solution to the mold problem in the induction curing process.

Figures V.11 and V.12 are photographs of the top and bottom rams after the initial trial. Both rams cracked during the initial test but neither was damaged severely enough to prevent its use in future trials. Logical explanations were presented for the cracks in both rams. The top ram cracked due to the expansion of the aluminum fitting (for receiving the handling eyebolt) which was heated by the induced magnetic field. The expansion of aluminum, being greater than the expansion of the castable, set up a "hoop" stress that exceeded the tensile strength of the "hydraulic set" castable. The lower face of the bottom ram was cast with a very slightly convex surface and the compressive load of 1000 lbs/in^2 set up a stress exceeding the ultimate flexural strength of the castable.

Induction curing trials Nos. 12-R and 13-R were conducted with the objective of reducing the heating cycle time. Figures V.13 and V.14 present the conditions and results of heating trials Nos. 12-R and 13-R, respectively. A comparison of the heating cycles of the three induction curing trials, Nos. 11-R, 12-R, and 13-R, shows that the heating cycle was progressively shortened. The total heating cycle times for each trial were 874, 775, and 575 minutes, respectively. This represented a maximum decrease of 299 minutes or 34.5 per cent in the heating cycle providing more efficient use of the equipment.

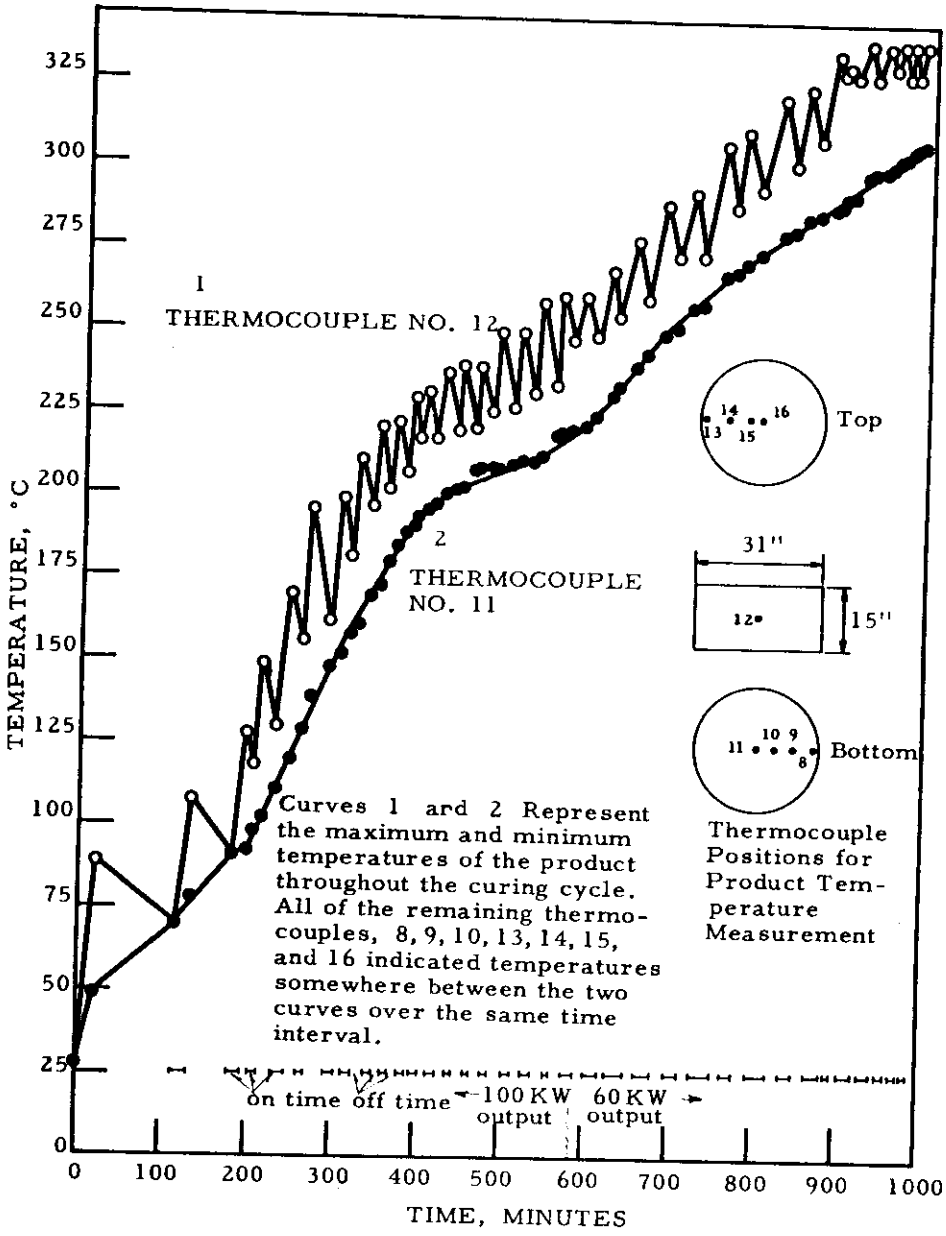

N-4136

Figure V.9. Trial No. 11-R, Induction Heating-Pressure Curing, RVA Grade, Conditions and Results

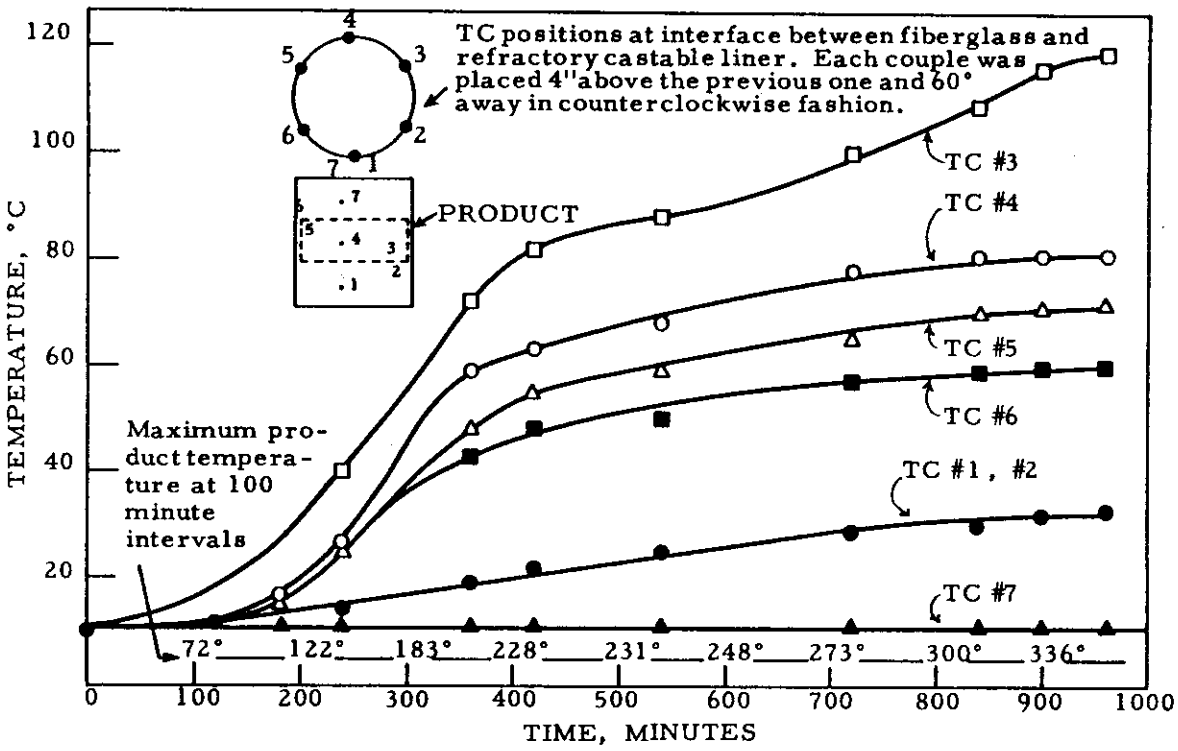

N-4137

Figure V.10. Trial No. 11-R, Induction Heating-Pressure Curing, Temperatures of the Fiber Glass-Castable Liner Interface

N-4138

Figure V.11. Top Pressure Ram for Induction Heating Pressure Curing Assembly

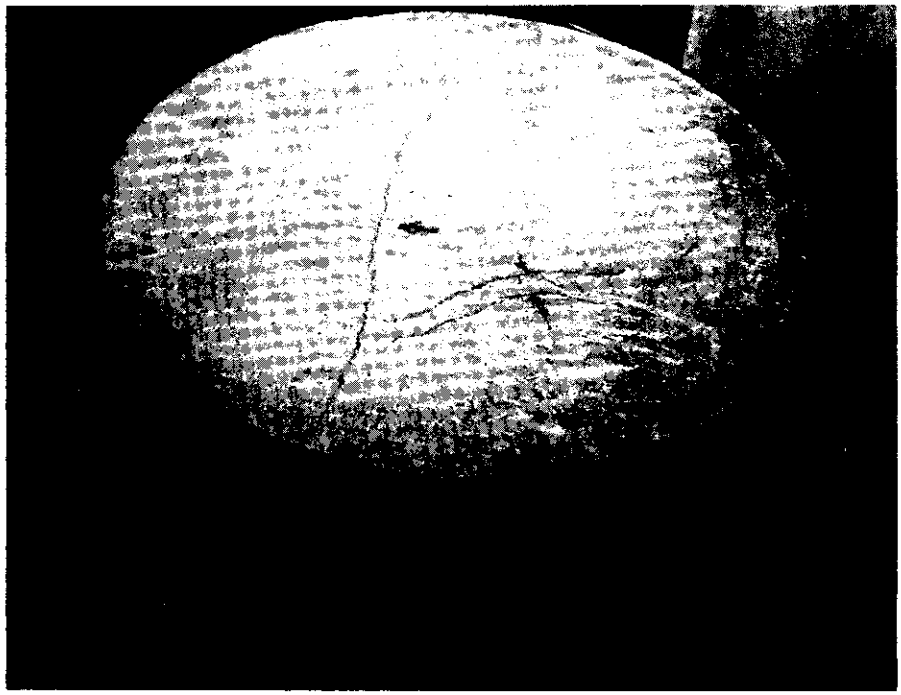

N-4139

Figure V.12. Bottom Pressure Ram for Induction Heating Pressure Curing Assembly

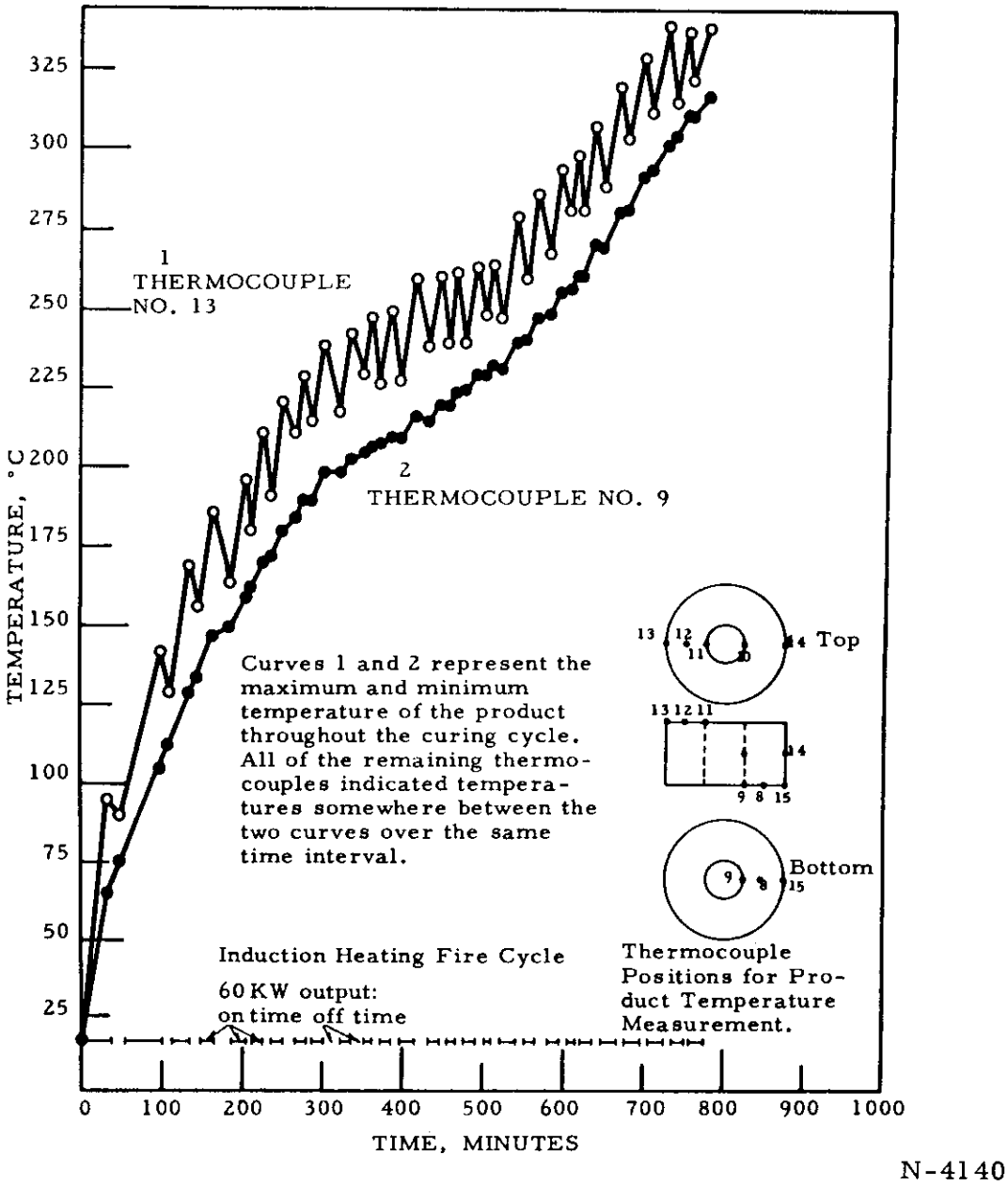

Figure V.13. Trial No. 12-R, Induction Heating-Pressure Curing, RVA Grade, Conditions and Results

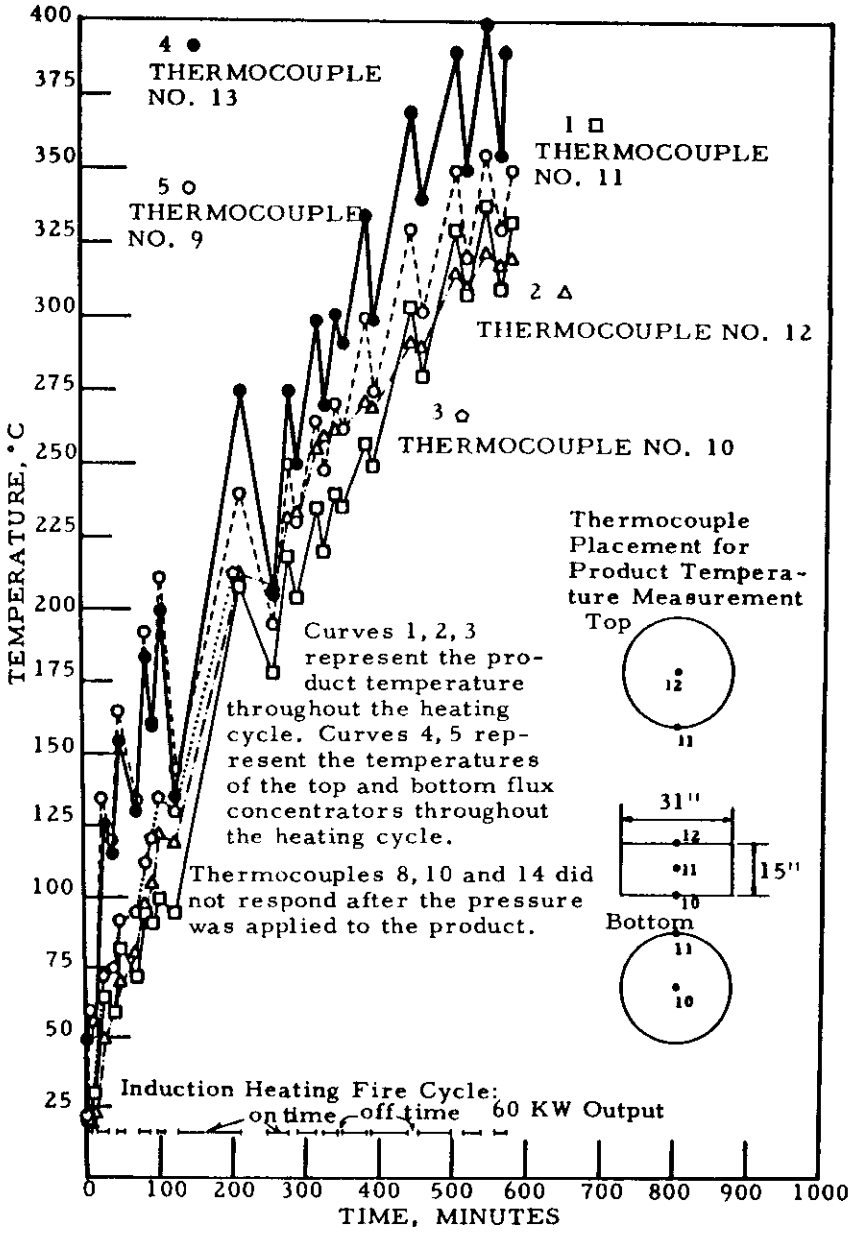

N-4141

Figure V.14. Trial No. 13-R, Induction Heating-Pressure Curing, RVA Grade, Conditions and Results

The decrease in the time of the heating cycle for trial No. 12-R was affected by a change in the geometry of the charge stock. A 10-inch diameter concentric hole was machined in the precompacted 31-inch diameter by 15-inch long RVA plug. This configuration increased the heating rate over two regions of the heating cycle, one from 20°C to 210°C and the other from 250°C to 330°C. However, the heating rate in the range from 210°C to 250°C was slower for trial No. 12-R than for trial No. 11-R. Despite the slower heating rate in the one region, the overall heating cycle was reduced from 874 to 775 minutes or decreased by 11 per cent.

The decrease in the heating cycle for trial No. 13-R was obtained by the use of two "heat concentrators" or graphite disks placed in the assembly as illustrated in Figure V.15.

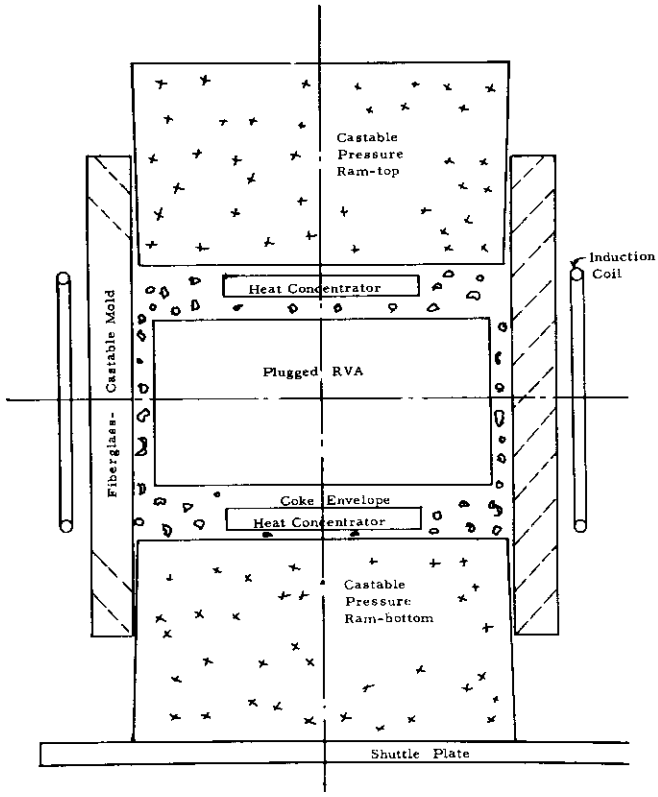

Figure V.15. Induction Heating Pressure Curing Assembly Showing Position of "Heat Concentrators"

The cured RVA plugs from the three trials were flaw free upon visual examination. Figures V.16. and V.17. are photographs of the cured plugs from trials Nos. 11-R and 12-R.

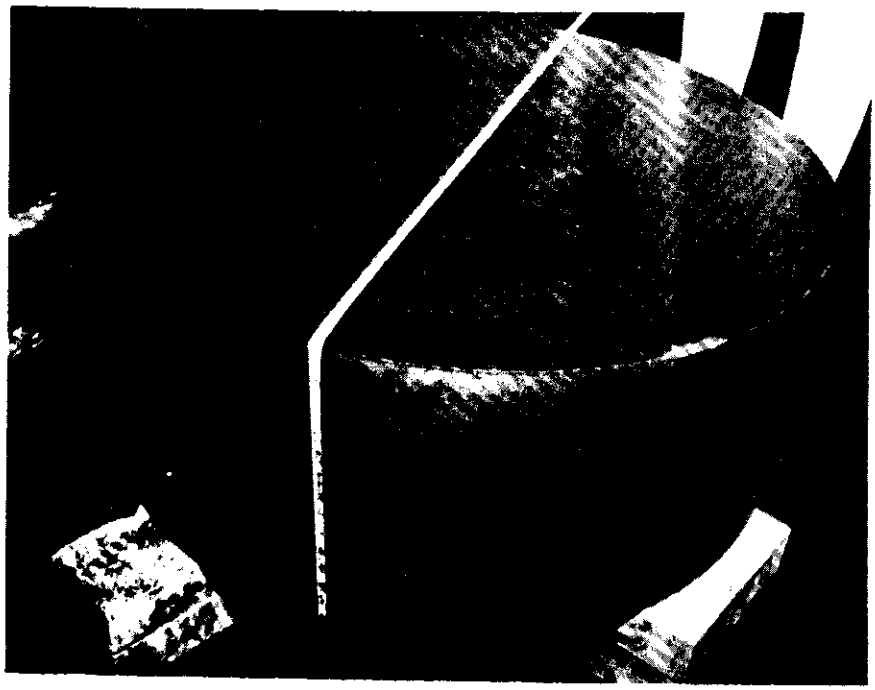

N-4143

Figure V.16. Trial No. 11-R, Induction Heated Pressure Cured RVA Plug

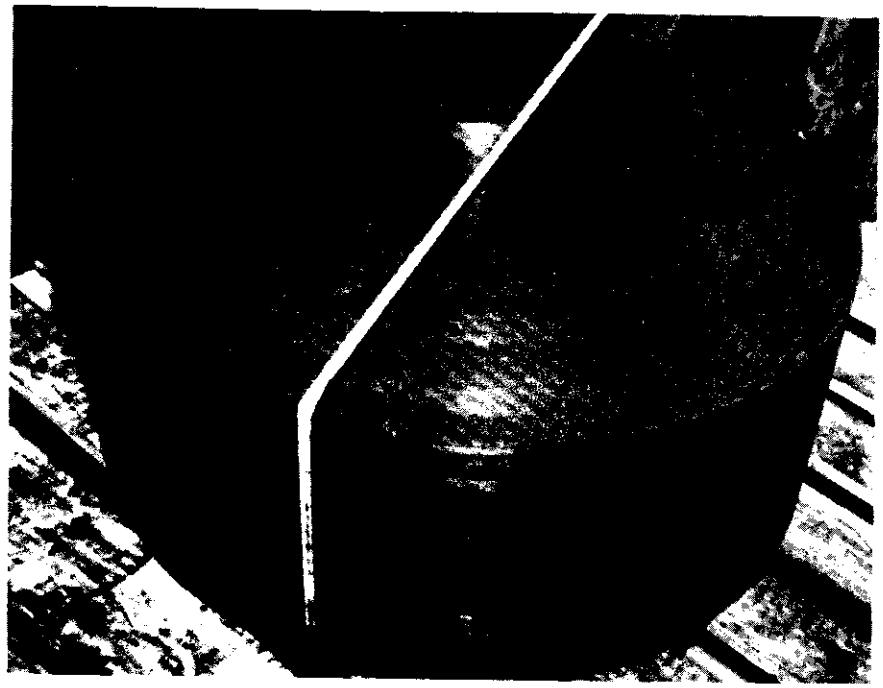

N-4144

Figure V.17. Trial No. 12-R, Induction Heated Pressure Cured RVA Plug

The cured plug from trial No. 13-R was indented on both ends, obviously caused by the heat concentrators. The effects of these indentations cannot be determined until the plug has been completely processed.

The dimensions and bulk densities of the three plugs, before and after curing, are given in Table V.1.

Table V.1. Induction Heating Pressure Curing, Before and After Cure Densities

	Trial No.		
	11-R	12-R	13-R
Before Cure			
Outside Diameter, inches	31.00	30.98	31.03
Inside Diameter, inches	---	9.98	---
Length, inches	15.30	14.94	15.40
Weight, lbs.	783	683	778
Bulk Density, g/cc	1.88	1.87	1.86
After Cure			
Outside Diameter, inches	31.20	31.12	30.90
Inside Diameter, inches		9.90	
Length, inches	13.50	12.88	13.11
Weight, lbs.	689	563.25	640
Bulk Density, g/cc	1.85	1.77	1.80

The cured bulk densities of the three plugs compared favorably with standard cured (resistance heated) RVA stock which is approximately 1.80 g/cc. Evaluation of the induction heating pressure curing process will be completed after the plugs have been graphitized.

The major conclusions made at this development stage concerning induction heated pressure cured RVA grade graphite were as follows:

1. Induction heating is adaptable to the pressure curing program.

2. The mold problem has been solved to such an extent that it can probably be scaled up to 120-inch diameter.

3. Further investigation may be needed for the development of better pressure rams to be used with induction heating. This is especially true if large diameter scale-up is to be considered.

APPENDIX VI

SPECIAL EXTRUSION TECHNIQUES

VI. 1. Introduction

The two most commonly used methods of forming bulk carbon or graphite shapes are pressure molding and hydraulic extrusion. The primary structural difference between stock made by the two methods is that orientation of the grain is normal to the direction of forming force for molding and parallel to the forming force for extrusion.

Most premium grade graphites are fabricated by pressure molding because:

1. Structural flaws are minimized.
2. Nonagglomerating mixes can be used thereby improving product property uniformity.
3. A wider range of binder levels can be used since a minimum plasticity is not a requirement as in extrusion. The opportunity to select the optimum level is thereby enhanced.
4. Larger cross sections of fine grain base materials can be produced by pressure molding than by extrusion.

Hydraulic extrusion presses are used for fabrication of the greater volume of bulk carbon and graphites. The advantage of this equipment is its larger production capacity as compared with the individual piece molding technique. The cross sectional areas of conventional hydraulically extruded products are limited to approximately 80 per cent of the cross section of the extrusion press mix chamber. This reduction is required between the mix chamber and die to compact and form the mix to the desired bulk density. Hydraulic extrusion is used primarily for fabricating large carbon or graphite shapes for application where minor structural flaws are not as critical as for premium grades of molded graphite such as ATJ or RVA. Structural flaws observed in extruded stock are attributed to the flow characteristics of the hot plastic mix during extrusion. Extrusion of premium grades of fine grain flaw free graphite is limited to relatively small diameters.

It was hypothesized that controlled particle orientation could be achieved and structural flaws minimized if back pressure could be applied to the mix at the die face during extrusion thus simulating pressure molding conditions.

VI. 2. Extrusion Through an Expansion-Reduction Die with Applied Back Pressure

The objective of this study was to determine the feasibility of semi-continuously forming carbon with controlled particle orientation and greater

in cross-sectional area than the extrusion mix chamber. The extrusion equipment used for these trials was a continuous auger extruder rather than the conventional hydraulic press. A hydraulic ram was installed in front of the extrusion die and pressure was maintained opposing the mix flow out of the die. This arrangement of auger extrusion--back pressure forming--is shown in Figures VI. 1. and VI. 2. and given diagrammatically in Figure VI. 3.

The die assembly used for these trials was such that the 4-½-inch diameter column of mix from the auger entered an 8-inch diameter expansion zone and was then reduced to a 5-inch diameter product. A detailed drawing of this die is given in Figure VI. 4.

The first trials were made using a blend of 1350°C calcined coke flour and particles. The blend consisted of 70 weight per cent 55 flour and 30 weight per cent through 20 on 35 mesh particles. Four mix types were produced in which the binder level varied from 28 to 32 pounds of 110°C melting point pitch per 100 pounds of filler. Mixing was accomplished in 30 minutes at 140-160°C and the mix was cooled to 120°C before extruding. The heating jackets on the auger extruded were maintained at 120°C during all the trials discussed in this report. The mix was extruded as 5-inch diameter by 24-inch long samples into a die sleeve (Figure VI. 3.) under 200 lbs/in^2 back pressure. The back pressure was applied to the mix during extrusion of the full 24-inch sample.

The initial trials to test the back pressure system were made with mix having 32 pounds of pitch per 100 pounds of dry blend. Additional trials were made using the previously discussed mix compositions to determine optimum binder levels for the back pressure system. The mix for further evaluation was selected on the basis of power requirements of the auger. The power requirements for the four types of mixes were as follows:

Mix Type	A	B	C	D
Pounds Pitch per 100 lbs Blend	34	32	30	28
Drive Motor Amps	24	25	30	40

Figure VI. 1. Extrusion with Applied Back Pressure, Back-Pressure Ram and Die Sleeve Assembly N-4145

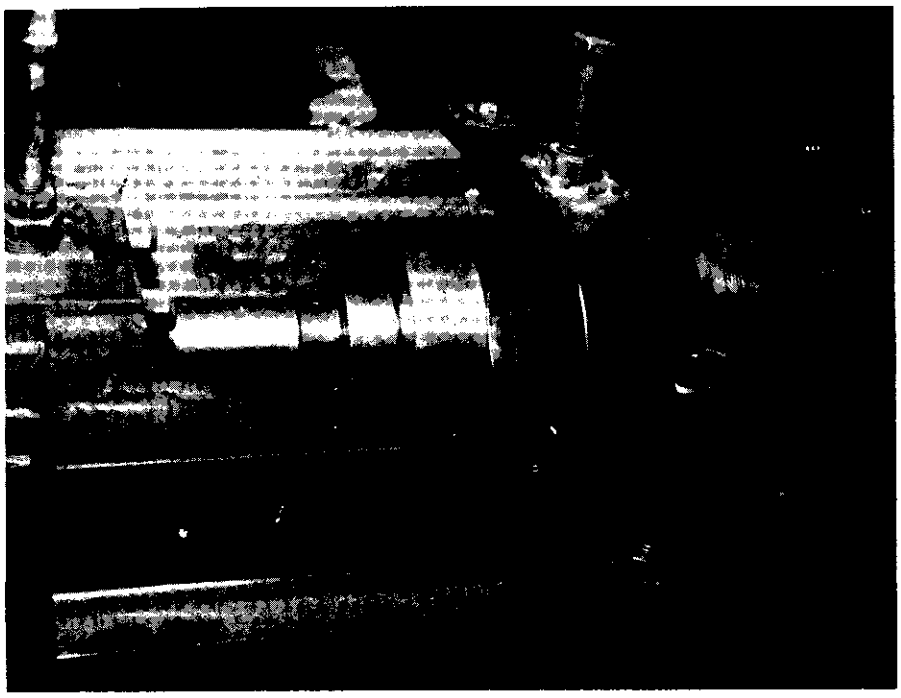

Figure VI. 2. Extrusion with Applied Back Pressure, Close-up View of Back-Pressure Ram and Die Sleeve N-4146

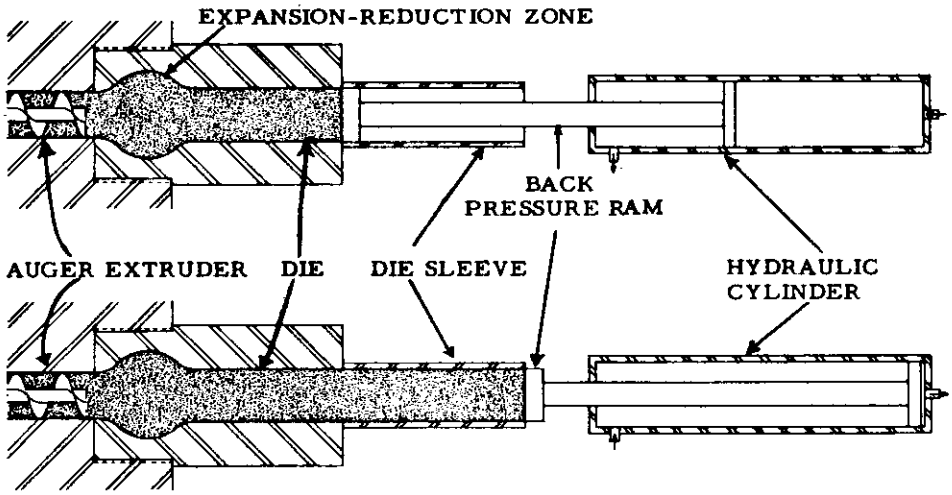

N-4147

Figure VI. 3. Auger Extruded with Expansion-Reduction-Back Pressure Assembly

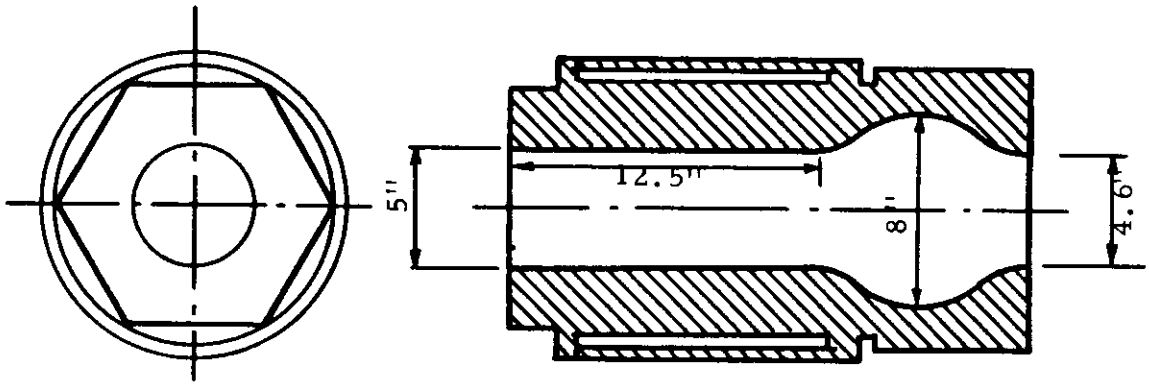

N-4148

Figure VI. 4. Expansion-Reduction Die Used in Back-Pressure Experiments

The sharp increase in power noted for mix "C" was due to increased side wall friction in the die and sleeve and resulted in shearing the bolts which fastened the back pressure assembly to the die. Mix "B", 32 pounds of pitch per 100 pounds of dry blend, was selected for further evaluation based on the relatively low power requirement and the near optimum binder level as indicated by previous experience. Five 5 inch diameter by 24 inch long samples of mix "B" were formed under 200 lbs/in^2 back pressure. In addition, five control samples were formed with no applied back pressure. Both groups of specimens were baked to 750°C.

The baked samples were sawed through the center parallel to the extrusion direction for visual inspection. Figure VI.5 shows the sawed sample which was extruded with the application of back pressure. Although difficult to see in this photograph, definite reorientation of the grain was obtained as evidenced by the flow lines which were approximately 45° to the direction of extrusion. The reference sample with no applied back pressure is shown in Figure VI.6 and the flow lines were nearly parallel to the extrusion direction. Flow line flaws were observed in both types of specimens. Green bulk densities of the back pressure and reference samples were 1.82 and 1.80 g/cc respectively while bulk densities of the baked materials were, respectively, 1.66 and 1.60 g/cc. These trials, though limited, were encouraging because the back pressure extrusion gave increased density and some degree of grain reorientation.

Diagrammatic sketches describing flow line patterns are shown in Figure VI.7, Examples 1 through 3. Example No. 1, no applied back pressure, shows the grain orientation approximately parallel to mix flow. Example No. 2, 200 lbs applied back pressure, shows the 45° orientation to the direction of mix flow. No further work is recommended with expansion-reduction extrusion since flow line flaws were observed in the specimens produced with the use of back pressure. Improvement can be made by machining the die to the configuration of Example No. 3 in Figure VI.7. This arrangement will permit the extrusion of 8 inch diameter stock from the 4-1/2 inch diameter continuous extrusion machine. The use of back pressure with the larger die should produce a grain orientation very similar to that obtained with pressure molding. The expected flow line pattern is given diagrammatically in Figure VI.7, Example No. 3. This method of fabrication of carbon and graphite shapes, if successful, will relieve the cross-sectional area limitations of available extrusion machines.

N-4149

Figure VI.5. Extrusion with 200 lbs. Back Pressure, Sawed Surface Showing Flow Line Patterns 45° to Direction of Mix Flow, 9X

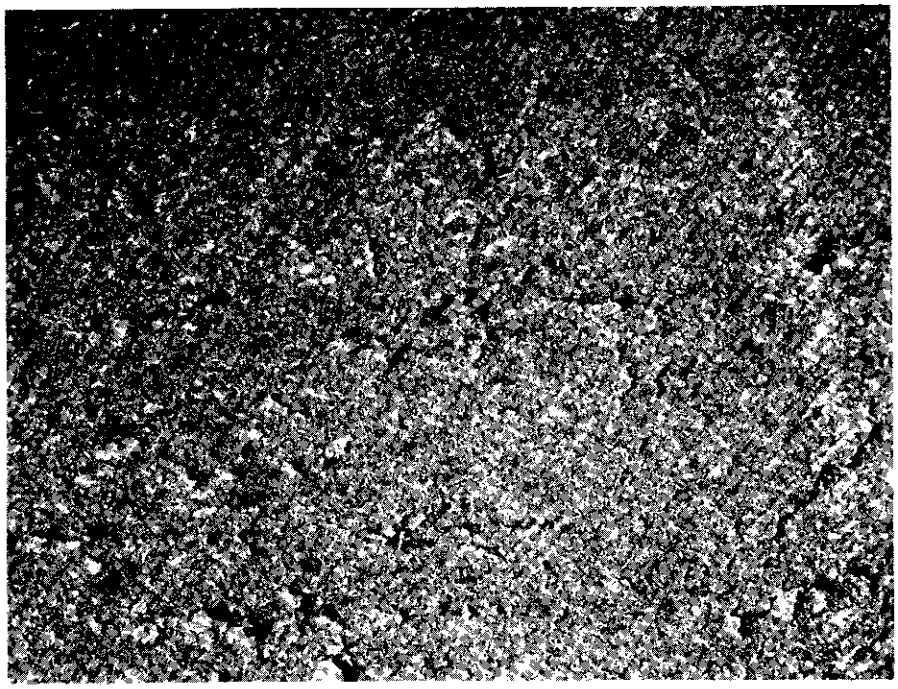

4150

Figure VI.6. Extrusion with no Back Pressure, Flow Lines Approximately Parallel to Direction of Mix Flow, 9X

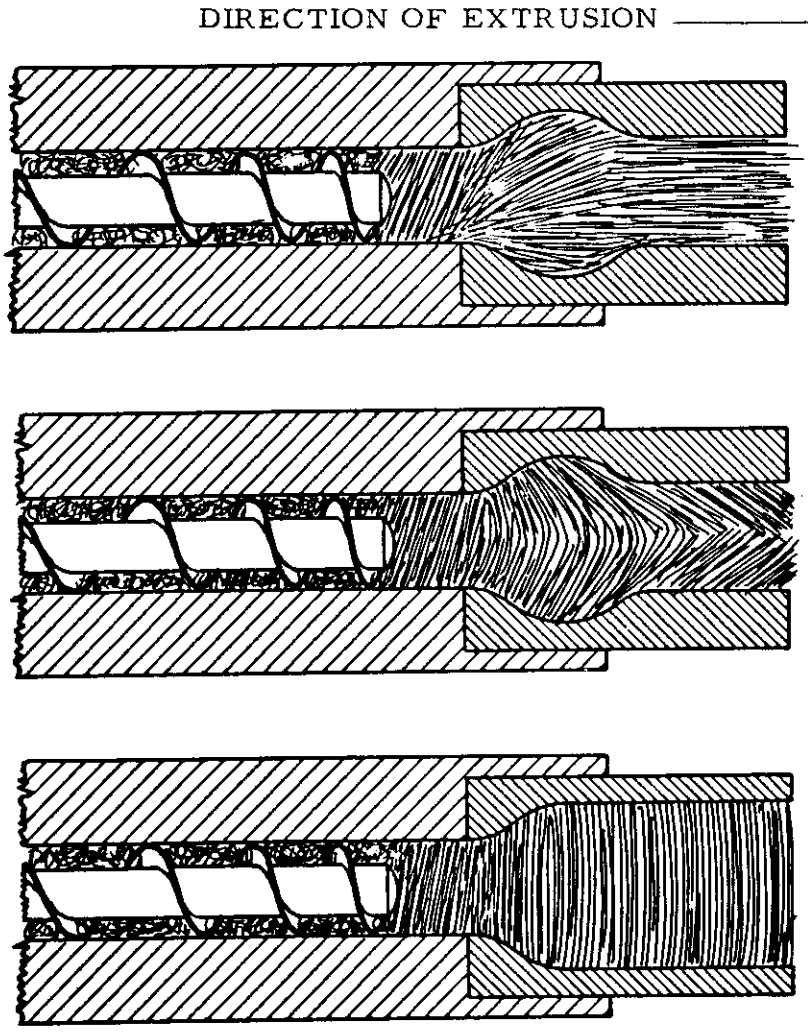

Figure VI.7. Grain Orientation Resulting from Various Types of Extrusion

APPENDIX VII

CARBON AND GRAPHITE WHISKERS

VII. 1. Introduction

Considerable interest has been generated during the past few years in metallic whiskers which show extremely high strengths; one area of interest has been in using high strength aluminum oxide whiskers for reinforcing 80 nickel-20 chromium alloys or other alloys useful in high temperature applications*.

Tensile strengths for bulk graphites are in the range of 2000 lbs/in^2. Some graphite fibers have been produced which, like the metallic whiskers, have extremely high strengths, in fact, approaching 3 million lbs/in^2. ** Interest has been shown in the discovery of two methods by which carbon or graphite whiskers may possibly be produced; the first of these two methods was discovered during investigations of the hot working or ZT process[62] and the second method was found during calcination of coke from the experimental delayed coker[56].

VII. 2. Graphite Whiskers From Hot Working Investigations

Graphite whiskers were produced during an investigative trial of the hot working process. The particular trial was made as an attempt to reorient or upset the grain structure of the graphite piece being hot worked; however, the piece fractured or opened up during the trial and a considerable quantity of graphite whiskers was present within the opening. Figure VII. 1. is a macrograph (10X magnification) showing some of the whiskers in their original environment, the whiskers being well formed and ranging from 1 ½ to 3 inches in length. The method by which the whiskers were formed is not definitely known, but it is theorized that they were grown by the deposition of sublimed graphite.

Metallographic examinations made on some of the individual whiskers are shown in Figures VII. 2. and VII. 3. Figure VII. 2. (100X magnification) shows a single whisker whose body has been cut longitudinally during the grinding process for metallographic sample preparation. Figure VII. 3. (500X magnification) is the center portion of Figure VII. 2. These two photographs give an indication of the typical scroll structure to be found in whiskers. Figures

---

* ASTIA Catalogue No. 261528, Studies of the Reinforcement of Metals with Ultra High Strength Fibers (Whiskers), Engineering Progress Report No. 4, by Bertram C. Raynes.

** National Carbon Company Internal Technical Report, TM-354, The Structure and Elastic Properties of Graphite Whiskers by R. Bacon, August, 1958. See also Appendix I to this Report.

VII. 4. and VII. 5. taken at 500X magnification show surface contours of the whiskers which have more the appearance of a bundle of rods than of scroll formation. The surface in each case is fluted and, in the original photographs taken in color, red striations appeared along the dark blue flutes. In both figures, minute hairs can be seen projecting from the whiskers. Figure VII.5. shows a partial "green tree" fracture in a whisker, a type of fracture not ordinarily found in graphite.

Figure VII. 1. Graphite Whiskers from the Hot Working Process in Original Environment, 10X N-4538

The whiskers have been purposely reproduced on two occasions, however, there was insufficient time to measure their physical properties.

VII. 3. Carbon Whiskers from Coke Calcination

Petroleum coke produced in the experimental delayed coker[56] is calcined to 1350°C by use of induction heating. Many carbon whisker or fiber growths were discovered while removing the susceptor from the induction calcining assembly after the calcination of slurry oil coke. These fibers measured up to 4 inches long and approximately 8 microns in diameter and were very shiny indicating a high degree of preferred orientation, which was confirmed by X-ray diffraction and is unusual in low temperature (1350°C) pyrolytic filaments. Such orientation is observed, although with less consistency, in filaments deposited at temperatures above 1800°C. An attempt was made to establish the

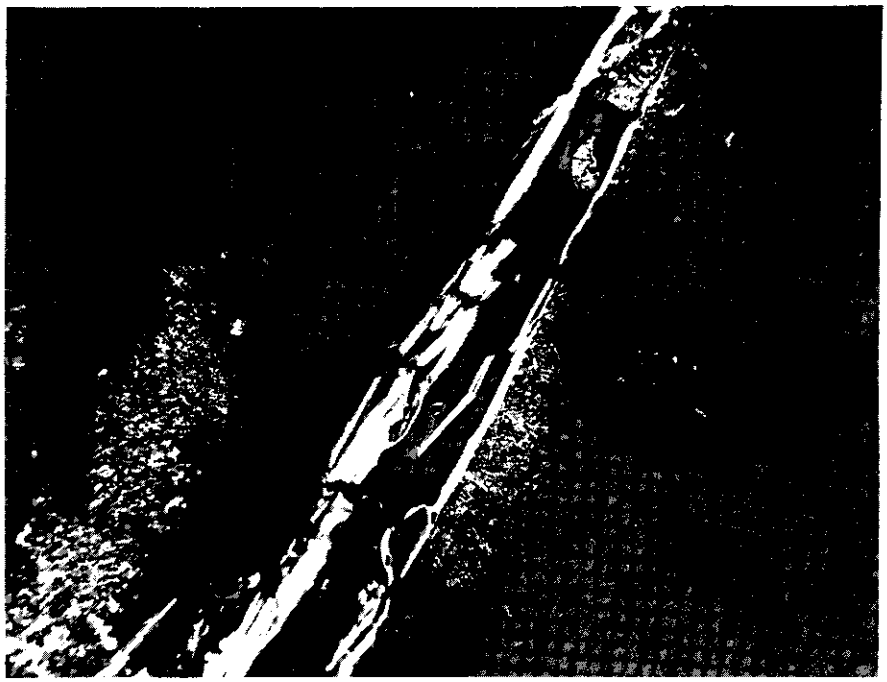

N-4539

Figure VII. 2. Graphite Whisker from Hot Working Process, Internal Section of Single Whisker, 100X

N-4540

Figure VII. 3. Graphite Whiskers from Hot Working Process, Internal Section of the Same Whisker as Figure VII. 2, 500X

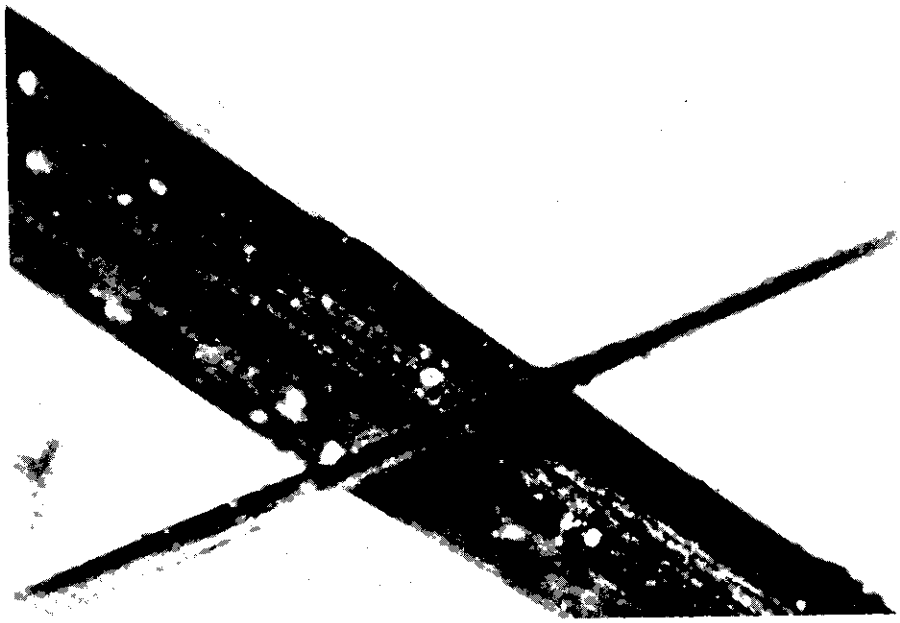

Figure VII. 4. Graphite Whiskers from Hot Working Process, Showing Surface Contour and Variation in Size, 500X

N-4541

Figure VII. 5. Graphite Whiskers from Hot Working Process, Showing Partial Fracture of Whisker, 500X

N-4542

necessary conditions for consistent reproduction because of the unique nature of these fibers.

VII.3.1. Discussion of Whisker Growth Area and Properties

The original carbon fibers under investigation were found in the 8 inch air gap of the 1350°C induction calcine assembly illustrated in Figure VII.6. The fibers were attached primarily to the inside perimeter of the susceptor that encompasses the 8 inch air gap. The growth was restricted to the surface of the susceptor with the long dimension of the fibers normal to the axis of the assembly.

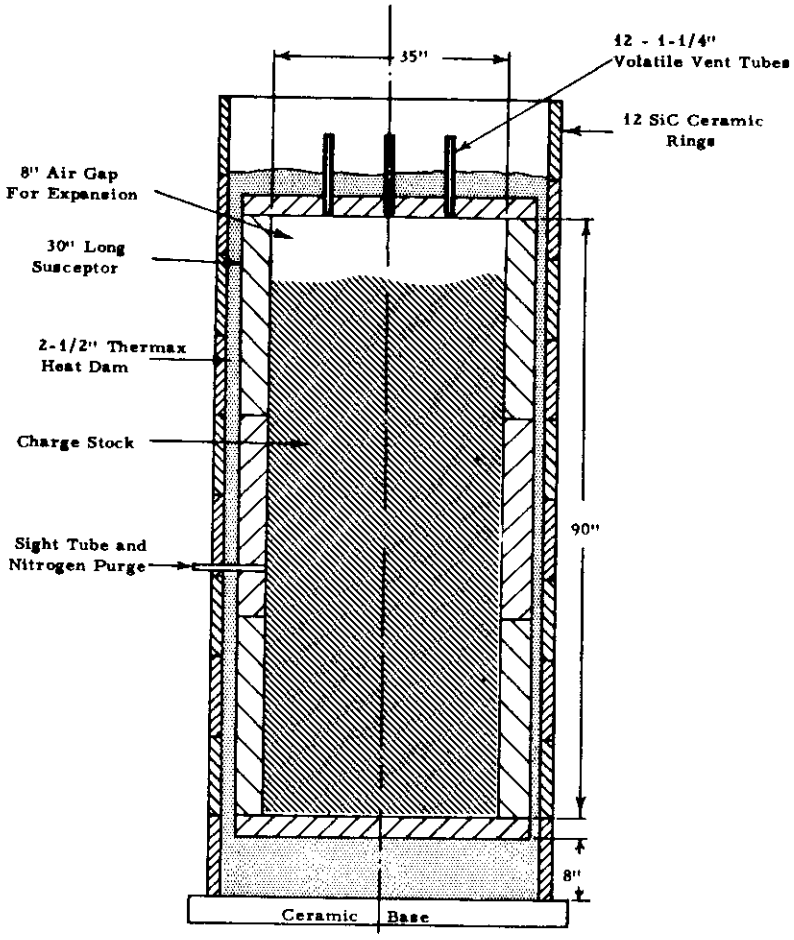

N-4543

Figure VII.6. 1350°C Induction Heated, Coke Calcination Assembly

Electron microscope studies indicated with fair confidence that these shiny filaments were composed of concentric pyrolytic layers similar to pyrolytic carbon formed on graphite substrates by conventional methods. Photomicrographs were made of several fibers and it was possible to distinguish concentric layers of material as shown in Figures VII.7, VII.8, and VII.9. X-ray

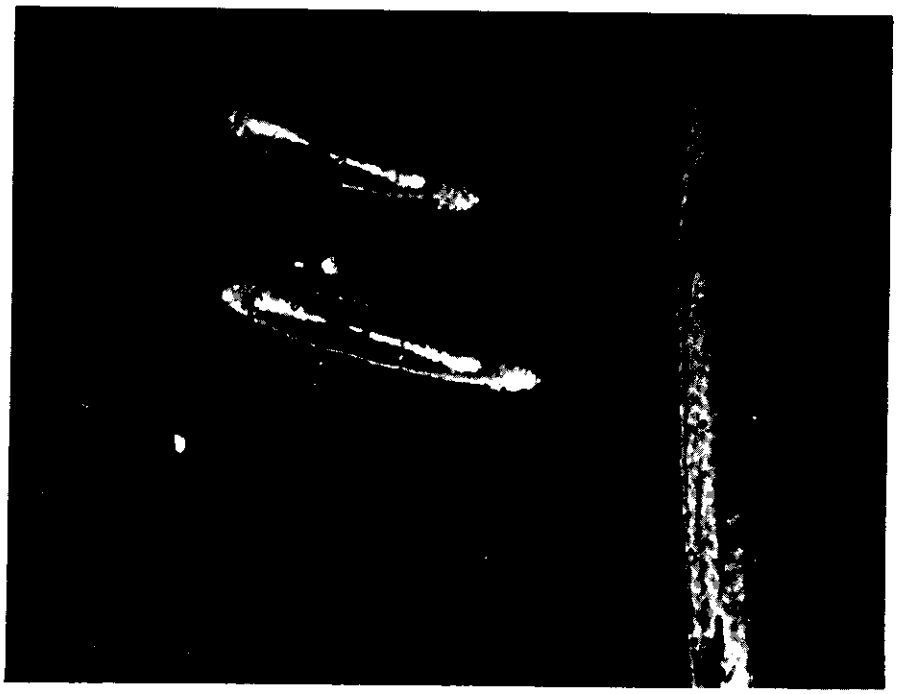

N-4544

Figure VII. 7. Carbon Whiskers from Coke Calcination, 1000X

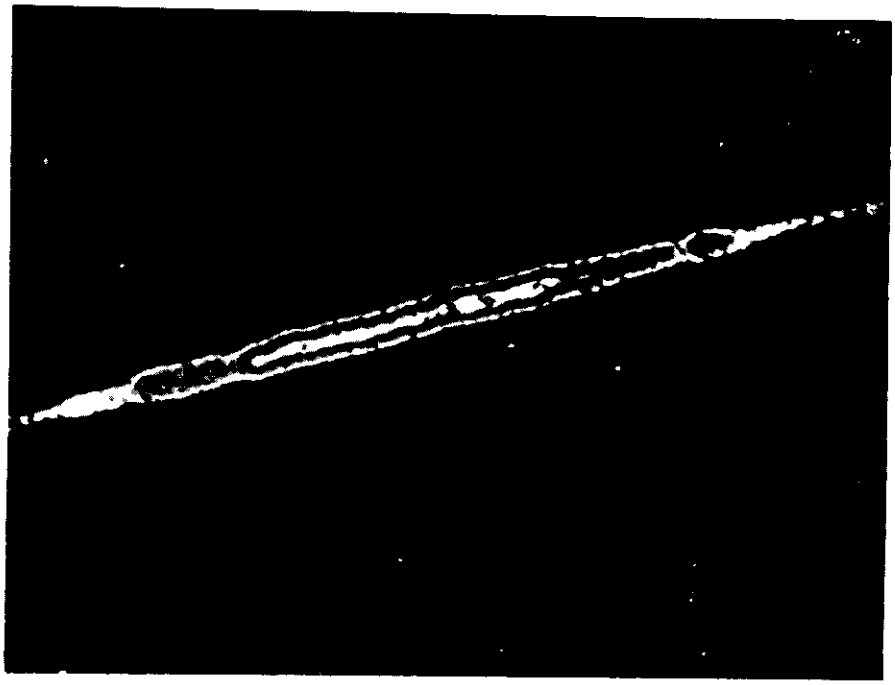

N-4545

Figure VII. 8. Single Carbon Whisker from Coke Calcination, 1000X

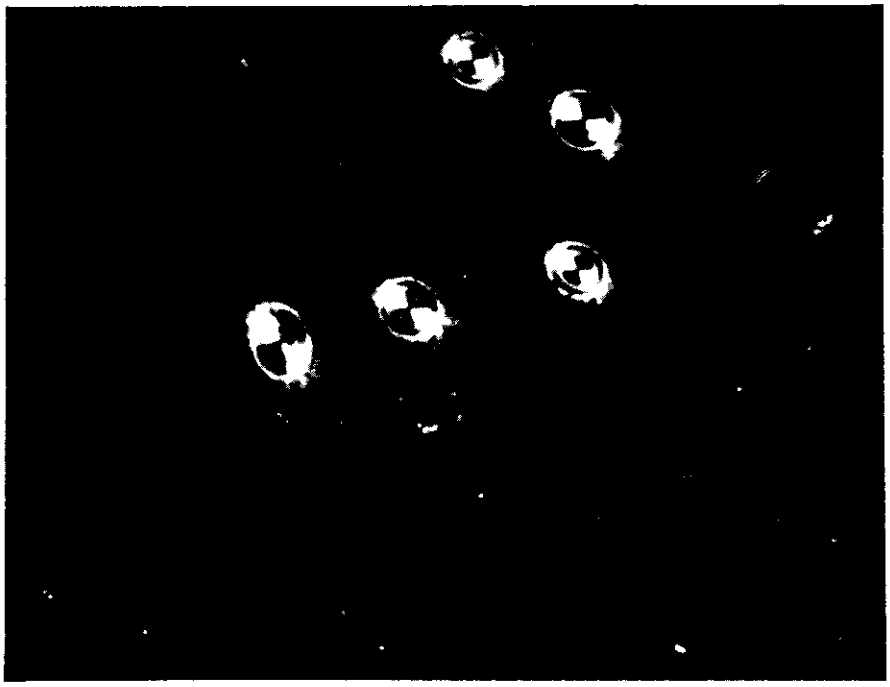

Figure VII.9. Carbon Whiskers from Coke Calcination, End View, 1000X N-4546

diffraction patterns showed this to be a highly polycrystalline material, as one would expect for a low temperature pyrolytic carbon, but that the crystallites were remarkably well oriented which is unexpected for such material. Measurable quantities of $CaCO_3$ were also found by X-ray diffraction and this may be the catalyst required for this unusual growth.

Tensile strength measured on the filaments was 127,000±17,000 lbs/in^2, much higher than for the reported pyrolytic filaments which seldom exceed 30,000 lbs/in^2. The filaments handled easily when they were extracted and mounted for testing and were quite flexible.

Several filaments were graphitized and produced tensile strengths up to 190,000 lbs/in^2. The electrical resistivity of the as-grown filaments were approximately 2,000 micro-ohm-cm which was reduced to less than 100 micro-ohm-cm by graphitization.

VII.3.2. Preliminary Investigation for a Whisker Growth Process

The preliminary investigation of a method for growing carbon whiskers had two objectives: first, to determine the conditions necessary to reproduce the previously described carbon fibers; and second, to prepare the whiskers in a large quantity.

The first step of this investigation was to set up an assembly (Figure VII. 10) similar in design to but much smaller than the large induction calciner. The materials utilized in this scaled-down equipment were also identical to the materials in the large calciner.

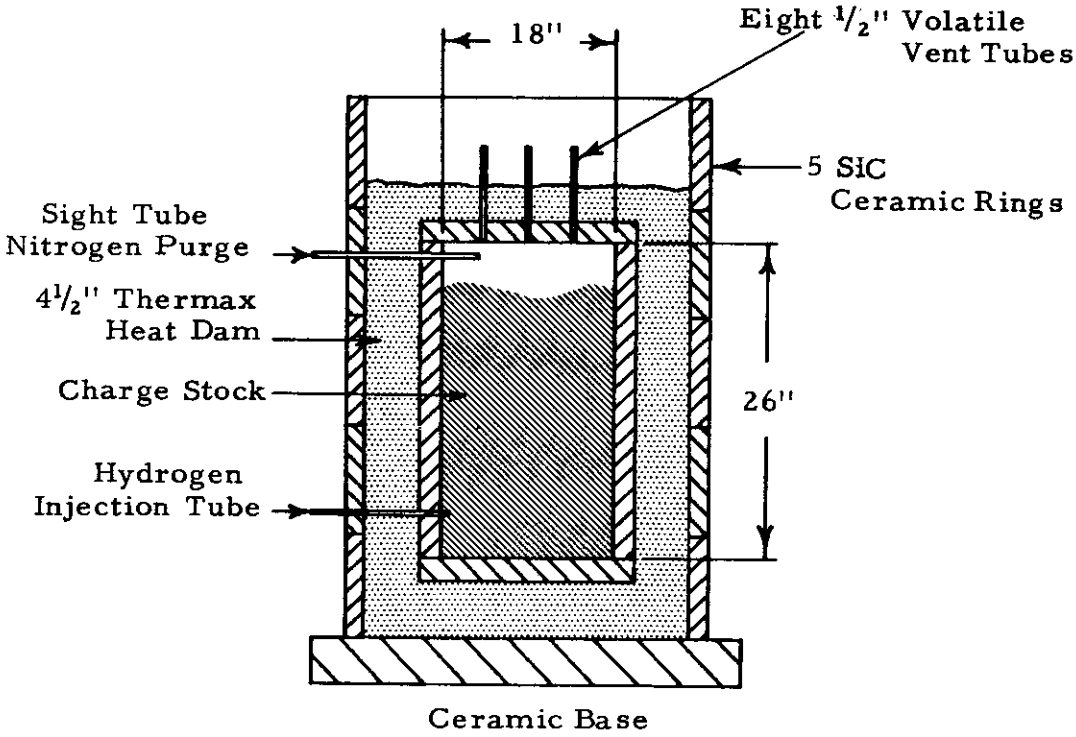

Figure VII. 10. Scaled Down 1350°C Induction Heated, Coke Calcination Assembly N-4547

The first "growth" trial in the scaled-down assembly duplicated the normal induction calcining cycle with the sole exception of the heating rate. The 18 inch diameter susceptor was charged with raw coke (1/16 to 3 inch particles) and heated to 1350°C in four hours instead of the normal two-day heating schedule. After coking, the inner surfaces of the susceptor and the calcined coke were carefully examined for carbon fibers. Numerous small carbon whiskers similar in structure to the original whiskers were found to be distributed over both areas. Figure VII. 11 shows the small fibers as they were grown on a coke particle. Although there was an abundance of the carbon fibers similar to the ones shown in Figure VII. 11, extraction of any quantity was impossible due to the random dispersion within the assembly.

A second trial was made during which hydrogen gas, at an approximate rate of 20 CFH, was admitted to the assembly and allowed to flow through the coke charge. The charging and the heating cycle duplicated the previous trial and again carbon whiskers were produced similar to those obtained in the full scale equipment. The quantity was small but there were areas in the assembly that allowed extraction of several carbon fibers.

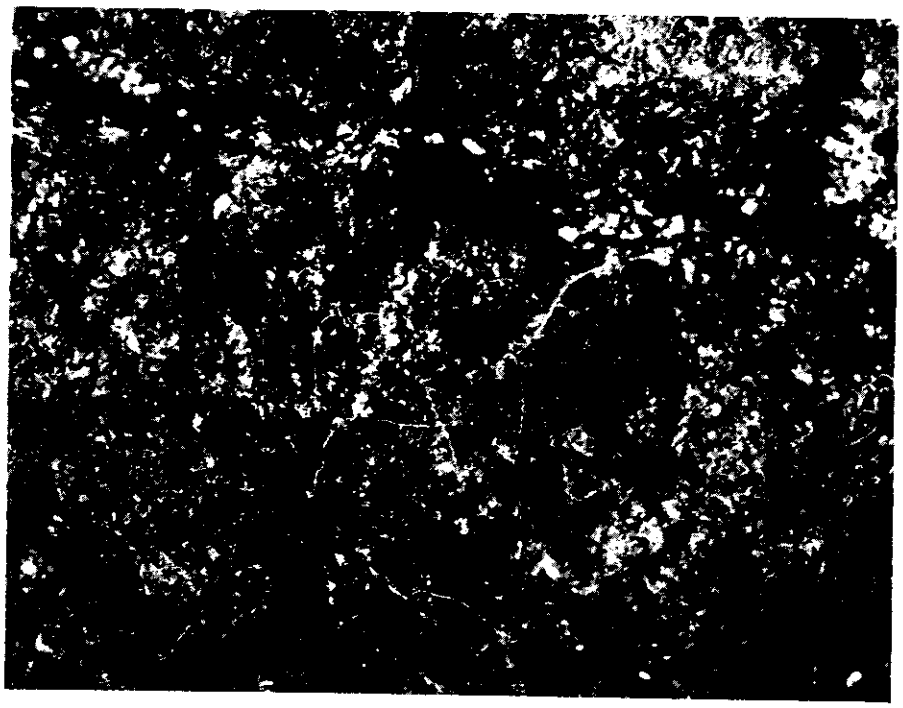

Figure VII. 11. Carbon Whiskers from Coke Calcination, Grown on Coke Particle, 15X

N-4548

A nitrogen injection tube (Figure VII. 10) protruded nearly 4 inches into the charge area and a quantity of whiskers up to $^1/_2$" long had grown on the end of the tube (Figure VII. 12).

Figures VII. 13 and VII. 14 show some of the fibers that were extracted from various areas on the side wall of the susceptor and include some individual whiskers up to 1 $^1/_4$ inches long.

The investigations are too limited to draw definite conclusions; however, it has been possible to grow carbon whiskers purposely but attempts to produce large quantities have as yet been unsuccessful.

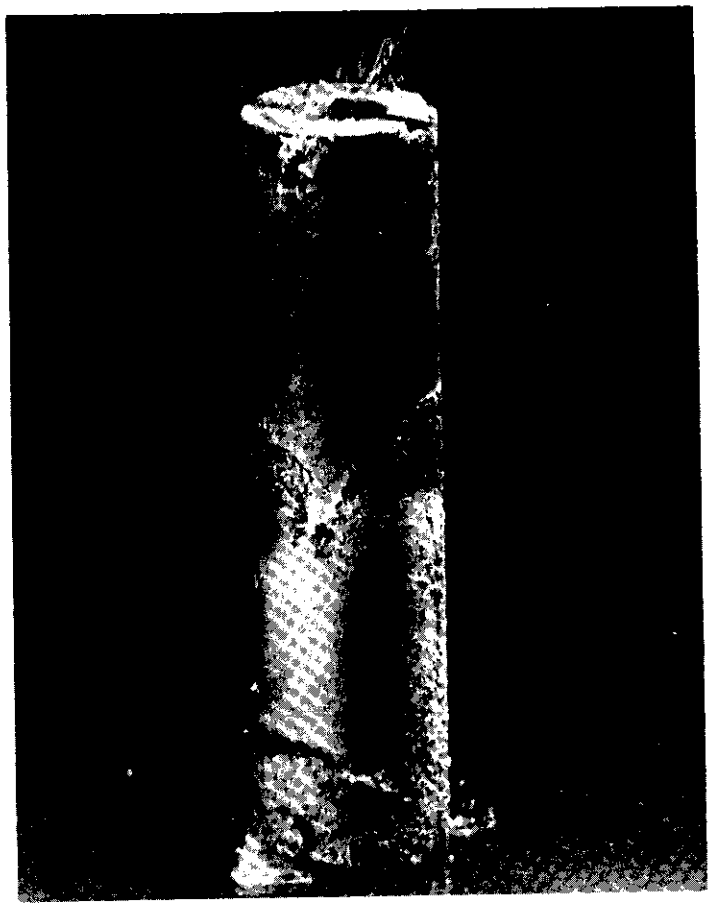

Figure VII.12. Carbon Whiskers from Coke Calcination, Grown on Exit End of Nitrogen Injection Tube, 2X N-4549

Figure VII.13. Carbon Whiskers from Coke Calcination, Extracted From Area on Side Wall of Susceptor, 15X N-4550

Figure VII.14. Carbon Whisker from Coke Calcination, 25X N-4551

APPENDIX VIII

CARBON AND GRAPHITE FOAMS - FEASIBILITY STUDIES

VIII. 1. Introduction

Various aerospace and industrial applications present a need for a solid form of insulating material having a relatively high mechanical strength and low bulk density with the thermal stability of graphite. Investigations by National Carbon Company * indicated that a carbon foam could be made having a lower thermal conductivity than previously attained with carbon foams. The initial experiments were limited to samples measuring about 1 x 1 x 3-inch and, therefore, a program was initiated to investigate methods of fabricating and scaling up the size of carbon foam. Graphitization of the carbon foams was also investigated in order to fabricate a material for higher temperature aerospace applications.

VIII. 2. Raw Materials

The prior work performed by National Carbon Company and the effort reported here were concerned with urethane base foam materials. The urethane foam was produced by mixing a three component system obtained from the Carwin Chemical Company under the trade name of Carthane 1003-10. A typical formulation of this foam system is presented in Table VIII. 1.

Table VIII. 1. Formulation of Urethane Base Foams

Component No.	Ingredient	Amount, Weight, Per Cent
A	A polyester resin	35
B	Polyaryl polyphenylisocyanate known as "PAPI"	60
C	Mixture of water, an amine, and a surfactant	5

VIII. 3. Carbon Foam - Fabrication and Scale-Up

The urethane foaming ingredients were batch mixed as follows: Components A and C (Table VIII. 1) were mixed together for one minute, Component B was added and stirring was continued for about 1.5 minutes. The mixture was then placed in a 60°C preheated oven for 30 minutes to complete the foaming. The foamed block, after the 60° heating period, possessed a high density skin which had to be removed before curing.

* Mitchell, C. V., "National Carbon Invention Disclosure LN 1960-19" National Carbon Company, 1960. Intercompany Report.

Curing of the foam was accomplished in two steps: (a) 50°C/hr to 200°C for 15-20 hours, and (b) 50°C/hr to 250°C for 18-25 hours. The hold period at 200°C was necessary to prevent cracking of the foamed piece and effected a weight loss of approximately 6 per cent. An additional 20-25 per cent weight loss occurred during the 200° - 250°C heating cycle. It was believed that the latter curing cycle significantly increased the cross linking. The curing reaction was time dependent on the size of the foamed sample with the larger samples requiring more time. Two reasons for the relatively long times required for curing are:

(1) The time required for oxygen to diffuse into the foam through a barrier of gaseous reaction products.

(2) The thermal conductivity of the foamed block was very low, and the center of the blocks reached curing temperatures slowly.

The large sizes also required slow cooling from the curing temperature (250°C) to prevent cracking by thermal stress. Typical results of curing a 5 x 5 x 10 inch block of foam are presented in Table VIII. 2.

Table VIII. 2. Curing Data - Urethane Foam System

200°C Curing Time hrs.	Wt. Loss Per Cent	Volume Shrinkage Per Cent	250°C Curing Time hrs.	Wt. Loss Per Cent	Volume Shrinkage Per Cent	Average Cooling Rate °C/hr.
16	6.3	5.1	20	17.7	17.1	75

Attempts to reduce the curing cycle time were made as follows:

(1) Curing in an autoclave under a pressure of 80 lbs/in^2 at 200-250°C with continuous air injection seemed promising and should be investigated further.

(2) Adding graphite cloth, phenolic resins or powdered graphite to the forming mixture did not appreciably decrease the curing time.

(3) Puncturing or drilling small holes in the foam did not reduce curing time.

The baking operation at 800°C to fully carbonize the foam was carried out in conventional furnaces. A 30 per cent volume shrinkage occurred during the baking operation and a slow heating rate (5-10°C/hr from 200-800°C) was required to prevent cracking. Foams which were not sufficiently cured, melted and cracked during the baking operation.

Foams containing uniformly sized, spherical cells were stronger than foams containing irregular and/or elongated shaped cells. Limited data (Table VIII. 3.) indicated that smaller cells also resulted in stronger foams.

Table VIII. 3. Flexural Strengths of Carbon Foam with Respect to Structure Type

Type of Cells in Structure	Flexural Strengths, lbs/in^2 N	Avg.
(1) Unsymmetrical shaped - large size	9	200
(2) Uniformly sized spherical shaped; about half the size of unsymmetrical shaped cells in (1)	2	450

Several difficulties were encountered in scaling up the fabrication of carbon foam. First, the largest piece of carbon foam produced by batch mixing with a 1/3 H. P. "Lighting" brand mixer measured 3 x 8 x 12 inches, but the foam structure was not uniform. The mixing equipment was not capable of producing blocks of foam larger than about 1 x 2 x 3 inches with a uniformly sized, spherical cell structure. A large batch mixer or continuous foaming equipment will be required for large size blocks of foam. Second, if the foam was not completely cured, it melted and cracked during baking. Several blocks larger than the 3 x 8 x 12 inch size mentioned above cracked during the baking operation and showed evidence of improper cure. Third, the curing, baking and cooling cycles became progressively longer as the size of the foamed blocks increased.

VIII. 4. Graphite Foams

Carbon foam with good structure was successfully graphitized at 2800°C in a conventional tube furnace at heating rates of 200-300°C/hr. Graphite foam was made having a bulk density of 0. 16 g/cc, but had a flexural strength of only 180 lbs/in^2. It was theorized that the strengths of graphite foams might be improved by the addition of various ingredients for structural reinforcement. Therefore, the following investigations were made:

(1) Graphite cloth fibers were added to the foaming ingredients. None of the foamed blocks made in this manner processed satisfactorily through the baking operation. Further effort did not appear justifiable.

(2) A phenolic-furane resin mixture was added to the foaming ingredients to act as a carbonizable reinforcement for the foamed body. Problems encountered in the curing operation indicated the need for appreciable further investigation to demonstrate the potential value of this approach.

(3) A powdered graphite and phenolic resin was blended with the foaming ingredients in the amount of 30 per cent by weight. This resulted in a flexural strength nearly four times as great as that for graphitized urethane (670 vs 180 lb/in^2) while the bulk density was doubled (0.33 vs 0.16 g/cc).

VIII. 5. Conclusions

1. Larger mixing equipment, either of the batch or continuous type, is required to produce urethane base foams with suitable structure.

2. Carbon foams with good structure can be graphitized readily.

3. A powdered graphite-phenolic resin mixture added to the foaming ingredients increased the strength of graphite foam by a factor of nearly four while the bulk density was increased by a factor of two.

APPENDIX IX

CEMENTS FOR USE WITH CARBON AND GRAPHITE

IX.1. Introduction

Many aerospace applications require very special properties and configurations of carbon and graphite materials. The size and shape of the desired article or the extremely fine grain and high density required in many cases make it impossible to manufacture the carbon or graphite in monolithic sizes large enough to accommodate the design. Therefore, a method is required for segmenting or building large shapes from smaller blocks and pieces. In some instances it is possible to segment using simple offset or step-wise mechanical joints in which no bonding or filler material is required. In other cases, a strong, gas tight joint is needed and must maintain strength over a considerable range of temperatures.

A small development program was undertaken in an effort to provide a cement which would yield flexural strengths of 3000 lbs/in^2 or greater at temperatures up to 2800°C. Various carbonaceous cements are commercially available but early attempts to use these cements on high density graphites such as ZT and pyrolytic were failures. A cement which would react with the graphite, thus forming a joint similar to a welded or brazed joint in metals, would seem to be more usable with the high density graphites. The theory was that such a cement would not rely on porosity in the graphite to provide a gripping surface. The basic ingredient selected for use in this study was finely divided titanium diboride.

National Carbon Company C-9 cement was used in order to establish a basis for comparison as well as to further evaluate a standard carbonaceous cement. It was decided that, if this evaluation so indicated, modifications would be made to the C-9 cement to improve its strength and high temperature capabilities.

IX.2. Investigation of Titanium Diboride Cement

The possibility of welding graphite with titanium diboride was investigated several years ago to join graphite electrodes. The results of these tests showed that TiB_2 would dissolve graphite at high temperatures and form an excellent bond upon subsequent cooling. The cement for this present study, made by mixing finely divided TiB_2 with a carbonizable binder (Table IX.1), was given the experimental designation of TS-341.

Table IX.1. Composition of TS-341 Cement

Ingredient	Amount, Weight Per Cent
Titanium diboride (100% through 200-mesh; Tyler Standard)	70
Phenol-furfural resin	30

A series of flexural strength measurements was made at elevated temperatures using ZTA graphite specimens cemented with TS-341. The size of the specimens was 1 x 1 x 4 centimeters. The specimens were divided into two groups. Group A was cured for sixteen hours at 110-120°C, and then heated to 2750°C to cause the TiB_2-graphite reaction. Group B was just cured to investigate the possibility of allowing the cement to react under the more rapid heating conditions used for testing. The flexural strength measurements for the two groups are presented in Table IX.2.

Table IX.2. Flexural Strength vs. Temperature of TS-341 Cemented Joints, ZTA Graphite Specimens

	Flexural Strength*, lbs/in^2				
Group	25°C	500°C	1000°C	1750°C	2500°C
A	3,179	--	3,854	2,169	1,856
B	2,075	2,805	1,276	1,724	1,409

* Single point loading: 1.25 cm span.

The encouraging results of the joint strengths prompted the test firing of a subscale ZTA segmented rocket nozzle assembled with TS-341 cement. The joints in the nozzle were reacted to 2750°C after a cure for 16 hours at 120°C. The nozzle was then installed in a 6-inch solid fuel rocket motor and fired for 72 seconds at 5600°F and 1,000 lbs/in^2 chamber pressure. Inspection of the nozzle after firing showed the joints still intact. Photographs of the tested nozzle are shown in Figures IX.1 and IX.2.

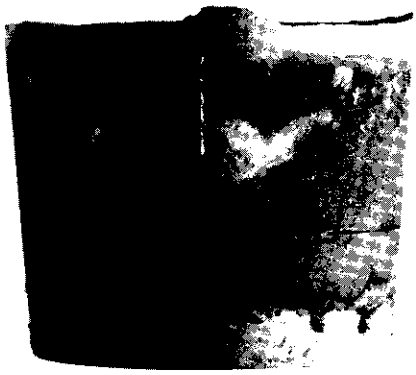

Figure IX.1. Side View of a Segmented Nozzle after Test Firing
N-4552

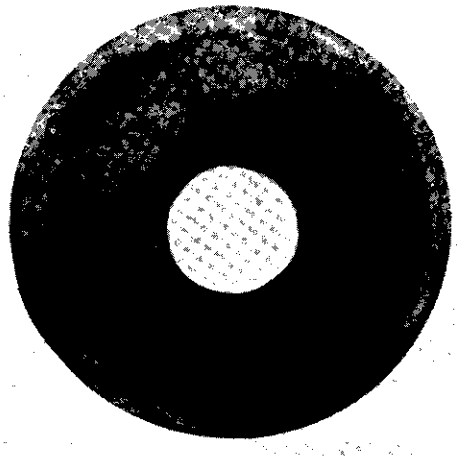

Figure IX.2. Top View of a Segmented Nozzle After Test Firing
N-4553

Reacting the cemented joints of all segmented nozzles to a temperature of approximately 2800°C prior to firing presents some problems because of indicated physical size of future nozzles. It may not be economically sound to provide graphitizing facilities for extremely large nozzles. Consequently, it was hoped that segmented nozzles using cured TS-341 cemented joints could be fired successfully, allowing the reaction between the cement and graphite to take place during the rocket firing. A segmented nozzle made using TS-341 cement cured to 120°C was test fired in the rocket motor under the conditions listed above but was not successful. Apparently the heating rate was too rapid to allow the cement to react and one section of the nozzle shifted during the firing, permitting hot combustion gases to melt and severely erode the backup material. No further tests were conducted on segmented nozzles with unreacted TS-341 cemented joints.

Cemented specimens were made to determine the optimum particle sizing of the TiB_2 for a given joint thickness. The initial trial using TS-341 cement made with TiB_2 of 2 microns size produced very low strengths. Specimens made with cement having TiB_2 of 74 micron size were then fabricated and proved to have excellent strength. Additional tests were conducted on cemented joints using 416 micron and 147 micron TiB_2. The curing and reaction temperatures were 120°C and 2600°C, respectively. The results of the flexural strength tests are shown in Table IX.3. The results in Table IX.3. indicated that TS-341 cement should be made with 74 micron TiB_2 filler.

Table IX.3. Flexural Strengths of TS-341 Cemented Specimens, Varying Grain Size of TiB_2

Size of TiB_2, Microns	Joint Thickness	n	Average Flexural Strength,* lbs/in^2	Remarks
416	1/32"	4	731	Some samples broke during preparation.
147	1/32"	3	2,701	Broke in joint
74	1/32"	4	3,541	Broke in stock

* Sample size was 1/2 x 1/2 x 5"; third point loading; room temperature.

Subsequent strength measurements with TS-341 cement have shown the importance of drying the graphite prior to applying the cement. If any moisture was present on the mating surfaces, water vapor trapped in the cement lowered the joint strength by the formation of gas bubbles which prevented the cement from reacting with the graphite. Flexural strengths were increased by drying the graphite as shown in Table IX.4.

Table IX.4. Flexural Strengths of TS-341 Cement Joints on Dried and Undried CFW Graphite

n	Final Curing or Baking Temperature, °C	Graphite Condition	Average Flexural Strength, lbs/in^2
6	120	Undried	1,586*
13	120	Dried	1,932*
10	2,850	Undried	3,179**
15	2,850	Dried	3,541* All samples broke in stock.

* Sample size was 1/2 x 1/2 x 5"; third point loading; room temperature.
** Sample size was 1 cm x 1 cm x 4 cm; single point loading; 1.25 cm span.

A carbon or graphite matrix homogeneously dispersed within the cement was investigated as a means for increasing the strength of TS-341 cemented joints. Graphite cloth as a graphite matrix was tried first as a whole sheet between the mating surfaces and then in the macerated form. The former reduced the cured flexural strength to an average of 1,189 lbs/in^2 and therefore was discontinued. The use of about 5 weight per cent of macerated cloth, blended with the TiB_2, produced some improvement in cured strengths and uniformity and was evaluated further. Flexural strengths of TS-341 cemented

specimens without and with macerated cloth filler are presented in Table IX.5. Standard deviations show the cured cement with the macerated cloth to be more uniform than that without the cloth. A comparison of standard deviations for the reacted specimens would be meaningless because many of the samples failed in the stock; however, it may be stated generally that the reacted cement containing the macerated cloth was more uniform since none of the specimens failed in the joints.

Table IX.5. Room Temperature Flexural Strengths of TS-341 Cemented Joints, With and Without Macerated Graphite Cloth Matrix, CFW Graphite Specimens

Final Curing or Baking Temperature, °C	Flexural Strength,* lbs/in^2 With Macerated Cloth	Location of Fracture**	Flexural Strength,* lbs/in^2 Without Macerated Cloth	Location of Fracture**
120	2823	C	687	C
120	2134	C	1833	C
120	2097	C	1930	C
120	2115	C	2272	C
120	2321	C	1794	C
120	2380	C	2340	C
120	2081	C	811	C
120	2239	C	2092	C
120	2526	C	2068	C
120	2098	C	2206	C
120	2387	C	2025	C
120	2710	C	1769	C
120	2175	C		
120	2445	C		
	Avg. 2324		Avg. 1932	
	Std. Dev. ± 163		Std. Dev. ± 507	
2850	3068	S	1570	C
2850	2931	S	4114	S
2850	2874	S	3491	S
2850	2940	S	2769	C
2850	3189	S	2321	C
2850	3343	S	4203	S
2850	3305	S	4664	S
2850	2915	S	3185	S
2850			3789	S
2850			1809	C
2850			4351	S
2850			4445	S
2850			4431	S
2850			3479	S
2850			4326	S
	Avg. 3071		Avg. 3541	

* Size of specimens 1/2 x 1/2 x 5 inches, third point loading.
** C-fracture located in cement, S-fracture located in stock.

IX.3. Comparison of TS-341 and C-9 Cements

A carbonaceous cement (National Carbon Company grade C-9) was also tested under this program. The purpose of these tests was to provide comparison data as well as to further evaluate an all-carbonaceous cement. In this way the advantages, if any, of TS-341 cement would be demonstrated.

Tensile strengths of the two types of joints were measured over a range of temperatures and results of these measurements are given in Table IX.6.

Table IX.6. Tensile Strength vs. Temperature of Reacted TS-341 and Cured C-9 Cemented Joints, CFW Graphite Specimens

Testing Temperature, °C	Tensile Strength,* lbs/in² TS-341 Cement**	Location of Fracture***	C-9 Cement	Location of Fracture***
20	1400	S	1401	C
20	565	C	1503	C
20	1705	S	1372	S
20			1649	S
20			1680	S
20			1544	S
20			1340	C
20			1694	S
20			1446	C
20			1659	S
20			1679	C
20			1473	C
20			1505	S
20			1714	S
500	1838	S	809	C
1000	1625	S	1766	C
1730			1522	C
1750	1900	C	728	C
2500	1257	C	2785	C
2500			2194	C

* Testing rate - 0.020 in/min. Specimen size, $\frac{1}{4}$-inch diameter by $1\frac{1}{2}$-inch gauge length.

** More than 50 per cent of the joints failed during machining of the TS-341 specimens.

*** C-fracture located in cement, S-fracture located in stock.

Figures IX.3. and IX.4. are photographs of CFW graphite specimens after tensile testing at room temperature. The two figures show, respectively, a sample which broke in the cemented joint and one which broke in the graphite stock.

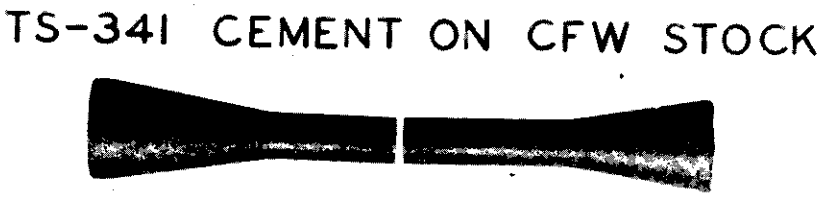

N-4554

Figure IX.3. Tensile Fracture for TS-341 Cement on CFW Graphite, Specimen Tested at Room Temperature, Fracture Located in Joint

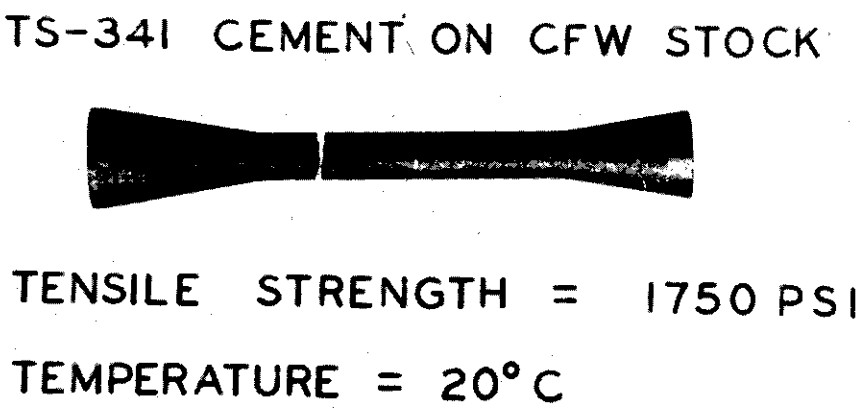

N-4555

Figure IX.4. Location of Tensile Fracture for TS-341 Cement on CFW Graphite, Specimen Tested at Room Temperature, Fracture Located in Stock

It was evident from the data reported above that cured TS-341 was not consistent in tensile strength since more than half of the TS-341 cemented specimens broke during sample fabrication while none of the C-9 cemented samples broke during machining. It also appeared from these data that at 2500°C C-9 was superior to TS-341.

The tests reported in Tables IX.3 through IX.6 were conducted on CFW grade graphite which is relatively porous stock as compared to the high density grades such as ZTA. Since it was felt that the TS-341 cement does not depend on the pore structure of the graphite to provide good bonds, additional trials were made using the higher density, low porosity Grade ZTA graphite to make the comparison of the two cements more conclusive. Samples of ZTA cemented with TS-341 (reacted to 2800°C) and C-9 (cured to 120°C) were tested in flexure over a range of temperatures. The results of the flexural strength tests are presented in Table IX.7 and are shown graphically in Figure IX.5.

Table IX.7. Flexural Strength vs. Temperature of TS-341 and C-9 Cemented Joints, ZTA Graphite Specimens

Testing Temperature, °C	Flexural Strength,* lbs/in^2	
	TS-341 Cement	C-9 Cement
20	2101	2844
20	1782	2961
20	1620	3030
20	1135	3057
20	960	2895
1000	2232	2299
1000	1704	2859
2500	4235	2654
2500	3039	3118

* Specimen size 1/4 x 1/4 x 2 inches, single point loading, testing rate 0.20 in/min., all samples broke in the cement.

The data shown in Table IX.7 and Figure IX.5 led to the following conclusions:

1. The flexural strength of C-9 cement remained essentially constant with increasing temperature.

2. The flexural strength of TS-341 cement increased with increasing temperature.

3. From room temperature to about 1650°C the C-9 cement was stronger than the TS-341 cement.

4. Above 1650°C the TS-341 cement was stronger than C-9 cement.

5. The C-9 cement produced more uniform strengths from sample to sample than did TS-341.

These conclusions point out that the TS-341 cement produced superior flexural strengths with low porosity graphites tested at temperatures approaching those expected under conditions of application. The TS-341 cement may prove to be of even greater value for bonding lower porosity materials such as pyrolytic graphite.

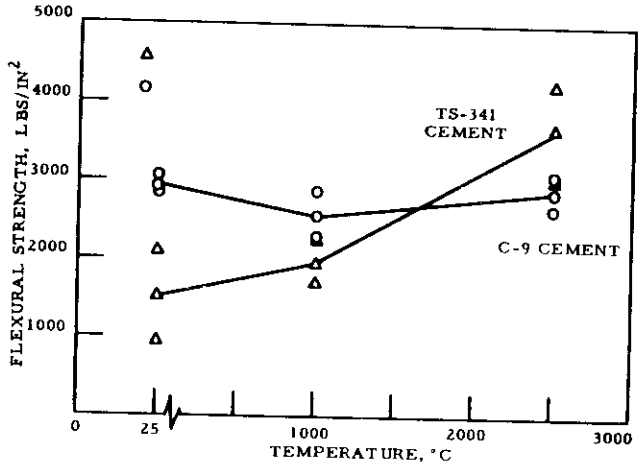

N-4556

Figure IX. 5. Flexural Strength vs. Temperature on TS-341 and C-9 Cemented Joints, ZTA Graphite Specimens

The nonuniform strength behavior of TS-341 cement was probably caused by the formation of gas bubbles within the cement. The gases could have been water vapor and/or the oxides of carbon. The C-9, being more porous, probably allowed such gases to escape during curing or baking.

IX. 4. Modified C-9 Cement

A limited effort was made to modify the C-9 cement and develop a carbonaceous cement superior in strength to C-9. The result of this effort was a cement consisting of coal tar pitch, thermosetting resin and graphite flour. The pitch was added to give the necessary plasticity to the cement. The composition of the modified C-9 cement is presented in Table IX. 8.

Table IX. 8. Composition of Modified C-9 Cement

Ingredient	Amount Weight Per Cent
Phenol-furfural resin	36. 8
175°C coal tar pitch	15. 8
High density graphite flour (74 micron size)	47. 4

Specimens of graphite were bonded with the modified C-9 cement using the same curing procedure as for C-9. Room temperature strength measurements made on these specimens produced a flexural strength of 2,798 ± 134 lbs/in^2 with all samples breaking in the cement. C-9 bonded joints using the same cementing techniques produced room temperature flexural strengths of 2,957 ± 100 lbs/in^2. There was no significant difference between the two cements; therefore, additional effort was not considered desirable.